IRE
Transactions
on Microwave Theory and Techniques

Volume MTT-4 **OCTOBER, 1956** Number 4

Special Issue

NATIONAL SYMPOSIUM ON

MICROWAVE TECHNIQUES

Held at
University of Pennsylvania
Philadelphia, Pa.
February 2-3, 1956

For complete Table of Contents, see page 191.

PUBLISHED BY THE
Professional Group on Microwave Theory and Techniques

IRE PROFESSIONAL GROUP ON

MICROWAVE THEORY AND TECHNIQUES

The Professional Group on Microwave Theory and Techniques is an association of IRE members with professional interest in the field of Microwave Theory and Techniques. All IRE members are eligible for membership and will receive all Group publications upon payment of the prescribed annual assessment of $2.00.

IRE TRANSACTIONS®
on Microwave Theory and Techniques

Published by the Institute of Radio Engineers, Inc., for the Professional Group on Microwave Theory and Techniques, at 1 East 79th Street, New York 21, New York. Responsibility for the contents rests upon the authors, and not upon the IRE, the Group, or its members. Price per copy: IRE PGMTT members, $1.85; IRE members, $2.75; nonmembers, $5.55. Annual subscription price: IRE members, $8.50; colleges and public libraries, $12.75; nonmembers, $17.00.

Address all manuscripts to Theodore S. Saad, Sage Laboratories, 30 Guinan St., Waltham, Mass.

IRE Transactions on Microwave Theory and Techniques

Published by the Professional Group on Microwave Theory and Techniques

Volume MTT-4 October, 1956* Number 4

TABLE OF CONTENTS

* *This Special Issue takes the place of the regular October issue.*

Foreword

In the spring of 1955 the Administrative Committee of PGMTT was looking for a new place to hold the yearly technical meeting of the group. The writer was present at the meeting where possible places were discussed, and he was asked whether he thought a meeting in Philadelphia could be arranged. The idea of holding a local meeting devoted to microwave relays had already been discussed by him with others of the Philadelphia area, and accordingly it seemed as though the situation demanded that the national and local meetings be combined. Presentation of the idea to the Executive Committee of the Philadelphia Section resulted in their approval and agreement to participate as a co-sponsor. Later, the PGAP also agreed to co-sponsor the meeting.

At the first meeting of the organizational group it was agreed that a symposium on microwave techniques would have more appeal than one devoted entirely to relays, and the date was set for February 2–3, 1956. The general plans were outlined accordingly, and the Committee Chairmanships agreed upon. The Steering Committee consisted of the following members.

R. F. Schwartz, *Chairman*,
Moore School of Electrical Engineering,
University of Pennsylvania.

Charles Polk, *Arrangements Committee*,
Moore School of Electrical Engineering,
University of Pennsylvania.

J. B. Williams, *Finance Committee*,
Government and Industrial Division.

D. R. Crosby, *Technical Program Committee*,
Radio Corporation of America.

S. M. King, *Secretary and Publicity Committee*,
I.T.E. Circuit Breaker Company.

I. L. Auerbach, *Treasurer*,
Burroughs Corporation.

E. I. Hawthorne, *Section Liaison*,
Moore School of Electrical Engineering,
University of Pennsylvania.
(Later replaced by J. B. Williams).

W. N. Sharpless, *PGAP and PGMTT Liaison*,
Bell Telephone Laboratories.

Ben Warriner, *PGMTT Liaison*,
General Electric Advanced Electronic Center.

D. D. King, *PGMTT Liaison*,
Johns Hopkins University.

Sanford Hershfield, *PGAP Liaison*,
Glenn L. Martin Company.

N. I. Korman, *Advisor*,
Radio Corporation of America.

Twenty-seven papers were selected from among the forty-two received as being of sufficiently general interest for the meeting. Sessions were devoted to microwave components, antennas, guided transmission, scatter propagation and radiation, ferrite theory, and ferrite components. Of particular interest was the panel discussion on guided transmission, in which authorities on a number of different types of transmission lines presented their respective viewpoints. Considerable discussion followed.

Thanks are due to all the members of the steering committee for helping to plan the symposium; to the chairman and members of the subcommittees who worked out the details for meeting; to the Moore School of Electrical Engineering for acting as host and making possible the securing of certain facilities; to the Physics Department, University of Pennsylvania, for the use of their auditoria; to I.T.E. Circuit Breaker Company for their aid in publicity and supplying a photographer; to Radio Corporation of America and the Philco Corporation for helping to support the cocktail party.

RICHARD F. SCHWARTZ,
Chairman, Microwave Symposium.

Nonuniform, Inhomogeneous, and Anisotropic Waveguides*

RALPH W. KLOPFENSTEIN†

Summary—**This paper discusses in a general way some of the properties of nonuniform, inhomogeneous, and anisotropic waveguides and transmission lines. No attempt is made to discuss in detail the behavior of any particular type of waveguide except for the purposes of example. Most of the points discussed are well known separately, but an attempt has been made to bring some of general properties of special types of waveguide together in order to unify them, and, thus, it is hoped, to contribute to the over-all understanding of guided wave phenomena.**

IN THIS paper I would like to discuss briefly some of the properties of *non*uniform, *in*homogeneous, and *ani*sotropic waveguides and transmission lines. This is, of course, too broad an area to cover in detail, but I will outline some of the special qualities of these types of waveguides.

The usual waveguide—which is uniform, homogeneous, and isotropic—has been commonplace in microwave applications for about two decades. The theory of such guide in dominant mode operation can be considered essentially complete, at least in its fundamentals. Important new work is being done today, however, on multimode propagation in uniform, homogeneous, isotropic waveguides.

It is my purpose to discuss here some of the *generalizations* of the usual waveguide structure. Recent researches have uncovered many interesting and useful properties of these generalized structures. They are generally referred to as *non*uniform waveguides, *in*homogeneous waveguides, and *ani*sotropic waveguides. For the sake of clarity, the meaning of these terms is illustrated in Fig. 1.

By the term *nonuniform waveguide* is meant a waveguide whose characteristics change in the direction of wave propagation. Ordinarily the basic structure remains the same, but the proportions of the guide may change. The continuous impedance matching taper shown at the top of the figure is such a structure. The change of dimension may also occur discontinuously as shown at the top right, and thus, the familiar impedance matching transformer is also an example of a nonuniform waveguide. Another example, not shown in the figure, is the tapered load commonly used in microwave practice.

An *inhomogeneous waveguide* is one whose properties remain constant in the direction of propagation, but they may vary across the cross section of the waveguide as shown in Fig. 1 (b). Here again the change may occur either continuously or discontinuously.

In an *anisotropic waveguide* the medium properties are constant across the guide cross section *and* along the direction of wave propagation. In this type of medium, however, the magnetic induction vector and the magnetic intensity vector are not necessarily colinear. But they still remain proportional. That is, if the magnetic induction is doubled in magnitude, so is the magnetic intensity. This situation is completely described by considering the magnetic permeability to be a tensor rather than a scalar. Such a condition exists in a waveguide filled with saturated ferrite, for example. Anisotropies may be present in the electrical properties of the medium, but this is not nearly so common in current microwave practice.

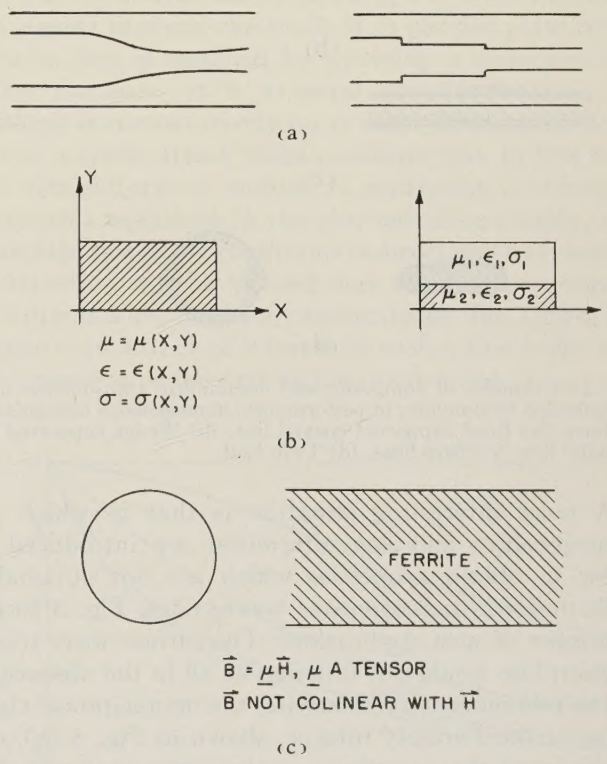

Fig. 1—Various waveguide types. (a) Nonuniform waveguides. (b) Inhomogeneous waveguide. (c) Anisotropic waveguide.

We ordinarily deal with various combinations of these waveguide types. An extreme example, perhaps, is a ferrite cylinder of finite length and tapered at the ends inserted into a larger circular waveguide. This configuration could be described as a *nonuniform, inhomogeneous,* and *anisotropic* waveguide.

*In*homogeneities and *non*uniformities are introduced into waveguides and transmission lines for *two* major

* Manuscript received by the PGMTT, July 16, 1956. Invited paper presented before the National Symposium on Microwave Techniques, Philadelphia, Pa., February 2, 1956.

† RCA Labs., Princeton, N. J.

reasons. Fig. 2 shows a number of transmission lines in which the desired behavior of the line is that of a uniform, homogeneous line. The deviations, in this case, are made for practical reasons such as the mechanical support of the conductors and suitability of the structure for printed circuit techniques. Here then, the special properties due to the *non*uniformities and *in*homogeneities are necessary evils, and are to be minimized as much as possible by suitable design. This situation is more characteristic of transmission lines than *uni*conductor waveguides. This is because of the multiplicity of conductors to be maintained in proper relation to each other in the case of transmission lines.

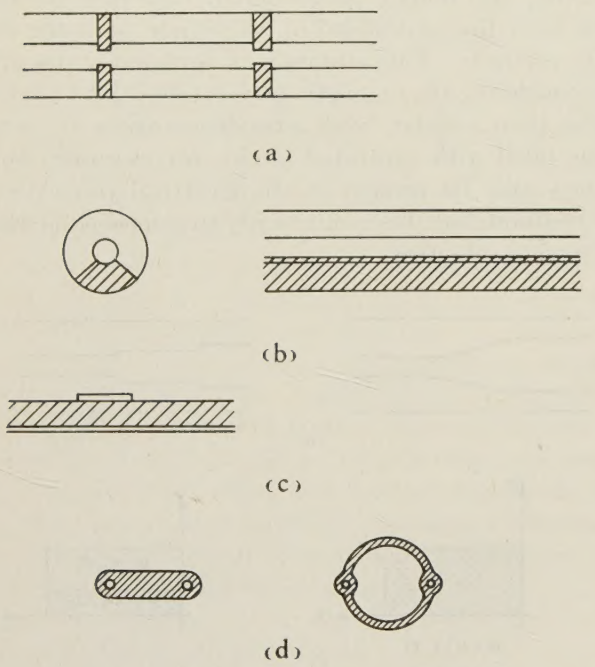

Fig. 2—Examples of composite and nonuniform transmission lines intended to simulate, in performance, homogeneous transmission lines. (a) Bead supported coaxial line. (b) Wedge supported coaxial line. (c) Strip lines. (d) Twin lead.

A more interesting situation is that in which *in*homogeneities and *non*uniformities are introduced in order to obtain properties which are not obtainable with uniform, homogeneous waveguides. Fig. 3 shows a number of such applications. The surface wave transmission line would not function at all in the absence of of the *in*homogeneity. Likewise, the nonreciprocal character of the Faraday rotator, shown in Fig. 3 (b), depends upon the *ani*sotropy of the ferrite material. For proper functioning of the elementary form of the linear accelerator shown, waves of slow phase velocity must be propagated in an empty space. This property depends on the inhomogeneity of the cross section.

A fourth application of considerable interest is shown at the bottom of Fig. 3. The structure consists of a rectangular waveguide with symmetrical dielectric slabs on each side. The investigation in which this structure was used dealt with the microwave resonances of the ammonia gas molecule. It was desired to expose a sample of ammonia gas to an essentially constant electric field at microwave frequencies, in order to determine the absorption spectrum. The unique thing about the structure shown is that in the dominant TE mode, proper proportioning of the dielectric constant or dielectric dimensions leads to a mode which has this property. The electric field in the empty space does not depend then on the cross-sectional coordinates, but is constant. Moreover, this condition is readily obtainable with low-loss dielectrics commonly used in microwave practice.

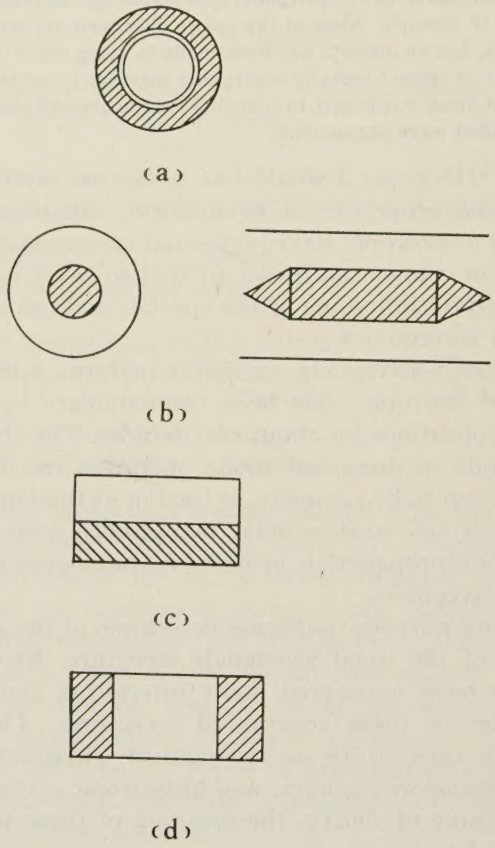

Fig. 3—Examples of inhomogeneous and anisotropic transmission systems in which the inhomogeneity and anisotropy is essential for the desired transmission properties. (a) Surface wave transmission line. (b) Nonreciprocal attenuator in circular waveguide. (c) Linear accelerator. (d) Composite rectangular waveguide for the investigation of microwave resonances of NH_3 molecules (E_y constant in open space).

The early theoretical investigations of *in*homogeneous waveguides dealt with particular types and their properties. In this manner, a number of unusual features of the mode structure of such guides were discovered. A general investigation of *in*homogeneous waveguides was undertaken by Professor Adler of M.I.T. as a topic for a doctoral dissertation. This was published in 1949. He found, among other things, that the free modes in an *in*homogeneous waveguide were *almost completely* of the hybrid type—that is, neither transverse electric nor transverse magnetic, but having axial components of both electric and magnetic fields. Professor Marcuvitz has more recently extended this work and shown that the set of free modes on a *closed in-*

homogeneous waveguide is complete—that is, that they are adequate to express the total field due to an arbitrary source distribution. This is not true, however, of *open inhomogeneous* guides, such as the dielectric rod waveguide. Here, an additional continuum of radiating modes is required for completeness.

Fig. 4 contrasts some of the properties of *in*homogeneous waveguides and transmission lines with those of homogeneous guides.

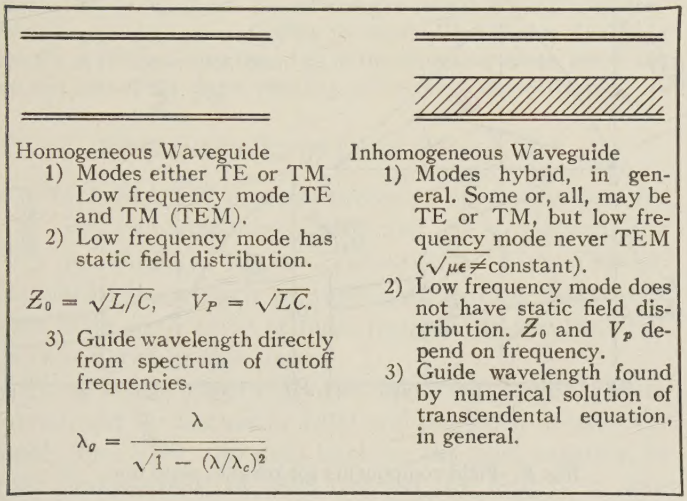

Homogeneous Waveguide
1) Modes either TE or TM. Low frequency mode TE and TM (TEM).
2) Low frequency mode has static field distribution.

$Z_0 = \sqrt{L/C}, \quad V_P = \sqrt{LC}.$

3) Guide wavelength directly from spectrum of cutoff frequencies.

$$\lambda_g = \frac{\lambda}{\sqrt{1 - (\lambda/\lambda_c)^2}}$$

Inhomogeneous Waveguide
1) Modes hybrid, in general. Some or, all, may be TE or TM, but low frequency mode never TEM ($\sqrt{\mu\epsilon} \neq$ constant).
2) Low frequency mode does not have static field distribution. Z_0 and V_p depend on frequency.
3) Guide wavelength found by numerical solution of transcendental equation, in general.

Fig. 4—Comparison of properties of homogeneous and inhomogeneous waveguide.

In the homogeneous guide the mode types are separable into two classes—TE and TM. When a low frequency mode exists, it is both TE and TM, that is, TEM. By way of contrast, in an *in*homogeneous guide the mode types are in general neither TE nor TM but hybrid in character. *Some* of the modes *may* be TE or TM, but the low frequency mode will never be TEM unless the free space propagation velocity is constant over the cross section.

For a homogeneous guide, the field distribution for the low frequency mode is that associated with the static charge distribution for the electric field and the static current distribution for the magnetic field. This field distribution does not depend on frequency, nor does the characteristic impedance and phase velocity which are expressible in terms of the static inductance and capacity. In an *in*homogeneous guide, on the other hand, the low frequency mode does not have the static field distribution except in the zero frequency limit. The characteristic impedance and phase velocity vary with frequency and only approach the static values in the zero frequency limit.

Another feature which leads to complications when one is dealing with an *in*homogeneous waveguide or transmission line is the determination of the guide wavelength, or phase velocity, for any particular mode. In a homogeneous waveguide, the guide wavelength is immediately obtainable for each mode, at any operating frequency, by means of the familiar relation shown on the figure. This situation no longer prevails with an inhomogeneous guide and the determination of guide wavelength normally requires the solution of a rather involved transcendental equation by numerical methods. The extent of the difficulties, naturally, depends on the merits of the individual problem.

These remarks may be illustrated by considering the simple example shown in Fig. 5.

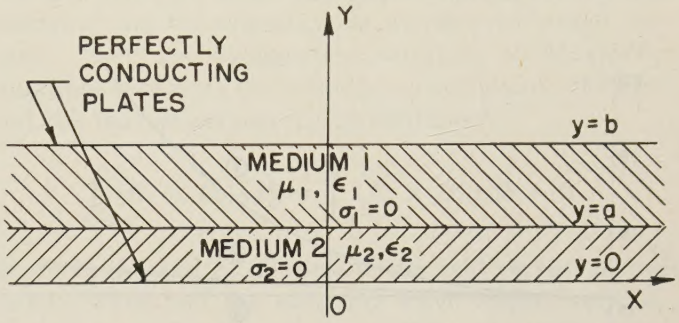

Fig. 5—Elementary type of inhomogeneous transmission line.

This is probably the simplest type of *in*homogeneous waveguide that one can think of. A parallel plate transmission line is modified by inserting a dielectric slab along one side. It is a useful example because the analysis is comparatively quite easy. There are a number of ways to attack these problems, but, in this case, the straightforward method of expressing solutions to Maxwell's equations in the two media separately, and matching boundary conditions is direct and convenient.

Attention will be focused here on the properties of this line as a low frequency transmission line. One of the primary quantities of interest in such a line is the cutoff frequency of the first higher order mode.

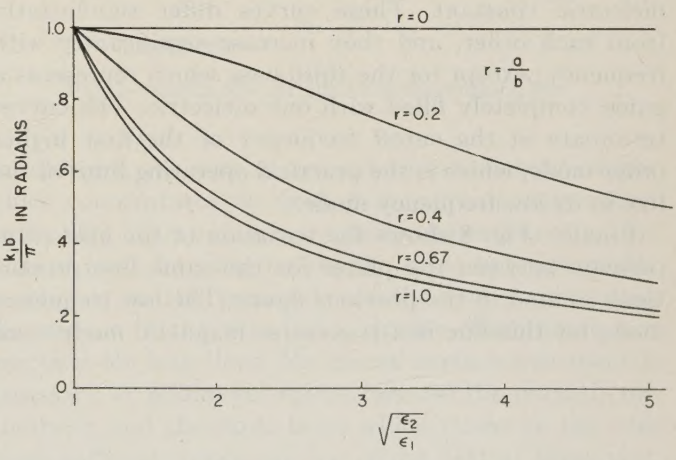

Fig. 6—Cutoff frequency of first higher order mode in parallel plate line.

Fig. 6 shows the cutoff frequency as a function of the relative dielectric constants of the two media for various amounts of dielectric. The line $r = 0$, and the curve $r = 1.0$, represent the limiting conditions in which the

guide is entirely filled with one dielectric or the other. There are two features of these curves of particular interest. Firstly, the cutoff frequency is always between the limiting values for one dielectric or the other. Another interesting thing to notice about these curves is that the cutoff frequency of the first higher order mode decreases much more rapidly than in proportion to the amount of dielectric inserted. When the guide is two-thirds full, the cutoff frequency is nearly as low as when the guide is completely filled.

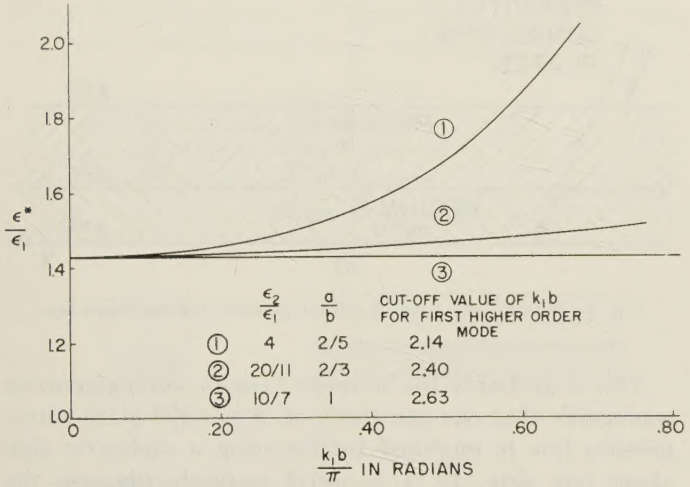

Fig. 7—Effective dielectric constant of parallel plate line.

Fig. 7 shows the "effective" dielectric constant of the guide for various proportions of dielectric. This is the dielectric constant from which the velocity, or guide wavelength, may be calculated. In the curves shown, the proportions are chosen so that the static "effective" dielectric constants are equal. The abscissa represents increasing frequency while the ordinate is the "effective" dielectric constant. These curves differ significantly from each other, and they increase significantly with frequency; except for the third case which represents a guide completely filled with one dielectric. The curves terminate at the cutoff frequency of the first higher order mode, which is the practical operating limit of the line in its low frequency mode.

Finally, Fig. 8 shows the variation of the field components between the plates for the same line proportions as used in the previous figure. The low frequency mode for this line is a transverse magnetic mode—not a TEM mode. The graph at the upper left shows the variation of the axial component of electric field. This can be compared to the transverse component, which is plotted to the same scale, in the curves at lower left. The transverse component of the magnetic field is shown at the lower right. A considerable variation of the field components is evident at this operating frequency which is near the cutoff frequency for the first higher order mode.

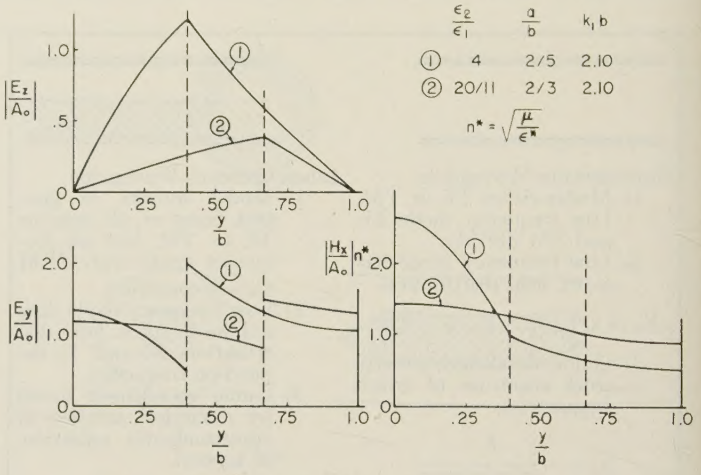

Fig. 8—Field components for parallel plate line.

The behavior of this prototype *in*homogeneous waveguide is qualitatively typical of all such guides. When a low frequency mode exists, it will not in general be transverse electromagnetic. It may be transverse electric, transverse magnetic, or hybrid. The characteristic impedance and phase velocity will depend on frequency to a greater or lesser extent depending upon the individual configuration. The cutoff frequencies will ordinarily lie between those of the corresponding homogeneous guide filled with dielectric of the maximum and minimum dielectric constants, respectively.

In summary, I would like to observe that we meet *non*uniformities, *in*homogeneities, and even *ani*sotropies almost continually in microwave transmission problems. Sometimes these occur as unavoidable necessities, and we minimize their effects as far as possible by suitable electrical design. In other cases, their effects are the very thing we need for the proper functioning of new devices. Their further study will undoubtedly throw new light on our general understanding of microwave transmission phenomena.

Open Wire Lines*

GEORG GOUBAU†

Summary—**The properties of two-wire lines and single wire lines (surface wave transmission lines) are discussed on a comparative basis. The two-wire line is actually a system of two coupled single wire lines and thus requires a high degree of symmetry to maintain the desired wave mode. While the single wire line is more affected by bends it has the advantages that it is simpler in construction and is less susceptible to weather conditions. The main domain of the two-wire lines lies in the frequency range below 100 mc and that of the single wire line in the range above 100 mc.**

Fundamentals of Open Wire Lines

THE MAJOR representatives of open wire lines are the two-wire line (TWL) and the single wire line or Surface Wave Transmission Line (SWL). Multiwire lines, such as three phase lines, have seen very little application at radio frequencies and shall not be considered in this paper.

The TWL is historically the oldest waveguide. It was introduced by Lecher in 1890 and has been in use ever since. The SWL too goes back to the past century, in that Sommerfeld[1] in 1898 derived the field of a nonradiating wave which is guided by a single wire with finite conductivity. However a single wire had not been used as a waveguide until recently. Sommerfeld did not suggest that the wave he derived might have applications. He actually intended to show in his paper that the velocity of waves on wires is affected by the conductivity of the wires, since Hertz had concluded from his experiments that the velocity is the same as in free space. Sommerfeld considered a cylindrical field on a single wire for simplicity reasons and suggested methods for the treatment of the "actual case" of a two-wire line.

Harms[2] in 1907 extended Sommerfeld's theory to an insulated wire in order to explain the fact that the resonance wavelength of an antenna made of insulated wire is greater than in the case of a plain wire. None of the early publications differentiated between truly guided waves (surface waves) and partially guided or radiating waves, as the waves may be called which are predominantly present on long wire antennas.

When the more rigorous theories on linear antennas were developed by Hallén, King, Schelkunoff, and others, these theories did not yield the Sommerfeld wave. Experiments too showed no evidence of a surface wave. A wire coupled to a power source in the usual manner does not behave like a waveguide since it radiates the energy into space. For these reasons it was frequently believed that surface waves on single wires are nonexistent. Now we know that both types of waves, the radiating and the nonradiating waves exist simultaneously. They are independent solutions of Maxwell's equations satisfying the boundary conditions on the wire and the mutual orthogonality relations:[3]

$$\int_S (E_s \times H_r) n dS = \int_S (E_r \times H_s) n dS = 0$$

where E_s, H_s and E_r, H_r denote the field vectors of the surface wave and the radiating wave respectively; n, the unit vector in the direction of the axis of the wire; and S, the surface of an infinitely extended plane perpendicular to the wire. It is the kind of excitation which determines whether the one or the other wave type is predominant. If the wire is excited by a concentrated source, for instance, by means of a little coil which is inserted into the wire and coupled to a transmitter, only the radiating wave is observed. In order to excite predominantly the surface wave, a special launching device must be used which preshapes a field to match the field distribution of the surface wave. Usually the launching is done with horns, as shown in Fig. 1.[4,5]

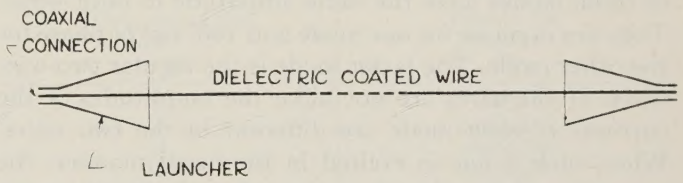

Fig. 1—Sketch of a surface wave transmission line.

In addition, the wire is covered with a dielectric layer which concentrates the field of the surface wave closer to the wire. This not only simplifies the excitation of the surface wave but also makes the wave less susceptible to objects in the proximity of the line. Corrugating the surface of the wire has a similar effect but is not practical for long lines. No special surface treatment is necessary at millimeter waves because the normal conductivity and the oxide layer which forms on the wire cause sufficient concentration of the field at these very high frequencies.

* Manuscript received by the PGMTT, July 17, 1956. Invited paper presented before the Panel on Guided Microwave Transmissions at the National Symposium on Microwave Techniques, Philadelphia, Pa., February 2–3, 1956.

† Signal Corps Engrg. Labs., Fort Monmouth, N. J.

[1] A. Sommerfeld, "Fortpflanzung elektrodynamischer Wellen an einem zylindrischen Leiter," *Ann. Phys. Chem.*, vol. 67, p. 233–290; March, 1899.

[2] F. Harms, "Elektromagnetische Wellen an einem Draht mit isolierender Hülle," *Ann. Phys.*, vol. 23, p. 44–60; January, 1907.

[3] G. Goubau, "On the excitation of surface waves," Proc. IRE, vol. 40, pp. 865–868; July, 1952.

[4] G. Goubau, "Surface waves and their application to transmission lines," *J. Appl. Phys.*, vol. 21, p. 1119–1128; November, 1950.

[5] G. Goubau, "Single-conductor surface-wave transmission lines," Proc. IRE, vol. 39, pp. 619–624; June, 1951.

The concentration of the field is associated with a reduction in phase velocity. However the reduced phase velocity is not a general requirement for surface waves. Barlow, Cullen, and Karbowiak[6,7] demonstrated recently that a dielectric rod with losses is able to guide a wave with a phase velocity greater than that of light. This is of particular interest as this wave is the cylindrical analog to the Zenneck wave, the reality of which has been the subject of many vigorous discussions. The Zenneck wave is guided by the interface between a nonconducting and a conducting dielectric and was introduced by Zenneck[8] in 1906 in a first attempt to explain the fundamental phenomena of wave propagation along the earth. One of the objections against the Zenneck wave was that its phase velocity is greater than that of light.

Returning to the TWL, the field on this line is not quite as simple as it is usually presented in text books. The standard derivation of the field from Maxwell's equations disregards the conductivity losses. The result is then a TEM wave which propagates with the velocity of light. The currents in the two wires are alike in amplitude, but 180° out of phase, whether the cross sections of the wires are the same or different. The finite conductivity is usually introduced as a perturbation whereby the assumption is made, that the cross-sectional field distribution is not substantially affected by the conductivity. This procedure, however, gives only the correct result, when the two wires are identical. Actually the TWL is a system of two coupled SWL's, and as such has two coupling modes with different phase velocities. If the wires are alike, the currents associated with each of these modes have the same amplitude in both wires. They are in phase for one mode and 180° out of phase for the other mode. The latter mode is the regular two-wire wave. If the wires are not alike the amplitudes of the currents of each mode are different in the two wires. When such a line is excited in the usual manner, the currents in both wires have the same amplitude at the input terminals. However since none of the two coupling modes has equal currents in both wires, the two modes are excited simultaneously. As they propagate with different phase velocities, the ratio between the resulting currents in both wires varies along the line. This effect is more pronounced with increasing frequency. Apparently a TWL with bare wires of different conductors has not been treated in the literature. The behavior of such a line must be essentially the same as in the case of coupled dielectric coated wires of different dimensions, a case which has been first investigated by Meyerhoff.[9]

In the following we consider only TWL's with identical conductors. The fact that the ordinary two-wire mode with equal currents in the two wires requires identical wires indicates that the mode is not stable, in that the wave splits into two waves if the dimensions of the wires vary somewhat along the line. This effect is usually of no importance, except in the microwave range. There, the normally present oxide layers on the wire have a considerable effect on the phase velocity, and if these layers vary along the line, the instability may become quite noticeable.

The TWL requires in general no launching devices. If the excitation of the line is symmetrical, the radiating fields of the currents in the two wires compensate each other to a large extent, provided the spacing d between the wires is very small compared to the wave length λ. However, since the spacing cannot be reduced arbitrarily without greatly increasing the conductivity loss, the condition $d/\lambda \ll 1$ is not satisfied at microwave frequencies. A microwave TWL therefore should also have a launching device if the efficiency of excitation is of importance. Apparently not much attention has been given to this problem. Fig. 2 shows a proposed device for the excitation of a two-wire line from a rectangular waveguide with TE_{10} excitation.[10] The drawings are self-explanatory. Presumably the efficiency of these launchers is not very good because a considerable fraction of the energy of the TE wave will escape where the side walls of the guide are cut away.

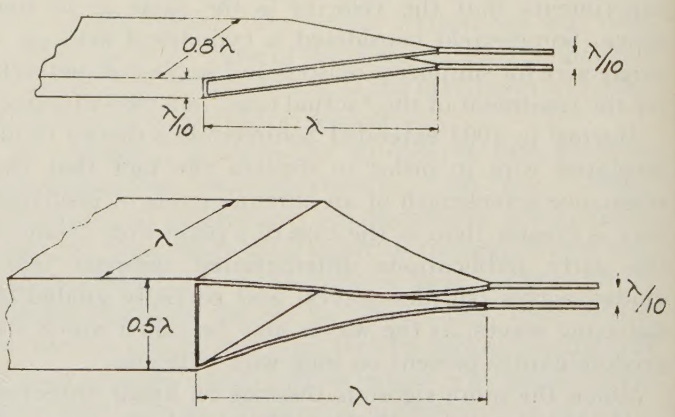

Fig. 2—Excitation of a two-wire line from a waveguide.[10]

Properties of Two-Wire and Single-Wire Lines

In the following the properties of the TWL and the SWL are discussed on a comparative basis. Data on

[6] H. E. M. Barlow and A. L. Cullen, "Surface waves," *Proc. IEE* (London), part III, vol. 100, p. 329–347; November, 1953.

[7] H. E. M. Barlow and A. E. Karbowiak, "An experimental investigation of axial cylindrical surface waves supported by capacitive surfaces," *Proc. IEE* (London), part III, vol. 102, p. 313–321; May, 1955.

[8] J. Zenneck, "Uber die fortpflanzung elektrodynamischer Wellen Langs eines Drahtes," *Ann. Phys. Chem.*, vol. 23, p. 846–866; September, 1907.

[9] A. A. Meyerhoff, "Interaction between surface wave transmission lines," Proc. IRE, vol. 40, pp. 1061–1068; September, 1952.

[10] French Patent Gr. 12-cl.6.#891,442.

single wire lines given during the panel discussion have been omitted since they will be published in a separate paper.[11]

Field Extension

The cross-sectional field of a two-wire wave on a TWL with bare conductors decreases, within a range of several wavelengths, with the square of the distance D from the line. At very large distances the decrease becomes exponential, due to the finite conductivity of the wires. The field of the wave on a SWL with dielectric coated conductor decreases first only with $1/D$, but approaches the exponential decrease much sooner. Therefore, assuming equal transmitted power, the field around a SWL is larger than that around an ordinary TWL if small distances are considered. However it is smaller around the SWL if the distances considered are several wavelengths. If a SWL of common design is compared with a TWL (with bare conductors) of equal loss per unit length, the field of the TWL exceeds that of the SWL in general at distances greater than 2 wavelengths. The SWL is more sensitive than the TWL to obstacles at a distance of less than 2 wavelengths. This fact restricts the applicability of SWL's to higher frequencies, say frequencies above 50 mc. Any line-supporting structures such as telephone poles must be kept farther away from the line than in the case of a TWL.[11]

Discontinuities

Bends: A bend in any open waveguide causes a certain amount of radiation loss. In the case of a TWL the radiation loss is small at low frequencies because the radiation field of the individual bends in the two wires compensate each other if $d/\lambda \ll 1$. The discontinuity produces primarily a reactive distortion which can be represented by an equivalent circuit shown in Fig. 3.[12] In

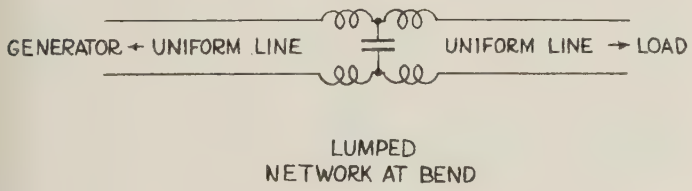

Fig. 3—Equivalent circuit for a bent two-wire line.[12]

the microwave range the radiation loss may become large particularly if the bends in the two wires are not identical or if d approaches or exceeds $\lambda/4$. In the case of the SWL with dielectric coated wire the radiation loss of bends is appreciable at all frequencies. It depends mainly on the ratio between outer and inner diameter (conductor diameter) and is only slightly dependent on the frequency.[11] The reactive distortion is usually negligible. The loss of bends in SWL's can be considerably reduced by appropriate supporting methods. One method which is mainly applicable within the uhf range is discussed in a separate paper.[11] Another method particularly adapted for 90° turns in microwave SWL's has been described by Chavance and Chiron.[13] The wire is laid around a dielectric pulley as shown in

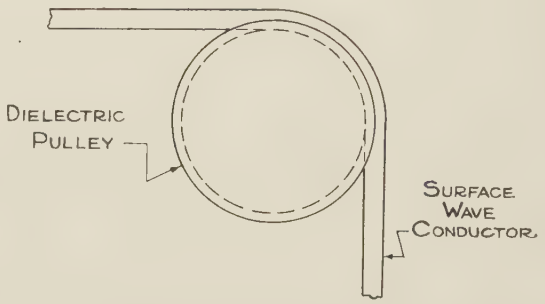

Fig. 4—Loss reducing support of a surface wave transmission line at a 90° bend.[13]

Fig. 4. By proper dimensioning of the pulley the loss of the bend can be made very small. The following table quotes results obtained by Chavance and Chiron at a frequency of 3150 mc with a polyethylene coated wire of 5 mm outer diameter and 2.5 mm inner diameter. The pulleys were made of polystyrol and had a diameter of 20 cm. The thickness of the pulleys was varied.

Thickness of the pulley in mm	Loss of the bend in db
5	0.2
8.5	negligible
10	negligible
15.5	negligible
31.5	0.8

Sag: Both the TWL and the SWL are insensitive to sag. However, the bends produced by the sag at the supporting points of long SWL's cause some loss. Results of loss measurements on SWL's requiring supports are given in the above mentioned separate paper.[11]

Spacers and Supports of TWL's: The TWL requires dielectric spacers. They constitute, as well as the support, discontinuities, and cause partial reflection and to some extent radiation. Part of this radiation is caused by the polarization currents induced in the dielectric material of the spacers. At low frequencies the effect of such discontinuities is mainly capacitive reactive and

[11] G. Goubau and C. E. Sharp, "Investigation with a model surface wave transmission line," submitted in February, 1956 for publication in IRE TRANSACTIONS.

[12] K. Tomiyasu, "The effect of a bend on a two-wire transmission line," Cruft Lab. Tech. Rep. No. 74, part II.

[13] P. Charance and B. Chiron, "Une étude éxperimentale de transmission d'ondes centimétrigues sur guides d'ondes filiformes," *Ann. des Télécommun.*, vol. 8, p. 367–378; November, 1953.

can be compensated, for instance, by inserting small inductances in series with the line. The effects of the spacers are severe at microwave frequencies. The discontinuities can be avoided by embedding the wires in a Polyethylene tape or tubing (twin-leads). Such lines, however, are more susceptible to weather conditions.

Supports of SWL's: The most simple method of supporting long SWL's is by means of slings of nylon cord. The loss caused by such cords is negligibly small. Experimental data are given in the above quoted paper.[11]

Weather Effects

The SWL with dielectric coat is much less sensitive to weather effects than the TWL (at the same frequencies) for several reasons. The dielectric layer of the SWL prevents rain, snow, or ice from reaching the region of highest field concentration. This is at least the case if the thickness of the dielectric layer is in the order of the wire radius. Such layer thicknesses are required for lines used in the uhf range. A TWL becomes unbalanced if the deposits of rain drops, snow, or ice are not equal on both wires. Expecially sensitive to weather effects are the twin-leads since a large area of highly concentrated field is exposed to the precipitation.

The SWL is surprisingly insensitive to weather effects. At frequencies below 500 mc the loss caused by rain or dry snow is hardly measurable and of no practical consequence even if lines of several miles length are considered. Ice as it forms under freezing rain conditions also causes no severe increase in loss. Up to now no data are available on loss measurements made during very heavy ice formation. The effect of weather conditions increases rapidly with frequency. At 2000 mc, for instance, an increase in loss during rain may be measured which exceeds 5 db per 100 feet for horizontally stretched lines. This increase is caused primarily by the drops adhering to the wire. These drops act as little radiating dipoles. If the line is used as an antenna feed and inclined against the ground the number of adhering drops is reduced and the loss due to rain is less than 1 db/100 feet. Preliminary measurements at 5000 mc indicate a loss increase of inclined lines of about 5 db/100 feet. Electric heating of the wire reduces the effect of rain considerably, presumably because the adhesion of the drops to the wire is reduced. An efficient remedy against the effect of rain in the upper microwave frequency range would be to remove the drops mechanically by shaking the line. However, the question is whether such a method is practical. The formation of ice has serious effects in the microwave range and must be prevented by electric heating.

Power Carrying Capacity

The cw-power-carrying capacity of the SWL is primarily determined by the heat breakdown of the dielectric layer and is smaller at low frequencies than that of a TWL. The peak-power carrying capacity (in the case of pulse modulation) however, is considerably greater. It is also high in comparison to that of closed waveguides. Fig. 5 shows the power-carrying capacity of a SWL at 3000 mc for a bare wire and a wire with a thin dielectric coat.[14]

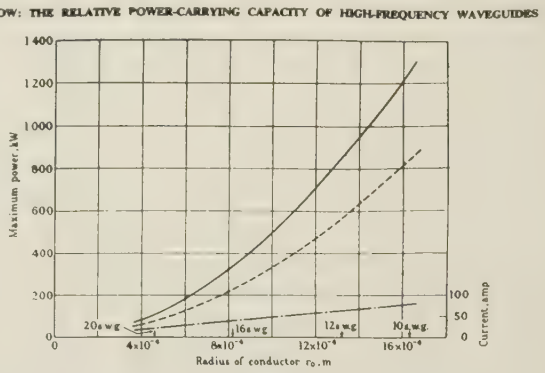

Fig. 5—Maximum power-carrying capacity of surface wave at 3000 mc supported by copper wires of various sizes.[14]
——— perfectly smooth surface.
– – – surface with enhanced reactance (radial decay factor ten times that of smooth surface).
–·–·– current corresponding to maximum power. (Reproduced from *Proc. IEE.*)

Conclusion

Compared to closed waveguides the open wire lines have advantages as well as disadvantages. They require little material, are inexpensive, easy to install, and have high power-carrying capacity. Their disadvantages are founded in the fact that they are open waveguides and as such are susceptible to weather conditions. The main domain of the TWL's lies in the frequency range below 100 mc and that of the SWL's in the frequency range above 100 mc. The applications of the two-wire line are well known. The SWL, as a newer device, has not yet seen a widespread application. However, it is successfully in use for antenna feeds in radio relay equipment[15] and recently has been applied also to long distance transmission in a community tv system.[16]

[14] H. M. Barlow, "The relative power-carrying capacity of high-frequency waveguides," *Proc. IEE* (London), part III, vol. 99, p. 21–27; January, 1952.
[15] C. E. Sharp and G. Goubau, "A uhf surface wave transmission line," Proc. IRE, vol. 41, pp. 107–109; January, 1953.
[16] A. S. Taylor and B. Hamilton, "Community television systems," presented at 1956 Seventh Region Technical Conference and Trade Show, Salt Lake City, Utah, April 13, 1956.

Rectangular and Ridge Waveguide*

TORE N. ANDERSON†

Summary—This paper describes the present state of the art with respect to rectangular ridge waveguide giving tables and data from standard waveguide sizes and constructional techniques for both rigid and flexible waveguide. The problems inherent in waveguide connectors are discussed along with the various methods for producing waveguide assemblies.

The problems inherent with present-day waveguide standardization are also discussed. It is essential that a series of standard waveguide for high pressure operation and for extremely broad-band operation (ridgeguide) be standardized.

The latest RETMA miniature standard flanges are shown along with present-day thinking on a series of pressurized contact flanges.

Introduction

SINCE THE title "Rectangular and Ridge Waveguide" is not technically correct according to the recently published IRE standards for waveguides, the proper definition is included here for clarification. This paper deals with the subject of "uni-conductor rectangular waveguides and ridged uni-conductor rectangular waveguides operating in the fundamental transverse electric (TE_{10}) mode" as defined by the IRE. However, by popular usage, "rectangular and ridged waveguide" are terms that will probably continue to be used for many years to come.

The field of rectangular waveguide is the one in which more work has been done from both the theoretical and practical point of view. Ridged waveguide has only begun to be important as a microwave transmission line for a number of specialized applications.

The history of rectangular waveguide, as far as we know, dates back only about 20 years for practical applications, although a number of early workers in electromagnetism discussed the possibility of propagating energy through hollow pipes. It was the work of G. E. Southworth, A. E. Bowen, A. P. King, A. J. Schelkunoff, and W. L. Barrow that resulted in practical use of rectangular waveguide. Despite the relative newness of the field, the basic mathematical relations describing waveguide propagation were set down by James Clerk Maxwell more than 83 years ago.

For a complete history of waveguides, the reader is referred to Dr. Southworth's book, "Principles and Applications of Waveguide Transmission." Dr. Southworth's historical description is probably the best written history of waveguides that can be found, and made all the more interesting since, as a graduate student at Yale, Southworth first noticed a peculiar behavior of electric waves propagated on a pair of wires in a trough of water. He went on later to investigate this phenomenon and this was the beginning of the practical application of waveguides.

* Manuscript received by the PGMTT, July 17, 1956. Invited paper presented before the Panel on Guided Microwave Transmissions at the IRE National Symposium on Microwave Techniques, Benjamin Franklin Center for Physical Sciences, University of Pennsylvania, Philadelphia, Pa., February 2, 1956.

† Airtron, Inc., Linden, N. J.

Rectangular Waveguides

Theory of Operation

The theory of operation of rectangular waveguides has been covered in a number of published works and will not be repeated here. Instead, a short review of the results and their practical considerations will be given.

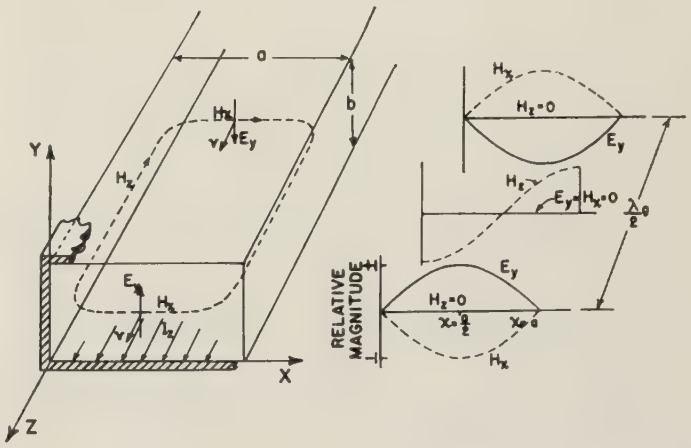

Fig. 1.

Fig. 1 shows in outline form the electric and magnetic fields which are present in a half-wavelength section of waveguide of dimensions a and b for the fundamental (TE_{10}) mode. The waveguide behaves as a high pass filter, with the cutoff wavelength and frequency given below:

$$\lambda c = 2a \text{ (for air dielectric waveguide)} \tag{1a}$$

$$fc = \frac{C}{\lambda c} = \frac{3 \times 10^{10}}{2a} \tag{1b}$$

where a and λc are in cm and fc is in cps.

For this mode of propagation, E_x, E_z, and H_y all equal zero. The electric field vector E_y reaches a maximum at the middle of the broad wall, which is an important point to keep in mind when designing waveguide components for operation at very high peak power levels. As there are no transverse currents flowing in the narrow walls of the waveguide, a vertical gap can exist without disturbing the field configuration. Conversely, there is no longitudinal component of current along the center line of the broad wall, thereby making it possible to slot the broad wall at this point without disturbing the fields.

As one goes higher in frequency, the first higher order mode is encountered, the TE_{20} mode, for which the following relations hold:

$$\lambda c_{20} = a \tag{2a}$$

$$fc_{20} = \frac{C}{\lambda c_{20}} = \frac{3 \times 10^{10}}{a}. \tag{2b}$$

It is between the TE_{10} and TE_{20} cutoff frequencies that most of the work in rectangular waveguide is done; however, in some extremely broad band applications, very broad or flat waveguide is used where the aspect ratio (a/b) is considerably larger than 2 to 1. In this case, operation may be in a frequency range which will allow the existence of the TE_{20} mode. This procedure is generally dangerous in that higher order mode resonances and mismatches may result, although techniques can be adopted to minimize these effects. However, as a general rule, it is advisable to operate only between the extremes of TE_{10} and TE_{20} cutoff.

The choice of dimensions for a waveguide involves several other considerations. The most important of these are attenuation and voltage breakdown. As TE_{10} cutoff is approached, the attenuation of a given waveguide increases quite rapidly, and the power handling capacity also decreases. Therefore, it is considered good practice to operate at frequencies no lower than 10 per cent above TE_{10} cutoff and up to a point of approximately 5 per cent below TE_{20} cutoff. Another consideration in choice of operating frequency for a given size waveguide is the rate of change of guide wavelength as a function of frequency. Guide wavelength for any mode is given by

$$\lambda g = \frac{\lambda_0}{\sqrt{1 - \left(\frac{\lambda_0}{\lambda c}\right)^2}} \tag{3}$$

where λ_0 = free space wavelength.

The attenuation of rectangular waveguide, neglecting dielectric losses, is given by

$$\alpha c = \frac{.00859}{a^{3/2}} \left[\frac{\frac{a}{2b}\left(\frac{2a}{\lambda_0}\right)^{3/2} + \left(\frac{2a}{\lambda_0}\right)^{-1/2}}{\sqrt{\left(\frac{2a}{\lambda_0}\right)^2 - 1}} \right] \text{db/meter.} \tag{4}$$

For minimum attenuation over the largest possible frequency range, the ratio of a/b should be exactly 2.0. Unfortunately, many of our standard waveguides were chosen from architectural tubing due to the wartime emergency, and therefore, these waveguides have aspect ratios which vary about the ideal figure of 2.0.

Table I is a tabulation of standard rectangular waveguide dimensions taken from the RETMA standard TR-108A. The numbering system employs the prefix WR (waveguide-rectangular) followed by a number giving the wide (a) dimension of the waveguide in one-hundredths of an inch. For example, WR-1500 measures 15.00 inches in the wide dimension. An original series of waveguide dimensions were chosen to meet the needs of the military in 1942, and these are now known as Series A, and remain military standard waveguides. To meet the needs for overlapping frequency ranges, a committee

TABLE I

DIMENSIONS, TOLERANCES, AND FREQUENCY RANGE FOR RIGID RECTANGULAR WAVEGUIDES

RMA+ Designation	Frequency Range (kmc/a) for Dominant (TE_{10}) Mode	Dimensions in Inches								Maximum Inner Radius
		Inner Dimensions			Outer Dimensions			Wall Thickness		
		A	B	Tolerance	C	D	Tolerance	Nominal	Deviation from Mean	
WR1500	0.47– 0.75	15.000	7.500	±0.015	15.250	7.750	±0.015	0.125	±0.015	3/64
WR1150	0.64– 0.96	11.500	5.750	±0.015	11.750	6.000	±0.015	0.125	±0.015	3/64
WR975	0.75– 1.12	9.750	4.875	±0.010	10.000	5.125	±0.010	0.125	±0.010	3/64
WR770	0.96– 1.45	7.700	3.850	±0.005	7.950	4.100	±0.005	0.125	±0.009	3/64
WR650	1.12– 1.70	6.500	3.250	±0.005	6.660	3.410	±0.005	0.080	±0.008	3/64
WR510	1.45– 2.20	5.100	2.550	±0.005	5.260	2.710	±0.005	0.080	±0.008	3/64
WR430	1.70– 2.60	4.300	2.150	±0.005	4.460	2.310	±0.005	0.080	±0.008	3/64
WR340	2.20– 3.30	3.400	1.700	±0.005	3.560	1.860	±0.005	0.080	±0.007	3/64
WR284	2.60– 3.95	2.840	1.340	±0.005	3.000	1.500	±0.005	0.080	±0.006	3/64
WR229	3.30– 4.90	2.290	1.145	±0.005	2.418	1.273	±0.005	0.064	±0.005	3/64
WR187	3.95– 5.85	1.872	0.872	±0.005	2.000	1.000	±0.005	0.064	±0.004	1/32
WR159	4.90– 7.05	1.590	0.795	±0.004	1.718	0.923	±0.004	0.064	±0.004	1/32
WR137	5.85 –8.20	1.372	0.622	±0.004	1.500	0.750	±0.004	0.064	±0.004	1/32
WR112	7.05– 10.00	1.122	0.497	±0.004	1.250	0.625	±0.004	0.064	±0.004	1/32
WR90	8.20–12.40	0.900	0.400	±0.003	1.000	0.500	±0.003	0.050	±0.004	1/32
WR75	10.00– 15.00	0.750	0.375	±0.003	0.850	0.475	±0.003	0.050	±0.004	1/32
WR62	12.4 –18.00	0.622	0.311	±0.003	0.702	0.391	±0.003	0.040	±0.003	1/64
WR51	15.00– 22.00	0.510	0.255	±0.0025	0.590	0.335	±0.003	0.040	±0.003	1/64
WR42	18.00–26.50	0.420	0.170	±0.0020	0.500	0.250	±0.003	0.040	±0.003	1/64
WR34	22.00– 33.00	0.340	0.170	±0.0020	0.420	0.250	±0.003	0.040	±0.003	1/64
WR28	26.50–40.00	0.280	0.140	±0.0015	0.360	0.220	±0.002	0.040	±0.002	1/64
WR22	33.00– 50.00	0.224	0.112	±0.0010	0.304	0.192	±0.002	0.040	±0.002	0.010
WR19	40.00–60.00	0.188	0.094	±0.0010	0.268	0.174	±0.002	0.040	±0.002	0.010
WR15	50.00– 75.00	0.148	0.074	±0.0010	0.228	0.154	±0.002	0.040	±0.002	0.008
WR12	60.00–90.00	0.122	0.061	±0.0005	0.202	0.141	±0.002	0.040	±0.002	0.006
WR10	75.00–110.00	0.100	0.050	±0.0005	0.180	0.130	±0.002	0.040	±0.002	0.006

on waveguides of the Radio Manufacturers Association (RMA), which is now active as the SQ-11.1 committee of the RETMA on waveguides and fittings, adopted a series known as Series B which provided an overlapping frequency range. The Series B waveguides can be identified from Table I by the right hand column of frequency ranges in the second column of the figure.

The power than can be handled by a rectangular waveguide operating in the TE_{10} mode is given by

$$P = 756ab\sqrt{1 - \left(\frac{\lambda_0}{2a}\right)^2} \text{ kilowatts.} \quad (5)$$

Mechanical Tolerances

Sudden changes in the internal dimensions of the waveguide, or differences in dimensions at the junction of two waveguides, may lead to objectionable reflections. These imperfections may be likened to sudden changes in characteristic impedance, and for the case of two similar waveguides with slightly different dimensions, the mismatch at the junction is given approximately by

$$r = \frac{Z_1}{Z_0} = \frac{a_0 b_1}{a_1 b_0} \text{ (neglecting frequency sensitive terms)} \quad (6)$$

where r = vswr, and a_1, b_1, a_0, b_0 = cross sectional dimensions of waveguides.

This equation, although not completely rigorous, is accurate enough for small mismatches and yields results sufficiently good for engineering purposes to establish practical tolerances. From this general consideration, it appears that satisfactory waveguide can be fabricated from sheet metal for the larger rectangular waveguide sizes. For the shorter wavelengths (12 cm to 1 cm), standard drawn seamless tubing is satisfactory for most applications. For wavelengths less than 1 cm, special techniques are required to obtain the necessary accuracy. Table I gives the standard tolerances which have been adopted by the RETMA. However, these tolerances are far from satisfactory for the most precise of applications, and are probably too loose for economical manufacture of precision waveguide components and assemblies. For these applications, special redrawn or broached waveguide tubing should be used. Tolerances held to a third of those specified in Table I are required for many applications and the engineers designing these components should carefully review the application for best results.

Materials

Since attentuation is not usually serious for the larger sizes of waveguide, the materials are dictated by mechanical considerations such as weight, rigidity, pressurization, etc. At the higher frequencies, however, attenuation may not be ignored and silver and copper waveguides are required. Since the attenuation losses are confined to an extremely thin layer of metal at microwave frequencies, laminated or bimetallic structures are fairly common. At the lowest waveguide frequency, neither corrosion nor minor variations in the surface of the waveguide structure appear to affect attenuation, but both are of importance at the higher frequencies. At frequencies above 9.0 kmc the attenuation is generally somewhat higher than calculated from direct current conductivity considerations. It is presumed that the differential is a result of surface imperfections in the waveguide. At the lower frequencies, thin films of low loss, low dielectric constant, dielectric materials are used occasionally as a protective finish without affecting attenuation seriously.

Constructional Techniques

In the larger waveguide sizes, WR-1500 to WR-975, sheet metal fabrication techniques are generally used with both copper-clad steel and aluminum waveguides finding popular acceptance. These are generally formed in two halves with a riveted or molded seam along the middle of the broad wall. In the middle range of waveguide sizes, WR-650 to WR-28, seamless rectangular waveguide tubes are obtained by metal drawing techniques. In the millimeter wavelength region, because of the extremely close tolerances that are required, sections are generally electroformed around hard steel mandrels which are subsequently removed. Fig. 2 illustrates the waveguide cross sections discussed.

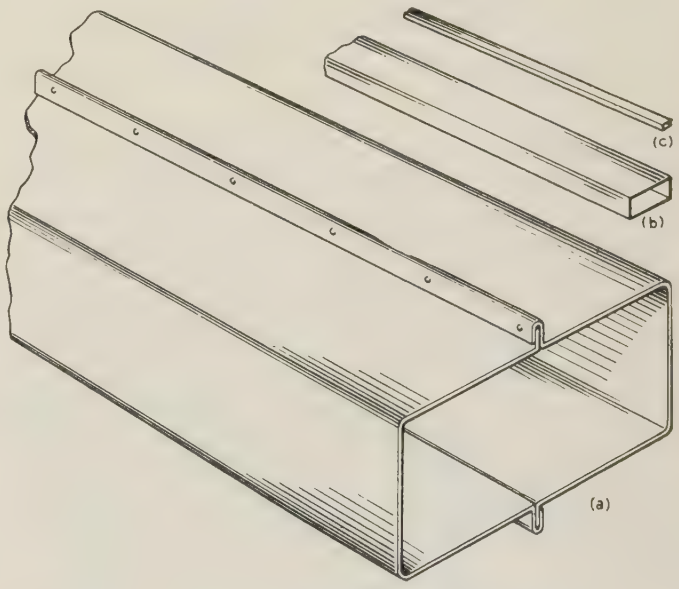

Fig. 2.

Waveguide Connectors

A considerable number of waveguide connector designs have evolved over the years; however, they can be roughly classified into two types, namely choke connectors (noncontacting) and contact flanges. Because of the large size of a choke design at the lower frequencies, chokes have become obsolete for frequencies below 2600 mc/sec. They are, however, in popular use for frequencies from 2600 mc/sec up to 40,000 mc/sec. The standard nominal dimensions for chokes covering this frequency range are shown in Table II.

TABLE II

NEW BROADBAND CHOKE DIMENSIONS AS PER APRIL, 1950

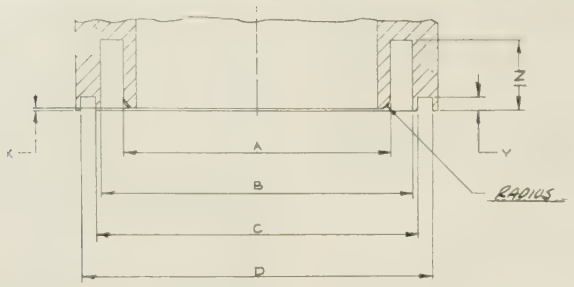

Size id	Size od	A	Tol.	B	Tol.	C	Tol.	D	Tol.
2.840×1.340	3.000×1.500	3.320	±0.005	3.880	±0.005	4.000	±0.005	4.450	±0.005
1.872×0.782	2.000×1.000	2.190	±0.003	2.556	±0.003	2.690	±0.005	2.949	±0.005
1.372×0.622	1.500×0.750	1.598	±0.003	1.860	±0.003	2.125	±0.003	2.429	±0.005
1.122×0.497	1.250×0.625	1.270	±0.003	1.495	±0.003	1.561	±0.003	1.765	±0.005
0.900×0.400	1.000×0.500	1.015	±0.002	1.225	±0.002	1.340	±0.003	1.540	±0.005
0.622×0.311	0.702×0.391	0.710	±0.002	0.828	±0.002	0.875	±0.003	1.195	±0.005

Size id	Size od	X	Tol.	Y	Tol.	Z	Tol.	Radius	Mates with Cover Flange	ANRFCCC Dwg. No.*
2.840×1.340	3.000×1.500	0.036	±0.001	0.165	±0.005	0.860	±0.005	0.090 R	UG-214/U	RE 49 F 334
1.872×1.782	3.000×1.000	0.025	±0.001	0.088	±0.003	0.570	±0.003	0.060 R	UG-149A/U	RE 49 F 279
1.372×0.622	1.500×0.750	0.017	±0.001 −0.000	0.108	±0.002	0.405	±0.003	0.040 R	UG-344/U	RE 49 F 456
1.122×0.497	1.250×0.625	0.015	±0.001	0.069	±0.002	0.345	±0.003	0.030 R	UG-51/U	RE 49 F 203
0.900×0.400	1.000×0.500	0.0115	+0.0010 −0.0000	0.073	±0.002	0.265	±0.003	0.020 R	UG-39/U	RE 49 F 197
0.622×0.311	0.702×0.391	0.0075	+0.0010 −0.0000	0.105	±0.002	0.190	±0.003	0.016 R	UG-419/U	RE 49 F 497

* For cover flange.

Choke-cover flange combinations have the advantage of being relatively simple to assemble, but since the flange faces do not make contact at the waveguide itself, mismatch contributions as large as 1.02 may be introduced by their use. At the present time, standard military drawings on choke-cover flange combinations suffer from several defects: 1) the dimensioning and tolerances allowed are not entirely correct; 2) the O-ring gasket groove is not properly designed, which is evidenced by a large number of O-ring failures. At the present time, RETMA committee SQ-11.1.1 is in the midst of preparing a joint comment on military waveguide flanges in an effort to clean up these dimensional problems.

Many contact flange designs have been evolved, their design having been dictated mainly by mechanical considerations. To effect a measure of standardization, the SQ-11.1.1 committee initiated a program several years ago to standardize on a series of miniature, unpressurized, contact flanges for use in complex waveguide assemblies as a means for connecting subassemblies internally. This procedure would allow for greatly simplified production and maintenance. The committee reviewed all of the various contact flange designs in existence, and decided on the outline shown in Fig. 3 and Table III (opposite). It is expected that this flange design will become an official RETMA standard by the end of 1956. This flange design does not use alignment pins, metal contacting fingers, or special gasketing. It has been found that a carefully machined surface of 63 microinches or better will yield excellent electrical results over the frequency range of 2.6 to 12.0 kmc and is economical to produce. By mounting the screws close to the waveguide and paying particular attention to the contact between the broad dimensions of the waveguides, a simple and economical waveguide connector design which yields a high order of performance has been obtained. Calculations and measurements have indicated that the mismatch contributions from a pair of properly mated contact flanges should be within 1.003 with the tolerances as specified. Predrilled flange blanks cannot be used due to the waveguide tolerances; therefore, the assembly procedure involves mounting a blank flange to the waveguide tubing by brazing or casting and then drilling after assembly. These flanges are asexual clearance, or tapped depending upon the particular mechanical requirements of the waveguide assembly, with one drill jig accomplishing all these operations. The design of this series of unpressurized contact flanges was done principally by A. F. Pomeroy of the Bell Telephone Laboratories.

To meet the needs for a pressurized version of the miniature contact flange, the SQ-11.1.1 committee has begun a program for the development and standardiza-

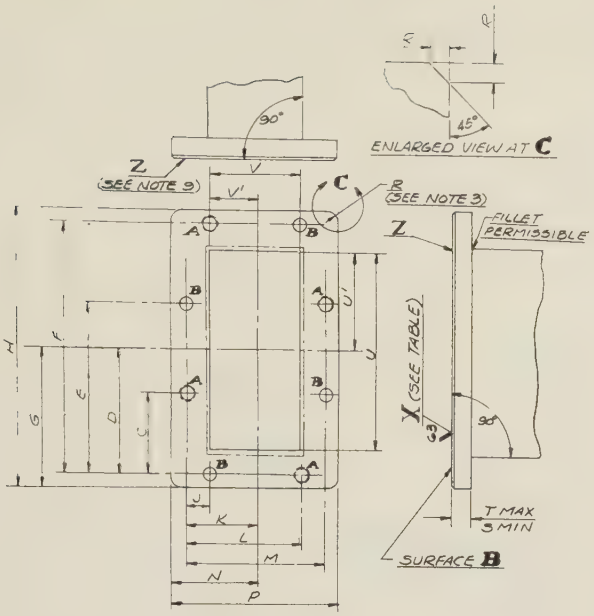

(a)

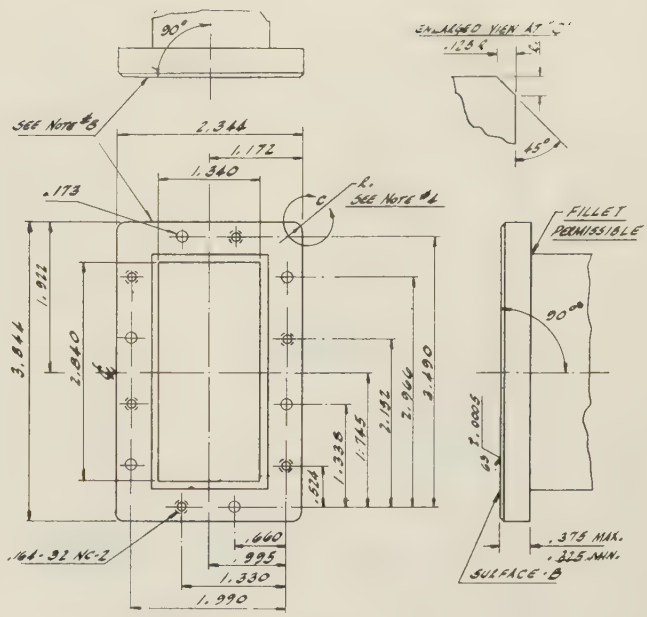

(b)

(a)—Notes:

1) After soldering and before machining holes, inside dim. of tubing at the flange shall be made to agree to dims. and tolerances shown as U and V and as per TR_{-108}. For centering tolerance of U' and V' see Y.
2) Surface B shall not exceed 63 rms microinches per ASA B_{46} surface roughness standard. X pertains to the whole flange face including end of waveguide.
3) R corner radius may be replaced by chamfer as shown at C.
4) Decimal tolerance ± 0.004 except where otherwise noted.
5) NC_{-2} tap refers to class 2 fit as specified in American Standard B-1.1.
6) Angular tolerance $\pm \frac{1}{2}°$.
7) Y tolerance on waveguide inner dimension per RETMA TR-108-A.
8) Break edge or slightly countersink all holes on mating surface.
9) Deburr edges Z.

b)—Notes:

1) The inside dimensions of the waveguide tubing U and V at the flange shall be made to agree to the dimensions and tolerances of waveguide tubing as per RETMA standard TR-108-A.
2) Tolerance on waveguide inner dimensions U and V as per RETMA TR-108-A.
3) Surface B shall not exceed 63 microinches per ASA, B46 surface roughness standard. X pertains to the flatness of the whole flange face including end of waveguide.
4) R corner radius may be replaced by chamfer as shown at C. Tolerance $\pm 1/64$.
5) Decimal tolerance ± 0.004 except where otherwise noted.
6) UNC-2B fit shall be as specified in American Standard ASA B.1.1.
7) Break edge or slightly countersink all holes on mating surface.
8) Deburr outside edges.
9) Refers to waveguide opening.
10) Angular tolerance $\pm 1/4°$.

Fig. 3—(a) Miniature, unpressurized contact flanges, RETMA for WR 229 to WR 90.
(b) Miniature, unpressurized contact flange WR 284, 12 hole.

TABLE III
DIMENSIONS FOR MINIATURE, UNPRESSURIZED CONTACT FLANGES**

WR	229	187	159	137	112	90	WR
A	0.138–32 NC-2 Tap (See Note 5)						
B	0.147	0.147	0.147	0.147	0.147	0.147	*B*
C	0.922	0.810	0.699	0.643	0.553	0.470	*C*
D	1.422	1.215	1.061	0.965	0.830	0.705	*D*
E	1.922	1.620	1.423	1.287	1.107	0.940	*E*
F	2.844	2.430	2.122	1.930	1.660	1.410	*F*
*G	1 37/64	1.392	1 1/4	1.142	1.007	0.882	*G*
*H	3 5/32	2.784	2 1/2	2.284	2.014	1.764	*H*
J	0.438	0.247	0.184	0.247	0.237	0.230	*J*
K	0.844	0.715	0.663	0.590	0.571	0.455	*K*
L	1.250	1.183	1.142	0.933	0.797	0.680	*L*
M	1.688	1.430	1.326	1.180	1.034	0.910	*M*
*N	1	0.892	7/8	0.767	0.694	0.632	*N*
*P	2	1.784	1 3/4	1.534	1.388	1.264	*P*
*R	1/8	0.125	1/8	0.125	0.065	0.065	*R*
S	0.200	0.200	0.200	0.200	0.200**	0.200**	*S*
T	0.250	0.250	0.250	0.250	0.250**	0.250**	*T*
U	2.290	1.872	1.590	1.372	1.122	0.900	*U*
V ***	1.145	0.872	0.795	0.622	0.497	0.400	*V*
U'	1.145	0.936	0.795	0.686	0.561	0.480	*U'*
V'	0.5725	0.436	0.3975	0.311	0.2485	0.200	*V'*
X	0.0005	0.0005	0.0002	0.0002	0.0002	0.0002	*X*
Y	0.005	0.005	0.004	0.004	0.004	0.003	*Y*

* Indicates a tolerance of ± 0.018.
** Aluminum and other than light alloy material for brass flanges dimensions S 0.145 dimension T 0.188.
*** For tol. see "Y," note 7.

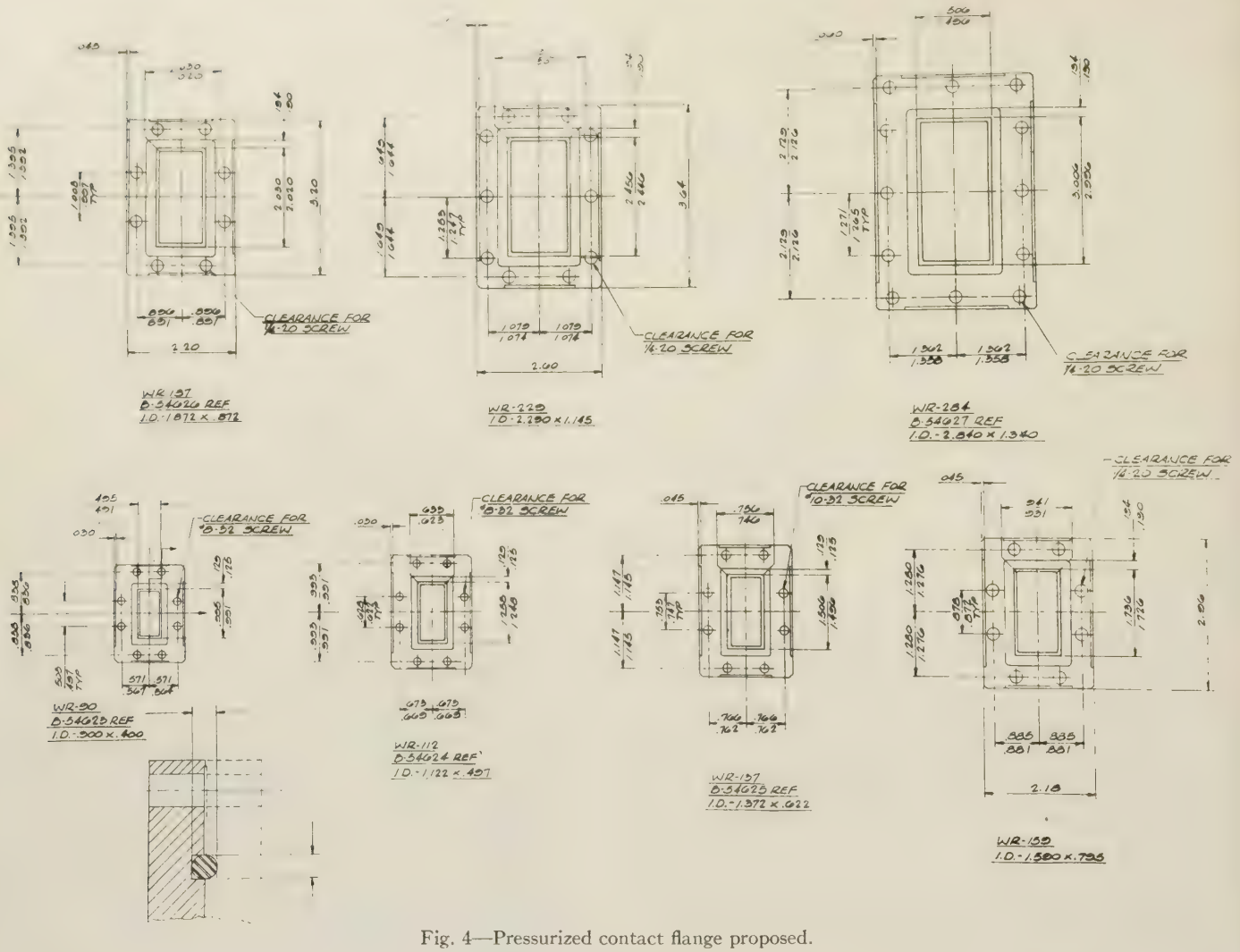

Fig. 4—Pressurized contact flange proposed.

tion of an asexual pressurizable contact flange. Fig. 4 shows a proposed design for such a flange. Because of mechanical problems, it was felt that it would be better to use through clearance holes and nuts and bolts to make the connection. Half of the gasket groove (in depth) is machined into each flange, thereby preserving the asexual characteristic. It is hoped that a standardized version of the pressurizable miniature contact flange will be arrived at within a year or two, since the waveguide designer faces a difficult problem in choosing the right flange design from the large number in existence. In the larger sizes of waveguide, contact flanges, both pressurized and unpressurized, are in use; however, the standardization here is far from complete.

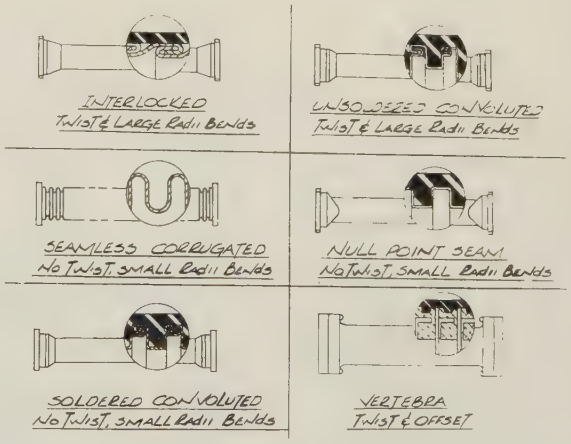

Fig. 5—Flexible waveguide types.

Flexible Waveguide

Flexible waveguide is essentially a rectangular corrugated metal hose assembly which provides for motional joints and tolerance build-up. The basic types of flexible waveguide are as follows: 1) soldered and unsoldered convoluted; 2) seamless split construction (single seam along each of the narrow edges of the waveguide); 3) interlock; 4) null point seam; and 5) vertebra. Fig. 5 illustrates the basic features of each type. With the exception of the interlock, all of the types listed above rely upon the mechanical flexure of the convolutions for motion. The interlock construction depends on the slipping of the joints to provide mechanical motion. Considerable development work has been done on flexible waveguide by several firms, and at the present state of the art, no real penalty is involved in using flexible waveguide. In fact, flexible waveguide which has a peak power capacity in excess of standard rigid waveguide and mates directly with the standard rigid

TABLE IV

Moderate Bandwidth Double Ridge Waveguide

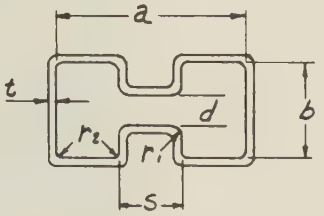

Ridge Guide (Airtron No's)	Frequency Range		Dimensions							Attenuation db/ft Midband Aluminum	Peak Power Handling Capability
	Series A	Series B	*a*	*b*	*d*	*s*	*t*	*r*1	*r*2		
ARA-1109	1.00 to 3.00		3.600	1.800	0.540	1.130	0.125	0.125	0.045 max.	0.0097	14,000
ARA-174		2.0 to 4.5	2.500	1.250	0.500	0.785	0.080	0.080	0.03 max.	0.021	7,000
ARA-148	2.6 to 5.2		1.750	0.875	0.350	0.555	0.080	0.080	0.03 max.	0.032	3,400
ARA-133		4.7 to 11.0	1.025	0.475	0.191	0.256	0.050	0.060	0.03 max.	0.06	900
ARA-136	5.2 to 9.6		1.222	0.611	0.403	0.351	0.064	0.060	0.03 max.	0.05	1,300

TABLE V

Extremely Broadband Single Ridge Guide

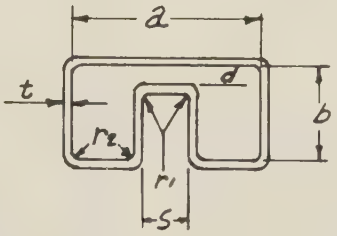

Ridge Guide	Frequency Range		Dimensions							Attenuation db/ft Midband (Al.)	Peak Power Handling Capability
	Series A	Series B	*a*	*b*	*d*	*s*	*t*	*r*1	*r*2		
50375	1.0 to 4.0		3.047	1.371	0.200	0.669	0.080	0.016	0.031	0.05	1500
50376	3.75 to 15.0		0.8125	0.3655	0.05315	0.1784	0.100	0.005	0.008	0.20	35
50437	10.0 to 40.0		0.306	0.133	0.0215	0.072	0.060	0.005	0.008	0.80	5

guide is now available. Attenuation of flexible waveguide is slightly higher than that of rigid guide; however, the mismatch contribution from well-designed flexible waveguide amounts to less than 1.05 in most cases. Flexible waveguide is usually protected by an elastomeric jacket generally made of neoprene or plastisol bonded to the outside surface of the guide. Flexible waveguide sections are available preformed to any desired shape or in standard straight lengths which are in multiples of six inches for field assembly use.

Ridged Waveguides

Practically all of the preceding material applies to ridged waveguide as well as to rectangular waveguide. Tolerances, materials, and constructional techniques are basically the same for ridged waveguide as rectangular waveguide. The connectors used are also similar; however, contact flanges are almost universally used with ridged waveguide due to the problems encountered in designing chokes for the broad bandwidths obtainable with ridged guide. Flexible ridged waveguide is also available in certain sizes.

The big advantage in the use of ridged waveguide is the extremely wide bandwidth obtainable between the TE_{10} and TE_{20} mode cutoff wavelengths. Frequency ranges of four to one or more for the fundamental mode of operation are easily obtainable with single and double ridged waveguide. It is also useful in that the lowered cutoff frequency permits a more compact cross section, and the wave impedance is lowered. Tables IV and V show the basic construction of some special single and double ridged waveguides. Single ridged and double ridged waveguides achieve the same effect; however, the choice between the two depends on the application and mechanical considerations. Double ridged guide is preferred for long transmission lines since the depth of each

ridge is roughly half that of a single ridge. This fact makes it easier to hold tolerances on the ridge, and flexible waveguide becomes simpler to fabricate. Single ridged guide is more practical for transitions to coaxial line and certain other specialized applications.

The ARA-136 double ridged waveguide shown in Table IV has found extensive use as a transmission line for commercial airlines weather radar, since *C*- and *X*-band radars may be used with the same transmission line in the aircraft. Also, the cross sectional dimensions are considerably less than that of standard *C*-band waveguide, thereby representing a considerable saving in space and weight for *C*-band installations.

Ridged waveguides cannot be analyzed by the simple methods of ordinary rectangular waveguide, and publications giving design data and theory of operation are quite limited.[1–3] Of these publications, the article by Hopfer gives the most advanced and accurate information. This article deals primarily with single ridged guide, although there is considerable design information also given for double ridged waveguide. Cohn's article includes design curves which can be used for both single and double ridged guide, but the data is not as accurate as Hopfer's, mainly because the step discontinuity susceptance effect is not included in the calculations.

Waveguide Assembly Constructional Techniques

Brazing

Brazed assemblies are still the most common type, although brazing is not necessarily the best method of fabricating waveguide assemblies. In this method, most of the parts are made from machined details and the entire assembly is brazed together generally by hand methods. With the large use of airborne radars, aluminum waveguide has become a major part of the production of waveguide components. Because of the fact that the melting point of aluminum brazing alloy is only 40 degrees lower than the melting point of the aluminum itself, hand brazing is a tricky and difficult job. It is also difficult to control the amount of distortion which occurs due to uneven heating. Therefore, hand brazing techniques should be confined to the relatively simple waveguide assemblies. Salt bath dip brazing techniques do much to eliminate the distortion problem and they also eliminate much of the flux entrapment which leads to corrosion problems. As a result, dip brazing methods are used for the more complicated assemblies. Extremely precise components can be produced by this method by the use of broached waveguide in conjunction with furnace brazing and suitable jigging techniques. An example of this technique is the precision crossguide directional coupler shown in the lower right hand corner of Fig. 6.

[1] S. B. Cohn, "Properties of ridge waveguide," Proc. IRE, vol. 35, pp. 783–788; August, 1947.
[2] Nathan Marcuvitz, "Waveguide Handbook," M.I.T. Rad. Lab. Series, vol. 10, pp. 399–402.
[3] Samuel Hopfer, "Design of ridged waveguides," IRE Trans., vol. MTT-3, pp. 20–29; October, 1955.

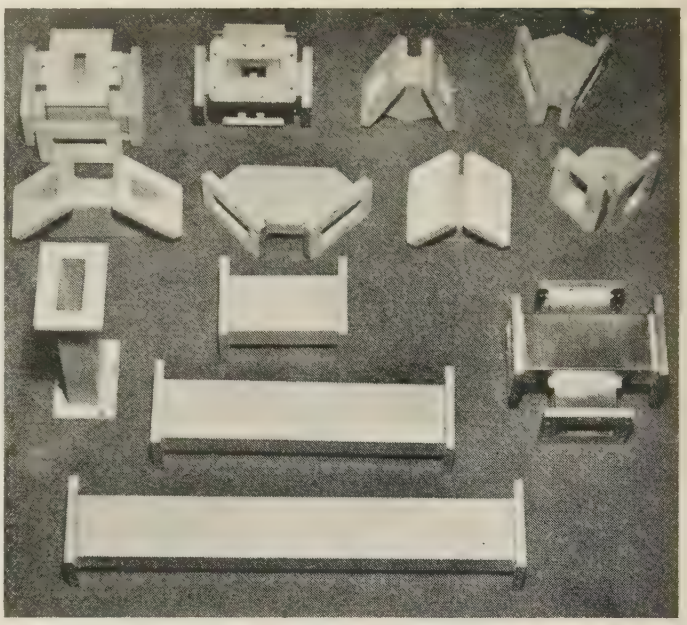

Fig. 6—Precision waveguide assemble fabricated by casting (upper) and by brazing and broading (lower).

Precision Casting

If a waveguide assembly is being produced in quantity, or if the complexity of the assembly increases beyond a certain level, it then becomes more economical to tool up for precision casting. The methods used most often for this application are plaster casting, the lost wax process, and die casting. The plaster and lost wax methods yield about the same order of precision (0.003 /inch) and are used in the majority of applications. Casting tools for die casting are relatively expensive and their use is limited to production of quantities in excess of several thousand.

Once the tools are worked out to give the proper dimensions, precision casting methods can readily duplicate parts economically in any quantity, whereas machining methods become very costly in comparison. Another advantage in casting is that adjustments can be made easily in the casting tools, thereby providing a means for finalizing the design right in the casting tools. This is an important advantage because, in precision waveguide assemblies, it is extremely difficult to translate the dimensions of a machined part to a set of drawings and then retranslate these every time a new part is produced. Fig. 6 also shows some waveguide components which have been produced by precision casting techniques.

Electroforming

Electroformed parts have found acceptance in some applications for complex and precise internal details, but the cost of electroforming is much higher than precision casting. Fig. 7 shows an electroformed hybrid ring circuit for *X* band; however, electroforming is more useful for applications in the millimeter wavelength region where the surface conductivity and roughness of normal casting alloys introduce severe attenuation.

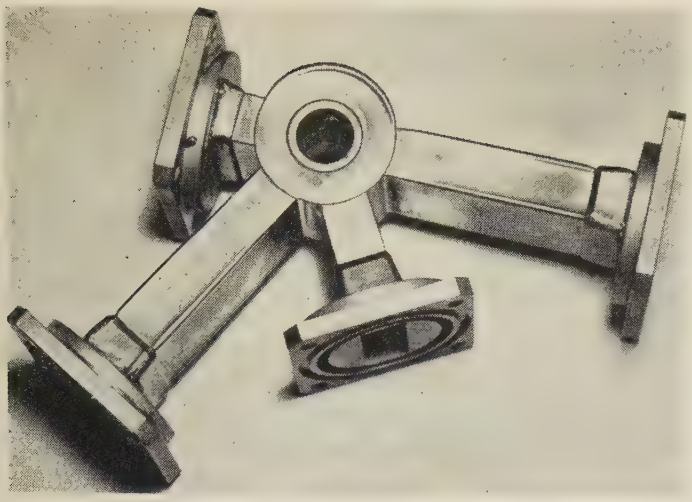

Fig. 7—Rat-race duplexer, electroformed.

With carefully machined and polished mandrels, an excellent surface finish can be obtained by electroforming. Furthermore, the purity of the metal is high, thereby providing good conductivity. There are, however, several difficulties encountered with electroforming. If the basic waveguide sections are electroformed and the flanges attached by brazing, distortions occur which nullify the inherent precision of electroforming. This problem can be eliminated by the expensive method of electroforming the flanges in place. Another serious problem is the reverse corner build-up that occurs as a result of the masking at the corners. This results in weak spots at the junctions of the flanges and electroformed waveguide. This problem can be alleviated by the use of suitable plastic compounds over the outer surfaces and by using special electrodes to "throw" metal into these corners. It must also be remembered that the electroforming process is only as accurate as the mandrel used, and therefore, the mandrel itself must be made to the tolerances required in the final product.

Pressurization of Waveguide for High Power

One of the major problems facing radar systems designers today is the ever increasing peak power which is becoming available. In order to increase the power handling capability of waveguide components, pressurization must be introduced. Unfortunately, rectangular waveguide is almost the poorest possible shape for pressure vessel design, and the standard wall thickness of waveguides larger than X band are far from adequate in this respect. Only a nominal amount of pressure can be applied without seriously distorting the waveguides. For example, pressures in excess of 5 psi will cause trouble in WR-650, especially since the tubing is usually in the annealed condition as a result of brazing. In the S-band region, 15 to 20 psi pressure is about the maximum for standard waveguide. At X band, pressures as high as 30 psi can be used with no difficulty. To meet the demand for high pressure waveguide in sizes larger than X band, a series of specially drawn waveguide tubing has been made available. This tubing was designed for negligible distortion at 60 psi pressure by using the principles outlined in Fig. 8.

Pressurization of waveguides for operation at extremely high altitudes and high power may not be the best choice, since the reliability of space born waveguide systems would be improved if pressurization could be eliminated. Of course, no voltage breakdown problems exist in the vacuum of outer space; however, the transition from the lower altitudes to outer space represents a serious problem. Towards this end, solid dielectric waveguide structures have been proposed and are under development.

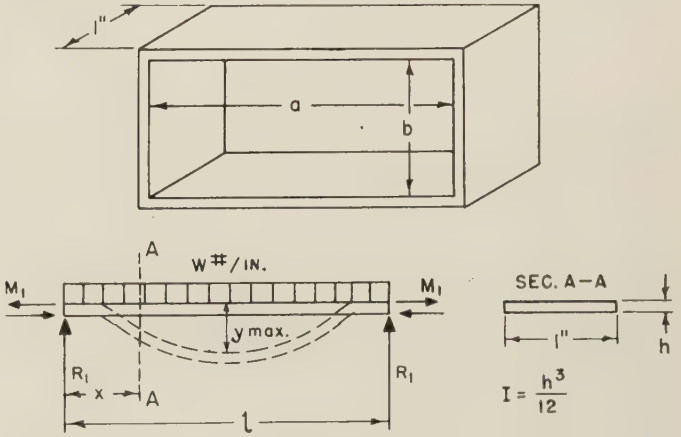

Fig. 8—Cross section of waveguide treated as uniformly loaded simple beam with end moments M_1.

General equation for deflection of pressurized waveguide:

$$EI\, y_{max} = \frac{(a^3 + b^3)wl_2}{96(a+b)} - \frac{5wl^4}{384}$$

where

E = modulus of elasticity,
I = moment of inertia = $b'h^3/12$ where b' (in this term) = 1 inch width of waveguide section chosen,
y_{max} = maximum deformation of pressurized waveguide section which occurs at the center of the face,
a = internal dimension of wide face of waveguide,
b = internal dimension of narrow face of waveguide,
w = pressure since element was chosen as a beam 1 inch in width,
$l = a$, when calculating y_{max} for wide face,
$l = b$, when calculating y_{max} for narrow face.

Standardization

At the present time, because of the tremendous activity in waveguide systems, there is very serious need for further standardization in this field. The need for standardization of flange designs has already been discussed in the section on waveguide connectors. The increasing use of pressurization for high power systems requires a program for standardizing on heavy walled waveguide tubing, since the application of nominal pressures introduces severe distortion in standard size waveguides. The most pressing need for standardization is in the field of ridged waveguide, where the wide variety of parameters can result in many different waveguide structures all designed for the same application. A program for the standardization of ridge waveguide is now under way by the RETMA SQ-11.1.3 committee and it is hoped that a suitable standard will be arrived at within the next year or two.

A Broad-Band Microwave Circulator*

EDWARD A. OHM†

Summary—The discovery of a simple, low loss way to hold Faraday rotation constant over a broad-band (coupled with the development of wide-band, high return loss, circular-to-rectangular waveguide transformers, and polarization couplers) has made it possible to design and build a high quality circulator for use in the 10.7 kmc to 11.7 kmc band.

The essential characteristics of the described unit include a more than 30-db return loss at each terminal, an isolation of 30 db or greater between "isolated" terminals, and a 0.35-db insertion loss between transmission terminals.

I. Introduction

THE PRINCIPLES of a four-arm Faraday rotation circulator were first published by Hogan in 1952.[1] Now with the discovery of a simple, low-loss way to hold Faraday rotation constant with frequency, it has been possible to design a good, practical circulator for use over at least a 10 per cent band.

The ideas and techniques which are discussed here can be applied to any waveguide frequency band. However, since there was a special interest in the 10.7-kmc to 11.7-kmc band, this data will be used for illustration.

The objective, of course, is to design an ideal circulator, and an ideal Faraday rotation circulator is shown in Fig. 1. Energy entering in arm 1 is polarized in the direction E_1 and on passage through the ferrite loaded region its polarization is rotated exactly 45° to the plane of E_2. Thus, all of the energy passes exclusively from arm 1 to arm 2. In a like manner energy entering arm 2 passes exclusively to arm 3, energy entering arm 3 passes exclusively to arm 4, and energy entering arm 4 passes exclusively to arm 1. This is shown symbolically in Fig. 2 (opposite).

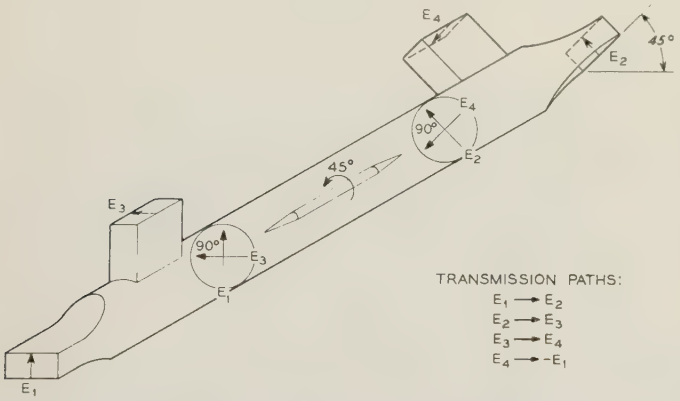

Fig. 1—An ideal circulator.

If the waveguide plumbing is nearly lossless and its reflections are small compared to those of the ferrite loaded region then all of the circulator characteristics will be determined by the ferrite-loaded region itself. This is a situation which can be approximated in practice and the necessary techniques for designing the waveguide components are described in part III.

In the design of a broad-band Faraday rotation circulator there are then three main things which degrade the performance from that of an ideal circulator.

1) The insertion loss of the ferrite assembly (*i.e.*, all of the materials which are inserted in the ferrite loaded region). This, of course, causes transmission loss between the transmission arms of the circulator.

2) A change of Faraday rotation with frequency. This causes adjacent arm leakages between nontransmission terminals as shown by the dashed lines in Fig. 3. For example (refer to Fig. 1), if energy entering arm 1 polarized as E_1 is not rotated exactly 45°, then its polarization will not be completely in the plane of E_2 but will have a component in the E_4 direction and this component will pass directly into arm 4. The isolation of this type of leakage can be computed and it is:

$$\text{Isolation} = 20 \log_{10} \csc \Delta\theta^\circ \text{ db} \qquad (1)$$

where $\Delta\theta^\circ$ is the departure in rotation from 45°.

3) Reflection from the ferrite assembly. This determines the return loss of each circulator arm and what is more important it causes alternate arm leakages as shown by the dashed lines in Fig. 4. For example (refer to Fig. 1), if energy from arm 1 is partially reflected by the far end of the ferrite assembly this reflected energy will reverse its direction, rotate another 45° to the polarization of arm 3 and pass directly into arm 3. The isolation of this type of leakage is equal to the return loss of the ferrite assembly.

Figs. 5–8 show four typical circulator applications first suggested by A. G. Fox, S. E. Miller, and W. W. Mumford of Bell Telephone Laboratories. The dashed lines indicate leakage paths which would most seriously interfere with the performance of each broad-band system. As seen from these figures both types of leakage are equally troublesome and therefore the design objective for this general purpose circulator was to attain an equal minimum of both types of leakage, commensurate with the smallest possible insertion loss.

The adjacent arm leakage due to a change in Faraday rotation with frequency has been the most serious obstacle in the design of a good broad-band circulator. The next section shows a general solution of this problem as well as a particular solution which more nearly satisfies the arbitrary design objectives.

* Manuscript received by the PGMTT, July 16, 1956. Presented before the National Symposium on Microwave Techniques, Philadelphia, Pa., February 2–3, 1956.

† Bell Telephone Labs., Holmdel, N. J.

[1] C. L. Hogan, "The ferromagnetic Faraday effect at microwave frequencies and its applications," *Bell Sys. Tech. J.*, vol. 31, pp. 1–31; January, 1952. See p. 25.

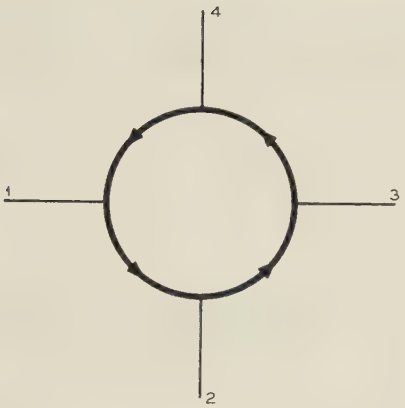

Fig. 2—An ideal circulator symbol.

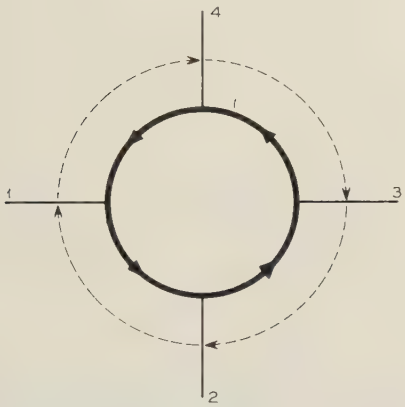

Fig. 3—A circulator with leakage due to a variation $\Delta\theta$, from 45° rotation.

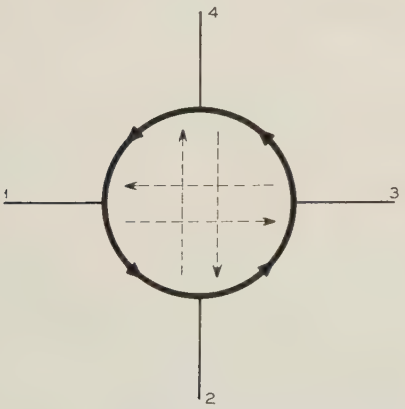

Fig. 4—A circulator with leakage due to ferrite assembly return loss.

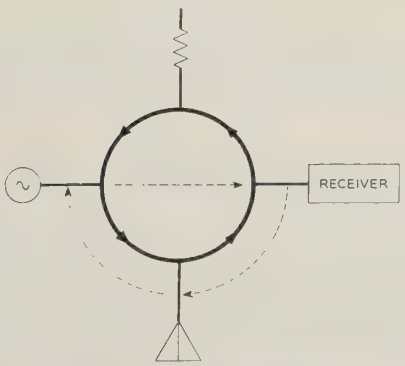

Fig. 5—A circulator duplexer.

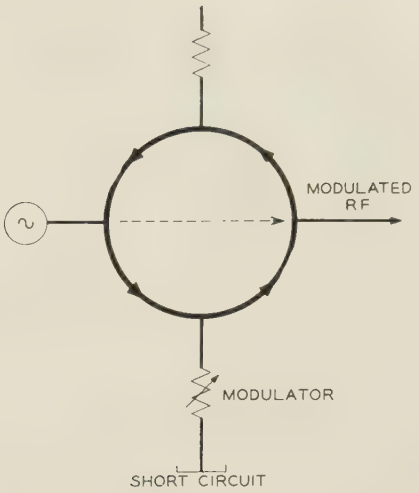

Fig. 6—A circulator microwave modulator.

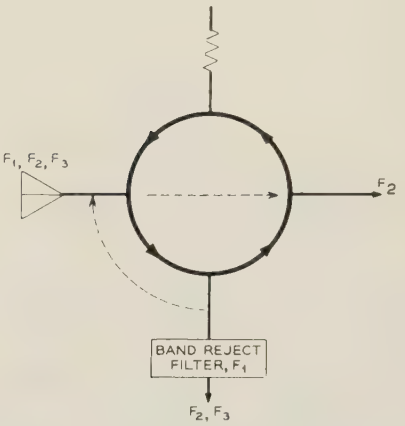

Fig. 7—A circulator channel brancher.

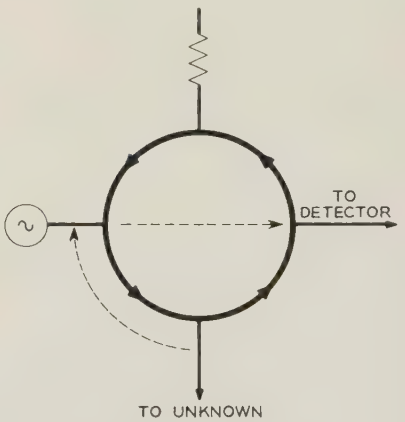

Fig. 8—A circulator as a no-loss directional coupler and isolator.

II. Broadbanding Faraday Rotation

The Faraday rotation of a ferrite cylinder (with conical matching tapers) centered in round waveguide increases considerably with frequency as shown by the upper curve of Fig. 9. Since a theoretical infinite medium of ferrite does not predict this frequency dependence it has been suggested that this is due to an increase in the percentage of energy in the ferrite (as the fre-

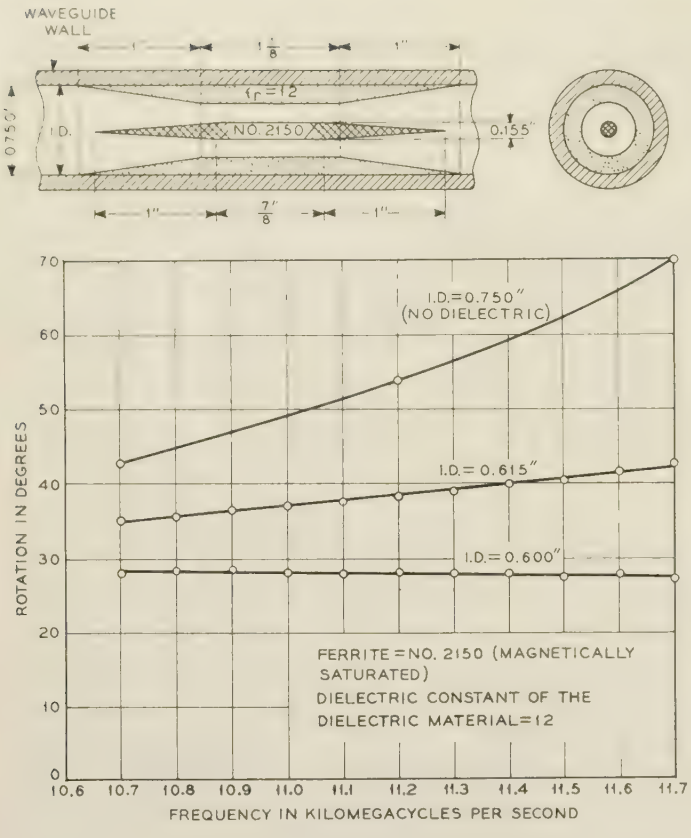

Fig. 9—Variation of rotation as a function of frequency and dielectric inside diameter ($\epsilon_r = 12$).

quency is increased) in a manner analogous to the dielectric waveguide effect.[2] If this is true, it seemed that a hollow concentric tube (with conical matching tapers) of high dielectric constant material could be inserted with its outside diameter contiguous to the waveguide wall and this would produce in the central region a compensating dielectric waveguide effect. Both of these ideas were confirmed by the curves of Fig. 9. As the dielectric material inside diameter was decreased (*ie.*, indicates an increase in the amount of dielectric material) the Faraday rotation decreased, the slope decreased, and it was even possible to obtain a negative slope in this manner. The lower curve of Fig. 9 shows a rotation characteristic of zero slope which is completely independent of frequency in this band.

The insertion loss of this latter ferrite assembly for 45° rotation was approximately 0.65 db and the major part of this loss was due directly to the loss tangent of the relatively high dielectric constant material ($\epsilon_r = 12$). Since lower dielectric constant materials generally have a lower loss tangent an effort was made to discover whether or not this phenomenon would be effective using lower dielectric constant materials. Some of these results using polystyrene ($\epsilon_r = 2.55$) and the same ferrite cylinder are shown in the top locus of Fig. 10. As the dielectric material inside diameter was decreased, the rotation ratio[3] decreased to a minimum before it again began to increase. By using smaller diameter cylinders of the same ferrite material the rotation ratio could even be reduced to less than unity and this is illustrated by the lowest locus of Fig. 10.

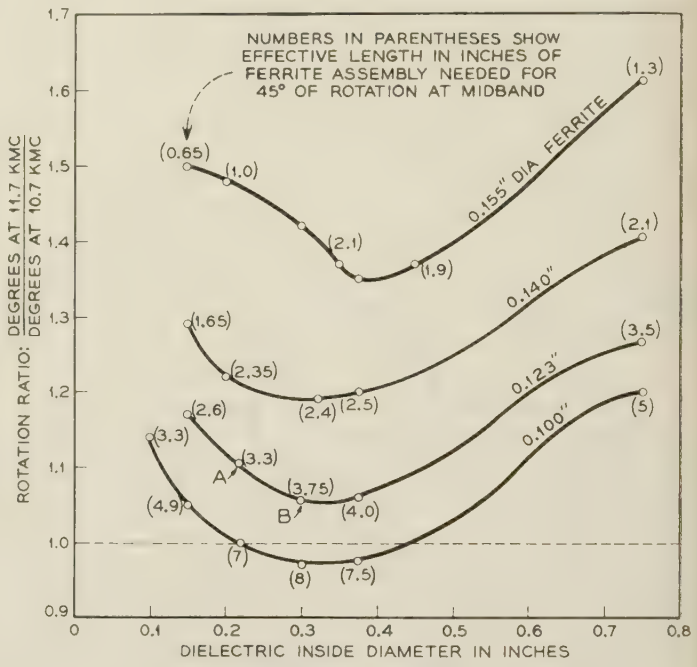

Fig. 10—Variation of rotation ratio for different ferrite diameters using $\epsilon_r = 2.55$ material in 0.750-inch diameter waveguide.

The insertion losses of ferrite assemblies using polystyrene were less than other materials tested (for similar rotations and rotation ratios) and most of the total losses were caused by either the loss tangent of the polystyrene or an increase in copper loss due to the polystyrene presence. Whatever the exact cause, losses were roughly proportional to the quantity of polystyrene especially for the smaller diameter ferrite samples. Since the optimum polystyrene inside diameter is nearly constant for the ferrite diameters of interest (see Fig. 10) it was concluded that the quantity of polystyrene and thus loss is roughly proportional to the ferrite assembly effective length.

[2] G. C. Southworth, "Principles and Applications of Wave Guide Transmission," D. Van Nostrand Co., Inc., p. 129; 1954.

[3] Since the rotation of each ferrite assembly under discussion here changes nearly linearly with frequency (as typified by the id = 0.615-inch locus of Fig. 9) the rotation ratio is a convenient index of the rotation vs frequency slope and can be easily used to predict $\Delta\theta$.

$$\Delta\theta = \frac{\theta_2/\theta_1 - 1}{\theta_2/\theta_1 + 1}\theta_0 \qquad (2)$$

where
θ_2/θ_1 = rotation ratio,
θ_2 = rotation at highest frequency in band,
θ_1 = rotation at lowest frequency in band,
θ_0 = desired rotation at midband (usually 45°),
$\Delta\theta$ = rotation departure from midband rotation.

The length of ferrite assembly required for 45° of rotation at midband increased as the minimums in rotation ratio approached the optimum goal of unity and these effective lengths in inches are shown in parenthesis in Fig. 10. Therefore, since the ferrite assembly losses are proportional to the effective length, a unity rotation ratio would also lead to a larger insertion loss.

Diverging for a moment, an investigation of the reflections of this type of assembly indicated that a minimum return loss of more than 33 db would be extremely difficult to achieve over the 10.7-kmc to 11.7-kmc band, and this of course would be a limiting factor in the alternate arm isolation.

Recalling now the design objective of equal values of alternate arm and adjacent arm isolations, it became apparent that a slightly greater than unity rotation ratio could maintain adjacent arm isolations equal to 33 db at the band edges [as per (1) and (2)] and at the same time reduce the transmission path insertion loss. Therefore, point B of Fig. 10 was selected as a good compromise and the ferrite assembly and its characteristics stemming from this point are in Fig. 11.

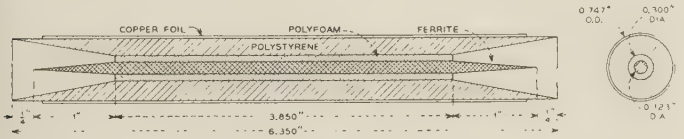

Fig. 11—Circulator ferrite assembly. Ferrite assembly characteristics (ferrite is magnetically saturated).
1) Rotation at 11.2 kmc = 45°.
2) Rotation ratio, θ at 11.7 kmc/θ at 10.7 kmc = 1.06; therefore, $\Delta\theta = 1.3°$.
3) Isolation at band edge (due to E component $\perp$ to the ideal rotation of 45°. Isolation (in db) = 20 $\log_{10}$ csc $\Delta\theta$ = 33 db.
4) Insertion loss = 0.19 db.
5) Return loss $\geq$ 28 db.

Note that the band edge adjacent arm leakage due to a change in rotation with frequency is 33 db and this is of the same general level as the return loss plotted in Fig. 12. This latter plot would be identical to the alternate arm leakage when the assembly is used in a circulator were it not for the adjusted phasing of smaller reflections from the other circulator components.

The measured insertion loss of this simple ferrite assembly was only 0.19 db and this was considered a reasonable price to pay for the greater than 30 db circulator isolations attainable over the 10.7-kmc to 11.7-kmc band.

III. Waveguide Components

Now that it is apparent that the isolations and return losses of the ferrite assembly can be made greater than 30 db over the 10.7-kmc to 11.7-kmc frequency band it will next be shown how these circulator characteristics were preserved by the improved design of wide-band waveguide components.

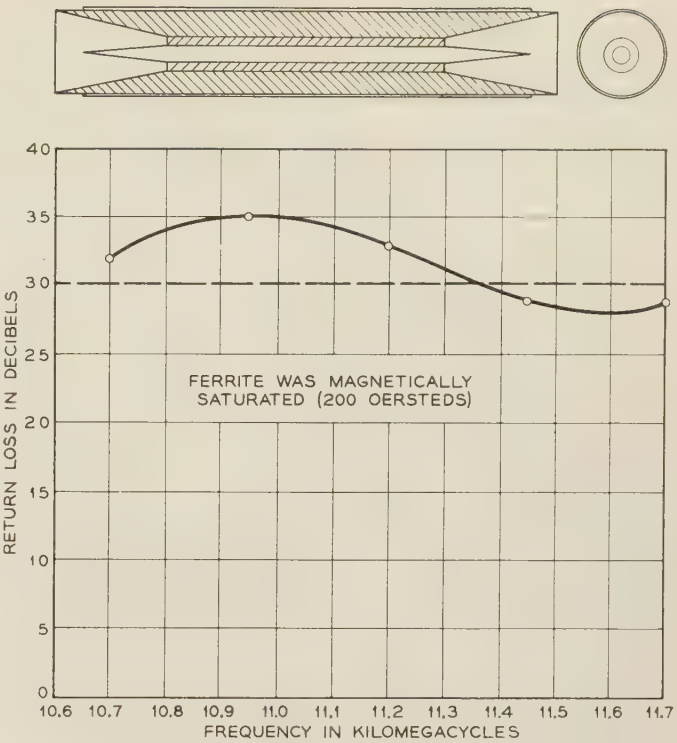

Fig. 12—Return loss of ferrite assembly.

Short Rectangular-to-Circular Waveguide Transformers

Fig. 13 shows a multiple quarter-wave rectangular-to-circular waveguide transformer designed so that each rectangular-to-rectangular junction has a net zero susceptance at midband. The capacitive shunt susceptance created by a step in waveguide height is cancelled at the same longitudinal location by an inductive shunt susceptance created by a step in waveguide width. Note that these steps are always in opposite directions, *i.e.*, the height of an adjacent section is larger when its width is smaller.

This makes it possible to nonsusceptively couple some waveguides of greatly different aspect ratios and since a standard rectangular waveguide has an aspect ratio of approximately 2 and a circular waveguide has an aspect ratio of 1, this approach automatically breaks up the total metallic discontinuity (of commonly used round and rectangular waveguides) so that it is distributed in a manner which (for a given number of intermediate transformer sections) yields the lowest possible Q at each junction. In this application all of the Q's were so low that they did not seriously effect the transformer characteristic even at the band edges so all junctions could be treated as pure resistive discontinuities.

Fig. 14 was developed to compute all of the intermediate waveguide transformer dimensions and the procedure is as follows.

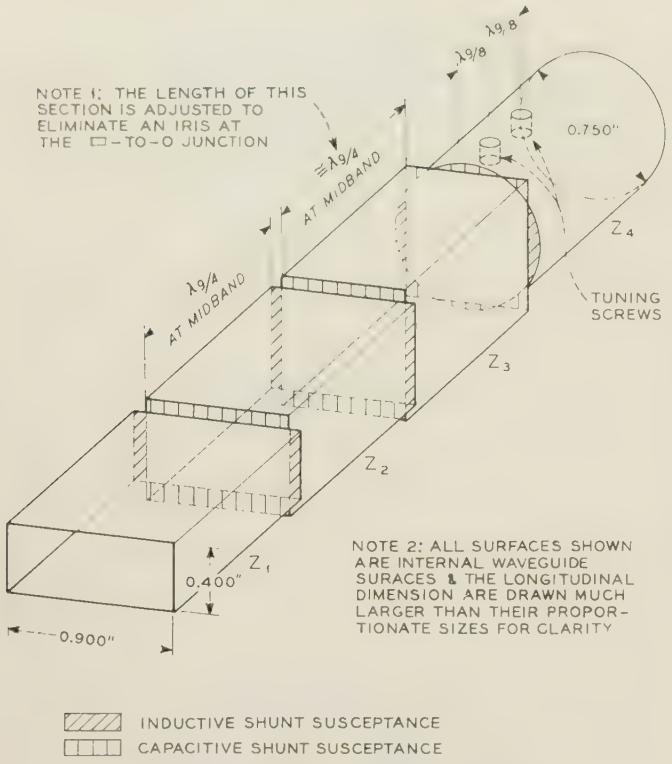

Fig. 13—A multiple quarter-wave transformer with junction susceptance cancellation.

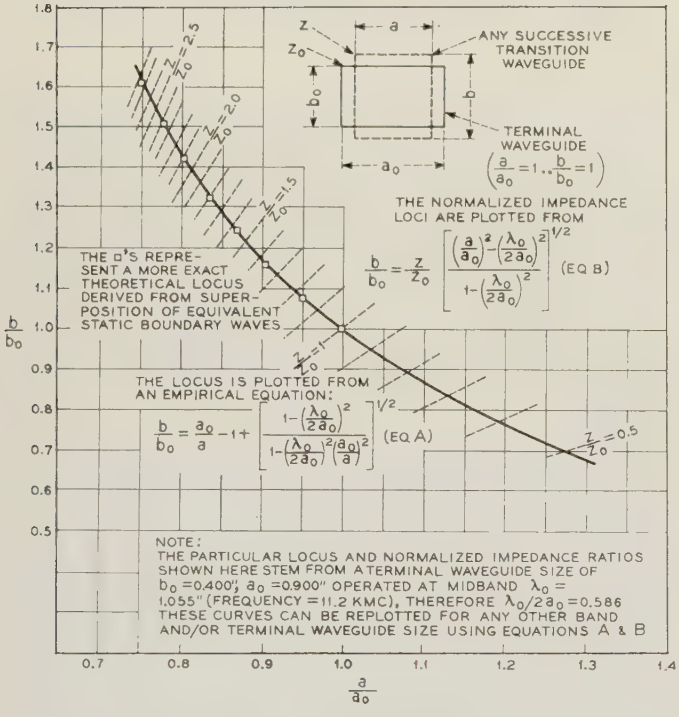

Fig. 14—A locus of waveguide dimension ratios which result in nonsusceptive junction.

1) Find the intermediate Z levels using any multiple quarter-wave transformer theory and normalize these to the terminal rectangular waveguide. These are Z/Z_0.

2) Plot these values of Z/Z_0. From the intersections

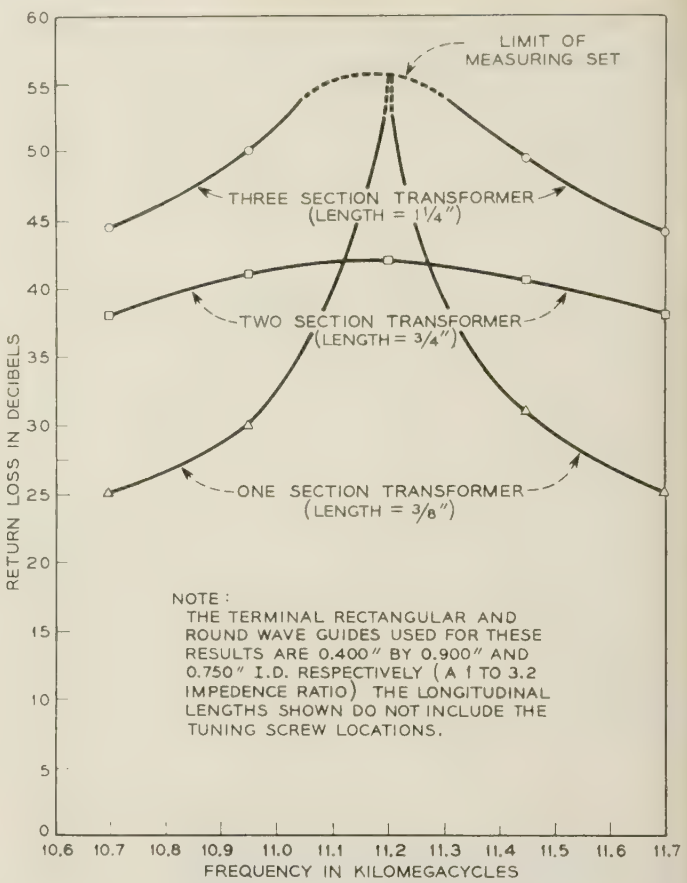

Fig. 15—Experimental results of 1, 2, and 3-section transformers.

of Z/Z_0 with the nonsusceptive locus read the required normalized height b/b_0, and width a/a_0, of each transformer section.

3) Denormalize, obtain height, b, and width, a, of each section.

4) Make each section $\lambda_g/4$ long at midband.

This in principle completes the transformer design. It turns out in practice that the arbitrary net susceptance at the rectangular-to-circular junction is fortuitously a small finite value and, in a manner shown by Cohn, a compensating iris at this junction is avoided by slightly altering the length of the waveguide section adjacent to the round waveguide.[4]

The two tuning screws located in the round waveguide were added to correct for a small systematic impedance level error inherent in this type of rectangular-to-rectangular junction and also to act as trimmers to compensate for machining deviations.

All of the over-all results are in excellent agreement with theory and Fig. 15 shows the measured return loss of a one, two, and three section rectangular-to-circular

[4] S. B. Cohn, "Optimum design of stepped transmission-line transformers," IRE TRANS., vol. MTT-3, pp. 16–21; April, 1955. See p. 18.

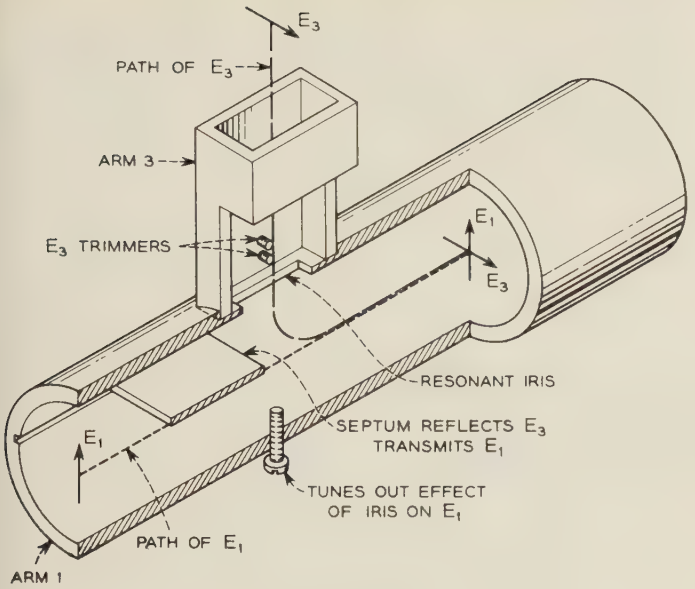

Fig. 16—A mode selecting coupler.

waveguide transformer used to connect the terminal waveguides of Fig. 13 (a 1 to 3.2 impedance ratio). The return loss of the three-section transformer is always greater than 44 db in the 10.7-kmc to 11.7-kmc band and therefore it was chosen for use with this circulator because its over-all reflections are so small that they can hardly interact with the reflections of the other components. In conclusion, note that this transformer is only $1\frac{1}{4}$ inches long (excluding the tuning screw locations) and this short length in itself reduces the copper insertion loss to a negligible value (less than 0.01 db).

A Mode Selecting Coupler

Fig. 16 shows the mechanical details of a mode selecting coupler which evolved at Holmdel of the Bell Telephone Laboratories through contributions by C. F. Edwards, C. B. Feldman, A. P. King, and D. H. Ring. It can be seen that the round waveguide on the right can be used as a mount for the ferrite assembly and by attaching a three-section rectangular-to-circular waveguide transformer to arm 1, the orthogonal polarizations of the round waveguide can be coupled directly and independently to standard rectangular waveguides.

By proper selection of the resonant iris dimensions and careful balancing of the tuning adjustments it was found that the return loss of each arm of the mode selecting coupler assembly could be maintained greater than 35 db over the 10.7-kmc to 11.7-kmc band as shown in Fig. 17, and that the isolation between arms 1 and 3 could be maintained greater than 45 db over this same frequency band. Although the reflections only 35 db down are large enough to degrade the over-all circulator characteristics (by interacting with the ferrite assembly reflections), these effects can be minimized by properly spacing the critical components as disclosed in section IV.

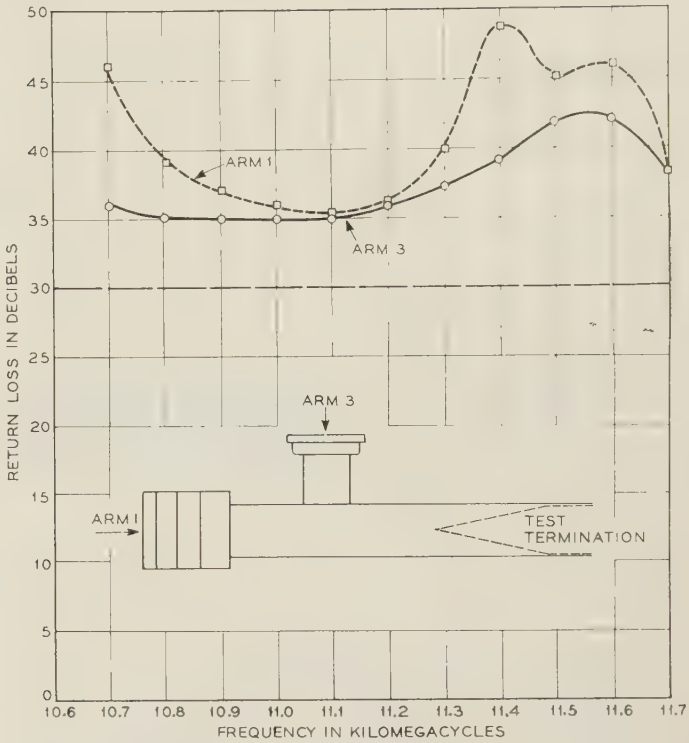

Fig. 17—Return loss of the mode selecting coupler assembly.

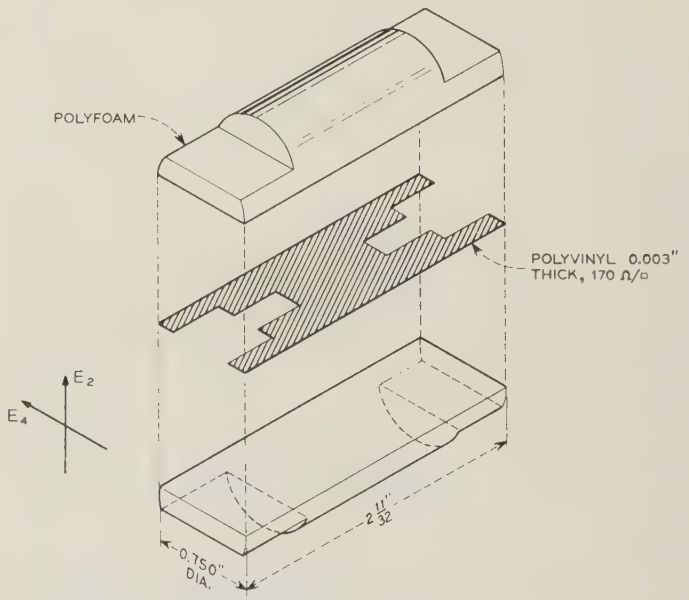

Fig. 18—A mode termination.
1) Return loss of $E_2 \geqq 45$ db.
2) Return loss of $E_4 \geqq 40$ db.
3) Insertion loss of $E_2 \cong 0$ db.
4) Insertion loss of $E_4 \cong 60$ db.

A Mode Selecting Termination

For many circulator applications it is necessary to terminate the 4th arm. Instead of externally terminating an arm of a mode selecting coupler assembly this can be accomplished directly in the round waveguide with negligible effect on the orthogonal polarization by using the mode selecting termination shown in Fig. 18.

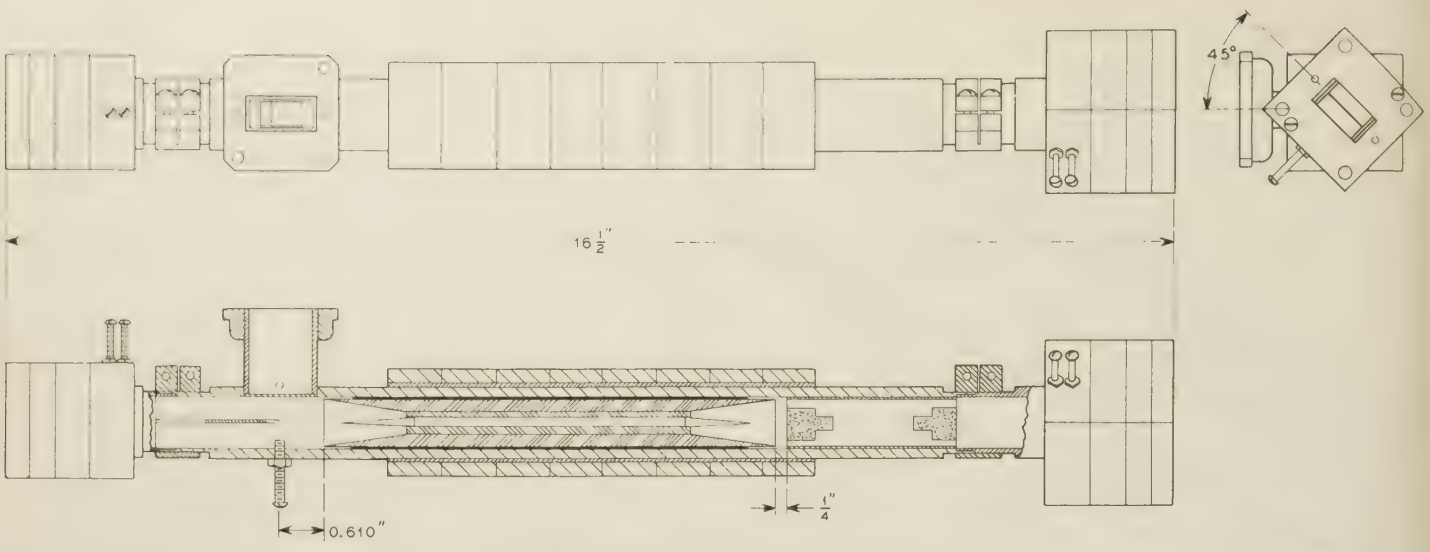

Fig. 19—Microwave circulator assembly.

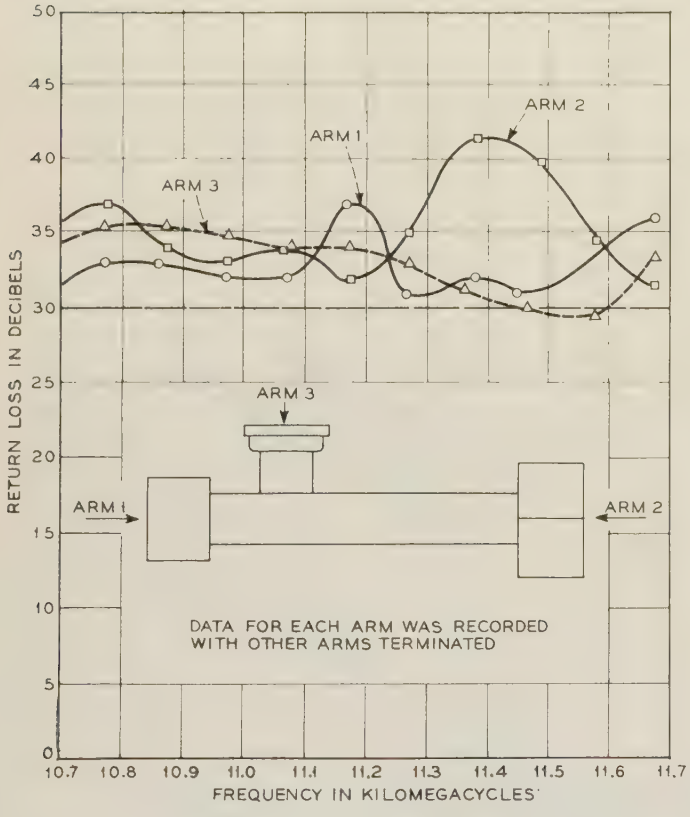

Fig. 20—Circulator return loss.

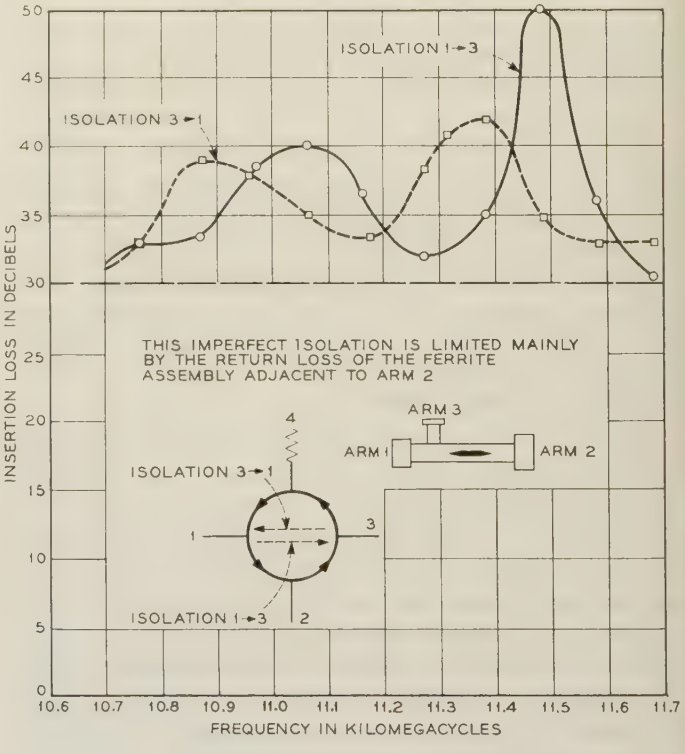

Fig. 21—Circulator isolation of alternate arms.

The return loss of the terminated polarization is more than 40 db and the return loss of the transmitted polarization is more than 45 db over the 10.7-kmc to 11.7-kmc band.

IV. The Circulator Assembly and Experimental Results

The circulator components were assembled as shown in Fig. 19 and the optimum longitudinal positions of the ferrite assembly and mode selecting termination were determined as follows.

The ferrite assembly was inserted in the mode selecting coupler assembly and after adjusting the magnets for 45° rotation it was located so that the reflections from the adjacent or left end of the ferrite assembly were partially cancelled by those of the mode selecting coupler assembly. Thus the reflections indicated by Figs. 12 and 17 were phased to give the best over-all return loss of arms 1 and 3 as shown in Fig. 20.

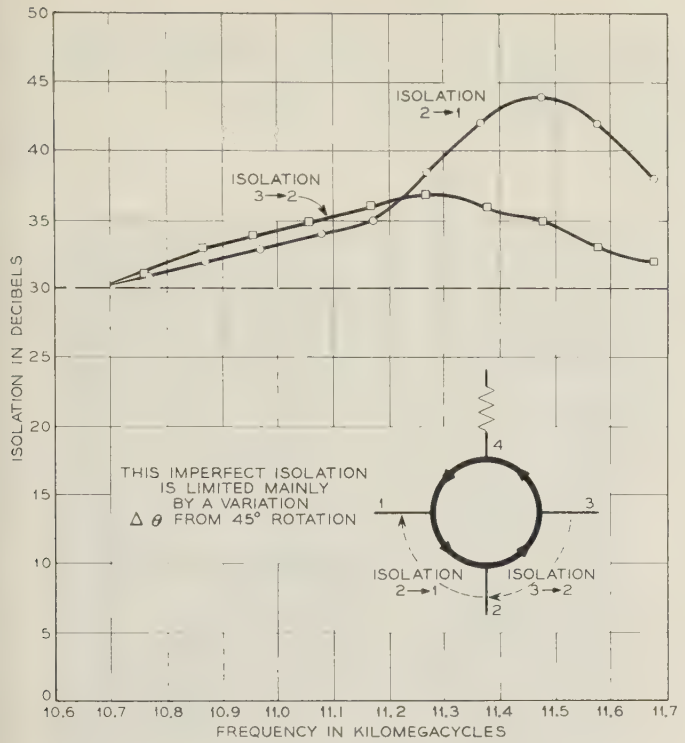

Fig. 22—Circulator isolation of adjacent arms.

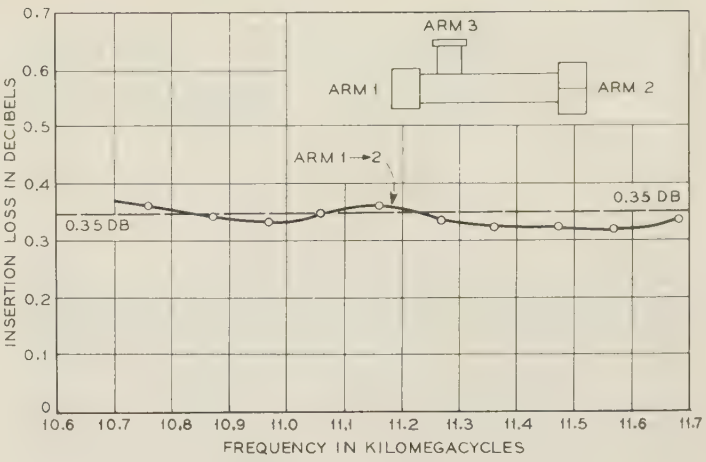

Fig. 23—Circulator insertion loss.

The mode selecting termination was then inserted and spaced longitudinally so that both orthogonal reflections from the arm 2 or right end of the ferrite assembly were partially cancelled by the smaller reflections from the mode selecting termination. The resultant reflections determined the alternate arm isolations and these results are shown in Fig. 21. Reflections from these same sources and the arm 2 transformer resulted in the over-all return loss of arm 2 and this data is shown in Fig. 20.

The measured adjacent arm isolations are shown in Fig. 22 and they are about as anticipated. The peaks are not infinite because of the residual brass and Faraday rotation ellipticites and these also account for the asymmetrical appearance of these isolation plots.

The insertion loss of a typical transmission path is shown in Fig. 23.

V. Conclusion

A practical broad-band Faraday rotation circulator can be built and adjusted using a moderate amount of care and a systematic tuning procedure.

Essential characteristics of this general purpose unit for the 10.7-kmc to 11.7-kmc band include a minimum 30-db return loss at each terminal, a minimum isolation of 30 db between nontransmission terminals and a 0.35-db insertion loss between transmission terminals.

The over-all length of this circulator is $16\frac{1}{2}$ inches and it would be difficult to significantly reduce this length below 13 inches without sacrificing bandwidth or some of the isolation characteristics.

The design objectives of this circulator resulted in equal nontransmission path isolations stemming from the ferrite assembly return loss and the Faraday rotation frequency dependence. However, the design emphasis can be readily shifted and in particular the Faraday rotation can be made frequency independent for this bandwidth if one is willing to allow a 0.1-db increase in insertion loss.

The Excitation of Surface Waveguides and Radiating Slots by Strip-Circuit Transmission Lines*

A. D. FROST,† C. R. McGEOCH,‡ AND C. R. MINGINS†

Summary—A variety of methods for coupling between a shielded strip-circuit transmission line, operating in the TEM coaxial mode, and a surface waveguide have been investigated. The arrangements include phased dipole arrays, series ground-plane slots and longitudinal slot excited probes. Impedance and matching conditions for each are discussed together with their relative efficiency and bandwidth. In the case of a single radiating slot, measurements on the effective equivalent circuit have been made as a function of the orientation angle of the slot with respect to the axis of the strip-line guide. Slots used ranged in length from 0.3 to 0.6 λ_g, having length /width ratios from 5 to 16.

Introduction

UNDER THE sponsorship of the Antenna Group of the Air Force Cambridge Research Center, the Research Laboratory of Physical Electronics at Tufts University has undertaken a continuing study of some of the basic properties of strip transmission lines. These studies have been made from both the theoretical and the experimental points of view.[1,2] The work has included investigations into the characteristic impedance, the power handling capabilities, and the losses of various types of lines using both air and solid dielectric. In addition, measurements have been made to establish typical design parameters for such simple line configurations as bends and steps. More recently our attention has turned to a consideration of the problems associated with the integration of strip-line components with existing or proposed microwave system elements. This paper is a report on one phase of this work having application in the field of antennas and radiating structures; that of the coupling of strip line to dielectric-coated conducting sheet waveguides, to surface waves guided by a corrugated ground plane, and to the radiation from slots in strip line.

The investigations reported here were carried out using a so-called balanced strip line with a dual center conductor etched on both sides of a copper-coated teflon glass base material 1/32 inch thick. The lines have an air dielectric and are supported between two parallel ground planes. All lines have a nominal characteristic impedance of 50 ohms and a ground-plane spacing of 0.500 inches. The center conductors have a width of 0.625 inches and are held in position at the lateral edges of the base material by posts which serve also to electrically connect the ground planes at frequent intervals.

Measurements on Radiating Slots

A theoretical expression for the radiation conductance of a narrow transverse slot in one ground plane of a strip-line structure having the configuration shown in Fig. 1 was contained in a paper presented by Dr. Arthur

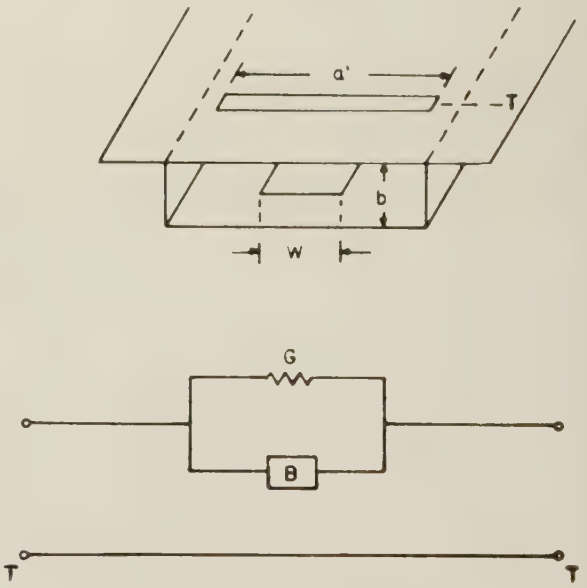

Fig. 1—Transverse slot in equivalent strip-line guide with midplane equivalent circuit representation.

Oliner at the Symposium on Microwave Strip Circuits held at Tufts University, October, 1954.[3] His evaluation gives the normalized conductance of a narrow slot in a thin ground plane with the axis of the slot perpendicular to the principal axis of the strip-line guide. This conductance is expressed as a function of the slot width a',

* Manuscript received by the PGMTT, July 16, 1956. Presented before the National Symposium on Microwave Techniques, Philadelphia, Pa., February 2–3, 1956. This work has been performed under Contract No. AF 19(604)-575 with the AF Cambridge Research Ctr., Air Research and Development Command.

† Dept. of Physics, Tufts Univ., Medford, Mass.

‡ Formerly at Dept. of Physics, Tufts Univ., now with Bomac Labs., Beverly, Mass.

[1] A. D. Frost and C. R. Mingins, "Microwave strip circuit research at Tufts College," IRE TRANS., vol. MTT-3, pp. 10–12; March, 1955.

[2] R. L. Pease and C. R. Mingins, "A universal approximate formula for characteristic impedance of strip transmission lines with rectangular inner conductors," IRE TRANS., vol. MTT-3, pp. 144–148; March, 1955.

[3] A. A. Oliner, "Equivalent circuits for discontinuities in balanced strip transmission lines," IRE TRANS., vol. MTT-3, pp. 134–143; March, 1955.

the wavelength, and a parameter related to the width of the center conductor.

The test fixture which was designed to permit measurement of such slot radiation effects and of the properties of other stripline components is shown in Fig. 2.

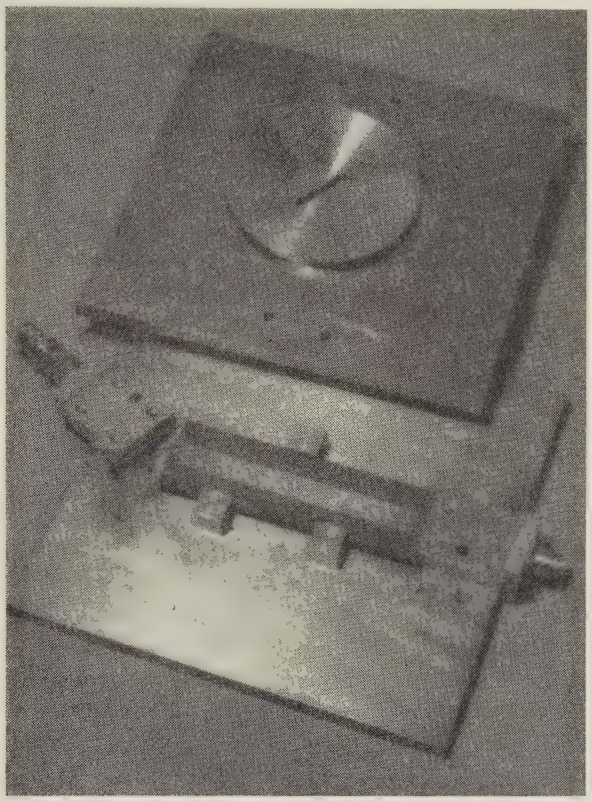

Fig. 2—Test fixture for slot radiation measurements.

The section is fitted with a circular removable center section which can be rotated for other measurements discussed in a later section of this paper. The strip line is joined at one end to a slotted line and at the other to a coaxial moving short using simple strip line to type *N* connector transitions such as those described by Fubini[4] and Fromm.[5] With a matched load at the terminal end of the system and a blank cover in place, the test section gave an over-all vswr of 1.1 in the operation range from 8 to 11 cm while with the movable short in position the vswr was under all conditions greater than 36 db.

Measurements of the input reflection coefficient of the test system as a function of the position of the moving short were taken for a number of slots ranging in length from 0.2 to 0.6 of a wavelength at orientations from 0° to 90°. In each case an approximate series conductance term introduced by the slot, as compared with the conditions with the blank in place, was determined.

The results for some of the measurements are shown in Fig. 3 together with the theoretical curve of normalized slot conductance as a function of slot length in wavelengths. The points shown represent slots which differ both in length and in length/width ratio. The posts which join the ground planes and incidentally serve to support the center conductor must have a lateral spacing measured at right angles to the axis of the strip line that is less than a half wavelength to insure dominant TEM mode operation. It is therefore not possible to excite a 90° slot which is a half wave long in the manner pictured in Fig. 1, in which it is presumed that the wave field in the guide is effective for the entire width. The use of additional grounding posts which has been made in some cases would not correspond to this situation. The possibility suggests itself, however, that operation of a slot rotated away from the 90° position could be substituted in some cases, providing sufficient line-to-slot coupling was achieved. In this way a slot of resonant length could be accommodated within the practical limits of a strip-line system. while maintaining the post spacing requisite for mode suppression.

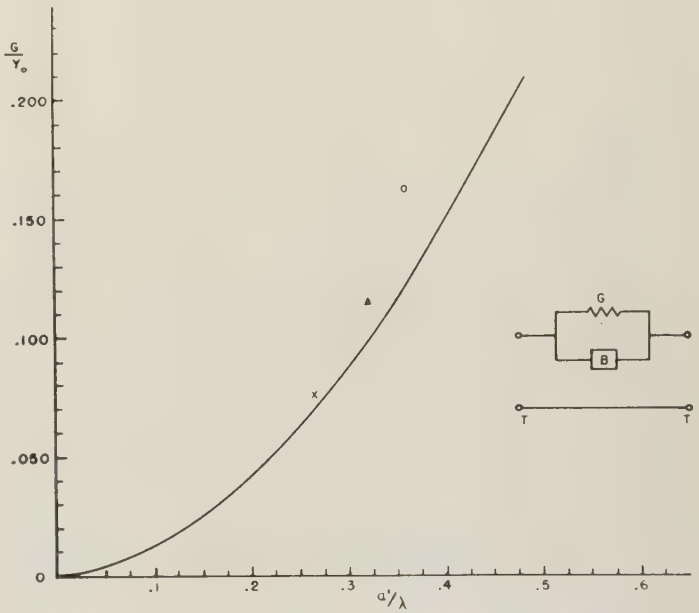

Fig. 3—Normalized slot conductance as a function of slot length. Measured values for finite width slots are shown.

A theoretical expression in integral form for the variation in slot conductance as a function of slot orientation angle has also been derived by Dr. Oliner but has not yet been evaluated. This derivation assumes, as does the previous one for the 90° slot, a thin ground plane and symmetrical orientation of slot and line.

Analysis of a range of measured values of slot conductance component as a function of rotation gives the

[4] E. G. Fubini, "Stripline radiators," IRE Trans., vol. MTT-3, pp. 149–156; March, 1955.

[5] W. E. Fromm, "Characteristics and some applications of stripline components," IRE Trans., vol. MTT-3, pp. 13–20; March, 1955.

data shown in Fig. 4. Relative conductance as compared to the value in the transverse or 90° position is plotted as a function of rotation angle. As was the case in the previous curve, these curves are for slots which differ both in length and length/width ratio. For shorter lines, those having a length a little more than twice the width of the center conductor, the variation in conductance is slow at small angles. In general most of the change takes place between 30° and 60°. Measurements on slots closer to resonant length than these confirm the sharp rise in conductance shown for angles less than 30°.

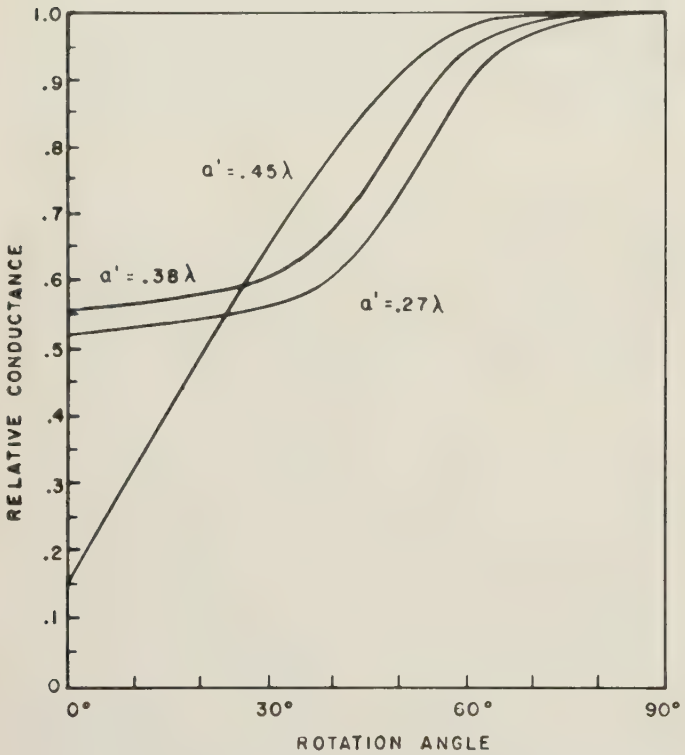

Fig. 4—Measured values of slot conductance as a function of slot orientation.

Excitation of Surface Waves from Strip Line

Studies have also been conducted on the coupling of strip line to surface waveguides of the kind provided by a grounded dielectric sheet and by a plane corrugated surface.

In the case of the dielectric waveguide three coupling techniques suitable for thick sheets have been explored. These include a single radiating dipole, multiple probes acting through a thick slot, and a phased array of dipoles.

In all cases the dielectric sheet used was a slab of polystyrene 1 inch thick as shown in Fig. 5.

Coupling by a single dipole was achieved with a probe passed through a $\frac{3}{8}$ inch hole in a thick ground plane, using a polystyrene bushing for support. The radiating probe was oriented within the slab so as to be symmetrically located between the long sides at a point approximately $\frac{3}{4}$ of a wavelength from one end. A cross-sectional view of the dielectric block, probe, and associated strip line is shown in Fig. 6. This view is at right angles to the axis of the strip line. With such a geometry the incident wave will be involved in a variety of mode transformations, some of which will radiate from the dielectric block in competition with the desired surface wave mode of present interest. A measure of the overall effectiveness of a radiating or mode conversion element can, within limits, be expressed in terms of the change in effective conductance as compared to some standard such as a dipole over an extended ground plane.

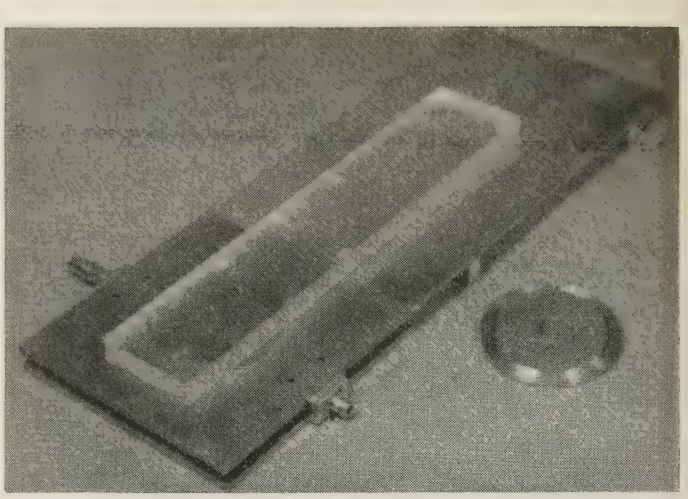

Fig. 5—Dielectric surface wave guide and associated strip-line connectors.

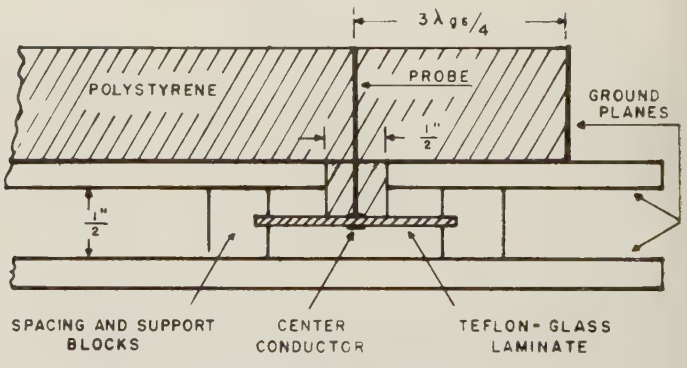

Fig. 6—Sectional view through dielectric guide showing single dipole coupling method.

Since all radiating modes will contribute to this single conductance term, it becomes necessary to isolate or eliminate, insofar as possible, the undesired modes which may be present. With this in mind and in an attempt to eliminate direct radiation from the near edges of the slab, conducting surfaces were provided at the end and for a short distance along the long dimensions of the slab. Since the critical angle for internal reflection is 42° in polystyrene, it was not necessary to continue

this shielding for the entire length. The presence of radiation from the extreme end of the slab was evidenced by a significant alteration in the probe input impedance when this end was covered. With the ends and a portion of the lateral sides covered as described above, the dipole admittance was only slightly greater than that introduced by the supporting polystyrene plug alone. The radiation from the extreme end of the slab was essentially due to the desired guided surface wave. By placing a metal barrier 3 inches high and somewhat wider than the slab perpendicular to the ground plane and to the long axis of the slab, it was possible both to provide an impedance matching section and to form a horn launching device. When adjusted for maximum effect the dipole conductance was appreciably increased. Measurements of the wavelength of the surface wave were made by moving a conducting bar along the principal surface of the slab and plotting the perturbation in probe conductance. The value of 7.6 cm, obtained for a free space wavelength of 10.6 cm, is in agreement with the predicted values for a TM wave over a polystyrene layer.[6]

Variation in the length of the dipole gave a maximum effectiveness, in terms of the conductance and measured with the matching radiating section in position, for a dipole length of 1.6 cm at 10.6 cm free space wavelength. This corresponds approximately to a quarter wavelength for a TEM wave in polystyrene. The normalized conductance in this case was 0.8 Y_0 as compared to a value of 0.55 Y_0 for a resonant dipole in air over a conducting ground plane.

A second technique employed for coupling strip line to a dielectric slab line is shown in Fig. 7. Three equi-

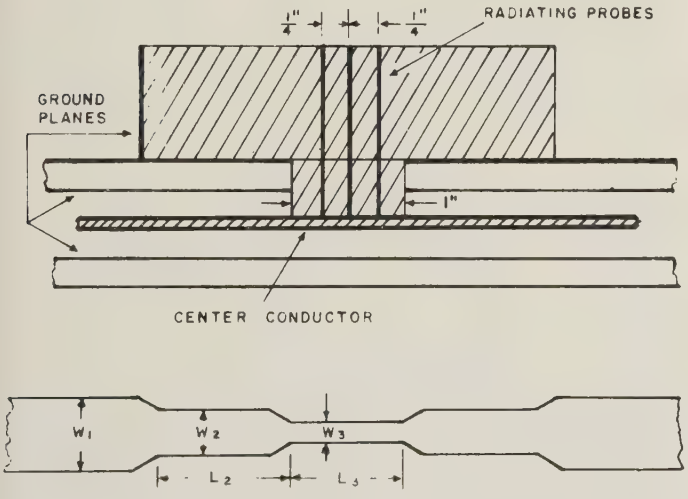

Fig. 7—Sectional view through dielectric guide showing slot-probe coupling method and associated strip-line center conductor.

[6] L. Hatkin, "Analysis of propagating modes in dielectric sheets," Proc. IRE, vol. 42, pp. 1565–1568; October, 1954.

spaced probes couple to the dielectric slab through a thick longitudinal slot. The strip-line center conductor has been tapered to adjust for the change in dielectric. To provide support and to preserve symmetry, a second polystyrene block not shown on the figure was positioned below the slot. Because of mutual coupling between the probes, the maximum mode conversion occurs with the probes extending the full thickness of the dielectric. In this case, with optimum end matching, the maximum system conductance was 0.65 Y_0. The variation in conductance with actual probe length was found to be less rapid than for the single probe.

In contrast to this system we have also considered the arrangement shown in Fig. 8.

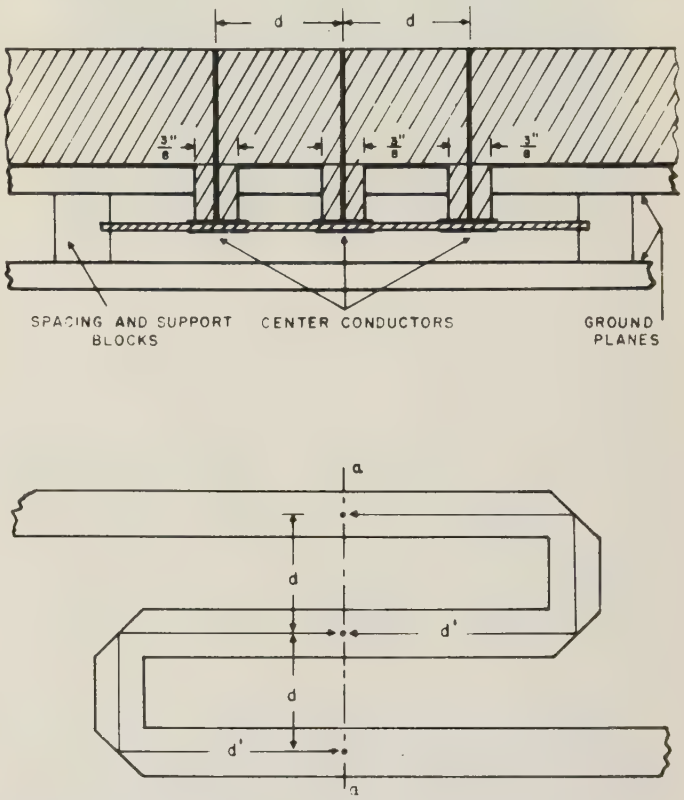

Fig. 8—Sectional view through dielectric guide showing plane dipole array coupling method and associated strip-line center conductor.

This comprises an array of spaced dipoles providing a cumulative end-fire array. Appropriate element phasing is provided by the use of an S-shaped strip line in which the differing phase velocities for waves in polystyrene and in the strip line are matched by an increased path length as shown. In this case the optimum probe length is near that for a single dipole but the change in relative effectiveness with a change in frequency is more rapid.

The properties of periodically corrugated surfaces as waveguides have been presented in the literature by

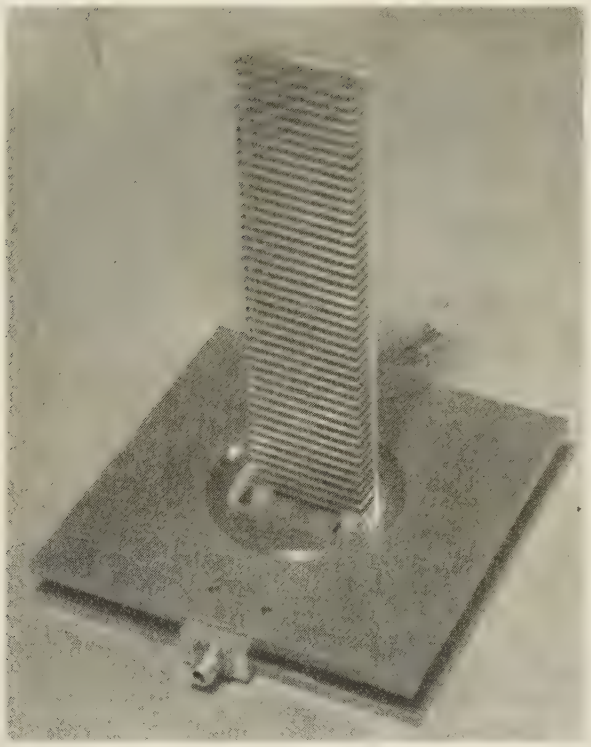

Fig. 9—Corrugated surface guide slot coupled to strip line.

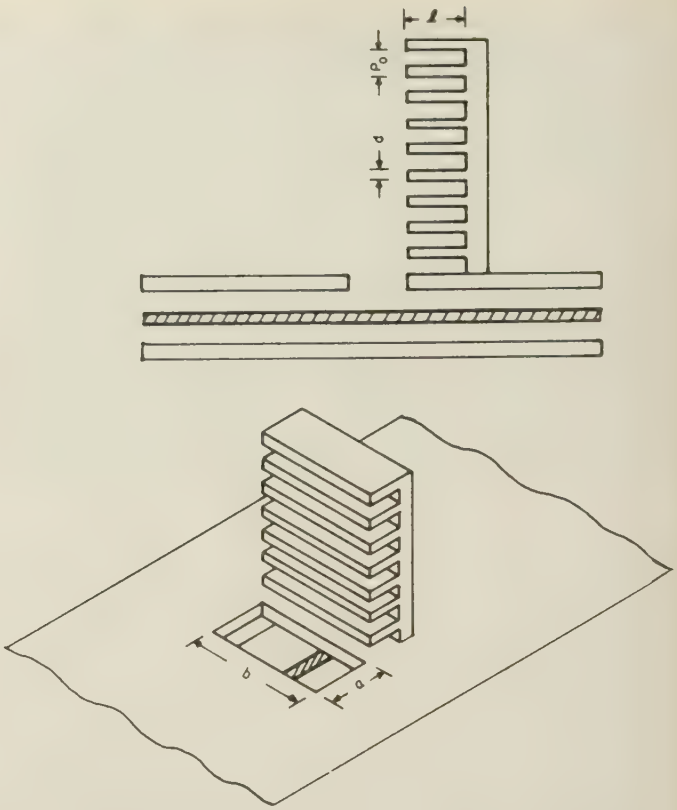

Fig. 10—Sectional and perspective view showing coupling method between corrugated surface guide and strip line.

various writers.[7,8] In the simple form which we have considered, parallel grooves, each less than $\lambda/4$ in length, provide an essentially inductive impedance to an incident wave and tend thereby to bind a progressive wave to the surface. The velocity of propagation is less than that of a free-space wave. The similarity between the TM wave in dielectric sheets and on such surfaces has led us to investigate the possibilities of the excitation of such waves using strip lines.

Of those methods considered, the one most successful to date has been that pictured in Fig. 9. A cross section showing the relationship between the slot, the strip line, and the corrugated guide is whown in Fig. 10.

The surface waveguide consists of a portion of corrugated surface which is slot-coupled to a strip-line as shown. As in the case of the excitation of a surface using a horn, the guided wave is mixed with a direct radiation component from the source, Measurements of the standing wave on the guide surface gave a λ_g or 5.80 cm at a source wavelength λ_0 of 10.6 cm. This is in agreement with the prediction for surface-guided wavelengths for a surface of limited width. Maximum surface wave component was obtained for a slot width of 0.85 cm.

[7] W. Rotman, "A study of single-surface corrugated guides," Proc. IRE, vol. 39, pp. 952–959; August, 1951.
[8] A. S. Dunbar, "Ridge and Corrugated Antenna Studies," Final Rept. on Project 199, Stanford Res. Inst., January 15, 1951.

The Turnstile Circulator*

PHILIP J. ALLEN†

Summary—**Theory and performance of a narrow band circulator employing but a single junction and a 45-degree Faraday rotator are discussed. Factors affecting bandwidth are considered and pertinent curves are plotted. Isolation bandwidth curves permit prediction of performance. This compact circulator, although frequency sensitive, is tunable and provides high reverse and cross isolations making it especially suited to duplexing, isolating and switching applications.**

ONE OF THE most valuable fundamental applications of the microwave gyrator[1] is in the realization of the microwave circulator,[1–6] a nonreciprocal multiport network having unique properties. A number of forms of microwave gyrator are now known and have been incorporated in a variety of circulators differing in geometry and performance capability. This paper describes still another circulator form—one of the simplest—incorporating a 45° Faraday rotator and a single turnstile junction. Although the circulator to be described is frequency sensitive, it is capable of high isolation with low insertion loss, is compact, and has a convenient terminal arrangement.

The Turnstile Junction

Before discussing the principle of the turnstile circulator, the pertinent properties of the basic turnstile junction[7–9] will be briefly reviewed. As illustrated in Fig. 1, the turnstile is a 6-port junction consisting of a circular waveguide symmetrically joining two intersecting rectangular waveguides. A symmetrical matching structure is located at the center of the junction. When the junction is properly matched and all ports are terminated in matched loads the junction exhibits the coupling properties listed in Tables I and II.

From symmetry of the junction its other coupling properties can be inferred.

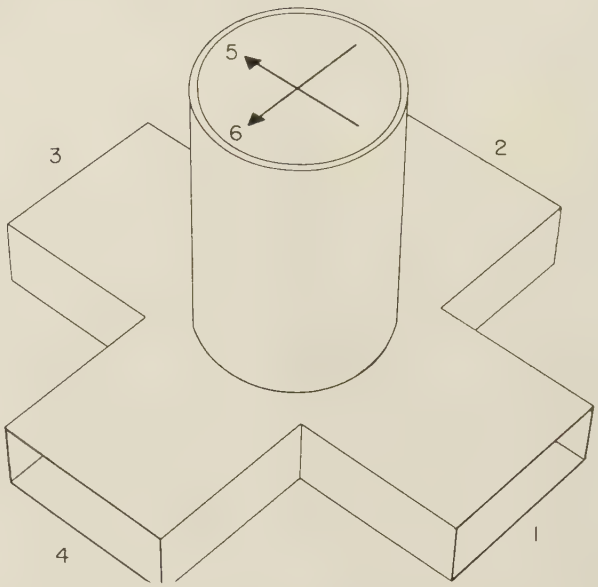

Fig. 1—The waveguide turnstile—a symmetrical 6-port junction.

TABLE I

Unit Power Input to Arm 1

Arm	Coupled Power	Voltage*	Coupling
1	—	—	(No reflection)
2	1/4	0.5	−6 db.
3	0	0	(Isolated)
4	1/4	0.5	−6 db.
5	1/2	0.707	−3 db.
6	0	0	(Isolated)

TABLE II

Unit Power Input to Arm 6

Arm	Coupled Power	Voltage*	Coupling
1	0	0	(Isolated)
2	1/2	−0.707	−3 db.
3	0	0	(Isolated)
4	1/2	0.707	−3 db.
5	0	0	(Isolated)
6	—	—	(No reflection)

* Voltage referred to Z_0 of rectangular waveguide arms.

The Turnstile Circulator

The turnstile circulator consists simply of a turnstile junction containing a 45° Faraday rotator in the circular waveguide which is short-circuited at an appropriate point. Circulator action will be explained by referring to Fig. 2. Consider a conventional turnstile junction

* Manuscript received by the PGMTT, July 16, 1956. Presented before the National Symposium on Microwave Techniques, Philadelphia, Pa., February 2–3, 1956.

† Naval Research Lab., Washington 25, D. C.

[1] C. L. Hogan, "The microwave gyrator," *Bell Sys. Tech. J.*, vol. 31, pp. 1–31; January, 1952.

[2] J. H. Rowen, "Ferrites in microwave applications," *Bell Sys. Tech. J.*, vol. 32, pp. 1333–1369; November, 1953.

[3] Robert H. Fox, "Bandwidth of Microwave Ferrite Devices," M.I.T. Lincoln Lab. Tech. Rept. no. 55; August, 1954.

[4] Robert H. Fox, "A Non-Reciprocal Four-Pole Ring Circuit," M.I.T. Lincoln Lab. Tech. Rept. no. 68; September, 1954.

[5] Robert H. Fox, "Ferrite Devices and Applications at Microwave Frequencies," M.I.T. Lincoln Lab. Rept. no. 69; September, 1954.

[6] A. G. Fox, S. E. Miller, M. T. Weiss, "Behavior and Applications of Ferrites in the Microwave Region," *Bell Sys. Tech. J.*, vol. 34, pp. 5–103; January, 1955.

[7] C. G. Montgomery, R. H. Dicke, E. M. Purcell, "Principles of Microwave Circuits," Radiation Lab. Series, vol. 8, p. 459; 1948.

[8] G. L. Ragan, "Microwave Transmission Circuits," Radiation Lab. Series, vol. 9, p. 375; 1948.

[9] M. A. Meyer, H. B. Goldberg, "Applications of the turnstile junction," IRE Trans, vol. MTT-3, pp. 40–45; December, 1955.

which is properly matched, with a signal entering arm 1, and the remaining three rectangular arms terminated in matched loads. The signal will divide at the junction and excite arms 2 and 4 equally and in phase, and will excite the circular arm with a linear TE_{11} mode polarized in the plane of arrow 5. Opposing arms of the junction are isolated from one another (Table I) and thus no power is coupled out arm 3.

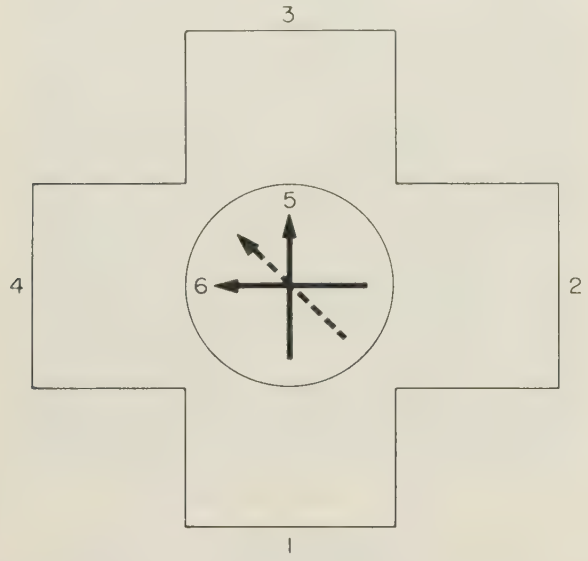

Fig. 2—In the turnstile circulator, polarization 5 is rotated 45 degrees, is reflected, then is rotated 45 degrees further to polarization 6.

After passing up through the 45° Faraday rotator, the component in the circular arm will be polarized at 45° as indicated by the dashed arrow. This component is then reflected by the short circuit back through the Faraday rotator causing an additional 45° rotation, so that the component is now polarized in the plane of arrow 6, at right angles to its original polarization. Ordinarily, on entering the junction, the power in such a component would divide equally but out of phase between arms 2 and 4 (Table II). However, assuming a lossless rotator, the voltage which this component excites in arms 2 and 4 is equal to exactly one-half the input voltage on arm 1. Since the polarization (in 5) has been rotated exactly 90° (to 6) there is no coupling of this component to arms 1 or 3.

By adjusting the position of the short circuit in the circular arm, vector 6 can be so phased at the junction that the *direct* and *reflected* components cancel at arm 4 and add in arm 2. The net result being that all of the power entering arm 1 leaves the junction by arm 2, while arms 3 and 4 are isolated from arm 1. Because of symmetry conditions and by similar reasoning, it should be apparent that a signal entering arm 2 couples only to arm 3, arm 3 couples only to arm 4, and arm 4 couples only to arm 1. This is the characteristic property of a circulator.

If the sense of Faraday rotation is reversed, as by reversing the applied magnetic field, or if the circular arm short circuit is moved a quarter of a wavelength, the order of the indicated coupling relationships will also be reversed. Arm 1 then would couple to arm 4, arm 4 to arm 3, etc.

Signal cancellation in the arm adjacent to the input arm is the result of cancellation between the *direct component* which couples directly from arm 1 to arm 2, and the *reflected component* which travels up and back the length of the shorted circular waveguide arm. It is this differential path length which makes the turnstile circulator frequency sensitive. Obviously, the shorter the circular arm the greater the bandwidth obtainable. In practice it is the physical length of the 45° Faraday rotator which limits the minimum length of the circular waveguide stub. A "turnstile circulator" with a *zero-length* Faraday rotator element need not be frequency sensitive.

Circulator Performance—Theoretical

A number of factors affect performance of the turnstile circulator. These include junction imperfections, rotator loss and mismatch, phase error, and deviation from correct Faraday rotation angle. For simplicity in the discussion which follows, a perfect junction is assumed, the rotator element is reflectionless and lossless, round-trip rotation is exactly 90°, and arms 2, 3, and 4 are terminated in matched loads.

If all voltages are referenced to the point in the turnstile junction at which vector addition of the direct and reflected components takes place, then with an input signal, v, on arm 1 the voltage at the junction terminus of arms 2 and 4 is

$$E_0 = \frac{v}{2} \pm \frac{v}{2} \exp(-j\beta l). \tag{1}$$

βl is the differential path length in radians, β being the effective phase constant, at the operating frequency, of the circular waveguide stub having a round-trip length l.

If l, the total path length in the circular guide is restricted to an integral number, n, of half guide wavelengths ($\lambda_{g0}/2$) at the design frequency, and β is expressed in terms of guide wavelength λ_g at the operating frequency, then (1) can be written

$$E_0 = \frac{v}{2}\left[1 \pm \exp\left(\frac{-j2\pi}{\lambda_g} \cdot \frac{n\lambda_{g0}}{2}\right)\right]. \tag{2}$$

Eq. (2) expresses the variation in outputs of arms 2 and 4 as a function of circular guide wavelength, λ_g. To make (2) more general, let $\lambda_{g0}/\lambda_g = \lambda_g'$, where λ_g' is what may be termed the "normalized guide wavelength." Then, substituting in (2) and expanding,

$$E_0 = \frac{v}{2}(1 \pm \cos n\pi\lambda_g' \mp j \sin n\pi\lambda_g'). \tag{3}$$

Eq. (3) has been plotted in Figs. 3 and 4 for various integral values of n, against the normalized circular guide wavelength, λ_g'. Note that the functions are periodic. Ordinarily, the turnstile circulator is operated in the vicinity of $\lambda_g' = 1$. For a given direction of Faraday rotation, *even* integral values of n place the null in one adjacent arm, while *odd* integral values of n place the

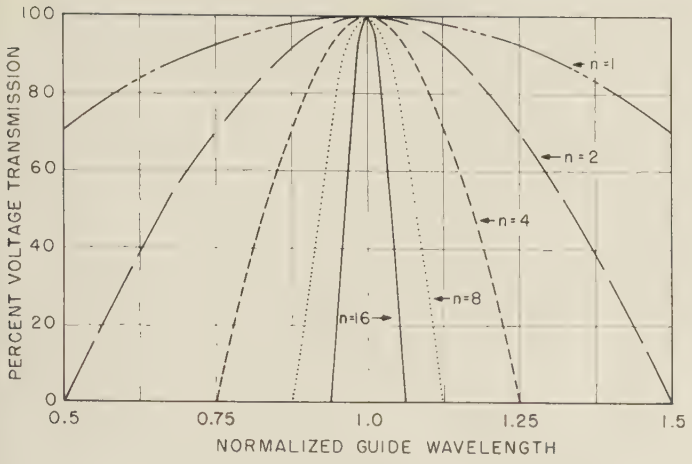

Fig. 3—Forward transmission characteristic of the turnstile circulator for various differential path lengths.

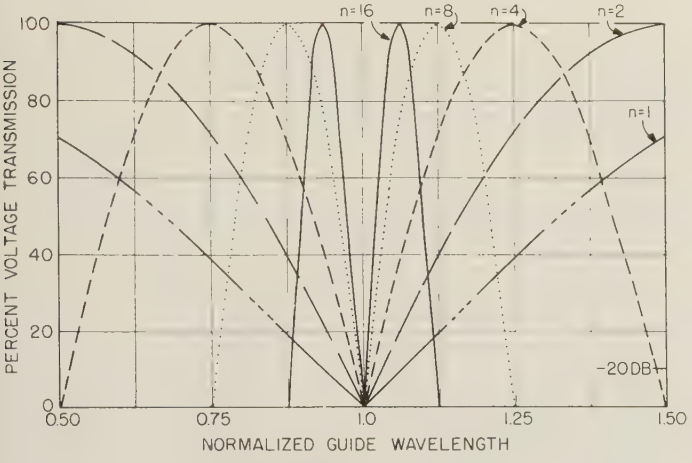

Fig. 4—Reverse transmission characteristic for various differential path lengths.

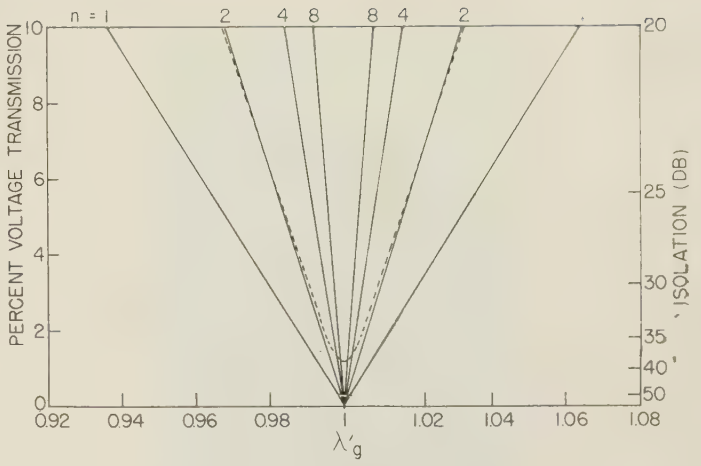

Fig. 5—Reverse isolation characteristic, and effect on isolation of a 0.2 db rotator loss.

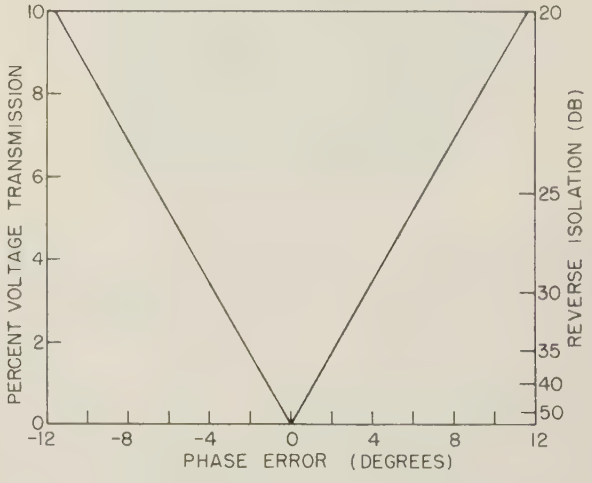

Fig. 6—Reverse isolation as a function of differential phase error.

null in the other adjacent arm. Reversing the direction of Faraday rotation also interchanges the isolated and transmission arms (*i.e.*, it reverses the direction of "circulation").

For small values of E_0 (less than $v/10$), (3) may be simplified and rearranged to

$$\left|\frac{E_0}{v}\right| \sim \frac{|\sin n\pi\lambda_g'|}{2}, \tag{4}$$

and the adjacent arm- or "reverse" isolation can be expressed directly in db.

$$\text{Reverse Isolation (db)} \sim 20 \log \frac{|\sin n\pi\lambda_g'|}{2}. \tag{5}$$

Eqs. (4) and (5) are illustrated in Fig. 5 where E_0 is expressed in per cent voltage transmission (*i.e.*, $100E_0/v$) and is plotted for various values of n against the normalized circular guide wavelength, λ_g'. The right-hand ordinate shows the reverse isolation in db.

The deterioration in reverse isolation (Fig. 5) as λ_g' deviates from unity is of course due to phase error between the direct and the reflected components. The effect of this phase error, ϕ, is expressed more explicitly in (6) and (7), plotted in Fig. 6.

$$\frac{E_0}{v} \sim \frac{\sin\phi}{2} \tag{6}$$

$$\text{Reverse Isolation (db)} \sim 20 \log \frac{\sin\phi}{2}. \tag{7}$$

When there is no rotation error and loss is negligible, these equations are accurate for phase errors as large as ± 12 degrees. Fig. 6 is convenient for determining the phase accuracy required for a desired reverse isolation, and of course applies regardless of n, frequency, or guide wavelength. (*Cross* isolation, on the other hand, is independent of phase error, but is affected by Faraday rotation error. This effect will be discussed later.)

The principal effect of a small amount of loss in the rotator is to reduce the maximum value of attainable reverse isolation. The dashed curve in Fig. 5 shows the effect of a rotator loss of 0.2 db for the case $n=2$. Incidentally, the insertion loss of the circulator is approximately one-half that of the rotator itself.

Bandwidth Determination

To obtain reverse isolation bandwidths of the turnstile circulator explicitly it is necessary to determine the frequencies which correspond to values of λ_g'. Upper and

lower limiting values of λ_g' for various reverse isolations have been computed for $n=1$ and are given in Table III as λ_{g1}', and λ_{g2}'.

TABLE III

Reverse Isolation (db)	λ_{g1}'	λ_{g2}'
20	1.06407	0.93593
30	1.02024	0.97976
40	1.00641	0.99359
50	1.00202	0.99798

$$\left[\lambda_{g1} = \frac{\lambda_{g0}}{\lambda_{g1}'},\ \lambda_{g2} = \frac{\lambda_{g0}}{\lambda_{g2}'}\right].$$

Now, if λ_{g0}, the circular guide wavelength at the design frequency is known, λ_{g1} and λ_{g2} can be determined, and using (8), the upper and lower frequency limits can be found.

$$f = 30\frac{\sqrt{\lambda_c^2 + \lambda_g^2}}{\lambda_c\lambda_g} \tag{8}$$

where f is in kmc, λ_c is cut-off wavelength in cm of the circular waveguide, and λ_g is the wavelength (λ_{g1} or λ_{g2}) in cm in the circular guide at the frequency in question.

For the bandwidths involved, the error is not serious if one considers the reverse isolation bandwidth to vary inversely with n. Thus, one might conveniently solve for bandwidth as above and divide by the value of n for the particular circulator in question.

The db bandwidths for a 15/16″ id circular waveguide have been computed for $n=1$ at a design center frequency of 9375 mc, and making the approximation that the bandwidth varies inversely with n, curves have been plotted in Fig. 7. It can be seen that if a turnstile circulator could be designed with a circular arm as short as $n=1$, then a 20 db bandwidth of 454 mc should be obtained. In practice, however, it may be difficult to realize such a short Faraday rotator. Usable bandwidths are readily obtainable, however, as shown in a later section which describes an experimental model.

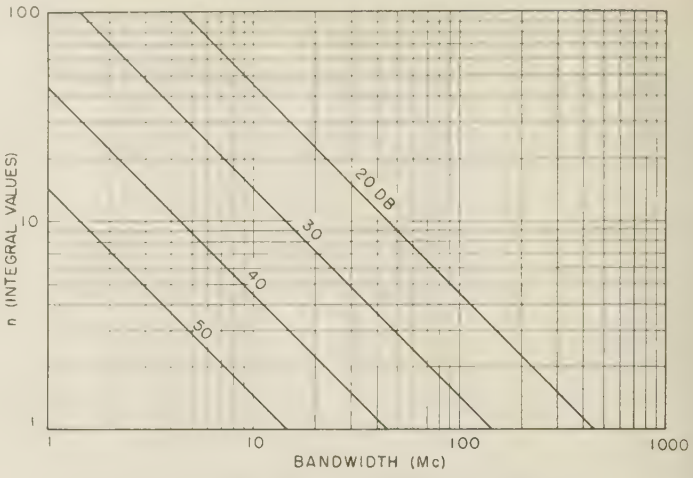

Fig. 7—Reverse isolation bandwidth curves as a function of differential path length.

Effect of Rotation Error

In the foregoing considerations it has been assumed that there was no Faraday rotation error. Now it will be assumed that there is no phase error, and the effect on isolation of rotation error will be considered. In the *ideal* turnstile circulator there is no coupling between opposing rectangular arms, that is, the *cross* isolation is infinite. Any departure from exact 90° total rotation, however, results in a field component in the plane of vector 5 (Fig. 2) which couples to arm 3 causing a deterioration in cross isolation, and to arm 1 causing input vswr to increase. Rotation error also causes a slight reduction in the amplitude of the component in the plane of vector 6 (Fig. 2) which has a secondary effect on the *reverse* isolation of the circulator.

It can be shown that with no other errors, the cross isolation in the turnstile circulator is determined by the Faraday rotation error (*i.e.*, the departure, ψ, from 90°) in accordance with the following expression.

$$\text{Cross Isolation (db)} = 20\log\frac{\sin\psi}{2} \tag{9}$$

where ψ is rotation error, that is, departure from 90° rotation.

Reverse isolation is also affected by rotation error but to a lesser extent as indicated by

$$\text{Reverse Isolation (db)} = 20\log\frac{1-\cos\psi}{2}. \tag{10}$$

It is assumed in (10) that there is no phase or attenuation error.

Eqs. (9) and (10) have been plotted in Fig. 8 to graphically illustrate the relative effect of rotation error on the reverse isolation (curve A) and the cross isolation (curve B). For comparison, curve C indicates the effect of rotation error on reverse isolation in a conventional Faraday rotation circulator, where

$$\text{Reverse Isolation (db)} = 20\log\sin\psi. \tag{11}$$

Ideally, *cross* isolation in the conventional rotation circulator is independent of rotation error.

In the turnstile circulator, if a change in rotation is introduced *after* the phase has been properly adjusted, a phase error may also be introduced which will result in a reverse isolation less than that indicated by (10). Correcting the phase will restore the isolation. This indicates that the proper way to adjust the turnstile circulator for maximum isolations is first to adjust Faraday rotation for best *cross* isolation, and then to adjust phase (circular arm length) for best *reverse* isolation, at the operating frequency.

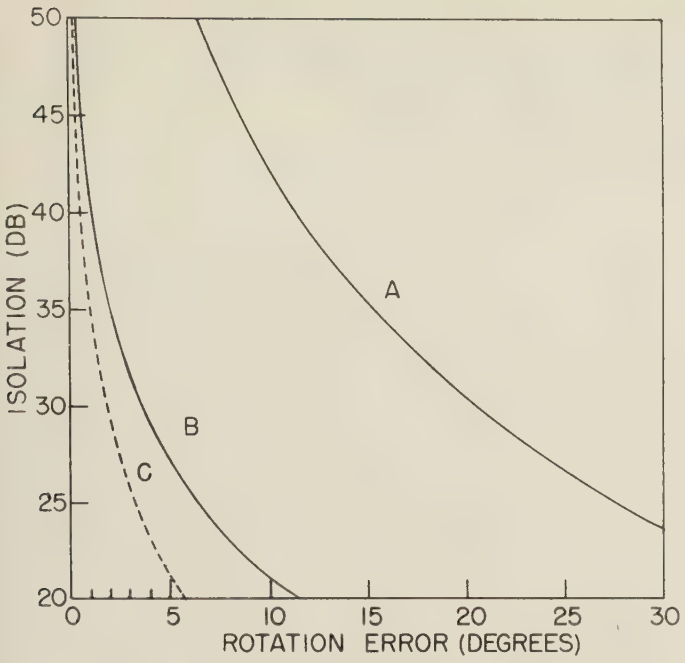

Fig. 8—Effect of rotation error on isolation. A) Reverse isolation. B) Cross isolation. C) Reverse isolation in a conventional rotation circulator.

Experimental Circulator Performance

An experimental turnstile circulator similar to the one pictured in Fig. 9 on the right, has been constructed and its performance measured. The circular waveguide arm had an inside diameter of 15/16 inch and, as determined from experimental measurements, a length of $n=8$. The Faraday rotator was a rod of Ferramic 1331 about one inch long and 7/32 inch in diameter. Polystyrene matching plugs on both ends of the ferrite rod made the unit about two inches long over-all. This was supported in a styrofoam cylinder which fitted the circular waveguide snugly. Magnetic field was applied by an external solenoid. A circular choke plunger was used as an adjustable short circuit.

Optimum adjustment of the circulator at 9375 mc resulted in a maximum cross isolation of 46 db, and a maximum reverse isolation of 46 db. Measured bandwidths were as follows: 20 db, 57 mc; 30 db, 18 mc; 40 db, 5 mc. Assuming n to be 8, these points fall exactly on the curves of Fig. 7, within an experimental measurement error of ± 0.5 mc. In this particular model the circular arm was somewhat longer than that required to accommodate the rotator. Circulator insertion loss was measured as 0.15 db, and input vswr was under 1.05:1 at the design frequency.

Application

Being a frequency-sensitive device, the turnstile circulator is perhaps best adapted to fixed frequency applications where a high performance circulator is required, although it can be made tunable over a wide band. Its relatively economical construction, simplicity, compactness, and convenient terminal arrangement make it acceptable for many circulator applications. The high cross isolation obtainable suggests its value as a duplexer in cw radar applications, for example. The high reverse isolation is of particular value in switching applications such as antenna lobe switching or for signal chopping. It should be pointed out that in this application, as the Faraday rotation passes through zero the cross isolation goes to 6 db and the input vswr goes to 3:1. In pulse systems, these undesirable effects can be avoided simply by synchronizing the switching cycle. The turnstile circulator should be of value in numerous other circulator applications.

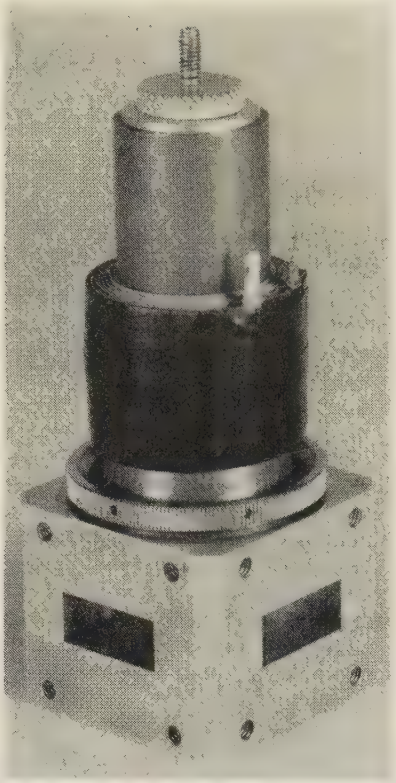

Fig. 9—Experimental X-band model of the turnstile circulator.

Conclusion

The turnstile circulator is a compact, narrow band, high-performance circulator, having convenient terminal arrangement, and since it employs but a single junction is relatively economical to construct. High values of cross and reverse isolation are obtainable in a circulator having very low forward loss. The device is especially well suited to fixed frequency duplexing, isolating, or switching. Although inherently "narrow band," the circulator can be designed to be tunable over a broad band. Average power handling capability is limited by ferrite heating, while peak power capability will be limited either by ferrite saturation effects or by voltage breakdown in the circular waveguide where standing waves occur. Turnstile circulators having low insertion loss and significant isolation bandwidths can be made with commercially available ferrite materials.

Acknowledgment

The author wishes to acknowledge the valuable assistance of R. D. Tompkins, in deriving, computing, and plotting some of the curves used in this paper.

Nonreciprocal Two-Ports Represented by Modified Wheeler Networks*

H. M. ALTSCHULER† AND W. K. KAHN†

Summary—**The extension of the (reciprocal) modified Wheeler network to include the more general nonreciprocal two-port is given. This representation is derived via a known decomposition of the general nonreciprocal network into two portions, one reciprocal, the other nonreciprocal. The reciprocal portion is then taken as the modified Wheeler network. Recombination of the elements results in the desired representation which is constituted of a minimum number, *i.e.*, of eight, passive elements. Each of these is a natural idealization of a physical microwave component. Since six of the elements belong to the class of "bilaterally matched" networks, some of the properties of this class are discussed. Two of the bilaterally matched elements embody the nonreciprocal properties of the network: a one-way attenuator and a one-way phase-shifter. Many of the characteristics of the (reciprocal) modified Wheeler network carry over directly to this nonreciprocal representation. The microwave measurement of the network parameters is also indicated.**

Introduction

A DIRECT extension of a representation of reciprocal two-ports to the case of nonreciprocal two-ports has recently been described by Haus.[1] In his paper he has given the decomposition of the general nonreciprocal two-port into a reciprocal two-port and a nonreciprocal one with certain useful commutation properties. His choice of the Weissfloch network for the reciprocal portion has resulted in essentially two different representations. One of these, consisting of eight elements, is "mixed" in that the elements of the reciprocal portion are expressed in standard impedance (*i.e.*, resistance and reactance) terms, while the nonreciprocal portion is expressed in terms of its *ABCD* coefficients. The other representation indicated employs three gyrators in conjunction with ten impedance parameters and is by comparison with the first representation quite complicated. Clearly these parameters are not all independent of one another. Their interdependence is expressed by relatively complex equations.

What appears to be a more attractive representation, and one more meaningful to the microwave engineer, may be obtained in a manner similar to that employed by Haus, when the modified Wheeler network,[2] instead of the Weissfloch network, is used to represent the reciprocal portion. In that case the nonreciprocal elements which are employed are, with the exception of their "one-way" properties, conceptually similar to the reflection coefficient transformer (or ideal attenuator) and the transmission lines which form part of the reciprocal modified Wheeler network. In this sense the present network representation is "homogeneous." Furthermore, at any single frequency this network is highly suggestive of a procedure for synthesizing a nonreciprocal microwave two-port structure with the properties exhibited by the network. The network consists of the minimum number of elements required to represent a nonreciprocal two-port, *i.e.*, of eight independent elements which are the natural idealizations of physical microwave components.

All but two of the network elements are "bilaterally matched." Hence special attention has been paid to the class of bilaterally matched networks. In particular, a simple multiplication rule for their scattering matrices has been stated which permits the ready manipulation of such elements. Appendix II summarizes the various bilaterally matched elements which are of interest here, together with their scattering matrices and the network symbols used to represent them.

In the evaluation of particular two-ports as components for use in a microwave system, it is pointed to distinguish certain "essential properties" of the component from those which may be adjusted by the addition of lossless reciprocal networks (tuners) at the ports. These "essential properties" of a two-port, dissipation and nonreciprocal behavior, are explicitly exhibited by distinct bilaterally matched elements in the modified Wheeler representation. The ultimate limitations on the performance of a tandem connection of such components may then be inferred by inspection.

As in the case treated by Haus, the measurement of the network parameters here consists of the known measurement of the reciprocal (modified Wheeler) network in conjunction with the measurements necessary to obtain the additional nonreciprocal parameters.

The Ideal Amplifier Phase Shifter

The general linear, nonreciprocal, (not necessarily passive) two-port can always be decomposed[3] into a reciprocal two-port in tandem with a nonreciprocal two-port, as shown in Fig. 1 and (1). (See Appendix I for definitions of *A*, *B*, *C*, *D*).

* Manuscript received by the PGMTT, July 16, 1956. Presented before the National Symposium on Microwave Techniques, Philadelphia, Pa., February 2–3, 1956. The work described in this report was conducted under Contract AF-19(604)-890 sponsored by the AF Cambridge Res. Ctr.

† Microwave Res. Inst., Polytechnic Inst. of Brooklyn, Brooklyn, N. Y.

[1] H. A. Haus, "Equivalent circuit for a passive nonreciprocal network," *J. Appl. Phys.*, vol. 25, pp. 1500–1502; December, 1954.

[2] H. M. Altschuler, "A method of measuring dissipative four-poles based on a modified Wheeler network," IRE TRANS., vol. MTT-3, pp. 30–36; January, 1955; and "Representation and measurement of a dissipative four-pole by means of a modified Wheeler network," IRE TRANS., vol. PGI 4, pp. 84–90; October, 1955.

[3] H. Schultz, "The transformation of the quadripole chain-matrix into diagonal form," *Arch. El. Übertr.*, vol. 5, pp. 257–266; June, 1951.

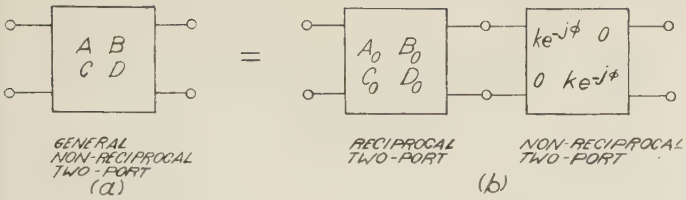

Fig. 1—Decomposition of general two-port.

$$\begin{pmatrix} A & B \\ C & D \end{pmatrix} = \begin{pmatrix} A_0 & B_0 \\ C_0 & D_0 \end{pmatrix} \begin{pmatrix} ke^{-i\Phi} & 0 \\ 0 & ke^{-i\Phi} \end{pmatrix}. \tag{1}$$

While this particular break-up is not the only one possible, it is unique when, in addition, it is required that the matrix representing the nonreciprocal two-port commute with *all* other matrices, *i.e.*, that it be a scalar matrix. It can be seen that this requirement can, in general, be met when one recalls that reciprocal two-ports must obey the condition

$$A_0D_0 - B_0C_0 = 1, \tag{2}$$

and when the matrix representing the general nonreciprocal two-port is decomposed as follows:

$$\begin{pmatrix} A & B \\ C & D \end{pmatrix} = \begin{pmatrix} A_0 & B_0 \\ C_0 & D_0 \end{pmatrix} \begin{pmatrix} ke^{-i\Phi} & 0 \\ 0 & ke^{-i\Phi} \end{pmatrix},$$

where

$$\begin{pmatrix} A_0 & B_0 \\ C_0 & D_0 \end{pmatrix} = \left[\frac{1}{\sqrt{AD - BC}} \begin{pmatrix} A & B \\ C & D \end{pmatrix} \right]$$

$$\begin{pmatrix} ke^{-i\Phi} & 0 \\ 0 & ke^{-i\Phi} \end{pmatrix} = \left[\sqrt{AD - BC} \begin{pmatrix} 1 & 0 \\ 0 & 1 \end{pmatrix} \right]. \tag{3}$$

This decomposition assures that $A_0D_0 - B_0C_0 \equiv 1$ and yields the definition $ke^{-i\Phi} \equiv \sqrt{AD - BC}$. The ambiguity in phase angle introduced by the square root is trivial.

The nonreciprocal two-port defined by the scalar matrix in (3) has been termed[1] "ideal amplifier phase shifter," and in a somewhat different context,[4] "ratio repeater." The scalar matrix $ke^{-i\Phi} \cdot I$ (where I is the unit matrix), of course, commutes with all other matrices. It follows that the ideal amplifier phase shifter represented by it "commutes" with *all* other networks; *i.e.*, its effect on the properties of a cascade of networks is completely independent of its position within the cascade.

For certain ideal or degenerate two-ports the terminal quantities (*e.g.*, V, I or a, b) at the in- and out-ports are not uniquely related. Examples are the one-way line ($S_{21} = 1$, $S_{12} = 0$) and the degenerate two-port consisting of two entirely separate one-ports. Transfer descriptions of such two-ports are singular. In terms of the scattering matrix and the particular transfer description employed (Appendix I) one has generally

$$AD - BC = 0 \qquad \text{if } S_{12} = 0.$$
$$A, B, C, D \text{ do not exist if } S_{21} = 0.$$

The physical content of (3), and the discussions based on it which lead to the extended form of the modified Wheeler network, is preserved by a limiting argument. It is assumed that S_{21} and S_{12} are always finite, no matter how small.

By the application of formulas given in Appendix I, the scattering matrix for the ideal amplifier phase shifter can be shown to be

$$\begin{pmatrix} 0 & ke^{-i\Phi} \\ 1/ke^{-i\Phi} & 0 \end{pmatrix}. \tag{4}$$

This class of two-ports, *i.e.*, those described by scattering matrices with $S_{11} = 0$, $S_{22} = 0$, and their properties are of special interest and consequently discussed below.

Bilaterally Matched Networks

Two-ports characterized by zero values for the coefficients S_{11} and S_{22} are said to be "bilaterally matched." This implies that no reflections arise at the in-port when the out-port is terminated in its characteristic impedance and vice versa. The general (normalized) scattering matrix of this class of networks is given by

$$\begin{pmatrix} 0 & S_{12} \\ S_{21} & 0 \end{pmatrix}, \tag{5}$$

where S_{12} and S_{21} are arbitrary complex numbers. Of course, the ideal amplifier phase shifter is a member of this class [see (4)]. From the well-known input-output (voltage reflection coefficient) relation

$$\Gamma_{in} = \frac{(S_{11}S_{22} - S_{12}S_{21})\Gamma_{out} - S_{11}}{S_{22}\Gamma_{out} - 1}, \tag{6}$$

one sees, by inspection, that for bilaterally matched two-ports

$$\Gamma_{in} = S_{12}S_{21}\Gamma_{out}. \tag{7}$$

In view of the absence of any reflections at their junction, when two such two-ports, say

$$\begin{pmatrix} 0 & S_{12}' \\ S_{21}' & 0 \end{pmatrix} \text{ and } \begin{pmatrix} 0 & S_{12}'' \\ S_{21}'' & 0 \end{pmatrix},$$

are placed in tandem it is recognized that the scattering matrix of the tandem combination is

$$\begin{pmatrix} 0 & S_{12}'S_{12}'' \\ S_{21}'S_{21}'' & 0 \end{pmatrix}.$$

One may then define the following multiplication rule:

$$\begin{pmatrix} 0 & S_{12}' \\ S_{21}' & 0 \end{pmatrix} * \begin{pmatrix} 0 & S_{12}'' \\ S_{21}'' & 0 \end{pmatrix} = \begin{pmatrix} 0 & S_{12}'S_{12}'' \\ S_{21}'S_{21}'' & 0 \end{pmatrix}, \tag{8}$$

where this product, which will be referred to here as "star-product," applies specifically to the scattering matrices of bilaterally matched two-ports which have been placed in tandem. Eq. (8) also implies that any

[4] Harold A. Wheeler, "Generalized transformer concepts for feedback amplifiers and filter networks," Wheeler Monograph no. 5; August, 1948.

bilaterally matched two-port may be arbitrarily decomposed, in accordance with the star-product rule, into two or more bilaterally matched two-ports in tandem. In addition it follows from (8) that all two-ports or network elements in this class commute with each other, *i.e.*, the order of any two or more adjacent bilaterally matched two-ports may be interchanged without affecting the properties of the over-all network.

The (Reciprocal) Modified Wheeler Network

The modified Wheeler network, which is shown in Fig. 2, and methods for its measurement have already

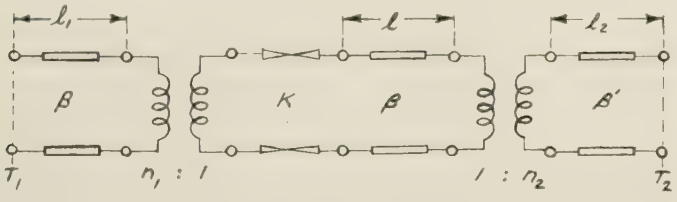

Fig. 2—Modified Wheeler network.

been described in detail elsewhere.[2] This network is a suitable representation of dissipative, *reciprocal*, passive, linear two-ports and consists of three lossless transmission lines l_1, l_2, and l, two ideal transformers $n_1:1$ and $1:n_2$, and a "reflection coefficient transformer" K. The latter element[5] is an ideal attenuator in that its scattering matrix is

$$\begin{pmatrix} 0 & K \\ K & 0 \end{pmatrix}, \qquad 0 \leqq K \leqq 1. \tag{9}$$

The phase constant β of the transmission lines l_1 and l is that associated with the in-port, while β', the phase constant of line l_2, is associated with the out-port. It is also pertinent to point out that the scattering matrix of a lossless transmission line of electrical length θ is

$$\begin{pmatrix} 0 & e^{-j\theta} \\ e^{-j\theta} & 0 \end{pmatrix}. \tag{10}$$

Extension of the Modified Wheeler Network to the Nonreciprocal Case

The method used by Haus[1] in conjunction with the Weissfloch network to represent nonreciprocal two-ports can also be employed advantageously with respect to the modified Wheeler representation. Assuming the network break-up given in Fig. 1 and (1), one may represent the reciprocal two-port by the modified Wheeler network shown in Fig. 2. The ideal amplifier phase shifter ($ke^{-j\Phi}I$) is then commuted to a new position between the elements K and l, and the three bilaterally matched elements (K, $ke^{-j\Phi}I$, l) now located between the two transformers are examined as indicated below in conjunction with Fig. 3.

[5] In terms of the notation used by Altschuler, *op. cit.*, K is defined by $K^2 \equiv |\Gamma_a|$.

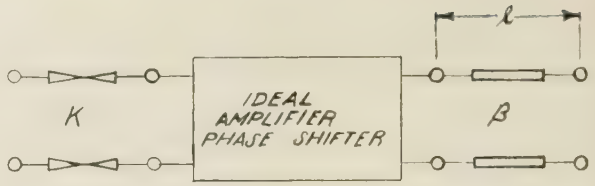

Fig. 3—Three bilaterally matched elements.

The three elements when taken together are represented by the star-product of their scattering matrices, [see (4), (9), and (10)] which when decomposed into a phase and a magnitude portion yields

$$\begin{pmatrix} 0 & Kk \\ K/k & 0 \end{pmatrix} * \begin{pmatrix} 0 & e^{-j(\theta+\Phi)} \\ e^{-j(\theta-\Phi)} & 0 \end{pmatrix}. \tag{11}$$

Since all the dissipation or amplification produced by the over-all network [such as in Fig. 1(a)] is expressed by the magnitude portion of (12), it is required that for *passive* networks this portion alone is also passive, *i.e.*, that the scattering parameters of the magnitude portion are subject to the condition

$$|S_{12}| = Kk \leqq 1 \text{ and } |S_{21}| = K/k \leqq 1. \tag{12}$$

Here K is restricted as indicated in (9) and k may consequently be larger than unity. In any case, one will have either $k \leqq 1$ or $1/k \leqq 1$. One can, therefore, demand a decomposition of the magnitude portion into two parts: one, a reciprocal passive element ($S_{12} = S_{21} \leqq 1$); the other, a nonreciprocal passive attenuator element of such a type that complete transmission takes place in one direction (*i.e.*, either $|S_{12}| = 1$, or $|S_{21}| = 1$). Depending on the magnitude of k one then has

$$\begin{pmatrix} 0 & k^2 \\ 1 & 0 \end{pmatrix} * \begin{pmatrix} 0 & K/k \\ K/k & 0 \end{pmatrix} \text{ for } k \leqq 1. \tag{13a}$$

or

$$\begin{pmatrix} 0 & 1 \\ 1/k^2 & 0 \end{pmatrix} * \begin{pmatrix} 0 & Kk \\ Kk & 0 \end{pmatrix} \text{ for } k \geqq 1. \tag{13b}$$

Analogously, the phase portion of (11) may be decomposed into

$$\begin{pmatrix} 0 & e^{-j2\Phi} \\ 1 & 0 \end{pmatrix} * \begin{pmatrix} 0 & e^{-j(\theta-\Phi)} \\ e^{-j(\theta-\Phi)} & 0 \end{pmatrix} \text{ or} \tag{14a}$$

$$\begin{pmatrix} 0 & 1 \\ e^{j2\Phi} & 0 \end{pmatrix} * \begin{pmatrix} 0 & e^{-j(\theta+\Phi)} \\ e^{-j(\theta+\Phi)} & 0 \end{pmatrix}. \tag{14b}$$

There is little reason to choose one alternative over the other in (14).

It is now seen from (13) and (14) that the elements in Fig. 3 can be represented by the star-product

$$\begin{pmatrix} 0 & k^2 \\ 1 & 0 \end{pmatrix} * \begin{pmatrix} 0 & K/k \\ K/k & 0 \end{pmatrix} * \begin{pmatrix} 0 & e^{-j2\Phi} \\ 1 & 0 \end{pmatrix} * \begin{pmatrix} 0 & e^{-j(\theta-\Phi)} \\ e^{-j(\theta-\Phi)} & 0 \end{pmatrix}, \quad \text{for } k \leqq 1 \tag{15a}$$

or by

$$\begin{pmatrix} 0 & 1 \\ 1/k^2 & 0 \end{pmatrix} * \begin{pmatrix} 0 & Kk \\ Kk & 0 \end{pmatrix} * \begin{pmatrix} 0 & 1 \\ e^{j2\Phi} & 0 \end{pmatrix} * \begin{pmatrix} 0 & e^{-j(\theta+\Phi)} \\ e^{-j(\theta+\Phi)} & 0 \end{pmatrix},$$

for $k \geqq 1$. (15b)

The reciprocal elements ($S_{12} = S_{21}$) of (15) are recognized to be of the form of the elements described by (9) and (10). The remaining elements ($S_{12} = 1$ or $S_{21} = 1$) are "one-way" devices, in particular "one-way attenuators":

$$\begin{pmatrix} 0 & k^2 \\ 1 & 0 \end{pmatrix} \text{ for } k \leqq 1 \quad \text{or} \quad \begin{pmatrix} 0 & 1 \\ 1/k^2 & 0 \end{pmatrix} \text{ for } k \geqq 1, \qquad (16)$$

and "one-way phase shifters"

$$\begin{pmatrix} 0 & e^{-j2\Phi} \\ 1 & 0 \end{pmatrix} \quad \text{or} \quad \begin{pmatrix} 0 & 1 \\ e^{j2\Phi} & 0 \end{pmatrix}. \qquad (17)$$

The associated network symbols, input-output relations, etc., are listed in Appendix II.

Based on the break-up given in (15) passive nonreciprocal two-ports can now be conveniently represented as shown in Fig. 4(a) or 4(b). Here $\theta_1 = \beta l_1$, $\theta = \beta l$, and $\theta_2 = \beta' l_2$. It is recognized that the particular break-up employed is only one of an infinite variety of possible ones; however, it is unique and meaningful in that each of the resulting elements performs a single well-defined function and is described by a single real number. Elements have been chosen in such a manner that (in the case of passive networks) all resulting elements are again necessarily passive. Clearly, when active networks are considered, elements such as "reciprocal amplifiers" or "one-way amplifiers" can be defined. As in the reciprocal case of the modified Wheeler network, all characteristic impedances are normalized to unity and the phase constant of the elements between transformers is arbitrarily assumed to be that associated with the in-port.

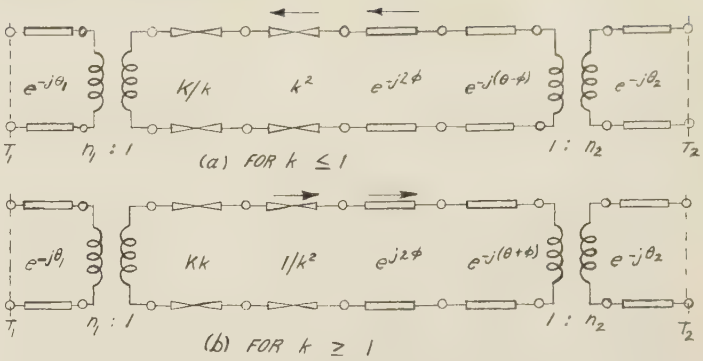

Fig. 4—Extension of the modified Wheeler network to the nonreciprocal case.

Each of the elements employed is particularly significant in context with certain practical microwave-structures in that close equivalences exist as shown in Table I (below). The elements of the network of Fig.

TABLE I

Idealized Element	Component Employed in Realization of Element	Representation of Component
Transmission line	Waveguide	
Ideal transformer	Lossless discontinuity	
Reflection coefficient transformer	Well matched practical attenuator	
One-way phase shifter	Well matched practical nonreciprocal phase shifter	
One-way attenuator	Well matched practical nonreciprocal attenuator	

4 consequently have physical meaning and lend themselves to a procedure for synthesizing physical two-ports with the properties of the network at the given frequency. The fact that the available microwave components are composite of our idealized elements is readily overcome in view of the commutivity of the bilaterally matched elements and the simple computations afforded by the star-product rule.

The break-up given here of the portion of the network between the transformers is to be looked upon as a systematic network description employing ideal elements which are defined in terms of their function and which may serve as a guide to synthesizing two-port structures with the properties of the network at the given frequency. With respect to such "synthesis," it is recognized that the reflection coefficient transformer, for example, must be realized by means of the attenuation of a practical nonreciprocal attenuator in conjunction with the small reciprocal attenuation inherent in such components. Once the present point of view is adopted, it is of course adequate for many purposes to lump the three bilaterally matched elements (in Fig. 3) into a single network. The scattering matrix of this combination is

$$\begin{pmatrix} 0 & Kke^{-j(\Phi+\theta)} \\ K/ke^{-j(\Phi-\theta)} & 0 \end{pmatrix}. \tag{18}$$

The distinction between the "essential properties" of a two-port and those properties which may be altered by the connection of lossless reciprocal networks (tuners) at the in-port and out-port has already been mentioned in the introduction. These "essential properties" are explicitly exhibited by the reflection coefficient transformer, the one-way attenuator and the one-way phase shifter of the modified Wheeler network. In this connection both the forms in Fig. 3 and in Fig. 4 are of interest.

One sees immediately that the nonreciprocal behavior of a two-port is an "essential property." Moreover, when the form of Fig. 3 is employed the net nonreciprocal behavior of any number of arbitrary two-ports connected in tandem may be computed simply by multiplication of the amplifier phase shifters of the individual networks. The dissipation associated with a two-port is also an "essential property" in the following sense: the ultimate gain (minimum attenuation) of a two-port in either direction is that which results from the two dissipative elements in the modified Wheeler representation of Fig. 4. The minimum attenuation which may be achieved through any number of arbitrary two-ports connected in tandem, with tuners at every junction, is directly given by the product of these dissipative elements.

Measurement of the General Nonreciprocal Network

The measurement procedure indicated by Haus[1] holds here also. Briefly, in view of (4) and (7) the input reflection coefficient of the (reciprocal) modified Wheeler network, corresponding to a given termination, is identical to the input reflection coefficient of the general (nonreciprocal) two-port when it is similarly terminated. It follows that the measurement of the general two-port, by impedance techniques as already described elsewhere,[2] will yield l_1, n_1, K, l, n_2, and l_2, the parameters of the (reciprocal) modified Wheeler network.

Assuming that the scattering matrix of the general two-port in Fig. 1 is given by S, that of the nonreciprocal (ideal amplifier phase shifter) portion by S_n, and that of the reciprocal portion by S_r, it is readily shown (by the consideration of incident and reflected waves at the various terminal planes) that the respective mutual elements are related by

$$S_{r_{12}}S_{n_{12}} = S_{12}; \qquad S_{r_{21}}S_{n_{21}} = S_{21}. \tag{19}$$

It follows readily from the fact that $S_{r_{12}} = S_{r_{21}}$, from (19) and from the definition of the amplifier phase shifter, which requires $S_{n_{12}} = 1/S_{n_{21}}$, that

$$S_{n_{12}} = 1/S_{n_{21}} = \pm = \sqrt{S_{12}/S_{21}}. \tag{20}$$

In consequence standard transmission type measurements of S_{12}/S_{21} yield all the additionally necessary information. Defining

$$S_{12} = |S_{12}|\, e^{j\Phi_{12}}, \qquad S_{21} = |S_{21}|\, e^{j2\Phi_{21}} \tag{21}$$

one can readily identify k and Φ in (4) in terms of the measurable quantities as

$$k = \sqrt{|S_{12}|/|S_{21}|}; \qquad \Phi = (\Phi_{21} - \Phi_{12})/2 + n\pi, \quad n = 0, 1. \tag{22}$$

The fact that only the *ratio* of magnitudes and the *difference* between phase angles need be known to obtain k and Φ obviates the necessity for determining the exact values of either magnitudes or phase angles. These quantities evidently need be determined only to within an additive (for the phase angles) or a multiplicative (for the magnitudes) constant so that certain scale or equipment calibrations may be avoided. For measurement procedures see especially Macpherson[6] and also Pippin.[7]

Appendix I

Relationships Between Scattering Matrix and *ABCD* Matrix

The voltages, currents, incident and reflected waves, and matrix elements are defined in the standard manner shown in Fig. 5 where

[6] A. C. Macpherson, "Measurement of microwave nonreciprocal four-poles," Proc. IRE, vol. 43, p. 1017; August, 1955.

[7] J. E. Pippin, "Scattering matrix measurements on nonreciprocal microwave devices," Proc. IRE, vol. 44, p. 110; January, 1956.

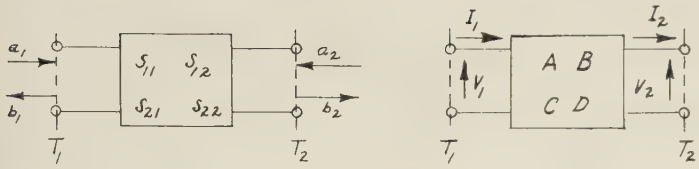

Fig. 5.

$$\begin{pmatrix} b_1 \\ b_2 \end{pmatrix} = \begin{pmatrix} S_{11} & S_{12} \\ S_{21} & S_{22} \end{pmatrix} \begin{pmatrix} a_1 \\ a_2 \end{pmatrix} \qquad \begin{pmatrix} V_1 \\ I_1 \end{pmatrix} = \begin{pmatrix} A & B \\ C & D \end{pmatrix} \begin{pmatrix} V_2 \\ I_2 \end{pmatrix}$$

For reciprocity: $S_{12} = S_{21}$ For reciprocity $AD - BC = 1$

The matrix elements are related as follows:

$$S_{11} = \frac{A+B-C-D}{A+B+C+D} \qquad A = \frac{S_{12}S_{21}+(1+S_{11})(1-S_{22})}{2S_{21}}$$

$$S_{22} = \frac{-A+B-C+D}{A+B+C+D} \qquad B = \frac{-S_{12}S_{21}+(1+S_{11})(1+S_{22})}{2S_{21}}$$

$$S_{12} = \frac{2(AD-BC)}{A+B+C+D} \qquad C = \frac{-S_{12}S_{21}+(1-S_{11})(1-S_{22})}{2S_{21}}$$

$$S_{21} = \frac{2}{A+B+C+D} \qquad D = \frac{S_{12}S_{21}+(1-S_{11})(1+S_{22})}{2S_{21}}.$$

Appendix II

TABLE II

Summary of Bilaterally Matched Elements

Name of Element	Scattering Matrix	Input-Output Relation	Network Symbol	Comments
Transmission Line	$\begin{pmatrix} 0 & e^{-j\theta} \\ e^{-j\theta} & 0 \end{pmatrix}$	$\Gamma_{in} = e^{-j2\theta}\,\Gamma_{out}$	$e^{-j\theta}$	Physical Length of Waveguide is ℓ $\theta = \beta\ell$
One-Way Phase Shifter	$\begin{pmatrix} 0 & 1 \\ e^{-j\theta} & 0 \end{pmatrix}$	$\Gamma_{in} = e^{-j\theta}\,\Gamma_{out}$	$e^{-j\theta}$	Wave Propagating In Direction of Arrow Undergoes Phase Shift; Wave in Opposite Direction Remains Unaltered
One-Way Phase Shifter	$\begin{pmatrix} 0 & e^{-j\theta} \\ 1 & 0 \end{pmatrix}$	$\Gamma_{in} = e^{-j\theta}\,\Gamma_{out}$	$e^{-j\theta}$	
Reflectional Coefficient Transformer (Ideal Attenuator)	$\begin{pmatrix} 0 & K \\ K & 0 \end{pmatrix}$	$\Gamma_{in} = K^2\,\Gamma_{out}$	K	$0 \leq K \leq 1$
One-Way Attenuator	$\begin{pmatrix} 0 & 1 \\ K & 0 \end{pmatrix}$	$\Gamma_{in} = K\,\Gamma_{out}$	K	Wave Propagating In Direction of Arrow Undergoes Attenuation; Wave in Opposite Direction Remains Unaltered
One-Way Attenuator	$\begin{pmatrix} 0 & K \\ 1 & 0 \end{pmatrix}$	$\Gamma_{in} = K\,\Gamma_{out}$	K	
Ideal Amplifier Phase Shifter (Ratio Repeater)	$\begin{pmatrix} 0 & ke^{-j\Phi} \\ 1/ke^{-j\Phi} & 0 \end{pmatrix}$	$\Gamma_{in} = \Gamma_{out}$	$ke^{-j\theta}$ $1/ke^{-j\theta}$	Network is Active In One Direction And Passive in The Other

Criteria for the Design of Loop-Type Directional Couplers for the L Band*

P. P. LOMBARDINI†, R. F. SCHWARTZ†, AND P. J. KELLY†

Summary—**For many years the design of loop type directional couplers has relied heavily on experiment. One of the most common varieties has been the loop coupler much shorter than a wavelength and having a built-in termination (vestigial arm). In this paper the criteria for the design of loop couplers of any length are considered, and their application to either coaxial line or waveguide are discussed. The theoretical basis for design is established by first considering the theory of coupled transmission lines. Several designs which utilize a quarter-wavelength or shorter loops and which have very desirable features with regard to coupling, directivity, and bandwidth are illustrated. Typical performance of couplers having couplings of 20–40 db and directivities of over 30 db are presented.**

Introduction

BY A LOOP type directional coupler is meant a directional coupler consisting of a segment of an auxiliary conductor located within either a coaxial line or a waveguide and brought out through the wall to the desired connectors or terminations. A loop type coupler may be thought of under some circumstances as a prolongation or segment of a secondary transmission line. The plane of the loop is normally approximately parallel to the axis of the main line to which the loop is coupled. All loop type couplers when properly constructed have intrinsic backward directivity; that is, the coupled energy in the secondary line travels in the opposite direction from that taken by the wave in the main transmission line or guide.

Although loop type directional couplers have found wide application for years in the measurement of standing wave ratio, reflection coefficient, and output power on commercial vhf, uhf, and microwave transmitters, their design has been largely an effort of cut-and-try. The literature, which is quite extensive on directional couplers in general, has been rather sparing in telling how one should go about designing loop type directional couplers. In the recent literature, Allan and Curling,[1] Monteath,[2] Oliver,[3] Firestone,[4] Knechtli,[5] and Wolf[6,7] have pointed out a number of features in the analysis and performance of loop type directional couplers. It is the purpose of this paper to bring together a number of these points and present the criteria which must be considered in actual design. It should be pointed out that cut-and-try is not eliminated, but has been given direction.

Several approaches may be used to analyze the loop type coupler. When the loop is of substantial length compared to a wavelength, we may apply the theory of multiconductor transmission lines. As the length of the coupler is reduced we reach a point (around $\lambda/12$) where lumped circuit analysis may be conveniently applied, the parameters of the equivalent circuit being simply related to the distributed parameters of the previous case. The advantage of this lies primarily in the ease of manipulation leading to results which *check* the much more formidable transmission line approach. Finally as the length of the loop is made still shorter, it may be necessary to abandon both approaches due to the difficulty in specifying the parameters.

The Transmission Line Approach

Starting from the well-known concepts of Maxwell's coefficients of capacity, induction, and potential in the case of a system of charged conductors, and their counterparts, the coefficients of self and mutual inductance in the case of a set of current carrying wires, the generalized telegraphers equations for a multiconductor transmission line can be derived. This has been done in a classical paper by Carson and Hoyt,[8] who were primarily concerned with cross talk on telephone lines. Later, Bewley[9] and Pipes[10] again treated the general equations, but from the viewpoint of studying surges on power transmission lines. Recent writers such as Oliver,[3] Knechtli,[5] and Wolf[6,7] treated the equations from the viewpoint of directional coupling effects.

Starting from the concepts cited we are led to the set of differential equations (1) representing the voltage and current situation on two coupled transmission lines

* Manuscript received by the PGMTT, July 16, 1956. Presented before the National Symposium on Microwave Techniques, Philadelphia, Pa., February 3, 1956. This work was done at the Moore School of Elect. Engrg. under AF Contract No. AF 30(635)-2801 with the Rome Air Dev. Ctr., Rome, N. Y.

† Moore School of Elect. Engrg., Univ. of Penn., Philadelphia 4, Pa.

[1] H. R. Allan and C. D. Curling, "The reflectometer," *Proc. IEE*, vol. 96, part III, pp. 25–30; January, 1949.

[2] G. D. Monteath, "Coupled transmission lines as symmetrical directional couplers," *Proc. IEE*, vol. 102, part B, pp. 383–392; May, 1955.

[3] B. M. Oliver, "Directional electromagnetic couplers," PROC. IRE, vol. 42, pp. 1686–1692; November, 1954.

[4] W. L. Firestone, "Analysis of transmission line directional couplers," PROC. IRE, vol. 42, pp. 1529–1538; October, 1954.

[5] R. C. Knechtli, "Further analysis of transmission line directional couplers," PROC. IRE, vol. 43, pp. 867–869; July, 1955.

[6] H. Wolf, "Zur theorie des reflektometers," *Arch. Elect. Ubertr.*, vol. 8, pp. 505–512; November, 1954.

[7] H. Wolf, "Anwendung der theorie des reflektometers," *Arch. Elect. Ubertr.*, vol. 9, pp. 221–227; May, 1955.

[8] J. R. Carson and R. S. Hoyt, "Propagation of periodic currents over a system of parallel wires," *Bell Sys. Tech. J.*, vol. 6, pp. 495–545; July, 1927.

[9] L. V. Bewley, "Traveling Waves on Transmission Systems," (1st ed.), John Wiley and Sons, Inc., New York, N. Y., ch. 6, 1933. (See also 2nd ed., 1951).

[10] L. A. Pipes, "Matrix theory of multiconductor transmission lines," *Phil. Mag.*, vol. 24, pp. 97–113; July, 1937.

with a common return conductor (see Fig. 1). Here V_1 and V_2 are the respective potential differences on the two lines; I_1 and I_2 are the respective currents; C_1, C_2, L_1, L_2 are the self parameters which it may be shown are respectively Maxwell's capacitance coefficients and the coefficients of self inductance; C_{12} and L_{12} are the corresponding mutual parameters.

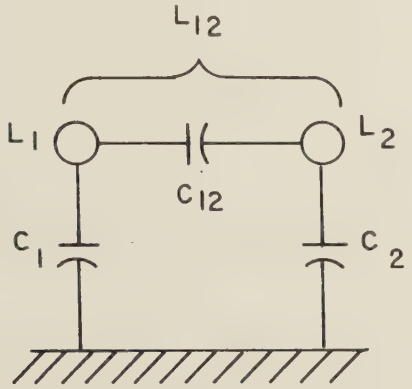

Fig. 1—Geometry of lines described by (1).

$$\begin{aligned}
\frac{\partial V_1}{\partial x} &= -j\omega L_1 I_1 - j\omega L_{12} I_2 \\
\frac{\partial V_2}{\partial x} &= -j\omega L_2 I_2 - j\omega L_{12} I_1 \\
\frac{\partial I_1}{\partial x} &= -j\omega C_1 V_1 - j\omega C_{12} V_2 \\
\frac{\partial I_2}{\partial x} &= -j\omega C_2 V_2 - j\omega C_{12} V_1. \qquad (1)
\end{aligned}$$

The solution of these equations yields not only a pair of forward and backward traveling waves as in ordinary transmission lines, but rather two such pairs (or normal modes) having, at least theoretically, different velocities as shown by (2).

$$\begin{aligned}
V_1 &= A_{11}\epsilon^{-\gamma_1 x} + A_{12}\epsilon^{-j\gamma_2 x} + A_{13}\epsilon^{+j\gamma_1 x} + A_{14}\epsilon^{+j\gamma_2 x} \\
I_1 &= B_{11}\epsilon^{-j\gamma_1 x} + B_{12}\epsilon^{-j\gamma_2 x} + B_{13}\epsilon^{+j\gamma_1 x} + B_{14}\epsilon^{+j\gamma_2 x} \\
V_2 &= A_{21}\epsilon^{-j\gamma_1 x} + A_{22}\epsilon^{-j\gamma_2 x} + A_{23}\epsilon^{+j\gamma_1 x} + A_{24}\epsilon^{+j\gamma_2 x} \\
I_2 &= B_{21}\epsilon^{-j\gamma_1 x} + B_{22}\epsilon^{-j\gamma_2 x} + B_{23}\epsilon^{+j\gamma_1 x} + B_{24}\epsilon^{+j\gamma_2 x}. \qquad (2)
\end{aligned}$$

The values of the new propagation constants γ_1 and γ_2 are defined by (3).

$$\gamma^4 - 2\gamma^2\beta_0^2\left[k_L k_C + 1 + \frac{(h^2-1)^2}{2h^2}\right] + \beta_0^4(1-k_C^2)(1-k_L^2) = 0 \qquad (3)$$

where

$$k_L = \frac{L_{12}}{\sqrt{L_1 L_2}}$$

$$k_c = \frac{C_{12}}{\sqrt{C_1 C_2}}$$

$$\beta_0 = \sqrt{\beta_1\beta_2} = \omega(L_1 C_1 L_2 L_2)^{1/4}$$

$$h = \sqrt{\frac{\beta_2}{\beta_1}}.$$

The constants k_C and k_L are measures of the capacitive and inductive couplings, and a new mean phase constant β_0 and a phase constant ratio h are defined. In general $\gamma_1 \neq \gamma_2 \neq \beta_1 \neq \beta_2$. This concept of multivelocity waves has been mentioned in the literature (*e.g.*, Bewley[9]), but under many conditions, *e.g.*, widely spaced open-wire lines, has been ignored due to the very slight differences between the constants in question.

For most cases β_1 and β_2 do not greatly differ, and under these conditions $\gamma_{1,2}$ is given by (4). This obviously *does not* include cases such as the coupling of a coaxial line with a hollow waveguide.

$$\gamma_{1,2} = \beta_0\sqrt{(1 \pm k_C)(1 \pm k_L)}. \qquad (4)$$

The sixteen integration constants shown previously in the solutions for V and I can be reduced to four, and these four are determined by the boundary conditions. Assuming the condition of (4), a generator voltage of 2 units in line 1, and termination of each line by its characteristic impedance we obtain the results shown in (5a) and (5b).

$$V_F \cong -j\sqrt{\frac{Z_{02}}{Z_{01}}}\sin\left[\beta_0\left(\frac{k_C + k_L}{2}\right)l\right]\epsilon^{-j\beta_0 l} \qquad (5a)$$

$$V_B \cong +\sqrt{\frac{Z_{02}}{Z_{01}}}\left(\frac{k_L + k_c}{4}\right)[1 - \cos(\beta_0(k_C + k_L)l)\epsilon^{-j2\beta_0 l}]. \qquad (5b)$$

The voltages coupled into the secondary line are dependent on the ratio of characteristic impedances, the capacitive and inductive coupling, and the length. Two TEM transmission lines in close proximity have k_C and k_L naturally of the same order of magnitude and of opposite sign. We call the resulting coupling "intrinsic backward coupling." Perfect (∞) directivity occurs when $k_C = -k_L$. This leads to the so-called "characteristic equation" $L_{12}/C_{12} = Z_{01}Z_{02}$. Usually, however, this condition is not obtained exactly, and we have the expressions for directivity and coupling as shown in (6) and (7).

$$C = -20\log_{10}\left(\frac{k_L - k_C}{2}\right)\sin\beta_0 l \qquad (6)$$

$$D = 20\log_{10}\frac{k_L - k_C}{k_L - k_C}\,\frac{\sin\beta_0 l}{\beta_0 l}. \qquad (7)$$

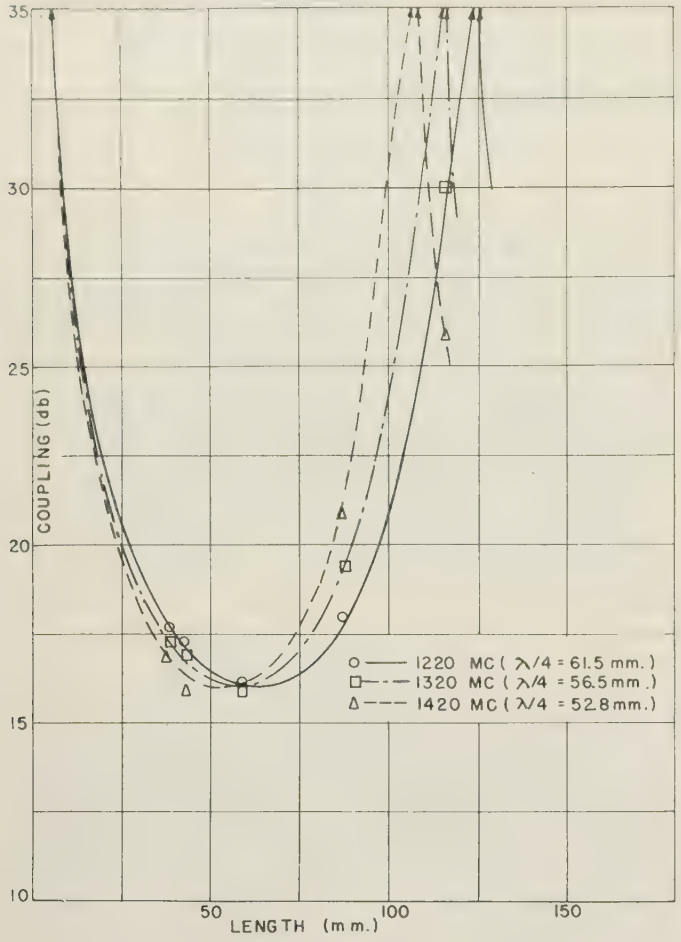

Fig. 2—Variation of coupling with length for a loop coupler (copper strip 9 mm in width penetrating 5 mm into RG-46/U coaxial line).

The coupling varies sinusoidally with length and thus is a maximum when the length of the coupling region or loop is a quarter-wavelength. Experimental verification of this for several frequencies is shown in Fig. 2. It is noted that in accordance with the conventional definition of coupling *a small number of db* means *a larger amount of coupling.*

When the length of the loop is $\frac{1}{4}$ wavelength the coupling is virtually insensitive to frequency. However as the length is reduced toward zero a greater variation is obtained, reaching a maximum slope of 6 db per octave when the loop is very short. This variation of coupling within a typical design band, with physical length is shown in Fig. 3.

The dependence of the directivity on $|k_L/k_C|$ or $|k_C/k_L|$ is shown in Fig. 4. It can be seen that the directivity goes up very rapidly as the condition for perfect equality of $|k_C|$ and $|k_L|$ is approached.

Whether $|k_C|$ or $|k_L|$ is the predominant factor can be determined if the loop is rotatable according to the method described by Allan and Curling.[1]

The directivity and coupling expressions both contain $\sin \beta_0 l$, and $(k_C - k_L)$. Consequently there is an interdependence between them as shown in Fig. 5 where

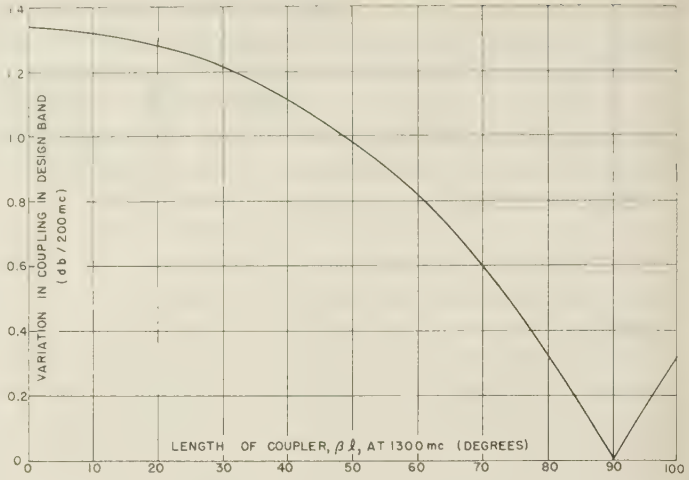

Fig. 3—Variation of coupling within 200 megacycle design band for different coupler lengths.

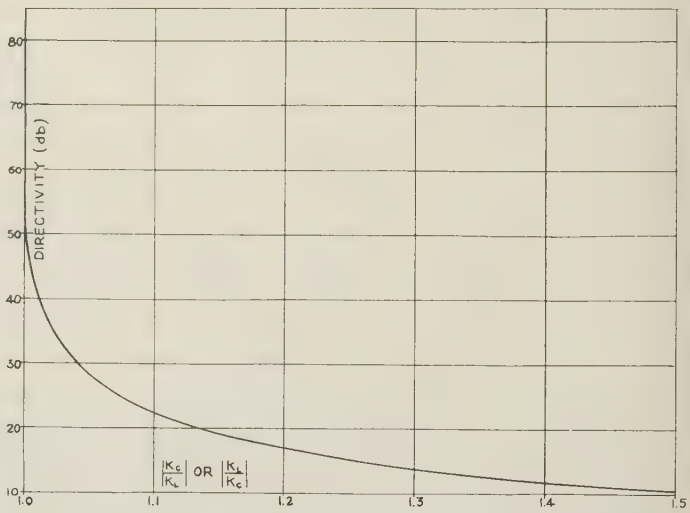

Fig. 4—Dependence of directivity upon $|k_c/k_L|$ or $|k_L/k_c|$ for quarter-wave loop coupler.

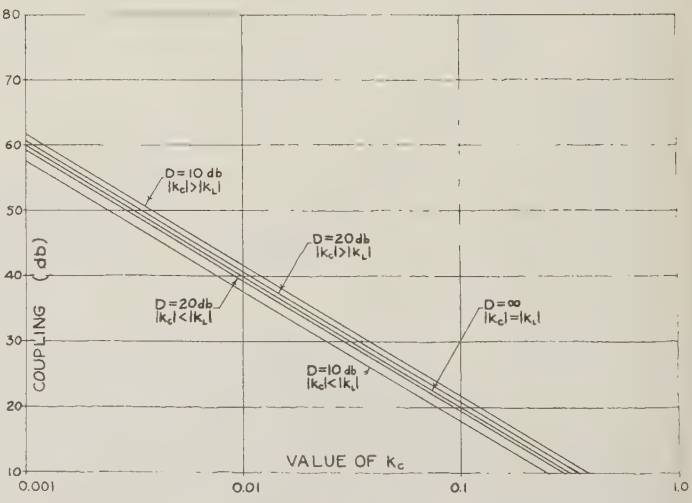

Fig. 5—Dependence of coupling upon k_c for various directivities for quarter-wave loop coupler.

coupling is plotted vs k_c for various conditions of directivity. This graph shows that the same directivity may be obtained for different combinations of k_L and k_C; however these *same* values of directivity yield *different* values of coupling. This curve is useful for estimating the tolerance which must be placed on directivity to ensure coupling within certain limits. It should be noted, however, that it assumes "perfect" termination of the secondary line (vswr <1.02).

Coupler Design for Coaxial Line

In designing directional couplers according to the general concepts outlined above, the principal stumbling block is that k_C and k_L cannot be theoretically predicted with great accuracy for most configurations. Furthermore the condition for $|k_C| = |k_L|$ is met by a number of different combinations of auxiliary conductor size and spacing, each one of which has a different characteristic impedance, and each one of which demands a different termination. Firestone[4] has shown that the termination on line 2 need not necessarily be equal to Z_{02}, but must then have a conjugate relationship to the termination on line 1 if high directivity is to be preserved. In the microwave region good terminations for values other than 50 ohms are not too common; usually also, the main line Z_0 is 50 ohms. This restricts the problem severely, and will be the matter first discussed.

In the necessary empirical part of the problem the first step is to secure a matched auxiliary line (vswr <1.02) when looking into the output terminal, the other end being properly terminated in a "good" termination. When the conductor spacing has been adjusted to give this condition to a given conductor, the coupling and directivity are checked. Then a new combination of conductor size and spacing is tried. In a relatively short time the high directivity needed can be secured. The coupling can then be secured by calculation of the needed length from the formula given. Of course, one is restricted as to the magnitude of coupling one can secure by this means. Fig. 6 shows the configuration and the results of a procedure such as this.

This procedure has been successfully used to design a directional coupler with four outputs as shown in Fig. 7. This device was made for use in an L band system utilizing RG-46/U, $1\frac{5}{8}$ inch, transmission line. The lengths of the loops were chosen to give a series of coupling values between 20 and 30 db. The directivity for each was over 30 db in the range 1200–1400 mc.

For smaller values of coupling (*i.e.*, actually tighter coupling) one must use a higher impedance secondary line requiring usually a vestigial arm (or built-in) termination. The empirical procedure would be much the same, only the condition of match in the secondary line cannot usually be conveniently determined by slotted line methods. It is useful to provide a tuning arrangement on the vestigial arm termination which has the effect of allowing adjustment of the reactance of the load and the loop itself, so that high directivity is obtained. See Fig. 8 for an example.

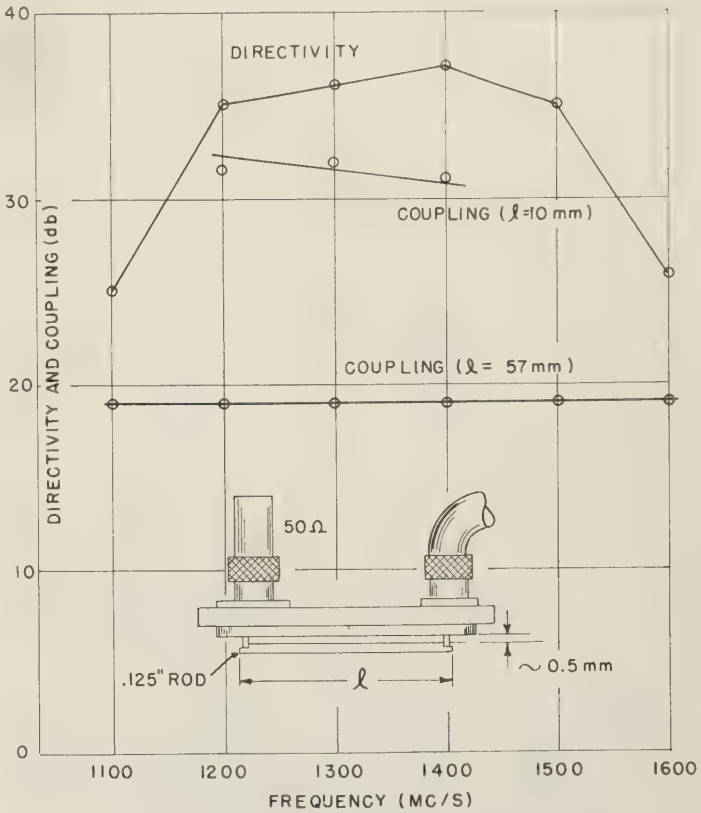

Fig. 6—Directivity and coupling of 50Ω loop type couplers of two different lengths applied to RG-46/U coaxial line.

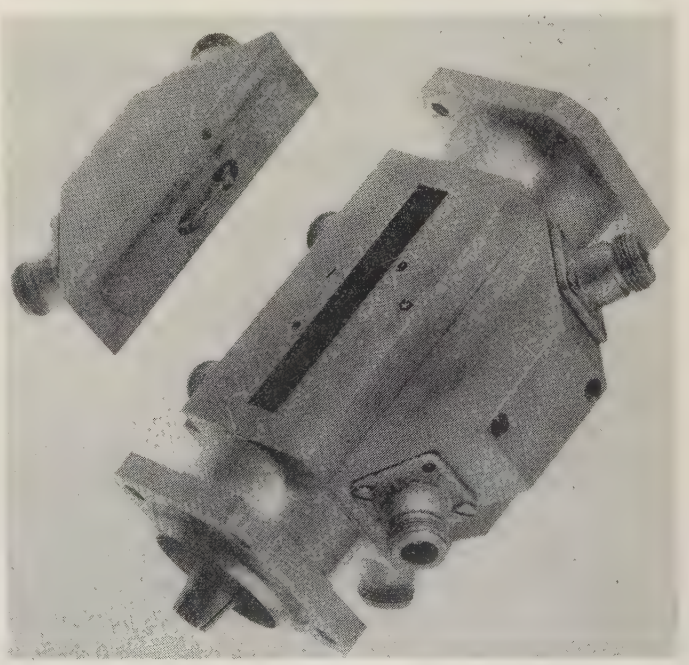

Fig. 7—Four-output directional coupler in RG-46/U coaxial line.

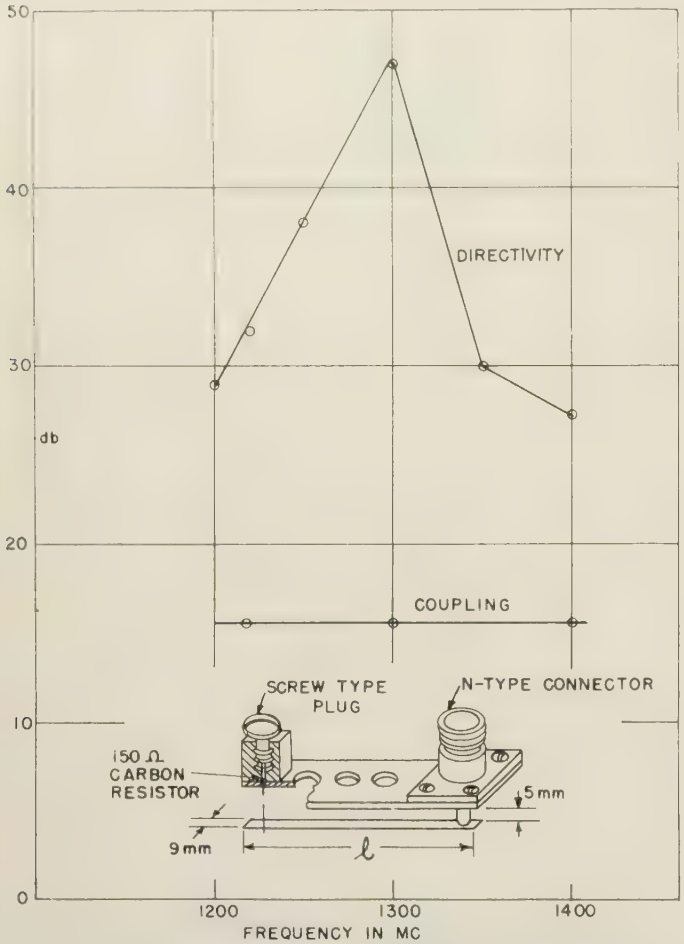

Fig. 8—Performance of quarter-wave loop coupler with vestigial arm termination for RG-46/U coaxial line.

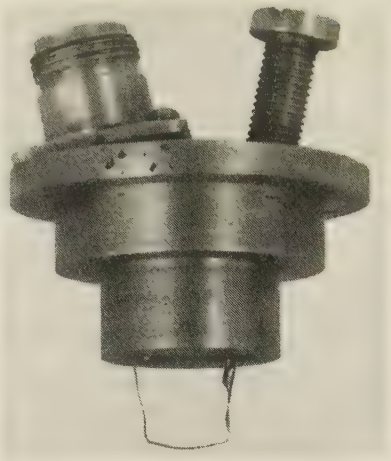

Fig. 9—Vestigial arm loop coupler for RG-69/U waveguide.

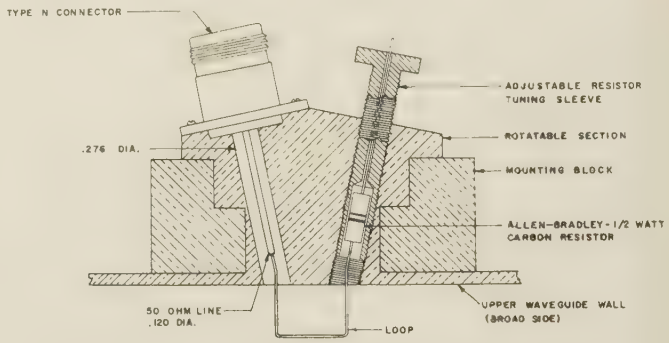

Fig. 10—Constructional details of vestigial arm loop coupler for RG-69/U waveguide.

Waveguide Loop Couplers

The theory of coupled transmission lines laid down above can be applied to the problem of coupling a coaxial line with a waveguide up to a point. However, the fact that the phase velocities in the two media are so different, and the difficulties in suitably defining the parameters of a waveguide, make the further application of the theory impractical.

Exhaustive experiments with coupling a coaxial line "naturally" through the broad wall of rectangular waveguide have shown that "intrinsic backward coupling" occurs for only one condition (extremely loose coupling), and is very frequency dependent due to the dependence of phase velocity upon frequency in the waveguide. This implies that loop couplers in waveguides based upon coupled transmission effects are not very practical.

However, if a very short loop is used, it no longer acts as a transmission line. It may be shown, however, that the perfect directivity condition given previously, *i.e.*, $C_{12}/L_{12}=Z_{01}Z_{02}$ is still valid, although some points of argument can be raised about the proper definition of the quantities involved.

Practically, a vestigial arm type of loop with a tuning device, as previously described, is used. Figs. 9 and 10 show one such coupler which was used in RG-69/U, *L* band waveguide. Each desired value of coupling requires a different area and consequently a different terminating resistance. For each condition selected, the "tuning sleeve" must be adjusted for optimum directivity. By this process fair results for coupling, directivity, and bandwidth were obtained for the L band as shown in Fig. 11.

It was found that a relationship exists between area of the loop and the coupling, nearly independent of the size and type of conductor used. This relation is presented in Fig. 12. The theoretical plot in the figure is obtained through the following approach.

The mutual inductance of a loop in the center of a rectangular waveguide excited in the dominant mode may be written

$$L_{12} = \mu_0 \frac{2A}{al} \tag{8}$$

where A is the area of the loop, a, the broad side of the guide, and l the length of the coupler. In the case of a short loop the coupling parameter will be defined as

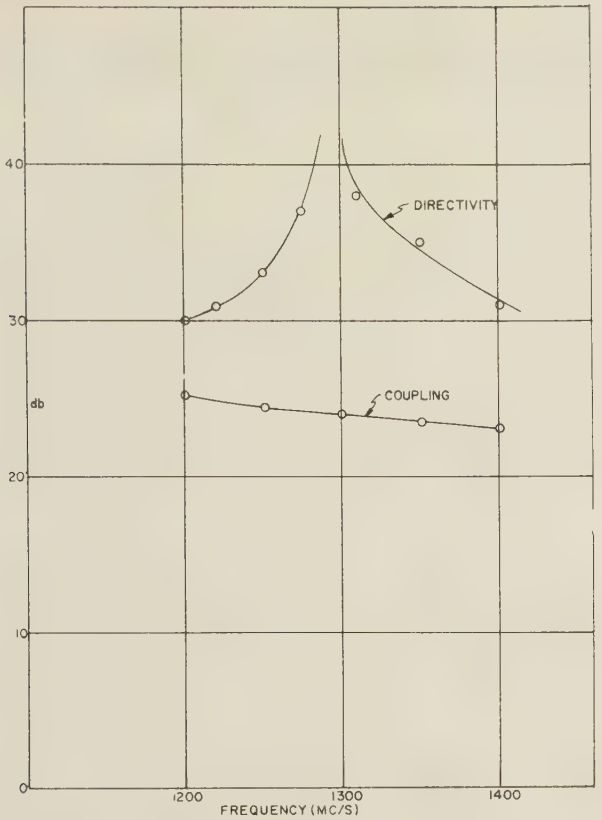

Fig. 11—Performance of vestigial arm loop coupler for RG-69/U waveguide.

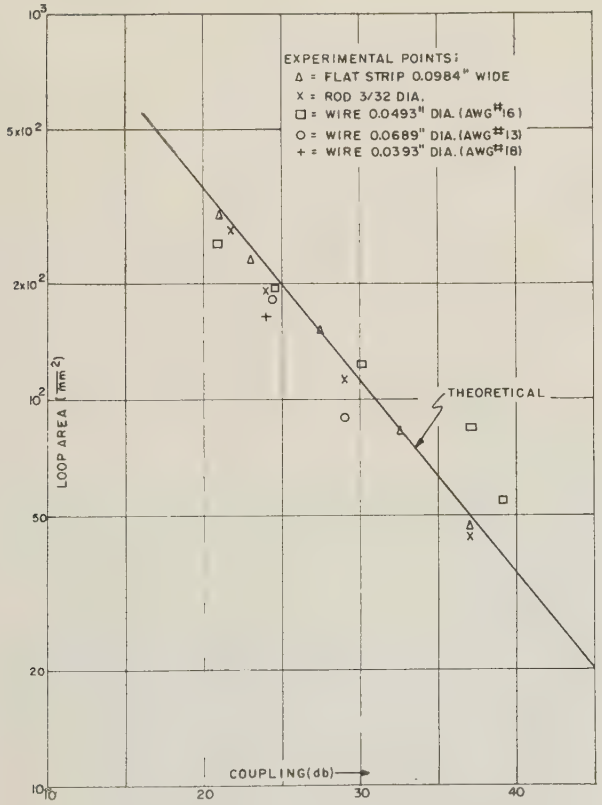

Fig. 12—Loop area—coupling relationship for vestigial arm loop coupler for RG-69/U waveguide. f = 1300 mc.

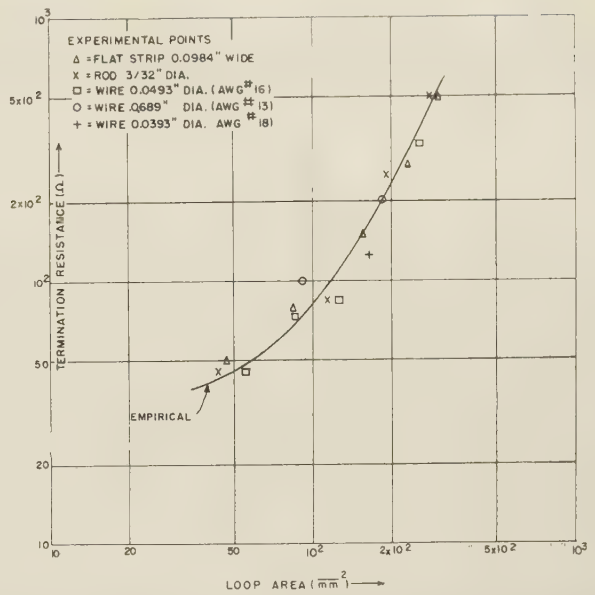

Fig. 13—Necessary loop area—terminating resistance relationship for vestigial arm loop coupler for RG-69/U waveguide. f = 1300 mc.

$k_L = L_{12}/L_1$ where L_1 is the equivalent distributed inductance for unit length of the waveguide which is taken to be

$$L_1 = \mu_0 \frac{2b}{a} \cdot \tag{9}$$

This expression for k_L is the same as that mentioned previously, $k_L = L_{12}/\sqrt{L_1 L_2}$ where $L_2 = L_1$, a condition that appears to be reached by adjustment of the "tuner," provided L_2 is initially large enough. No reason other than the fair agreement shown in Fig. 12 can be given here, for L_2 is neither accurately measurable nor calculable.

Using (6) with $|k_C| = |k_L|$ the coupling is

$$C = 20 \log \frac{b\sqrt{\lambda_g \lambda_0}}{2\pi A} \cdot \tag{10}$$

Eq. (10) is plotted in Fig. 12, for an RG-69/U waveguide, and a frequency of 1300 mc.

Each value of area selected demands a unique value of terminating resistance for preservation of good directivity. The empirical relationship is shown in Fig. 13.

When designing an L band loop coupler, use may be made of Figs. 12 and 13. For any required value of coupling, Fig. 12, or (10), gives the area of the loop to be used. Entering the curve of Fig. 13 with the above area, an indication of the order of magnitude of the resistor to apply in the vestigial end of the coupler is obtained. Note that the resistor should be "tuned" in the receptacle; *i.e.* the distances of the resistor with respect to the short-circuit, and of the plunger with respect to the loop (Fig. 10) should be chosen so as to have a maximum of directivity and bandwidth.

Improved Rectangular Waveguide Resonance Isolators*

MAX T. WEISS†

Summary—**The early resonance isolators, using nearly full waveguide height ferrite slabs, gave a high reverse loss per unit length but a disappointingly low reverse-to-forward loss ratio. By substantially reducing the height of the ferrite slabs, the reverse-to-forward loss ratio can be increased at the expense of reverse loss per unit length. More recently, it has been found that the addition of certain dielectric loading in rectangular waveguide resonance isolators results in generally improved performance. Thus, the reverse-to-forward loss ratio of these isolators is high (150 to 1 at X band) and the reverse loss per unit length is also high (20 db/inch at X band). The broad-banding problem will also be briefly discussed.**

Introduction

With the realization of nonreciprocal behavior of ferrites in rectangular waveguides[1] several years ago, it had been expected that the resonance isolator would prove to be a simple and effective device. It was indeed simple since it merely involved the placing of a thin ferrite slab in a rectangular guide, as shown in Fig. 1, and the application of magnetic field sufficient to give ferromagnetic resonance at the operating frequency. However, it was not very effective, with the best backward-to-forward loss ratio in db being only about 20 to 1. For a thick ferrite slab, the forward loss would be expected to be larger since not all of the ferrite can be at the point of pure circularly polarized rf magnetic field. The early work of Fox[2] on resonance isolators showed, however, that making the ferrite slab thin did not entirely eliminate the presence of considerable forward loss. It was further observed that for ferrite slabs extending completely from top to bottom of the waveguide, the back-to-forward ratio was much poorer than for ferrite slabs with heights substantially less than the full waveguide height.

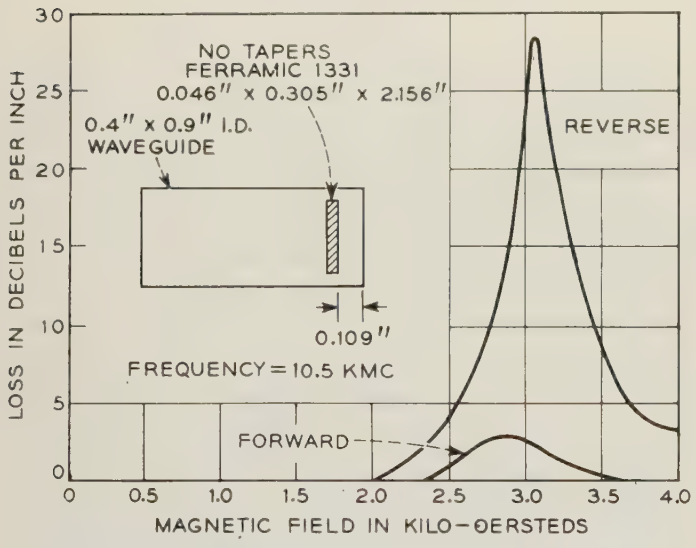

Fig. 1—Performance of an early resonance isolator.

H-Plane Ferrite Slab Isolator

Recently, reduction of the height of the ferrite slab has been carried to a successful extreme in commercial high power resonance isolators. In these isolators the ferrite slabs are placed in the *H*-plane on the top and bottom walls of the waveguide as shown in Fig. 2. This not only permits better heat dissipation for high power applications, but also results in better performance. The data taken by us of forward and reverse loss as a function of applied magnetic field for this configuration are also shown in Fig. 2 for 10.5 kmc operation. It is seen that at a field of 4800 oersteds, the reverse loss is 29 db with a forward loss of less than 0.4 db, giving a ratio of about 75 to 1. The side wall to ferrite spacing for the above isolator was found not to be too critical with results remaining substantially the same for spacings varying between 0.100 inch and 0.120 inch.

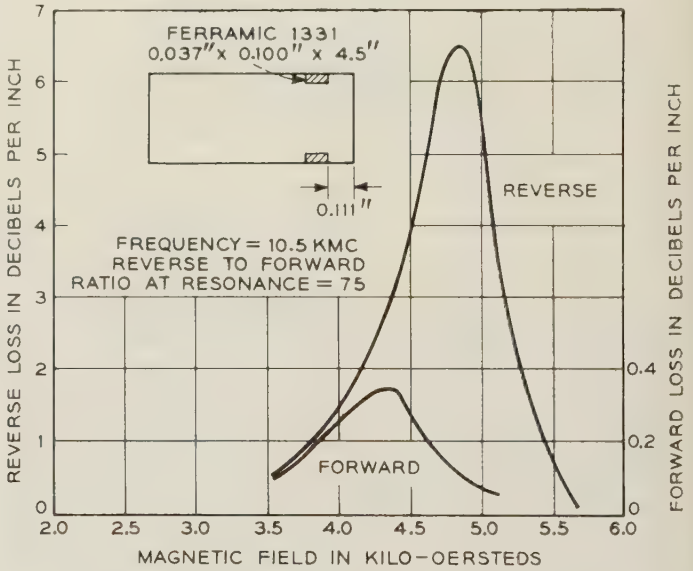

Fig. 2—Performance of an *H*-plane resonance isolator.

* Manuscript received by the PGMTT, July 16, 1956. Presented before the National Symposium on Microwave Techniques, Philadelphia, Pa., February 2–3, 1956.

† Bell Telephone Labs., Inc., Holmdel, N. J.

[1] N. G. Sakiotis and H. N. Chait, "Properties of ferrites in waveguides," IRE Trans., vol. MTT-1, pp. 11–16; November, 1953.

[2] A. G. Fox, S. E. Miller, and M. T. Weiss, "Behavior and applications of ferrites in the microwave region," *Bell Sys. Tech. J.*, vol. 34, pp. 5–103; January, 1955.

The above results for the H-plane isolator are to be compared with the results for the more usual type of E-plane isolator shown in Fig. 1, with a reverse-to-forward loss ratio of only about 10 to 1. Although better ratios have been obtained with lower saturation ferrites, these ratios never exceeded about 25 to 1.

The improved performance of the H-plane isolator is obtained, however, at the expense of several disadvantages. Not only is the magnetic field strength required higher (4.8 kilo-oersteds as compared to 3 kilo-oersteds) but the magnetic field must be applied over a larger volume. The high field requirement is due to the high dc demagnetizing factor for the H-plane configuration. Furthermore, the reverse loss per unit length of isolator is much smaller: only about 6.5 db/inch compared to 29 db/inch for the E-plane isolator.

Ferrite-Dielectric Isolator

In order to increase the reverse loss/unit length for the H-plane isolator, high dielectric constant material was added to the ferrite, as shown in Fig. 3. The purpose

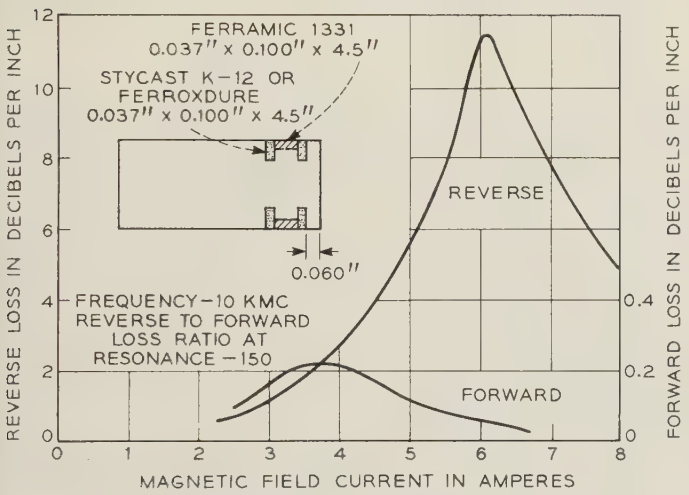

Fig. 3—Performance of an H-plane ferrite-dielectric resonance isolator.

of the dielectric was to concentrate more of the rf energy near the ferrite and to eliminate edge effects. The dielectric used was Stycast K-12 having a dielectric constant of 12 manufactured by Emerson and Cuming of Canton, Mass. Ferroxdure is also satisfactory since it has a high dielectric constant with an rf permeability of very nearly unity at frequencies below 24,000 mc. It is seen that the reverse loss for this configuration has increased from 6.5 db/inch to over 11 db/inch, while the forward loss actually decreased somewhat, thus resulting in increasing the reverse-to-forward loss ratio to 150 to 1.

Split-Ferrite E-Plane Isolator

In order to reduce the applied magnetic field strength required to produce resonance, one must go back to the E-plane type of isolator, which has a much lower dc demagnetizing factor and smaller air gap as shown in Fig. 4. As one can see, the magnetic field requirement is reduced to 3400 oersteds, but with no dielectric loading, the loss per inch is only 8 db, while the ratio is 60.

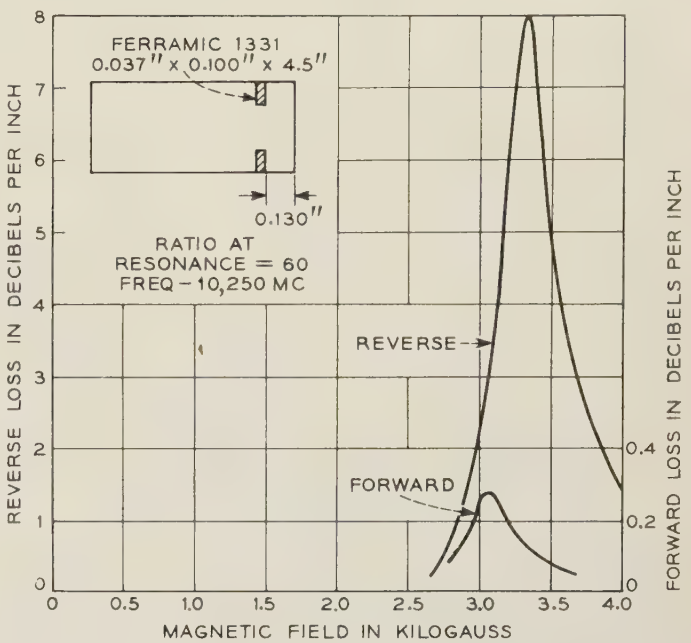

Fig. 4—Performance of a split-ferrite E-plane isolator.

To increase the reverse loss per unit length value as well as to improve the reverse-to-forward loss ratio, one can add Stycast on both sides of the ferrite as shown in Fig. 5. For this configuration the magnetic field require-

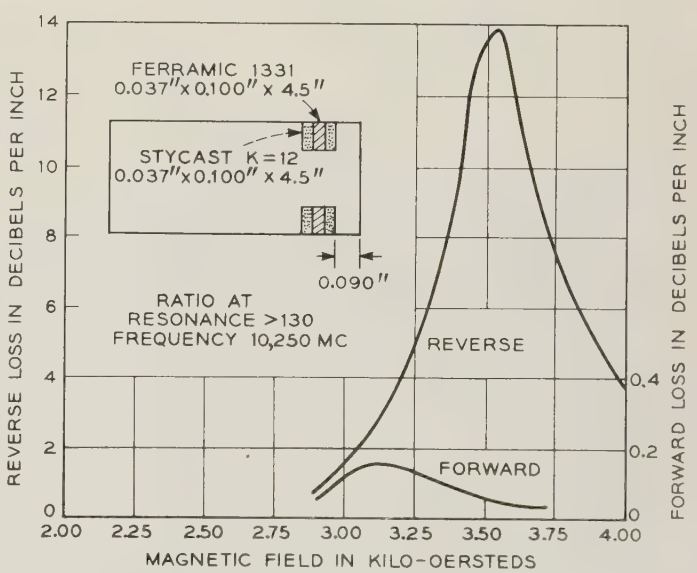

Fig. 5—Performance of a split-ferrite and dielectric E-plane isolator.

ment is 3500 oersteds, the reverse-to-forward loss ratio is better than 130 to 1, while the peak loss has risen to about 14 db/inch. One gets similar results by placing all the Stycast on one side, as shown in Fig. 6.

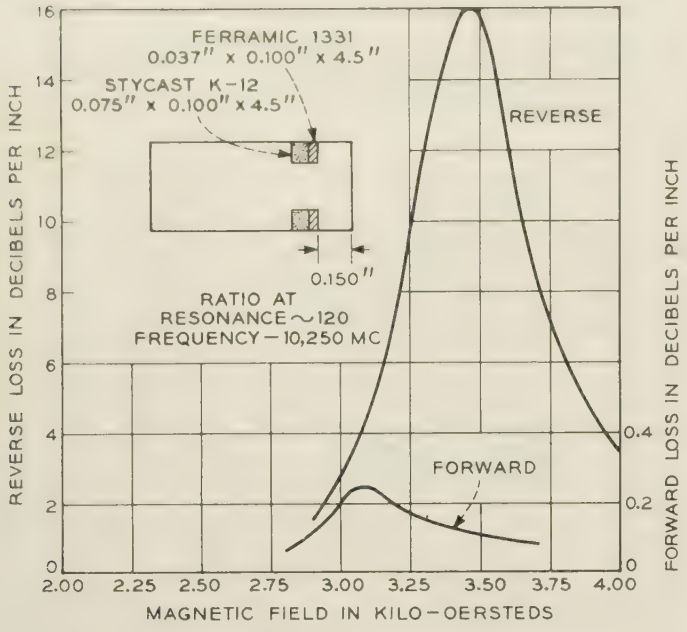

Fig. 6—Performance of a split-ferrite *E*-plane isolator with all the dielectric on one side.

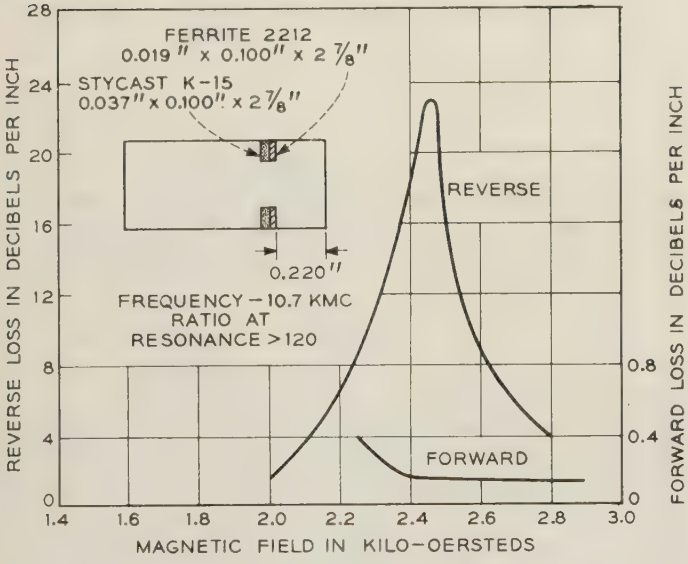

Fig. 7—Performance of a dielectric and split-ferrite *E*-plane isolator using a high saturation magnetization ferrite.

In order to reduce further the magnetic field requirement, a high saturation ferrite (No. 2212 produced by L. G. Van Uitert of the Metallurgical Research Department) having a saturation magnetization of about 4500 gauss was used. Experiments showed that this material required a higher dielectric constant material for dielectric loading and therefore Stycast K-15 with $\epsilon = 15$ was used. It was also found that best results were obtained with the Stycast on only one side of the ferrite, as shown in Fig. 7. The magnetic field requirement dropped to 2500 oersteds, the peak loss for a $2\frac{7}{8}$ inches sample was over 70 db, giving a loss per inch of over

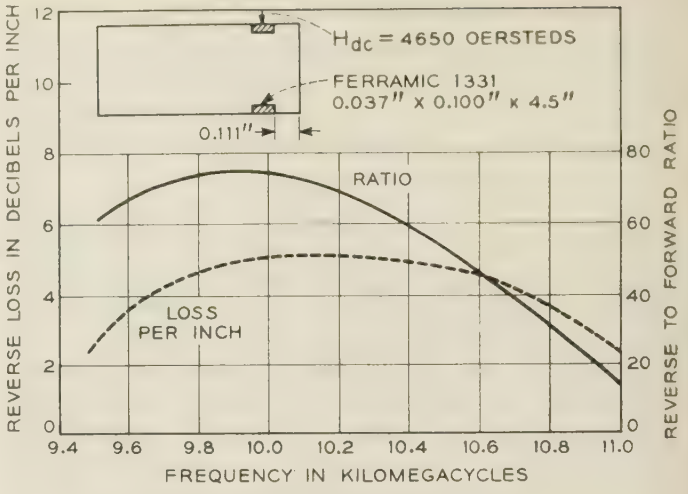

Fig. 8—Frequency response curves for the *H*-plane isolator of Fig. 2.

23 db. The forward loss also remained quite low at about 0.25 db. However, Stycast K-15 appears to have an appreciable dielectric loss, so that the total forward loss was about 0.5 db, resulting in a reverse-to-forward ratio of about 140 to 1.

Broad-banding Problems

Since the peak resonance loss in a ferrite occurs at increasing values of applied magnetic field for increasing operating frequencies, it is evident that a resonance isolator is not inherently a broad-band device. Fig. 8 is a plot of reverse loss/inch and reverse-to-forward loss ratio as a function of frequency over a 9.5 kmc to 11 kmc band for an *H*-plane ferrite slab isolator. It is seen that between 9.65 and 10.65 kmc the loss/inch remains above 4 db while the reverse-to-forward loss ratio remains above 40 to 1.

Fig. 9 shows similar curves for a split ferrite *E*-plane isolator using Ferramic 1331. Although these curves are much more peaked, this configuration still gives substantially better over-all performance over the 9.5 to 10.4 kmc region. The frequency response curves for an isolator using Ferrite 2212 are shown in Fig. 10 for the 11 kmc band. In all of the above isolators the applied magnetic field was chosen to give equal loss/inch values at the two ends of the band. Over narrower bands, one could obtain better results by choosing appropriate applied fields.

An attempt to improve the broad-band performance of a Ferrite 2212 isolator was made by using different thicknesses of ferrite for the top and bottom slabs as shown in Fig. 11. With a top slab thickness of 0.016 inch and a bottom slab thickness of 0.019 inch, the resonance curve of loss vs applied field became double peaked. The resulting reverse loss and reverse-to-forward loss ratio as a function of frequency over a 10.7 kmc to 11.7 kmc band is shown in Fig. 11. As can be

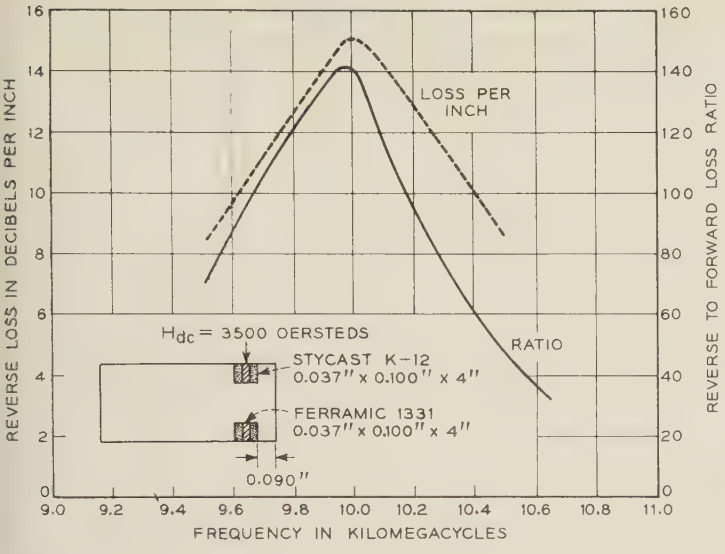

Fig. 9—Frequency response curves for a split-ferrite and dielectric E-plane isolator.

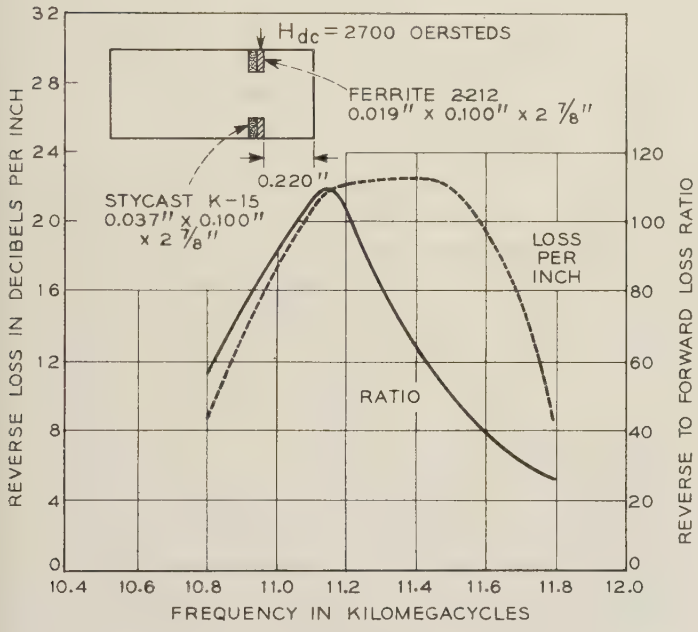

Fig. 10—Frequency response curves for a split ferrite and dielectric E-plane isolator.

seen, these curves are substantially flatter than those shown in Fig. 10 where no attempt was made to broad-band the device.

Other possible broad-banding schemes might include

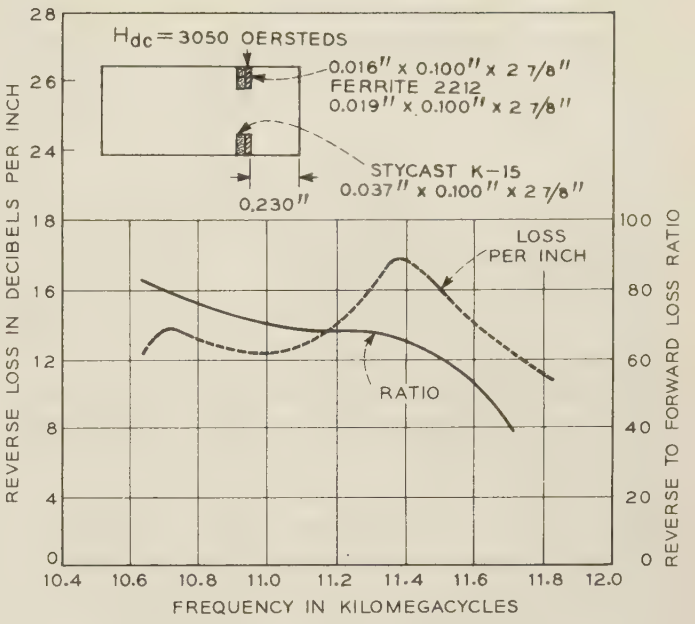

Fig. 11—Frequency response curves for a split-ferrite isolator constructed with different ferrite thicknesses on top and bottom.

tapering of the ferrite slabs, tapering of the magnetic field by means of tapered pole faces, using different types of ferrite, or using different thicknesses and heights of ferrite in tandem. Some of these schemes have been investigated, but all require substantial development time for improved results.

Explanation

A theoretical explanation for the improved performance of the dielectric loaded resonance isolators which have been described is not possible at present, since even a good qualitative theory appears to be extremely difficult to formulate for the ferrite configurations used. One can, however, say that the dielectric loading causes the electromagnetic energy to concentrate in the ferrite, thus increasing the loss per unit length in the reverse propagation direction. One could also use a qualitative perturbation argument to explain the excellent reverse-to-forward loss ratios obtained. These perturbation arguments can show that the dielectric loading causes the rf magnetic field to be circularly polarized over a wider cross-section of the waveguide. However, it seems to me that perturbation theory is not quite valid when ferrites are operating near resonance.

An Automatic Gain Control System for Microwaves*

JORGEN P. VINDING†

Summary—This paper describes a system which can keep the power level in a microwave set-up constant with good accuracy in spite of variations of the input power level.

The system uses a variable attenuator based on the Faraday rotation in magnetized ferrite and thereby achieves a frequency response up to about 500 cps with the present equipment and much better potential response.

Variations in input power are reduced by a factor varying from 10 to 400 depending on available power and on the detector used to detect the output power.

IN ORDER to keep the power level in a microwave set-up constant with good accuracy, it is necessary to have a system consisting of three parts.

1) A sensing element.
2) A control element.
3) A comparator and amplifier element which detects changes in the output from the sensing element and feeds an error signal back to the control element.

In the *X*-band system to be described here, the sensing element is a standard crystal detector, the control element is a ferrite modulator—the Gyraline R-920 NA—and the comparator-amplifier is a special unit made for this application.

Fig. 1 shows a block diagram of the set-up. The output voltage from the crystal is compared to a reference voltage, the difference is amplified and the output current controls the attenuation introduced by the Gyraline. The stabilization factor or loop gain is then determined by the components used and also by the level of the microwave power. Loop gain $= P_1/P_2 + P_2 \times S \times A \times M$ where

P_1 = input power in μW,
P_2 = output power (regulated) in μW,
$a = P_1/P_2 = a(ig)$ = attentuation of Gyraline,
ig = Gyraline current in mA,
S = detector sensitivity in $mV/\mu W$,
A = amplifier gain in mA/mV,
$M = da/di_g = M(ig)$ = slope of attenuation characteristic.

The system in its present form uses the Gyraline R-920 NA as a control element in spite of the rather poor modulation frequency response of this unit, because this Gyraline combines a very good sensitivity M with a microwave characteristic that covers the whole *X*-band.

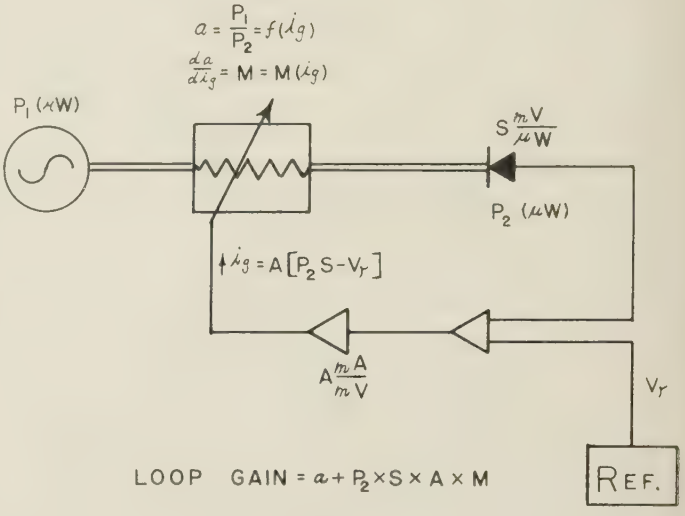

Fig. 1.

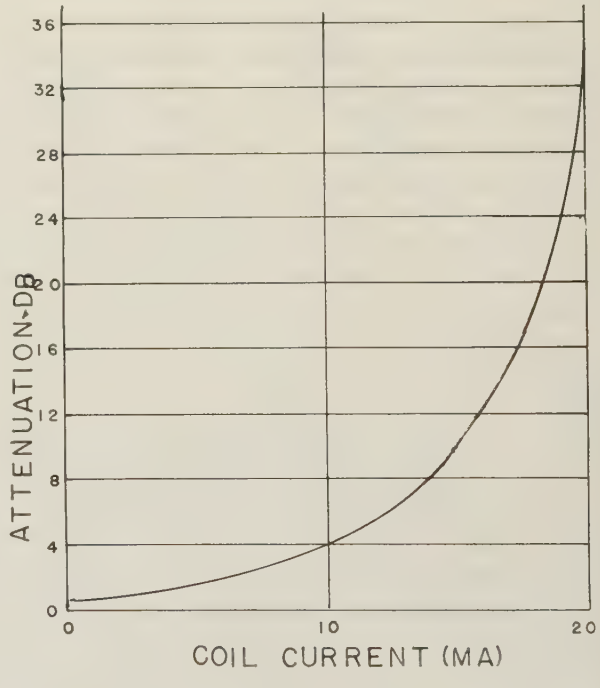

Fig. 2.

The Gyraline is a microwave variable attenuator using the Faraday rotation in magnetized ferrite. This type of unit has been described in several places so that only an outline of the principle is required here. The rectangular waveguide is coupled to a circular guide excited in the TE_{11} mode; a rod of ferrite in the center of the waveguide will rotate the plane of polarization so

* Manuscript received by the PGMTT, July 16, 1956. Presented before the National Symposium on Microwave Techniques, Philadelphia, Pa., February 2–3, 1956.

† Cascade Research Corp., Los Gatos, Calif.

that only a part of the power can be accepted by the rectangular output waveguide while the rest is dissipated in an absorber, the angle of rotation and therefore the attenuation depending on the magnetic field applied to the ferrite. In the Gyraline this magnetic field is supplied by a coil wound around the waveguide so that the attenuation is determined by the coil current. Fig. 2 shows a typical characteristic for Gyraline R-920 NA. In this Gyraline the coil has a very high number of turns which gives a good sensitivity but also a high inductance with corresponding poor response at high frequencies. Fig. 3 shows the frequency response of the R-920 NA and it is seen that the 3 db point is around 110 cps.

If a better response is required, it would be possible to use a less sensitive Gyraline, such as the R-920 or R-920 HF, which have 3 db points at 3 kc and 50 kc, respectively, but the stabilization factor would then be reduced by a factor of 6 and 30, respectively. However, even the present system has a response much faster than anything possible with mechanical attenuators.

Fig. 4 shows a block diagram of the comparator-amplifier unit or agc amplifier. The incoming dc voltage is compared to a reference voltage and the difference voltage is fed to a crystal chopper driven from a square wave oscillator. The resulting ac signal is amplified and rectified in a synchronous rectifier which, in turn, drives the dc output amplifier. This system reduces drift of the amplifier to a negligible value but also introduces some problems of its own, mainly the need for filtering between the rectifier and dc amplifier, which necessarily gives phase shift and therefore must be closely controlled to insure the stability of the whole system.

In order to give this filtering and also to compensate to some extent for the poor response of the Gyraline, a filtering network was built around the dc amplifier so that the chopper frequency 3 kc is attenuated more than 40 db while the over-all system has a reasonably flat response up to 500 cps which was thought to be be sufficient for most applications; *e.g.*, a bwo covering the *X* band with 30 sweeps per second.

The agc system described here uses a standard crystal detector as the sensing element because this is the most sensitive, but for some applications where the microwave frequency is swept over a wide range, the available crystal detectors have too wide variation in sensitivity—a variation that will not be counteracted by the agc because it will try to keep the dc output from the detector constant even if this requires the microwave power level to vary. In such cases, the input comparator must be modified to work with a barretter or thermistor, *e.g.*, in a bridge set-up where the feed-back through the Gyraline tends to make the bridge self-balancing, but this would require a redesign of the input and would probably be far less sensitive, *i.e.*, a good stabilization could only be achieved at much higher power levels.

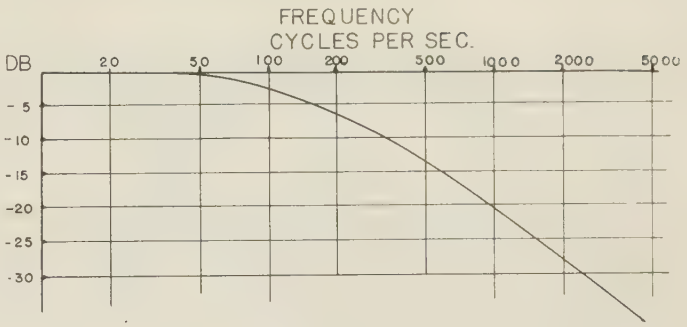

Fig. 3.

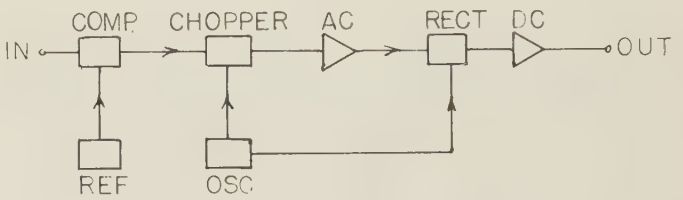

Fig. 4.

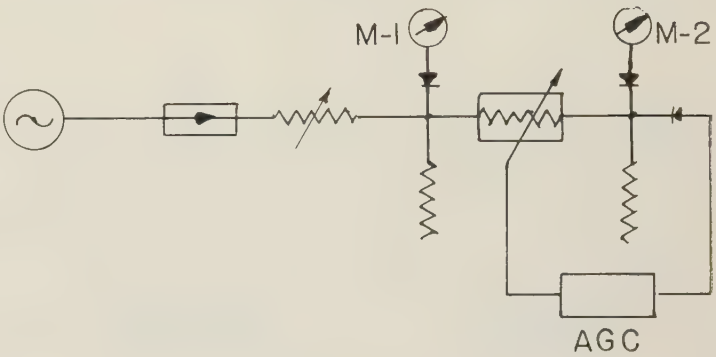

Fig. 5.

Fig. 5 shows a set-up for rapid testing of tw Tubes where the power level from the bwo is held constant during the sweep so that the output from the twt amplifier is directly proportional to its gain. In this case, it does not hurt that the crystal detectors are frequency sensitive as long as the two detectors are closely matched over the frequency range. In a typical case, the bwo has an output varying from 10 mw to 50 mw, the Gyraline works with a minimum attenuation of 5 db and the directional coupler attenuates 10 db giving a power level at the agc detector of 300 μw. This would give a stabilization factor around 100. In a broad-band set-up the directional coupler should be of the multihole type to avoid too much frequency sensitivity in the coupling.

The agc amplifier described here can be used with the proper detectors and Gyralines to obtain a constant power level in other frequency ranges from about 6 kmc to about 35 kmc. At lower frequencies, the Gyralines become more lossy because of imperfections in the ferrite material and, at the same time, they require more driving current than the present agc amplifier can deliver, but the same principle can still be applied.

A Method of Analysis of Symmetrical Four-Port Networks*

J. REED† AND G. J. WHEELER†

Summary—An analysis of four-arm symmetrical networks such as a branched directional double stub coupler or the hybrid ring (rat race) is presented. The input wave is broken into an even and an odd mode and the vector amplitude out the various arms is computed from the sums or differences of the reflection or transmission coefficients for the two modes. A zero decibel directional coupler is described and its possible use as a duplexer is proposed. The design of multiple stub directional couplers for any degree of coupling is discussed. A method of computing the bandwidth of all these couplers is outlined, and the bandwidth curves, the power out the various arms with respect to frequency of the zero decibel coupler, are computed. A tabulation is made for six different 3 db couplers (even-power split) and their standing wave ratio, evenness of power split and isolation of the fourth arm as a function of frequency assuming perfect performance at the band center.

Introduction

A SYMMETRICAL network is defined as one which has a plane of symmetry as illustrated in Fig. 1. The four arms in the network may be coaxial lines, waveguides, or strip-lines, but this discussion will be limited to coaxial lines, shunt connected.

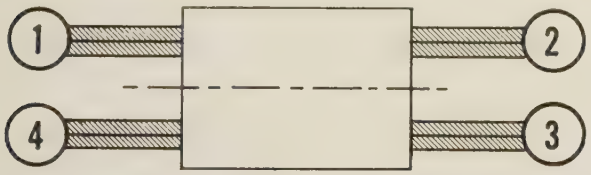

Fig. 1.

It is assumed that the network is lossless, and the ratio of wavelength to line size is very large so that junction effects are negligible.

A signal of unit amplitude is applied at arm 1 and divides in the network. The method of analysis to be described makes possible the determination of the resultant signals appearing at the four arms and how they vary (in phase and amplitude) with frequency.

Symmetry Analysis[1]

If two signals of amplitude $\frac{1}{2}$ and *in* phase are applied at arms 1 and 4, by symmetry a voltage maximum occurs at every point on the line of symmetry. That is, at these points $Z=\infty$ and $Y=0$. This is the equivalent of an open circuit as illustrated in Fig. 2.

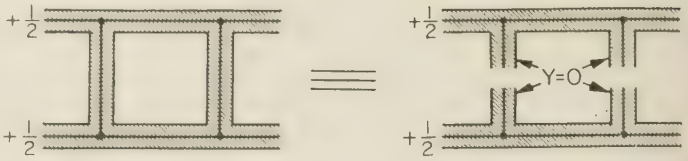

Fig. 2.

Similarly, if two signals of amplitude $\frac{1}{2}$ and *out of* phase are applied at arms 1 and 4, a voltage minimum occurs at every point on the line of symmetry. That is, at these points $Z=0$ and $Y=\infty$. This is the equivalent of a short circuit as in Fig. 3.

Fig. 3.

In each case, the problem reduces to that of a two-arm network. For the even mode, a reflection coefficient $\frac{1}{2}\Gamma_{++}$ and a transmission coefficient $\frac{1}{2}T_{++}$ are determined. Similarly, for the odd mode, $\frac{1}{2}\Gamma_{+-}$ and $\frac{1}{2}T_{+-}$ are determined.

By superposition, the sum of the two cases is a single signal of unit amplitude in arm 1. The resultant signals out of the four arms are also the superposition of the results obtained in the even mode $(++)$ and odd mode $(+-)$ case.

Thus the vector amplitudes of the signals emerging from the four arms are:

$$A_1 = 1/2\Gamma_{++} + 1/2\Gamma_{+-},$$

$$A_2 = 1/2T_{++} + 1/2T_{+-},$$

$$A_3 = 1/2T_{++} - 1/2T_{+-},$$

$$A_4 = 1/2\Gamma_{++} - 1/2\Gamma_{+-}.$$

Matrix Analysis[2]

The analysis of a cascade of two-terminal pair networks may be carried out by use of the $ABCD$ matrix. In Fig. 4 the voltages and currents of two-port junctions are related by matrix equations. The matrices of several useful circuit elements are shown in Fig. 5.

* Manuscript received by the PGMTT, July 16, 1956. Presented before the National Symposium on Microwave Techniques, Philadelphia, Pa., February 2–3, 1956.

† Raytheon Mfg. Co., Wayland, Mass.

[1] B. A. Lippmann, "Theory of directional couplers," M.I.T. Rad. Lab. Rep., No. 860; December 28, 1945.

[2] W. L. Pritchard, "Quarter-wave coupled waveguide filters," *J. Appl. Phys.*, vol. 18, pp. 862–863; October, 1947.

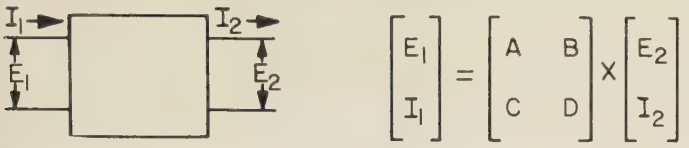

Fig. 4.

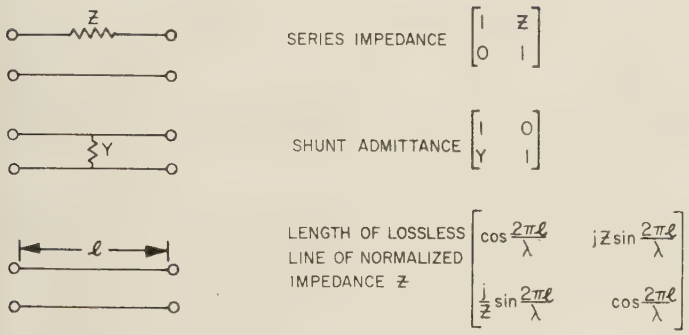

Fig. 5.

The impedance and admittances are all normalized with respect to that of a matched generator and load.

For reciprocity $AD-BC=1$; for forward-to-back symmetry, $A=D$.

$T=\dfrac{2}{A+B+C+D}=$ insertion voltage transmission coefficient between matched generator and load.

$Z_1=\dfrac{E_1}{I_1}=\dfrac{A+B}{C+D}=$ input impedance with matched load.

$\Gamma=\dfrac{A+B-C-D}{A+B+C+D}=$ voltage reflection coefficient with matched load.

Design at Band Center

The following analysis is for coaxial lines of quarter wavelength long, shunt connected neglecting discontinuity effects. By duality this analysis is valid for waveguide junctions with series connections.

To illustrate an application of the method, consider the 4-arm network illustrated in Fig. 6. Here each line represents a coaxial line, all characteristic admittances are unity, and all lines are a quarter of a wavelength between the pure, shunt junctions.

The matrices for the even and odd modes become:

$$M_{++}=\begin{bmatrix}1&0\\j&1\end{bmatrix}\begin{bmatrix}0&j\\j&0\end{bmatrix}\begin{bmatrix}1&0\\j&1\end{bmatrix}\begin{bmatrix}0&j\\j&0\end{bmatrix}\begin{bmatrix}1&0\\j&1\end{bmatrix}=\begin{bmatrix}0&-j\\-j&0\end{bmatrix},$$

$$M_{+-}=\begin{bmatrix}1&0\\-j&1\end{bmatrix}\begin{bmatrix}0&j\\j&0\end{bmatrix}\begin{bmatrix}1&0\\-j&1\end{bmatrix}\begin{bmatrix}0&j\\j&0\end{bmatrix}\begin{bmatrix}1&0\\-j&1\end{bmatrix}=\begin{bmatrix}0&+j\\+j&0\end{bmatrix}.$$

The even mode matrix is the product of five matrices; the first, third, and last are those of an open-circuited stub one eighth wavelength long; the second and fourth

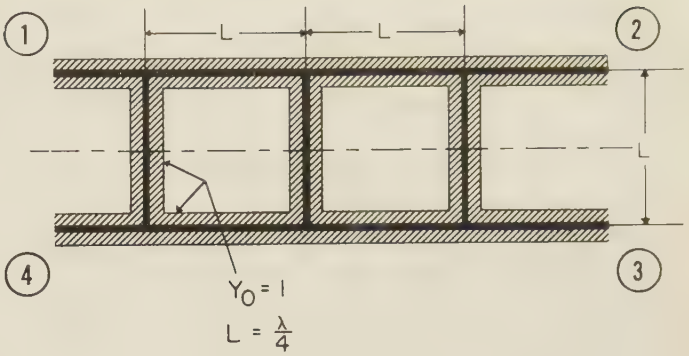

Fig. 6.

are those of a quarter wavelength line. The matrix for the odd mode proceeds similarly except that short circuited stubs are imagined.

$$\Gamma_{++}=\Gamma_{+-}=0 \qquad A_1=A_4=0$$

$$1/2T_{++}=\frac{1}{-2j} \qquad A_2=1/2(T_{++}+T_{+-})=0$$

$$1/2T_{+-}=\frac{1}{2j} \qquad A_3=1/2(T_{++}-T_{+-})=j.$$

Thus $P_1=P_2=P_4=0$ and $P_3=1$ or all the power comes out of arm 3; that is, it is coupled diagonally across the network. The phase is indicated by the value of A_3 which in this case shows a shift of 90°.

A possible application of this device is as a duplexer illustrated in Fig. 7. This is the waveguide analog of the

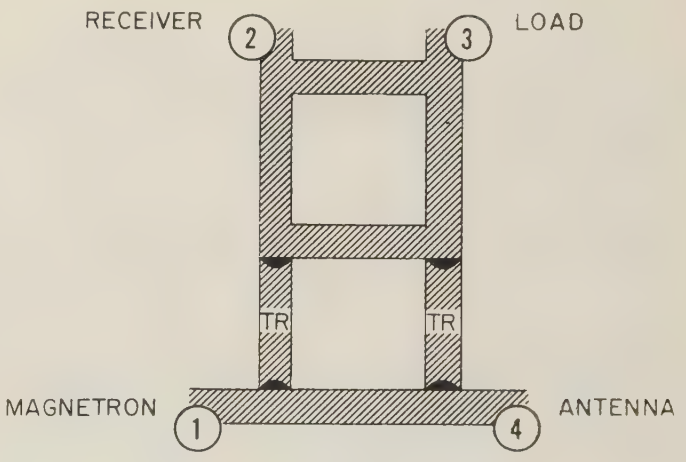

Fig. 7.

circuit of Fig. 6. The magnetron fires the TR tubes and all the power travels to the antenna. Any leakage through the TR's goes diagonally across the network to the load. On reception the tubes look like matched lines and energy travels diagonally across the circuit from the antenna to the receiver.

Another device which can be easily analyzed by this method is the two-stub coupler shown in Fig. 8. (As in Fig. 6, each line in this and all succeeding diagrams represents a coaxial line.)

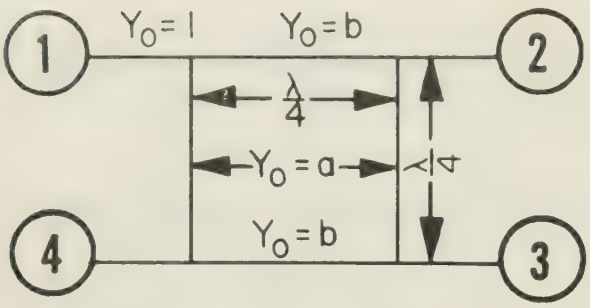

Fig. 8.

Writing the even and odd mode matrices together

$$M_{+,} = \begin{bmatrix} 1 & 0 \\ \pm ja & 1 \end{bmatrix} \begin{bmatrix} 0 & \frac{j}{b} \\ jb & 0 \end{bmatrix} \begin{bmatrix} 1 & 0 \\ \pm ja & 1 \end{bmatrix}$$

$$= \begin{bmatrix} \mp\frac{a}{b} & \frac{j}{b} \\ j\left(b - \frac{a^2}{b}\right) & \mp\frac{a}{b} \end{bmatrix}.$$

The device will be matched and perfectly directive if $\Gamma_{++} = \Gamma_{+-} = 0$, that is, if $B = C$ in both the even and odd mode matrices: $1 + a^2 = b^2$. Thus the coupling into arm 3 is

$$20 \log \frac{1}{|A_3|} = 20 \log \frac{\sqrt{b^2 - 1}}{b}.$$

These are the same results as given by Montgomery.[3]

For the special case where $a = 1$ and $b = \sqrt{2}$ the device is a 3 db directional coupler for which power in arm 1 divides evenly between arms 2 and 3.

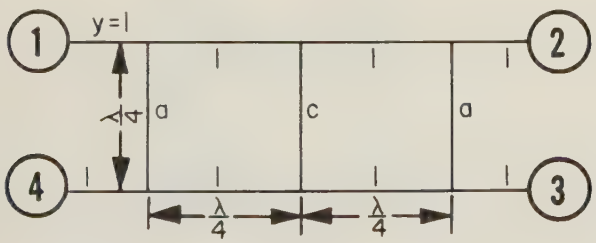

Fig. 9.

If three cross arms are used instead of two (see Fig. 9) it is not necessary to change the admittance of the main lines to achieve match and directivity.

$$M_{+\pm} = \begin{bmatrix} ac - 1 & \mp jc \\ \mp j(2a - a^2c) & ac - 1 \end{bmatrix}.$$

[3] C. G. Montgomery, R. H. Dicke, and E. M. Purcell, "Principles of Microwave Circuits," McGraw-Hill Book Co., Inc., New York, N. Y., pp. 309–310.

For match

$$c = \frac{2a}{1 + a^2} \qquad a = 1 - \frac{\sqrt{1 - c^2}}{c}.$$

Then

$$\text{coupling} = 20 \log_{10} \frac{1}{c} = 20 \log_{10} \frac{1 + a^2}{2a}.$$

Note that for $a = c = 1$ the coupling is 0 db which means that there is no loss in going from arm 1 to arm 3 as noted previously.

A broader band device for three cross arms results when the impedance of the main lines may be changed (see Fig. 10).

$$M_{+,} = \begin{bmatrix} \frac{ac}{b^2} - 1 & \mp j\frac{c}{b^2} \\ \mp j\left(2a - \frac{a^2c}{b^2}\right) & \frac{ac}{b^2} - 1 \end{bmatrix}$$

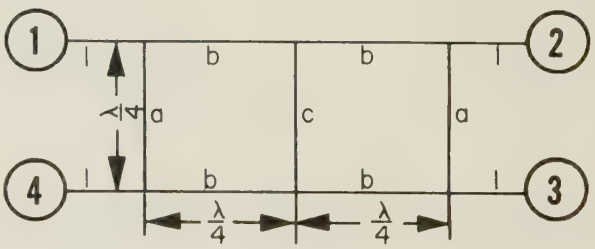

Fig. 10.

For match and perfect directivity

$$B = C \text{ or } c = \frac{2ab^2}{1 + a^2}.$$

Then

$$\text{coupling} = 20 \log_{10} \frac{1}{|A_3|} = 20 \log_{10} \frac{1 + a^2}{2a}.$$

When coupling = 3 db, $a = \sqrt{2} - 1$. A useful form is when $b = c = \sqrt{2}$.

A wider band directional coupler may be made with four cross arms (see Fig. 11).

$$M_{+\pm} = \begin{bmatrix} \pm(a + c - ac^2) & j(c^2 - 1) \\ j(-ac^2 + 2a^2c + a^2 - 1) & \pm(a + c - ac^2) \end{bmatrix}.$$

The values of a and c again can be calculated for perfect match and directivity as before for any coupling.

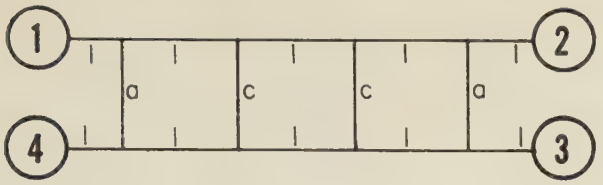

Fig. 11.

With five or six cross arms there could be a third different size for the center arms. However, if the center arms are all kept at the same value, the results for equal power division in arms 2 and 3 are indicated in Table I.

TABLE I

	a	c	
3 arms *aca*	0.4141	0.7071	(Fig. 9)
4 arms *acca*	0.2346	0.5412	(Fig. 11)
5 arms *accca*	0.2088	0.3810	
6 arms *acccca*	0.1464	0.3179	

These values were obtained by setting all the terms in the $M_{+\pm}$ matrix equal in magnitude to $1/\sqrt{2}$. Care was taken that the lowest root of the equation was chosen for broadest band performance.

The rat race ring[4] can also be analyzed (see Fig. 12) and is interesting.

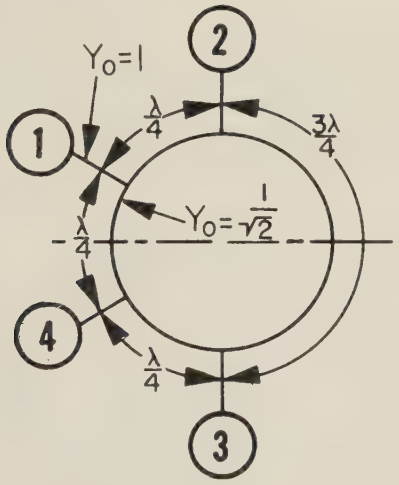

Fig. 12.

$$M_{+\pm} = \begin{bmatrix} 1 & 0 \\ \pm j\frac{1}{\sqrt{2}} & 1 \end{bmatrix}\begin{bmatrix} 0 & j\sqrt{2} \\ \frac{j}{\sqrt{2}} & 0 \end{bmatrix}\begin{bmatrix} 1 & 0 \\ \mp j\frac{1}{\sqrt{2}} & 1 \end{bmatrix}$$

$$= \begin{bmatrix} \pm 1 & j\sqrt{2} \\ j\sqrt{2} & \mp 1 \end{bmatrix}.$$

The matrix product is that of an eighth wavelength stub, a quarter wavelength of line and then a three-eighth wavelength stub, all of admittance $1/\sqrt{2}$. Note that in the final matrix $A \neq D$.

As before

$$\Gamma_{++} = \frac{-j}{\sqrt{2}} \qquad A_1 = \frac{\Gamma_{++} + \Gamma_{+-}}{2} = 0,$$

$$\Gamma_{+-} = \frac{j}{\sqrt{2}} \qquad A_4 = \frac{\Gamma_{++} - \Gamma_{+-}}{2} = \frac{-j}{\sqrt{2}},$$

$$T_{++} = \frac{-j}{\sqrt{2}} \qquad A_2 = \frac{T_{++} + T_{+-}}{2} = \frac{-j}{\sqrt{2}},$$

$$T_{+-} = \frac{j}{\sqrt{2}} \qquad A_3 = \frac{T_{++} - T_{+-}}{2} = 0.$$

The result is that power fed in arm 1 divides evenly *in* phase between arm 2 and arm 4 and none is reflected. A similar analysis shows that power fed in arm 2 divides equally and *out of* phase between arms 1 and 3. Similar analysis may be used for the $7/2\lambda$ hybrid ring.[5] (See results, Fig. 15).

Frequency Sensitivity

To calculate the frequency sensitivity of the devices the junctions are assumed still to be pure shunt or series connections. The frequency dependent values, the lengths of line in the matrices are expressed in terms of $t = \tan \pi l/\lambda$ where l is the length of the line. This makes the value of t unity when l is a quarter wavelength. In the case of the three-arm coupler with all elements the same as in Fig. 6 the matrices are as follows:

Even mode stub Odd mode stub Length of line

$$\begin{bmatrix} 1 & 0 \\ jt & 1 \end{bmatrix} \qquad \begin{bmatrix} 1 & 0 \\ -\frac{j}{t} & 1 \end{bmatrix} \qquad \begin{bmatrix} \frac{1-t^2}{1+t^2} & \frac{j2t}{1+t^2} \\ \frac{j2t}{1+t^2} & \frac{1-t^2}{1+t^2} \end{bmatrix}$$

where $t = \tan \pi l/\lambda (t = 1 \text{ if } l = \lambda/4)$

Note:

$$\cos 2\theta = \frac{1 - \tan^2\theta}{1 + \tan^2\theta} \qquad \sin 2\theta = \frac{2\tan\theta}{1 + \tan^2\theta}.$$

Substituting these in the matrix for the even and odd modes we obtain

$$M_{++} = \frac{1}{(1+t^2)^2}\begin{bmatrix} 1 - 12t^2 + 11t^4 & j(4t - 8t^3) \\ j(7t - 26t^3 + 15t^5) & 1 - 12t^2 + 11t^4 \end{bmatrix},$$

$$M_{+-} = \frac{1}{(1+t^2)^2}\begin{bmatrix} t^4 - 12t^2 + 11 & j(-4t^3 + 8t) \\ j\left(-7t^3 + 26t - \frac{15}{t}\right) & t^4 - 12t^2 + 11 \end{bmatrix}.$$

[4] W. A. Tyrrell, "Hybrid circuits for microwaves," Proc. IRE, vol. 35, pp. 1294–1306; November, 1947.

[5] L. J. Cutrona, "The theory of biconjugate networks," Proc. IRE, vol. 39, pp. 827–832; July, 1951.

Note that for $t=1$ these expressions reduce to those following Fig. 6. For any frequency a value of t can be found and the matrices evaluated and then the vector amplitudes of the waves out all arms calculated.

On the graph in Fig. 13 (below) are plotted the powers out the various arms expressed in decibels below incident power as a function of t and, assuming coaxial lines, also as a function of the ratio of frequency to design frequency. Note the change in scale for the power out arm 3.

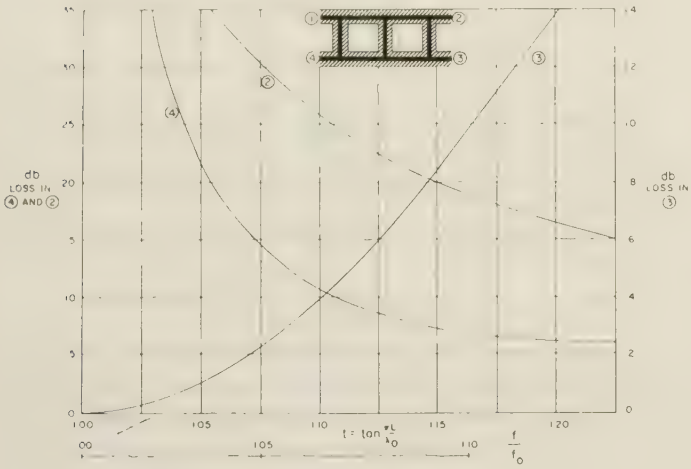

Fig. 13.

The values on these curves for a given value of t are exactly equal to those for $1/t$. Thus for a design over a band of frequencies the arithmetic average frequency should be used for the value of length to get equal performance at the edges of the band.

In the calculations of these curves and of the others that follow, a simplification can be made which makes it unnecessary to multiply out the M_{+-} matrix as a function of t. To obtain the numerical values of the M_{+-} matrix for a given t, the value $1/t$ is put in for t in the M_{++} matrix. Then if the exponent of the term $(1+t^2)^n$ is odd, the sign of the A and D components are changed; if even, those of the B and C components are changed.

In Fig. 14 are shown the theoretical preformance curves calculated by this method for the two simplest four-arm junctions, the rat race, and the double stub 3-db coupler. Both of these can be considered as 3 db directional couplers and will divide power equally between two arms shown with arrows and no power will go out the fourth arm with no arrow, as was shown previously.

On the graph the curves sloping *up* to the right indicated the input vswr with matched loads on the other three arms. Also the curves sloping *down* to the right show the ratio of power coupled to the fourth arm (arm 3 in the case of the rat race) to the incident power. These curves are plotted as a function of t and also as a function of f/f_0 assuming free space variation of wavelength as before. The rat race is a solid line and the square hybrid a dashed line.

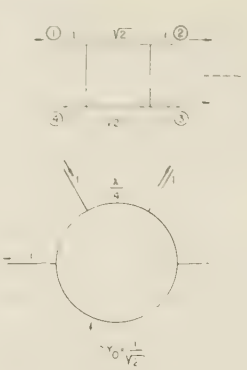

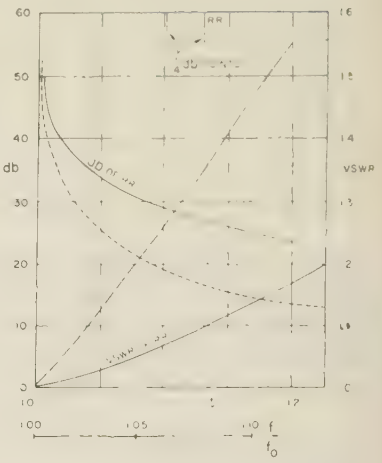

Fig. 14.

While the power will divide evenly between the two arms with arrows when $t=1$, that is, when all values are a quarter wavelength, it will not divide evenly at other frequencies. The values of t at which the ratio goes up to a quarter of a decibel are shown as the little vertical lines at the top of the graph.

The M_{++} matrices are given below for reference for these 3-db couplers. The M_{+-} matrices are not needed if the rule mentioned before is used.

Square hybrid of Fig. 8:

$$M_{++}=\frac{1}{1+t^2}\begin{bmatrix} 1-(1+\sqrt{2})t^2 & j\sqrt{2}t \\ j[(2+2\sqrt{2})t-(2+\sqrt{2})t^3] & 1-(1+\sqrt{2})t^2 \end{bmatrix}$$

Rat race of Fig. 12:

$$M_{++}=\frac{1}{1+t^2}\begin{bmatrix} \dfrac{1-10t^2+5t^4}{1-3t^2} & 2j\sqrt{2}t \\ j(3\sqrt{2}t-\sqrt{2}t^3) & 1-3t^2 \end{bmatrix}.$$

A tabulation of calculated results for six different 3-db couplers described in the text appears in Fig. 15 in order of increasing bandwidth. For $t=1.1$ and 1.2 the first column shows the input vswr, the second shows the ratio of power delivered to arm 4 (arm 3 in the hybrid rings cases) to that incident and the third column shows the ratio of power delivered to arms 2 and 3, (2 and 4 for the hybrid rings cases).

The method outlined in this paper has been the subject of many experimental checks. We have built a coaxial line model of Fig. 7, the duplexer, in $\frac{3}{8}$-inch line at L band. The data taken on this device checked quite consistently with the theory. Also a square hybrid (Fig. 8) has been constructed at L band in $\frac{3}{8}$ inch coaxial

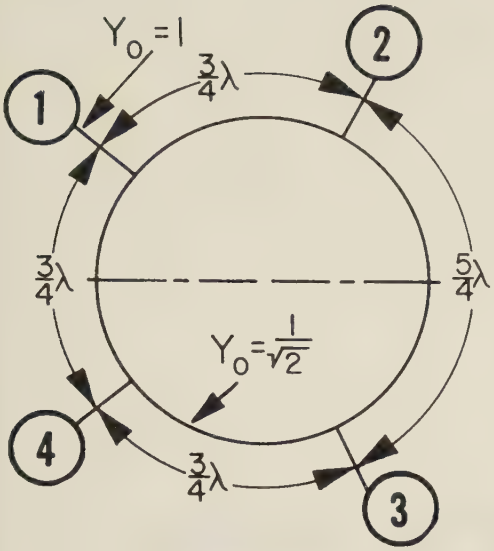

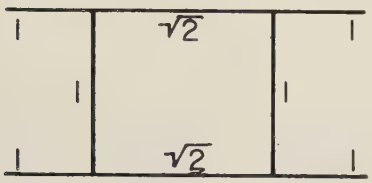

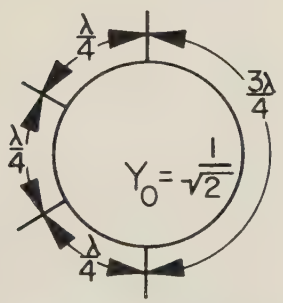

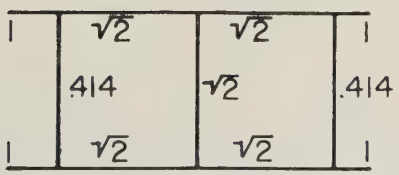

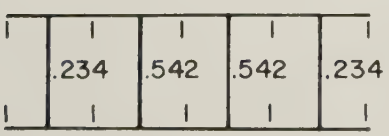

$t = 1.10$ ($\frac{f}{f_o} = 1.06$)			$t = 1.20$ ($\frac{f}{f_o} = 1.13$)		
VSWR	DB	DIFF IN DB	VSWR	DB	DIFF IN DB
1.37	17.7	1.47			
1.26	19.0	.24	1.57	13.8	.74
1.08	27.4	.18	1.20	20.5	.60
1.07	29.3	.14	1.17	23.3	.51
1.03	37.0	.12	1.12	25.3	.49
1.01	45.0	.10	1.05	32.0	.45

Fig. 15—Tabulation of theoretical results on 3-db directional couplers.

line and its performance checked the curves presented almost exactly. The curves presented on the rat race check very well with published data.[6]

Again it must be emphasized that pure shunt junctions are assumed neglecting fringing effects. This will only be true if the ratio of wavelength to line size is very high. This first approximation is valuable anyway. To make a coaxial 3-db directional coupler with many arms as shown in Fig. 11 requires excessively small center conductors since the characteristic admittance varies as the logarithm of the size ratio. But with waveguide a branch guide 3-db coupler, with many arms appears to be a definite possibility since the impedance of the arms varies as the height of the guide and the fringing effects get smaller as the height of the guide is decreased.

[6] H. T. Budenbom, "Some quasi-biconjugate networks and related topics," Proc. of the Symposium on Modern Network Synthesis, Polytech. Inst. of Brooklyn, New York, N. Y., 1952, pp. 312–326.

Broad-Band Waveguide Series *T* for Switching*

J. W. E. GRIEMSMANN† AND G. S. KASAI‡

Summary—**By use of properly proportioned half-wavelength transformer sections in the arms of a waveguide series *T* broad-band performance can be obtained for switching applications. Over the frequency band 8200 to 9765 megacycles per second, corresponding to a bandwidth of 17.4 per cent, an experimental model showed an insertion vswr of less than 1.15 for transmission through the aligned arms and 1.30 for transmission around the bend. Further bandwidth improvement is possible with the use of a special arrangement of quarter-wave transformer sections but at the expense of further impairment of power-carrying capacity.**

Introduction

ONE APPLICATION of a *T* junction is duplexing. The transmitter and antenna are usually connected to the aligned arms and the receiver to the side arm. Power flow from transmitter to antenna and not to the receiver can be considered to be so directed by an appropriately positioned effective short in the side arm. The received signal can be considered to be directed from antenna to side arm by an appropriately positioned effective short in the transmitter arm. An inherent bandwidth limitation for the ordinary *T* is that the effective short positions are correct only for the center frequency and thus give rise to "branching loss,"[1] principally through reflection of energy back out through the antenna. The device discussed in this paper provides one means for minimizing this branching loss over a broader range of frequencies.

In any practical case of duplexer design many special problems relating to positioning of the shorts and special means of solving them are introduced.[1] This paper is directed chiefly at the frequency sensitivity of the stubbed *T* structure itself and means for overcoming it. Fixed metallic shorts are assumed to replace the effective shorts indicated above. For this reason the device is called a switching *T* rather than duplexer.

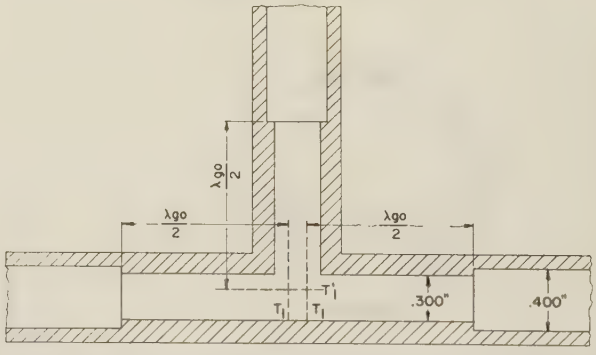

Fig. 1—Waveguide switching *T* cross section—side view.

Shown in Fig. 1 is a dimensioned sketch of the broad-banded series (*E* plane) *T* in the *X* band, RG-52/U rectangular waveguide designed for a center frequency of 9000 mc and a theoretical bandwidth of 16 per cent for a maximum vswr of 1.08. This design was based on circuital computation of a pure series arrangement of the arms and use of the equivalent circuit[2] for the *E* plane *T* at 9000 megacycles per second. At appropriate reference planes the particular equivalent circuit chosen is a good approximation to a series con-

* Manuscript received by the PGMTT, July 16, 1956. Presented before the National Symposium on Microwave Techniques, Philadelphia, Pa., February 2–3, 1956. This work was performed under Signal Corps Contract No. DA-36-039-sc-42489. The work is in part the subject of a thesis for the M.E.E. degree by Mr. Kasai at the Polytech. Inst. of Brooklyn.

† Microwave Res. Inst., Polytech. Inst. of Brooklyn, Brooklyn, N. Y.

‡ North American Aviation Corp., Downey, Calif.; formerly with Microwave Res. Inst., Polytech. Inst. of Brooklyn, Brooklyn, N. Y.

[1] L. Smullin and C. Montgomery, "Microwave Duplexers," Rad. Lab. Ser., McGraw-Hill Book Co., Inc., New York, N. Y., vol. 14, ch. 7, 1948.

[2] N. Marcuvitz, "Waveguide Handbook," Rad. Lab. Ser., McGraw-Hill Book Co., Inc., vol. 10, pp. 337–351, 1951.

nection of the arms, and was thus assumed for the design. The discontinuity susceptances of the steps were compensated for by foreshortening of the transformer sections.[3]

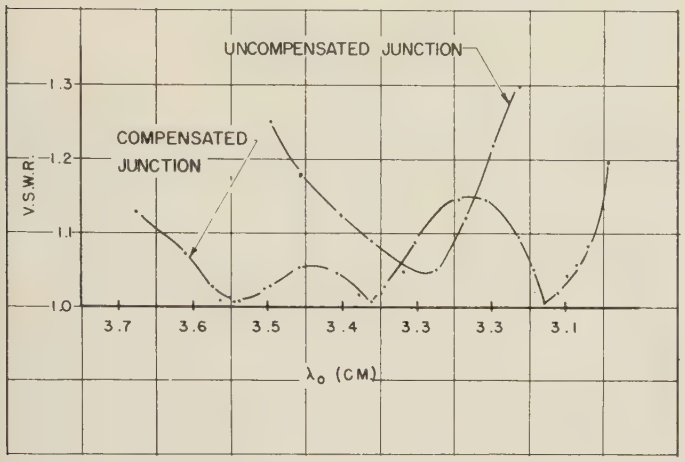

Fig. 2—Experimental results: insertion vswr vs free space wavelength for transmission between parallel arms.

Shown in Fig. 2 is a plot of measured insertion vswr vs free space wavelength for transmission through the aligned arms of the broad-band T along with the same for an uncompensated T. At a vswr of 1.15 the bandwidth for the broadband T is measured to be 19.1 per cent whereas that for the uncompensated T is 6.2 per cent.

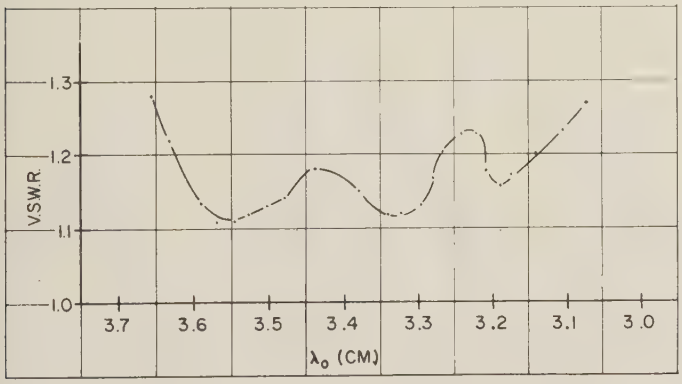

Fig. 3—Experimental results: insertion vswr vs free space wavelength for "around the corner" transmission of the compensated junction.

Shown in Fig. 3 is a plot of measured insertion vswr vs free space wavelength for transmission around the bend of the broad-banded T. For a vswr of 1.23 the bandwidth is found to be 15.8 per cent while for a vswr of 1.29 the measured bandwidth is in excess of 17.4 per cent. The minimum insertion vswr value that could be measured on the uncompensated T junction for around the bend transmission at 9.0 kmc was 1.30.

The degree of correspondence between theoretical and measured vswr data is shown in Fig. 4 for transmission through the aligned arms. Considering the magnitude of the scales used and the fact that the model represents an initial paper design the agreement is good. For the transmission around the bend the same theoretical data would be valid and the discrepancy is beyond that anticipated from the equivalent circuit. Further improvement in performance could be expected if additional investigations were conducted, particularly with respect to compensation for the around the bend transmission.

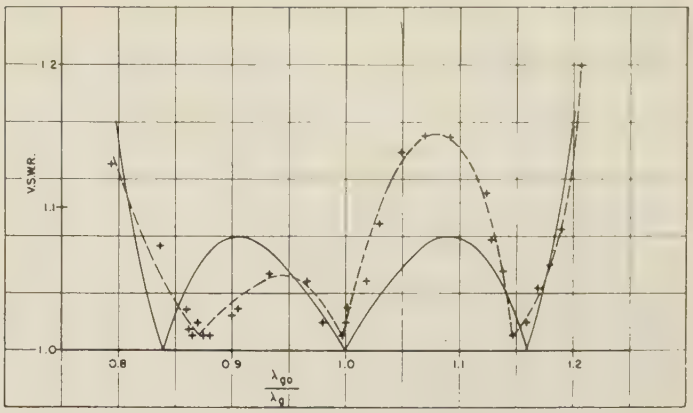

Fig. 4—Comparison of experimental and theoretical results for the compensated junction: – – –=experimental; ———=theoretical.

General Circuit Analysis

The following analysis assumes that the T may be represented by the simple circuit consisting of the three arms connected in series.

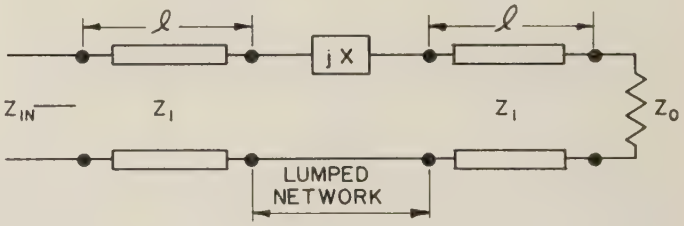

$$\frac{X_r}{Z_1} = \frac{2\left[\left(\frac{Z_0}{Z_1}\right)^2 - 1\right] \tan \beta\ell}{1 + \left(\frac{Z_0}{Z_1}\right)^2 \tan^2 \beta\ell}$$

$$\frac{dX_r}{d(\beta\ell)} = \frac{2\left[\left(\frac{Z_0}{Z_1}\right)^2 - 1\right] \sec^2 \beta\ell \left[1 - \left(\frac{Z_0}{Z_1}\right)^2 \tan^2 \beta\ell\right]}{\left[1 + \left(\frac{Z_0}{Z_1}\right)^2 \tan^2 \beta\ell\right]^2}$$

Fig. 5.

In Fig. 5 is shown the circuit used for the analysis when there is but a single transformer in each leg. The circuit is somewhat more general than need be for design and is used to determine the values of the series reactance, x_r, required to match the over-all structure.

[3] *Ibid.*, pp. 307–310.

By appropriate analysis of the half structure,[4,5] the value of x_r shown in Fig. 5 was determined. In accordance with Foster's reactance theorem, the expression for the derivative of x_r with respect to frequency as given in Fig. 5 is positive for $(z_0/z_1)>1$ and for values of l/λ_g ranging less than $\frac{1}{8}$ on either side of $l/\lambda_g=\frac{1}{2}$, corresponding to an approximate limit of the guide wavelength ratio of 5 to 3 (per cent λ_g bandwidth = 50). For small values of tan Bl the reactance x_r can be approximated by a shorted arm or stub having a length equal to that of the transformer section. A match can be obtained at two other frequencies by appropriate choice of the characteristic impedance of the stub.

Analysis for Half-Wave Transformer Case

If the T is to be used as a switching junction with equal transmission for the transmit and receive condition, the stub must also be made up of a line of characteristic impedance, Z_1, of length, ι, and shorted at the end of this length. For this condition, the input reflection factor is

$$\Gamma = \sin\tan^{-1}\left[\frac{\tan\beta l}{\frac{z_0}{z_1}(1+\tan^2\beta l)}\left(\frac{3}{2}-\left[\frac{z_0}{z_1}\right]^2\cdot\left[1-\frac{1}{2}\tan^2 BL\right]\right)\right]$$

The junction is matched for $\Gamma=0$. This occurs for tan $\beta l=\tan 2\pi l/\lambda g_0=0$ corresponding to $l/\lambda g_0=\frac{1}{2}$ and for

$$\tan\beta l \equiv \tan\frac{2\pi l}{\lambda g_0} = \pm\left|\left[2-3\left(\frac{z_1}{z_0}\right)^2\right]^{1/2}\right|.$$

Thus, there are three frequencies for which $\Gamma=0$. Shown in Fig. 6 the curve is the ratio (z_0/z_1) plotted as a function of $\lambda g_0/\lambda g_c$, where λg_c is taken to correspond to the highest frequency of reflection cancellation. Between midband, corresponding to λg_0, and the cancellation frequencies the reflection coefficient and corresponding insertion

$$\text{VSWR} = \frac{1+|\Gamma|}{1-|\Gamma|}$$

go through a maximum value. Plotted as curve B in Fig. 7 is this maximum vswr as function of $\lambda g_0/\lambda g_c$, giving one measure of bandwidth. Shown for comparison are the maximum vswr values measured at λg_c for the uncompensated junction ($z_1=z_0$). Typically for a vswr of 1.08 and a design centered at 9.0 kmc in RG-52/U guide, the per cent frequency bandwidth for the compensated junction is 16 per cent as compared to 2.5 per cent for the uncompensated junction. The value of z_0/z_1 to give this condition is 1.329. The basic circuit is seen to be capable of considerable broadbanding as compared to that of the uncompensated with, of course, the attendant decrease in power carrying capacity associated with the reduction in height of the guide, the standing waves in the transformer section, and the corner of the discontinuity.

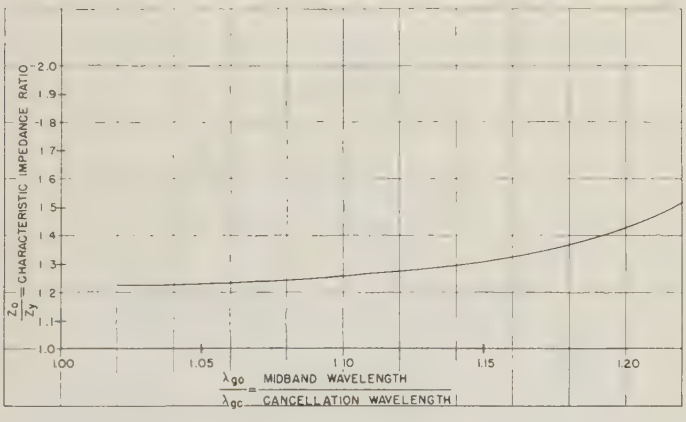

Fig. 6—Transformer characteristic impedance ratio vs cancellation wavelength.

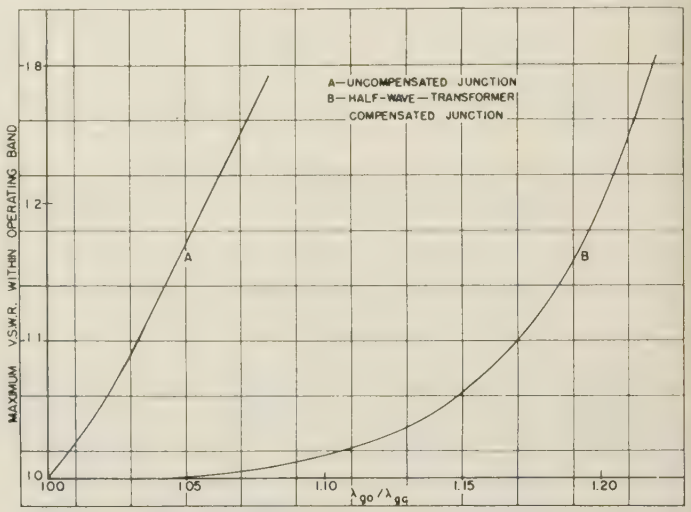

Fig. 7—Maximum insertion vswr vs cancellation wavelength.

Double Quarter-Wave Case

Further improvement in broadbanding is feasible if instead of one-half wave transformer in each arm, two quarter-wave transformers are used in each arm as shown in Fig. 8. The analysis can again be accomplished in terms of the open circuit and short circuit half structures, but is considerably more complicated.

Shown in Table I are the maximum vswr values occurring at frequencies between the matched condition at the center frequency corresponding to λg_0 and the matched conditions at the frequencies corresponding

[4] J. W. E. Griemsmann, "Microwave Broadbanding," Proc. of the Symposium on Modern Network Synthesis, Polytech. Inst. of Brooklyn, Brooklyn, N. Y., pp. 330–331, April, 1952.
[5] H. Bode, "Network Analysis and Feedback Amplifier Design," D. Van Nostrand and Co., Inc., pp. 363–364; 1945.

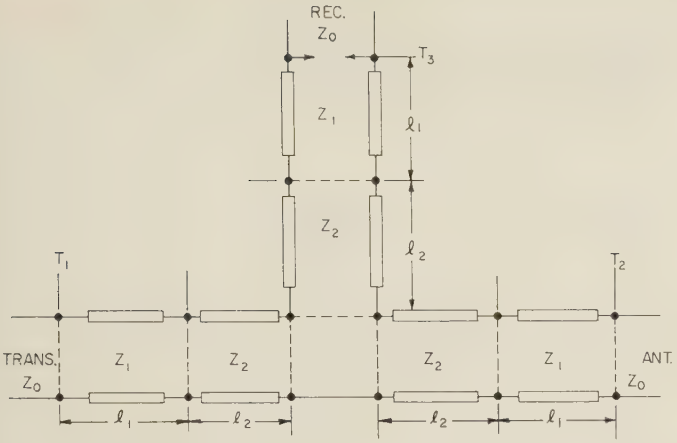

Fig. 8—Double quarter-wave transformer circuit.

to λg_c for given values of $\lambda g_0/\lambda g_c$ (where λg_c corresponds to the highest cancellation frequency) and various values of the transformer impedance ratio Z_1/Z_2. The analysis shows that for a given selection of $\lambda g_0/\lambda g_c$ there is a relationship between z_1/z_2 and z_0/z_1 given implicitly by

$$(2b - 3a^2)y^4 + (6a^2b - 3b^2 - 2b + 3)y^2 + (2b - 3a^2b^2) = 0$$

where

$$a = \frac{z_1}{z_0}, b = \frac{z_1}{z_2}, \text{ and } y = \cot\frac{\beta l}{2}.$$

TABLE I

Double Quarter-Wave Performance Characteristics (Calculated Values)

$\lambda_{g0}/\lambda_{ge}$	1.16	1.20	1.25
z_1/z_2	Maximum Insertion VSWR		
0.300	1.0212	1.2121	
0.500	1.0456	1.1386	1.7682
0.700	1.0586	1.1530	1.5899
0.800	1.0651	1.1649	1.5956
1.000	1.0786	1.1935	1.6519
1.100	1.0854	1.2095	1.7139
1.200	1.0926	1.2266	1.7657

For each value of vswr given in the table there is also a value of z_1/z_0 inferred.

The table shows that for a given bandwidth the maximum vswr values may be reduced below the value for the half-wave transformer junction, $z_1/z_2 = 1.00$, by using the double quarter wave arrangement. For example for $\lambda g_0/\lambda g_c = 1.16$ corresponding to that for the previously considered half-wave transformer design, the maximum vswr value could be reduced from 1.079 to 1.046 using $z_1/z_2 = 0.500$ and $z_0/z_1 = 0.9044$. For $\lambda g_0/\lambda g_c = 1.20$ and $\lambda g_0/\lambda g_c = 1.25$, the values for the maximum vswr values are noted to pass through minimums as the transformer dimensions are varied. The upper bound for bandwidth is changed very little, if any, over that of the half-wave transformer.

In order to achieve the improvement indicated above for $\lambda g_0/\lambda g_c = 1.16$, the height of the guide in the second transformer section would have to be considerably increased over that corresponding to z_0. This brings into doubt the practicability of the double transformer arrangement particularly in view of the degree of improvement obtained. From the design viewpoint, the question of higher modes and discontinuities would make the realization difficult. Reducing the value of z_0 below that of standard RG-52/U guide by transformers or tapers so as to minimize the mode and discontinuity problems would mean considerable complication of the design and reduction in carrying capacity.

Comments

For some switching purposes T's can be broadbanded up to approximately a limit of 16 per cent. This is not an open recommendation for use of the broad-banded switching T as the basis for radar duplexing. There is competition from short slot duplexer which has about the same bandwidth, and in some cases can provide better magnetron starting characteristics.

Some of those having long acquaintance with the microwave art will recognize this as analogous to the broadbanding of stub supports for coaxial lines. It will be recalled, however, that these used a parallel circuit for the stub and quarter-wave transformers sections. This paper is felt to give the first open suggestion for use of this device in rectangular waveguides and to give the first thorough bandwidth analysis for the half-wave transformer case.

A Traveling-Wave Directional Filter*

FRANKLIN S. COALE†

Summary—A new type of microwave filter is presented in which resonance occurs in the form of a traveling wave rather than in the conventional form of a standing wave. This device is a constant-resistance circuit, and therefore presents a very low input vswr. Formulas for loaded Q and insertion loss are given. Experimental results verify the theoretical approach. This filter, which is constructed of a transmission-line loop and two directional couplers, finds application in multiplexing filters as well as in matched band-pass and band-rejection filters.

Introduction

MICROWAVE filters usually employ one or more elements which are resonant in the sense that a high standing wave is present. It is possible, however, to obtain resonance in another sense. Consider a directional coupler in which the coupled and isolated arms are connected to form a ring of electrical length corresponding to n wavelengths. A signal incident at the primary arm of the directional coupler will cause in the secondary, a resonance, that is in the form of a traveling wave circulating about the loop.[1–3] This process of build-up to resonance is similar to standing-wave build-up in a microwave cavity.

If two directional couplers are connected in the loop (as shown in Fig. 1) at the resonant frequency of the loop all the energy will pass from the primary arm of one directional coupler (arm 1) to the primary arm of the other (arm 4). The device will then behave as a band-pass filter with an unloaded Q equal to the Q of the transmission line, and a loaded Q dependent upon the voltage coupling coefficient of the directional couplers. At resonance, the through arm of the directional coupler behaves as a band-rejection filter (arm 1 to arm 2). This type of filter will be referred to as a "traveling-wave directional filter."

The traveling-wave directional filter is a four terminal-pair network with the frequency response shown in Fig. 2, and lends itself quite naturally to multiplexing filter applications. By using traveling-wave directional filters as basic building blocks, it is possible to construct multiplexing filters with a perfect match, since the input vswr of a directional filter is theoretically unity both at resonance and off resonance, and thus avoid the off-resonance mismatch that is probably the most difficult problem associated with the ordinary multiplexing filters (*i.e.*, those constructed with simple band-pass, band-rejection, high-pass, and low-pass filters).

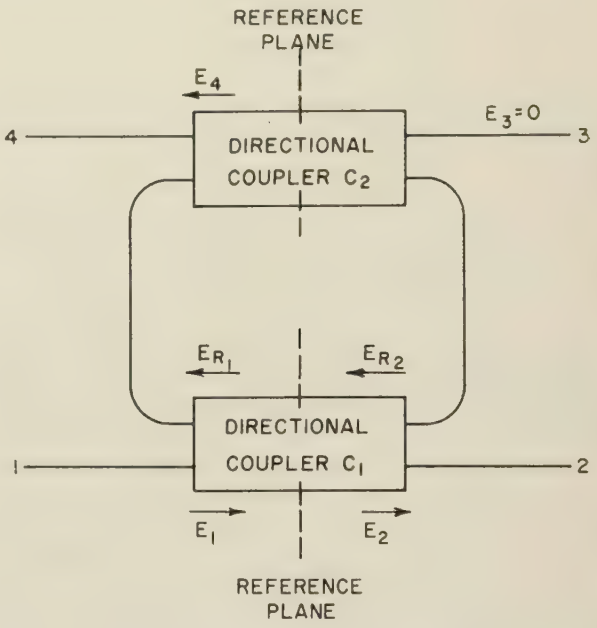

Fig. 1—Schematic of traveling-wave directional filter.

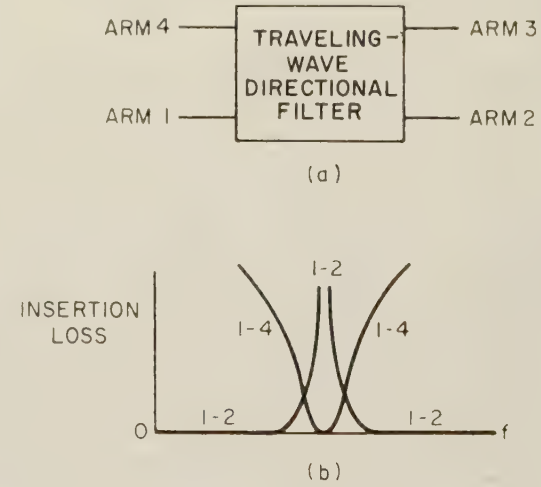

Fig. 2—Response of a traveling-wave directional filter.

Theoretical Analysis

Two different approaches are used to analyze the traveling-wave directional filter. By assuming that all elements of the filter are adjusted so that a pure traveling wave exists in the loop, it is possible to calculate such quantities as loaded Q and insertion loss simply, in terms of the coupling and the length and attenuation constant of the loop transmission line. The second ap-

* Manuscript received by the PGMTT, July 16, 1956. Presented before the National Symposium on Microwave Techniques, Philadelphia, Pa., February 2–3, 1956. The work described here was supported by the Signal Corps under Contract No. DA-36-039-SC-64625.

† Stanford Res. Inst., Menlo Park, Calif.

[1] B. H. Ring, U. S. Patent 2,639,326, issued May 19, 1953.

[2] P. J. Sferazza, "Traveling wave resonator," *Tele-Tech*, vol. 14, pp. 84–85, 142–143; November, 1955.

[3] K. Tomiyasu, "A new annular waveguide rotary joint," PROC. IRE, vol. 44, pp. 548–553; April, 1956.

proach is somewhat more involved, but is capable of predicting anomalies due to imperfect adjustment of the filter. Because of the presence of the directional couplers, it is possible to have two mutually orthogonal standing-wave resonances in loop, corresponding to electric and magnetic coupling. When the two resonant frequencies are made to coincide, the field components of the two resonant modes superimpose to form a pure traveling wave in the clockwise direction around the loop.

It is assumed that: 1) all transmission lines have the same characteristic impedance, 2) all directional couplers are perfectly matched and have infinite directivity, and 3) no points of reflection exist in the loop and therefore a pure traveling wave exists. The expressions for loaded Q and insertion loss are derived for the TEM-transmission-line case, and the expression for loaded Q must be modified as shown later to be applicable to the waveguide-loop case. The voltages shown in Fig. 1 at the terminals of the directional couplers are, for convenience, referred in amplitude and phase to the midplanes of the directional couplers. The total length of the loop at resonance, including the lengths of the coupling regions, is $l=n\lambda$, where n is an integer. It is seen that the following voltages are excited during the first traversal of the loop by the traveling wave:

$$E_1 = 1\angle 0 \tag{1}$$

$$E_2 = \sqrt{(1-c_1^2)}\angle 0 \tag{2}$$

$$E_3 = 0 \tag{3}$$

$$E_4 = c_1c_2e^{-\alpha l/2}\angle 0 \tag{4}$$

$$E_{R_1} = c_1\angle -90 \tag{5}$$

$$E_{R_2} = c_1\sqrt{(1-c_2^2)}e^{-\alpha l}\angle -90 \tag{6}$$

where c_1 and c_2 are the voltage couplings of the directional couplers, and α is the attenuation constant of the loop transmission line.

For the nth traversal of the loop, the voltages may be written in terms of E_{R_2} as follows:

$$E_2 = \sqrt{(1-c_1^2)} - c_1E_{R_2}\angle 0$$

$$E_3 = 0$$

$$E_4 = \frac{c_2e^{\alpha l/2}}{\sqrt{(1-c_2^2)}}E_{R_2}\angle 0$$

$$E_{R_1} = \frac{e^{\alpha l}}{\sqrt{(1-c_2^2)}}E_{R_2}\angle -90$$

where

$$E_{R_2} = c_1\sqrt{(1-c_2^2)}e^{-\alpha l} \cdot \left\{1+\sum_{m=1}^{m=n}(1-c_1^2)^{m/2}(1-c_2^2)^{m/2}e^{-m\alpha l}\right\}\angle -90.$$

Letting $n\to\infty$ and summing this expression in closed form, we obtain

$$E_{R_2} = \frac{c_1\sqrt{(1-c_2^2)}e^{-\alpha l}}{1-\sqrt{(1-c_1^2)}\sqrt{(1-c_2^2)}e^{-\alpha l}}\angle -90. \tag{7}$$

The condition for perfect rejection between arms 1 and 2 may be obtained by setting $E_2=0$, which yields

$$e^{2\alpha l} = \frac{1-c_2^2}{1-c_1^2}. \tag{8}$$

For perfect rejection, (8) requires that $c_2<c_1$ if $\alpha>0$. With $c_2=0$, the case of a single line coupled to a loop is obtained. The condition for maximum output from E_4 for a given bandwidth can be shown to be $c_1=c_2=c$. Thus, when attenuation of the loop is considered, the conditions are different for obtaining $E_2=0$ and E_4 = maximum.

The loaded Q of the filter may be calculated assuming $c_1=c_2=c$. At resonance the output voltage is

$$E_4 = \frac{c^2e^{-\alpha l/2}}{1-(1-c^2)e^{-\alpha l}}. \tag{9}$$

At a different frequency which corresponds to an electrical length around the loop equal to $2\pi n+\theta$, the output voltage is

$$E_4 = \frac{c^2e^{-1/2(\alpha l+j\theta)}}{1-(1-c^2)e^{-(\alpha l+j\theta)}}. \tag{10}$$

Defining $Q_L=f_o/2(f_o-f_1)=n\pi/\theta_1$, where f_1 and θ_1 are values at the half-power point, we have from (9) and (10),

$$E_4 = \left|\frac{c^2e^{-1/2(\alpha l+j\theta_1)}}{1-(1-c^2)e^{-(\alpha l+j\theta_1)}}\right|$$

$$= \frac{\sqrt{2}}{2}\frac{c^2e^{-\alpha l/2}}{1-(1-c^2)e^{-\alpha l}}.$$

Taking absolute magnitudes of each side and simplifying, we may solve for θ_1 in terms of c and α:

$$\cos\theta_1 = 1-\frac{[1-(1-c^2)e^{-\alpha l}]^2}{2(1-c^2)e^{-\alpha l}}. \tag{11}$$

If θ_1 is small, we may replace $\cos\theta_1$ by $1-(\theta_1^2/2)$ which yields

$$\theta_1 = \frac{1-(1-c^2)e^{-\alpha l}}{\sqrt{(1-c^2)}e^{-\alpha l/2}}. \tag{12}$$

The loaded Q of this filter[4] is

$$Q_L = \frac{n\pi\sqrt{(1-c^2)}e^{-\alpha l/2}}{1-(1-c^2)e^{-\alpha l}}. \tag{13}$$

It should be noted that this expression gives the true loaded Q of the resonator as it would be measured, and

[4] When a waveguide loop is used in the filter, Q_L as given in (13) must be multiplied by $(\lambda g/\lambda)^2$ where λg is the guide wavelength and λ is the free-space wavelength. Eq. (14) for insertion loss applies without change to the waveguide case.

takes account of the external loading of the couplers combined with the losses in the transmission of the loop.

The insertion loss at resonance is given by 20 log E_1/E_4, and, since $E_1=1$, we have

$$\text{Insertion Loss} = 20 \log \frac{1-(1-c^2)e^{-al}}{c^2 e^{-al/2}} \cdot \quad (14)$$

Eqs. (13) and (14) were derived assuming equal characteristic impedances of the transmission lines and assuming c to be the voltage coupling, but they apply correctly to unequal impedance of the ring and input and output arms if c^2 is defined as the power coupling of the directional couplers. For small couplings, c^2 may be expressed as a function of Q_2 and insertion loss as

$$c^2 = \frac{n\pi}{Q_L 10^{I.L./20}} \cdot \quad (15)$$

If the insertion loss is small we have

$$c^2 = \frac{n\pi}{Q_L} \cdot \quad (16)$$

The foregoing analysis is applicable only when the filter is perfectly tuned. It is possible, however, to analyze the problem by assuming two resonant orthogonal modes corresponding to electric and magnetic coupling from the external transmission lines to the loop. The discussion will now be confined to shielded-strip-line directional couplers as developed at Stanford Research Institute.[5,6] (The principle applies equally well for all directional couplers.) The analysis of footnotes 5 and 6 utilizes the two basic TEM modes that may exist on the pair of coupled strips (*i.e.*, the even and odd modes). Fig. 3 shows the electric fields of these two modes, in which the strips are either at the same potential or at opposite potentials (corresponding to even and odd modes, respectively). The impedance of the strip line is dependent upon the polarity of the strips in the coupling region. It has been shown that $Z_o' = \sqrt{Z_{oo}Z_{oe}}$ where Z_o' is the characteristic impedance of a single strip line that will match the directional coupler; Z_{oo} and Z_{oe} are the odd- and even-mode characteristic impedances of the coupled strips, respectively. The odd mode corresponds to electric coupling between the strips, and the even mode to magnetic coupling. Because of the differences in impedance of the resonant loop, it may be treated as a length of nonuniform transmission line as shown in Fig. 4. In general, the resonant frequency of the even-mode transmission line will differ from that of the odd-mode line. It must be noted that, in this analysis, the directional coupler is considered to be a device which couples energy (nondirectionally)

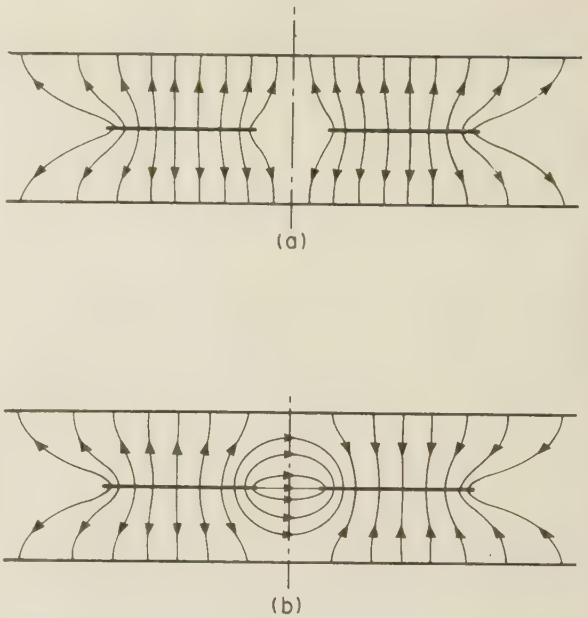

Fig. 3—Odd and even mode electric field distributions existing in a pair of coupled strips. (a) Even-mode electric field distribution. (b) Odd-mode electric field distribution.

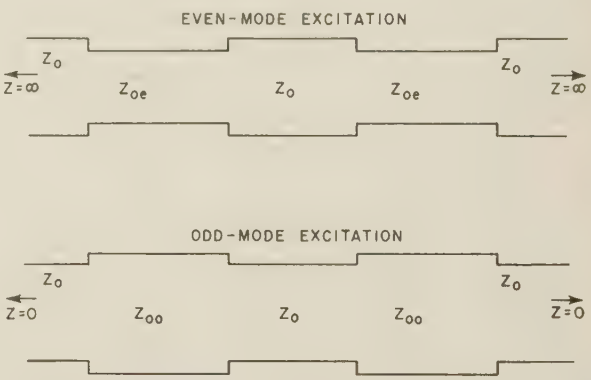

Fig. 4—Nonuniformity of even and odd mode traveling-wave loop transmission lines.

to the loop in the form of two orthogonal resonant modes. At a frequency for which the electric (odd) mode is resonant, waves travel in opposite directions in the loop, forming a standing wave with voltage maxima at the centers of the coupling regions and voltage minima at the sides of the loop. Fig. 5 illustrates this case and also the magnetic coupling case for which resonance may occur at a slightly different frequency. Each resonant mode alone yields no directivity, but if the modes are made to resonate at the same frequency—either by a judicious choice of the strip lengths and widths in the loop or by reducing the higher resonant frequency by means of tuning screws at the voltage maxima—the two modes superimpose into a pure traveling wave. Under these conditions the filter obeys the theory derived in the previous section.

The difference in resonant frequency of the two modes may be made equal to zero by choosing the characteristic impedance of the sides of the loop to be $Z_o = \sqrt{Z_{oe}Z_{oo}}$. However, tuning devices are usually still

[5] S. B. Cohn, "Shielded coupled-strip transmission lines," IRE TRANS., vol. MTT-3, pp. 29–38; October, 1955.

[6] E. M. T. Jones and J. Bolljahn, "Coupled strip line filters and directional couplers," IRE TRANS., vol. MTT-4, pp. 75–81; April, 1956.

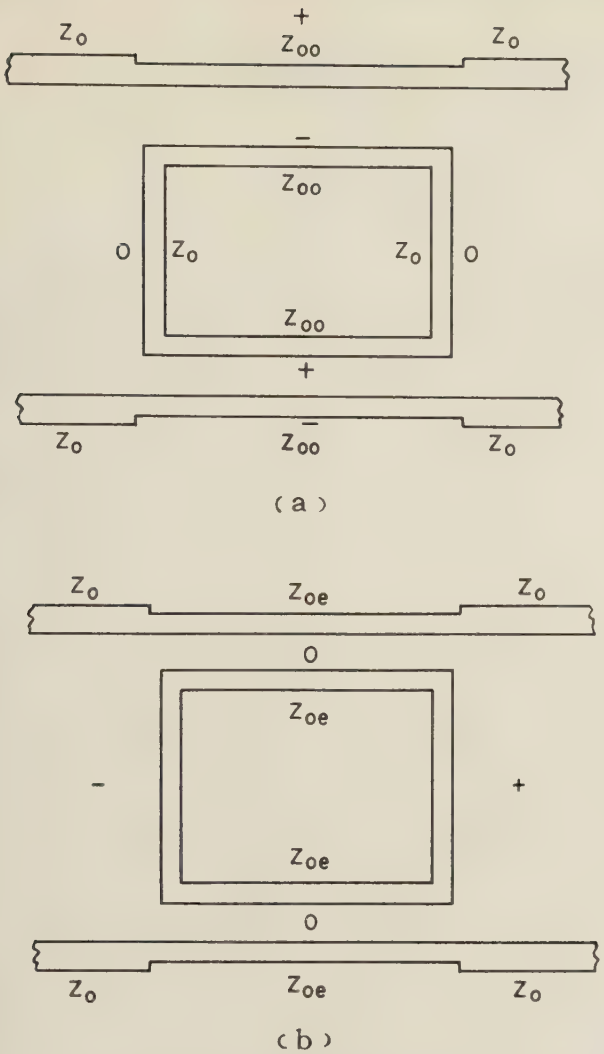

Fig. 5—(a) Electric field coupling to loop. (b) Magnetic field coupling to loop.

necessary to compensate for points of reflection that might otherwise destroy the orthogonality of the two modes. It can be shown that three shunt capacitive susceptances, spaced at quarter-wavelength intervals around the loop, will serve both to tune the two modes to the desired frequency, and to eliminate any spurious coupling between the modes. However, in practice, four susceptances are somewhat easier to tune and offer less deterioration of the insertion loss.

Design and Experimental Results

A typical design procedure for a traveling-wave directional filter might be as follows.

The filter specifications should include such items as resonant frequency, loaded Q (or bandwidth), maximum allowable insertion loss in the pass band, and the characteristic impedance of both the input and output. It is first necessary to select tentatively a strip-line cross section and perform a preliminary theoretical check to ascertain whether the desired loaded Q and an acceptable pass-band loss may be obtained with the attenuation constant[7] afforded by this cross section.

From (13) and (8), it is possible to calculate the values of c_1 and c_2, which will be equal in the case of minimum pass-band loss and unequal in the case of perfect rejection. Eqs. (13) and (14) are generally accurate for the case of low attentuation when $c_1 \neq c_2$ if one uses the average value of c_1 and c_2 for c. The formulas in the article on directional couplers by Jones and Bolljahn[6] may be employed to calculate, from c_1 and c_2, the characteristic impedances Z_o, Z_{oo}, and Z_{oe}. From Cohn's article on coupled strip line,[5] the width, w, of each strip and the spacing, s, between the strips may be found from a knowledge of Z_o, Z_{oo}, and Z_{oe}. It is probably best to make the length of the coupling region one-quarter wavelength because the separation, s, is then a maximum for a given coupling value, and because the more nearly square shape of the loop allows the resonant modes to approach a common frequency.

As shown in Fig. 7, the corners of the loop are mitered. Square and round corners were also used, but resulted in a wide frequency separation between the two orthogonal resonant modes.

Since it is impossible to design a loop which will resonate perfectly at a given frequency, it is necessary to provide some means of tuning not only the orthogonal modes but any reflections that might exist in the loop. A simple but effective means of tuning may be achieved by means of four pairs of screws placed at one-quarter wavelength spacings around the loop, preferably at the voltage maxima of the two orthogonal modes.

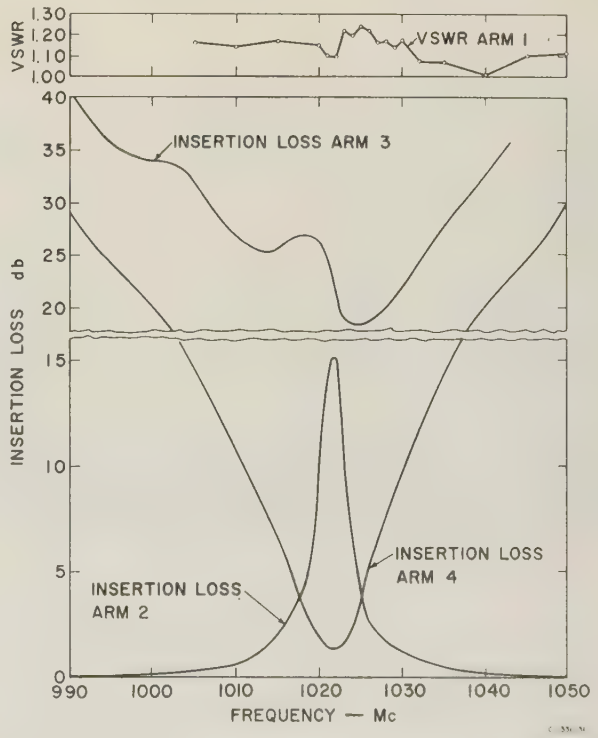

Fig. 6—Frequency response of traveling-wave directional filter.

[7] S. B. Cohn, "Problems in strip transmission lines," IRE Trans., vol. MTT-3, pp. 119–126; March, 1955.

The screws are so located that they may be screwed in evenly from opposite ground planes towards the center of the strip; this affords a symmetrical tuning which will not excite the TEM mode between the parallel ground planes. It should be noted that the screws may be used only to reduce the resonant frequency of the loop. Copper tuning screws allow tuning from 1080 to 1020 mc with a change in insertion loss from 1.1 to 1.3 db.

Fig. 6 gives experimental results for a traveling-wave directional filter. A more complex filter circuit (Fig. 7), containing two separate resonant loops, was also constructed and tested. This circuit separates two frequencies in the 1000 mc region from a spectrum of frequencies incident at the input arm. The experimental loaded Q's of this filter agreed with the theoretical value within 5 per cent. The directional couplers were designed to have 16-db coupling at the low-frequency loop and 17-db coupling at the high-frequency loop. One-half-inch plate spacing with polystyrene dielectric was used in this design. The over-all dimensions of this dual filter were 9 by 4.5 by 1 inches. Fig. 7 gives the measured

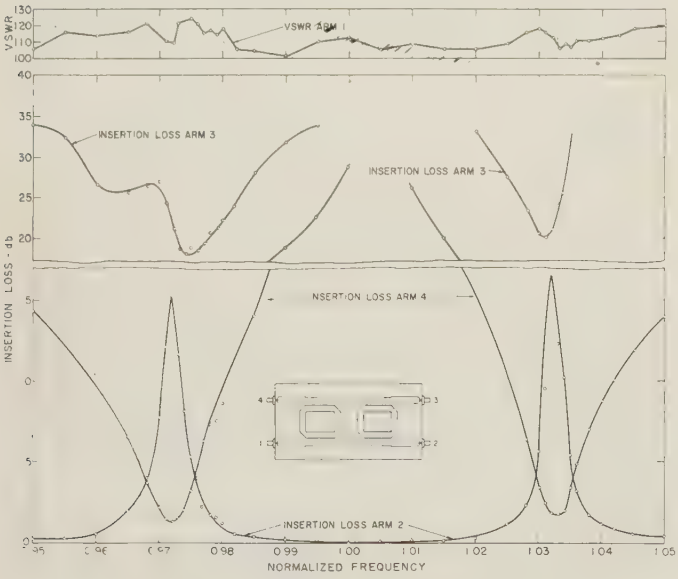

Fig. 7—Frequency response of dual directional filter.

response of this dual-loop filter. A high-power test with 3 kw of CW power at the resonant frequency of the higher loop showed no sign of voltage breakdown. The maximum average power that may be tolerated over a long period of time is limited by the dissipation loss of the filter and the thermal properties of the dielectric employed.

Fig. 8 shows a diagram of a double loop filter which has been designed and tested. The typical double-tuned-circuit response is obtained both for the band-pass and band-rejection cases. The coupling coefficient between two identical loops for small coupling values and narrow bandwidths is $K = c/n\pi$, where c is the coupling coefficient of the directional coupler between the two loops and n is the length of the loop in wavelengths. The exact coupling coefficient for two coupled loops is given by

$$K = \frac{1}{n\pi} \tan^{-1} \frac{c}{\sqrt{1 - c^2}}. \tag{17}$$

The output voltage for such a filter is given as

$$E_4 = \frac{c_1 c_2 c_3 e^{-1/2(\alpha + j\beta)l}}{(1 - \bar{c}_1 \bar{c}_2 e^{-(\alpha+j\beta)l})(1 - \bar{c}_2 \bar{c}_3 e^{-(\alpha+j\beta)l})(1 - \bar{c}_1 c_2^2 \bar{c}_3 e^{-2(\alpha+j\beta)l})} \tag{18}$$

where c_1, c_2, and c_3 are the voltage coupling coefficients of the directional couplers, $\bar{c}_1 = \sqrt{1 - c_1^2}$ etc.

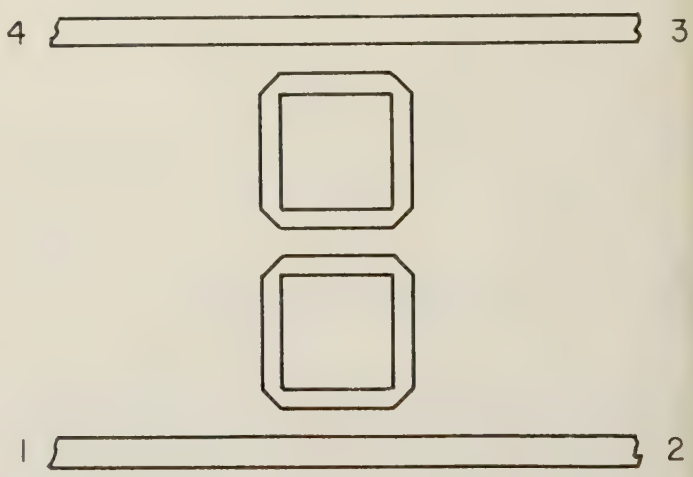

Fig. 8—Layout of double-tuned traveling-wave directional filter.

Conclusion

It may be seen that this type of filter and related types of filters present to the microwave engineer a new type of circuit which is simple in construction, small in size, light weight, and has excellent electrical performance.

Acknowledgment

The author wishes to express his thanks to S. B. Cohn, and E. M. T. Jones for their valuable contributions in the course of this work.

Miniaturization of Microwave Assemblies*

LEONARD LEWIN†

Summary—A method of construction is described in which waveguides are arranged in a single plane with adjacent walls common. An assembly is made from a top and bottom plate between which partition walls are arranged to constitute the transmission region. A hybrid-*T* is made from a 3 db coupler, and a microwave repeater is described consisting of five band-pass filters, two hybrid-*T*'s, an isolator, and several other component aspects.

Setting up in situ is achieved by the use of a Bethe hole coupler to monitor the reflection or transmission at a number of specially located check ports.

No electric coupling can be measured across a soldered fabricated waveguide wall.

THERE ARE two basic ways of reducing the bulk and weight of microwave assemblies. The first consists in the reduction in the transverse dimensions of the transmission system employed. This method includes the use of stripline, loaded guide, and ridge guide, and in many cases leads to a loss in performance and tighter tolerances as compared to standard rectangular guide construction. The second method consists in the use of waveguide of standard cross section rearranged topologically so as to form a compact geometrical configuration of components.

Examination of some existing waveguide systems shows that most of the bulk is taken up by flanges, connecting lengths, corners, twists, etc., and by the space which has to be provided to assemble or get at the various pieces. Much of this is occasioned by the three-dimensional layout, the main cause of which would appear to be the familiar hybrid-*T* with its *E*, *H*, and side arms all at right angles to each other. With space at a premium a three-dimensional construction is a luxury. Accordingly a first step towards a compacted arrangement consists in the planarization of the system. This calls for a planar type hybrid-*T*, and a convenient type to use is a simple 3 db directional coupler. The multipost coupler described by Tomiyasu and Cohn[1] is convenient for this purpose and a unit 5.7 inches long with five posts has been constructed for the 4000 mc band. The directivity is in the 20 db range and the power in the straight through arm varies from 44 per cent to 56 per cent in the 7.2 to 8.1 cm band. These figures could no doubt be improved considerably, but for a microwave crystal mixer they are probably adequate.

A second step involves the elimination of connecting pieces and flanges. This brings the walls of adjacent waveguides into contact and makes way for the third step, in which an integral construction is achieved by milling slots in a baseplate and cover-plate and inserting partitions into the slots, thereby creating several waveguide channels side by side. The component aspect is built into these channels before the top plate is fixed on. It has been found that by screwing the partitions to the plates at intervals of one inch the coupling between guides, even in the absence of soldering, is very low. The side walls were a light push fit into the milled grooves, and with the screws loosened the coupling rose to −50 db. Thus despite the fact that the constructional gaps (such as they are) cut the lines of current flow it is possible, for some applications at least, to avoid the necessity of soldering the partitions. It is not easy to say just how small the leakage is when the screws are tight. The limit of detection in these measurements was about −75 db, and at about the −70 db level there was some slight coupling due to leakage at the input flanges; this was in excess of any leakage there may have been through the partition walls themselves. No difficulty was experienced in soft-soldering. An alternative, which was not tried, is to plate the partition wall edges with a thin coating of indium, and to rely on mechanical pressure to achieve an adequate cold weld.

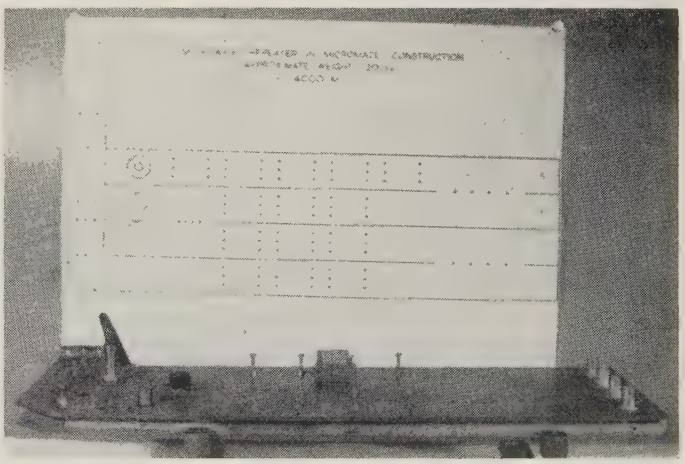

Fig. 1.

Fig. 1 shows schematically the waveguide part of a microwave repeater, together with a block diagram of the functioning parts, made according to the principles outlined above. It has been possible to save an entire repeater bay by this means and to reduce the weight of waveguide by a factor of four. Much of this latter came from the elimination of flanges. The repeater comprises five band-pass filters, two hybrid-*T*'s, a directional

* Manuscript received by the PGMTT, July 16, 1956. Presented before the National Symposium on Microwave Techniques, Philadelphia, Pa., February 2–3, 1956.

† Standard Telecommunication Labs., Progress Way, Enfield, Middlesex, England.

[1] K. Tomiyasu and S. B. Cohn, "The Transvar directional coupler," PROC. IRE, vol. 41, pp. 922–926; July, 1953.

coupler, a load, one unbalanced crystal mixer, two balanced mixers, an isolator, a corner, a local oscillator, and an output for a traveling wave tube. The over-all dimensions are about 1 foot×2 feet 6 inches×1 inch. The isolator, of the resonance absorption type, buffers the local oscillator, which also serves as an output tube, from unwanted frequency components produced in the mixer. Its performance is about 1 db/20 db and its permanent magnet can be seen in Fig. 2. A saving in

Fig. 2.

length of the band-pass filters was achieved by using triplets of posts across the guide instead of single posts, thus permitting quarter-wave separation of the tuned cavities without higher order mode coupling between them. It is not known how typical this example may be, but a comparison of the new, compact assembly with the arrangement which it replaced was certainly very striking.

The price to be paid for an integrated construction is lack of versatility and inability to alter the design and change components on the one hand, and the need to align components and test them in situ, on the other. The first point makes the method unsuitable for laboratory work, or design of early models. Only at a late stage in the design of equipment is it suitable to go over to the compacted form, or Micromaze, as we have called it.

With regard to testing and matching components in situ, the absence of long and movable connecting pieces between elements makes possible a certain amount of mutual compensation which can be sufficiently broadband for many purposes. In order to align filters, match crystals, etc., it is necessary to insert a signal at certain positions and also to monitor the response at other positions. In the case of the repeater of Fig. 1, there are a number of "natural" entry points, such as the local oscillator input, the crystal mount positions, and so on. A complete test procedure has to be prescribed, with each component tuned or lined up in order, and it was found that to do this efficiently eight additional monitor positions were needed. Each of these took the form of a hole, $\frac{5}{8}$ inch diameter, which was plugged under normal conditions. (No discontinuity at a plugged hole could be detected.) In order to insert or extract a signal the plug is removed, and a monitor guide is coupled by means of a short boss with a $\frac{5}{8}$ inch diameter bore. The coupling is of the type known as a Bethe hole coupling, and with the monitor guide at about 35° to the main axis—the angle is not critical to within a degree or two—a directivity of 30 db is readily obtained. In order to improve this to a figure in excess of 40 db over a 20 mc band a slight screw insertion in the coupled arm is used to cancel out the small remaining wave. In use, the monitor arm is clamped to the sides of the repeater, as shown in Fig. 2. and once the angle is set it can be maintained for any movement of the guide over the test piece. In fact the monitor is set up, once and for all, by using a subsidiary guide mounted parallel to the repeater axis and the correct angle and trimmer screw insertion found. Although it is not certain to what extent the accuracy of setting is maintaned, test filters in isolated guide tuned by this "in situ" method had responses in no way inferior to those tuned by more conventional methods. For these measurements a swept frequency bench and cro display were used. By the use of a movable and calibrated probe in the coupled arm it is possible to produce a reflection which exactly cancels the reflection produced by the test piece, and in this way measurements of both the amplitude and phase of the reflections can be made. For example, the input to the repeater, consisting of a tuned filter and an unbalanced mixer could be tuned readily under active conditions to a (voltage) reflection of the order of 1 per cent over a 14 mc band, this being the limit provided by the filter.

A fuller description of the test apparatus will appear in a later paper. It may be added here, however, that one of the difficulties encountered was the need to deal with very small signals, since the Micromaze is tested under low signal conditions. Thus, if 10 microwatts of input signal incident on the input mixer crystal is reflected with a one per cent voltage reflection coefficient then it becomes necessary to measure signals at the −60 dbm level. The coupling coefficient of the coupler is −35 db so that when there is no direct entry a further attenuation of the signal occurs: fortunately in these positions a somewhat larger incident signal can be used. In order to deal with these small signals a superheterodyne receiver is used, and since the frequency is being swept over something like 120 mc the local oscillator must keep closely in step if the necessary signal to noise is to be achieved. It was eventually decided to derive the local oscillator signal directly from the swept frequency oscillator by beating in a high level crystal mixer. An intermediate frequency of 1000 mc was chosen so that the various beat frequencies and other harmonics could be adequately dealt with. The 1000 mc signal after detection was mixed with a subsidiary signal at 940 mc and the resulting signal amplified in a conventional 60 mc receiver.

The author wishes to acknowledge the assistance of his colleagues in carrying out the work described above, in particular, H. Grayson who originally conceived the idea of compacting the waveguide, and G. Craven who did much of the associated design and measurements.

Recent Advances in Finline Circuits*

SLOAN D. ROBERTSON†

Summary—**Detailed studies of transmission properties of the finline coupler have revealed existence of certain phenomena which adversely affect the transmission characteristics. A discussion of the origin and successful elimination of such effects is described.**

New applications for the finline coupler have been found in the design of hybrid junctions, twists and bends in multimode waveguide, and other polarization selective devices.

The paper concludes with a presentation of theoretical and experimental results in the application of finline techniques to low-pass microwave filters.

WITH THE demand for ever wider frequency bands in microwave communication systems, it is evident that means for broadbanding various circuit elements must be found. Finline techniques already offer the means of accomplishing this in several devices and may be expected to be of use in others.

Some finline circuits are capable of operating over at least a three-to-one frequency range. One of these, the basic finline coupler, announced last year,[1] is shown in Fig. 1. It consists of a length of circular waveguide

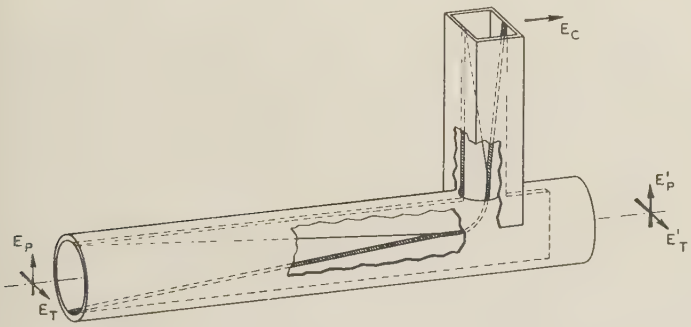

Fig. 1—Finline coupler.

fitted with a pair of diametrically opposite, thin metal fins which taper in from the outer wall of the guide until their opposing edges are separated by a narrow gap or slot at the center. Thus, substantially all of the energy associated with the electric field E_p (where the subscript p denotes that the vector is parallel to the plane of the fins) is transformed from the dominant mode of propagation in the circular waveguide to a finline mode in which the energy is largely confined to the gap and its immediate vicinity. This energy may then be removed from the circular guide by curving the finline and bringing it out through a small hole in the side wall. It may then be launched into another waveguide as shown.

* Manuscript received by the PGMTT, July 16, 1956. Presented before the National Symposium on Microwave Techniques, Philadelphia, Pa., February 2–3, 1956.

† Goodyear Aircraft Corp., Litchfield Park, Ariz.

[1] S. D. Robertson, "The ultra-bandwidth finline coupler," PROC. IRE, vol. 43, pp. 739–741; June, 1955.

On the other hand, a wave characterized by the transverse field E_T will pass on through the guide, relatively undisturbed by the presence of the fins, and will emerge as E_T'.

One can readily see that the finline coupler offers a means whereby it is possible to separate two waves perpendicularly polarized to one another. The fact that this is done with smooth tapers several wavelengths long suggests that the coupler ought to work over very wide bands. Such has been found to be the case.

If only one wave is present in the guide, it is found that one may abstract any desired proportion of its energy by simply rotating the coupler about its axis so that the plane of the fins makes an angle with respect to the plane of polarization of the wave. The abstracted field will then be proportional to the cosine of the angle.

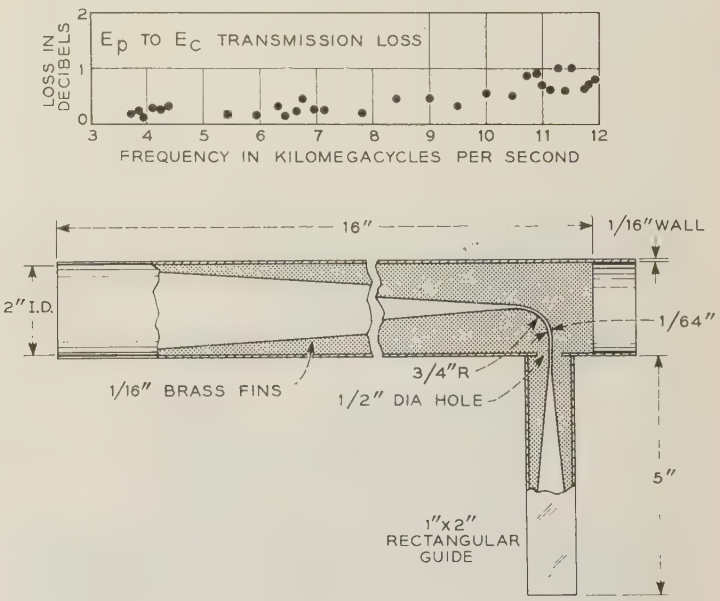

Fig. 2—Transmission characteristics of a coupler having the dimensions shown.

Fig. 2 shows a plot of the transmission losses from E_p to E_c for a coupler having the dimensions shown in the lower part of the figure. It will be observed that, for the most part, the losses are less than one db over the entire range of frequencies from 3.75 to 12.0 kmc. Over most of this range the losses are only a few tenths of a db. The losses encountered by the transverse mode in going from E_T to E_T' are less than 0.1 db, and are not plotted in the figure.

Mode Resonances in the Finline Coupler

Recent detailed transmission measurements on the finline coupler have uncovered several sharp peaks in

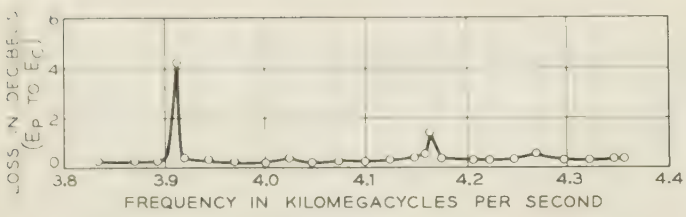

Fig. 3—Half-cylinder mode resonant loss peaks in the 4 kmc band.

the transmission loss curves which have not been observed in the earlier measurements of Fig. 1. A sample transmission loss curve showing two of these peaks in the 4 kmc band is shown in Fig. 3. It will be noted that the higher frequency peak is much smaller than the lower frequency one. In fact, careful measurements with swept frequency oscillators covering the bands between 5.8 and 6.6 kmc and also between 10.5 and 12.1 kmc have not shown any of these sharp peaks at all.

Studies have shown that these loss peaks are due to the excitation of a dominant mode in each of the half-cylinders separated by the fin. The field configurations of these dominant modes are sketched in the end view of the coupler in Fig. 4. The dominant modes are very

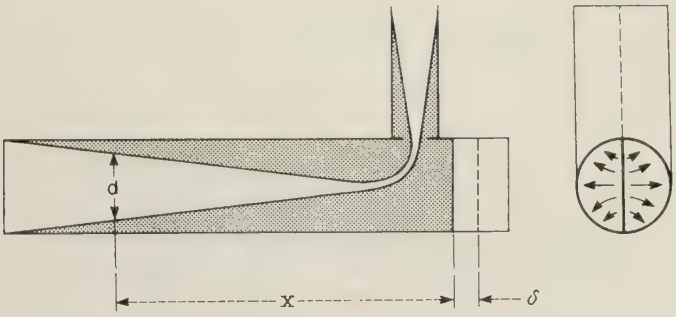

Fig. 4—Geometry of half-cylinder resonant modes.

likely generated in the vicinity of the curved portion of the finline. The geometry causes them to be 180° out of phase in the two half-cylinders. After being launched, the modes are propagated in both directions along the guide. Those propagated to the right soon encounter the edge of the fin and are reflected, since the vectors in each half-cylinder are out of phase and cancel beyond the fin edge. Likewise, the waves propagated to the left ultimately reach a point where the fin separation d is sufficient to permit the vectors to cancel and reflect the waves. If the spacing x between these two reflecting points is an integral number of half wavelengths, the sections will resonate and will absorb some of the useful power from the finline. This is believed to be the origin of the loss peaks in the curve.

These peaks will not all be equally objectionable. If the point where the finline launches the half-cylinder modes is at a position in the standing wave pattern of the resonant section where there is a favorable coupling between the finline and the resonant modes, the loss peaks may be rather high. At other frequencies the coupling may be unfavorable and the loss peaks may be low or even negligible. The absence of these peaks at the higher frequencies is possibly due to two factors. The increase of the electrical length of the tapers with frequency results in a better impedance match between the guide and the finline gap and lowers the coupling to the half-cylinder modes. On the other hand, increased ohmic losses at the higher frequencies would be expected to dampen the resonant peaks.

The identification of the loss peaks of Fig. 3 with half-cylinder mode resonances was easily confirmed. It was found that the locations of the peaks could be shifted by extending the back edge of the lower fin by a distance δ as shown in Fig. 4. With the fin extended, the length of the resonant chamber becomes $x+\delta$, and at resonance it must include an integral number of guide half-wavelengths.

$$x + \delta = n\lambda_g/2. \tag{1}$$

With the well-known relation between λ_g and the cut-off frequency f_c, (1) can be solved for the resonant frequency.

$$f = [n^2c^2 + 4f_c^2(x + \delta)^2]^{1/2}/2(x + \delta). \tag{2}$$

Observations of the shift in resonant frequency for three different, known values of δ made it possible to solve for the three unknowns x, n, and f_c. For the coupler of Fig. 2, x is found to be 27.6 cm, n is 3 for the 3.92 kmc peak, and f_c is 3.54 kmc. The latter is slightly higher than the theoretical cut-off frequency of 3.47 kmc for the half-cylinder mode in 2 inch diameter guide. This is due to the reduction in half-cylinder cross section caused by the thickness of fins. It is perhaps of interest that the fin separation d at the left-hand reflection point is about 62 per cent of the waveguide diameter.

Resonant peaks have been successfully eliminated by introducing loss at a point where it can absorb energy from the half-cylinder dominant modes. Fig. 5 shows the results of one experiment in which this was done. A 12.5 ohm per square resistive strip was placed in the plane of the fin adjacent to the right-hand edge. This strip absorbs energy from the half-cylinder modes which would be reflected at this point and kill the resonances. Since it lies in an equipotential plane of the transverse mode, the resistive strip will have little effect upon the transmission from E_T to E_T'.

Applications of Finline Couplers

Fig. 6 shows how two finline couplers may be arranged to form a hybrid junction. When the planes of the fins are inclined at an angle of 45 degrees, as shown in the

figure, one obtains a 3 db hybrid. A wave entering at E_1 passes through the left-hand coupler without modification. Upon entering the second coupler, however, it is split into two equal components, one of which emerges at E_3, and the other emerges at E_4. Likewise, a wave entering E_2 travels through the first coupler and is split by the second coupler into two equal components. Degrees of coupling other than 3 db may be obtained by inclining the fins at angles other than 45 degrees.

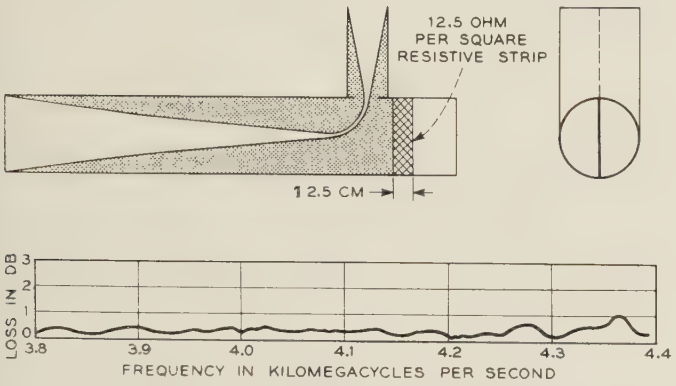

Fig. 5—Elimination of mode resonances.

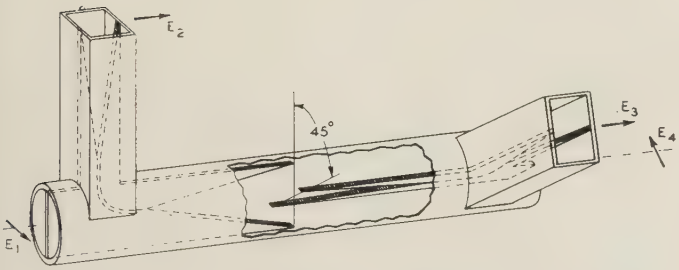

Fig. 6—Ultra-broadband hybrid junction using two finline couplers.

Fig. 7 shows another application of finline techniques to form a flexible waveguide joint or bend. As seen in the figure, the device comprises input and output waveguide sections containing 8-inch long tapers for matching in and out of the flexible finline section between. The fins in this case are exposed to free space in the region between the waveguide sections. It has been found that, for the device shown, the transmission losses are reasonably low in the 4 kmc band even when the flexible fins are bent or twisted. Lower losses are obtained by placing a sheet of dielectric between the fins in the exposed portion of the path. Apparently the action of the dielectric in confining the fields more closely to the gap, thereby reducing the radiation losses, exceeds the added dissipation due to the dielectric. The dielectric has been tapered at the ends for purposes of impedance matching. In the lower part of the figure a curve of the insertion loss over the 4 kmc frequency band is plotted. The joint can be bent or twisted through angles of as much as 45 degrees without substantial change in the transmission losses.

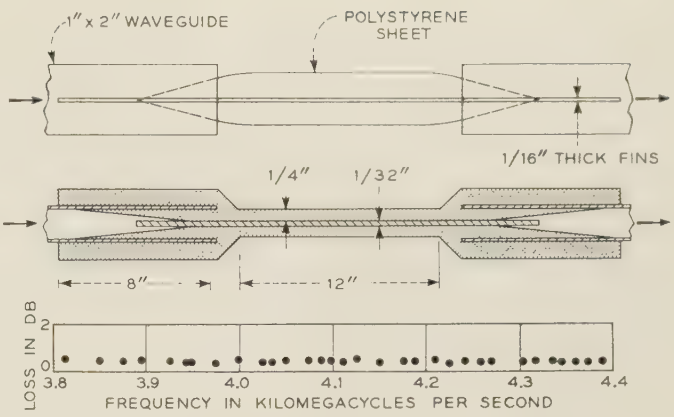

Fig. 7—Flexible finline bend or twist. Curve shows loss vs frequency.

It has been suggested that four finline couplers can be combined as shown in Fig. 8 to form a broad-band, right-angled, waveguide bend. The figure is of a model and is for illustrative purposes only. The large wooden cylinders represent hollow metal waveguides, and the brass strips represent finlines. It can be seen that the vertical component of a wave entering the lower waveguide will be collected by a finline coupler and will emerge through the side of the guide along the finline path shown and can then be launched into the upper waveguide by means of another coupler. Similarly, the horizontal component of the input wave will be collected by the horizontal coupler and will then be launched into the upper guide. It will be noticed that the arrangement possesses complete symmetry, and that the path lengths traveled by the two components are equal. Hence, there will be no phase difference between the two components as they emerge from the upper guide. Such a bend is expected to operate over the same broad frequency band over which the individual couplers have been found to operate.

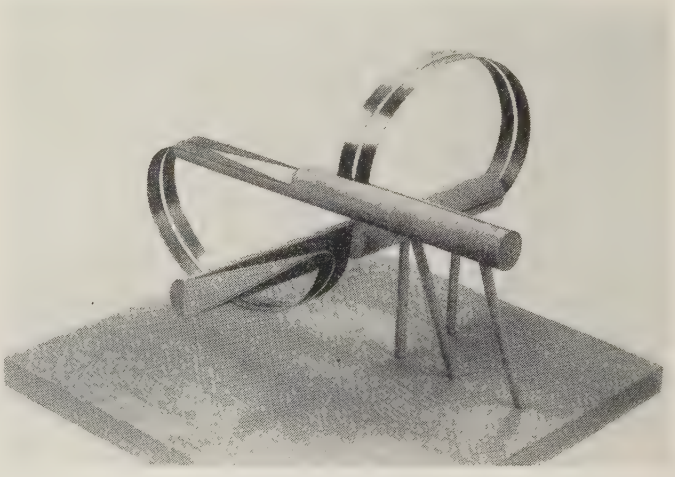

Fig. 8—Model showing the arrangement of four finline couplers in a broad-band, right angle bend in circular waveguide.

Finline Filters

With finline techniques it has been found possible to design frequency filters using the ordinary lumped-circuit theory that is used in low-frequency filter design. Analogs have been found which correspond to the series or shunt inductors and capacitors required for building up conventional π or T networks. Some of these analogs are shown in Fig. 9. It is seen that the finline equivalents for series inductance and shunt capacitance are quite simple, consisting only of a slot less than $\lambda/4$ in depth for the former, and a short tab protruding into the gap for the latter.

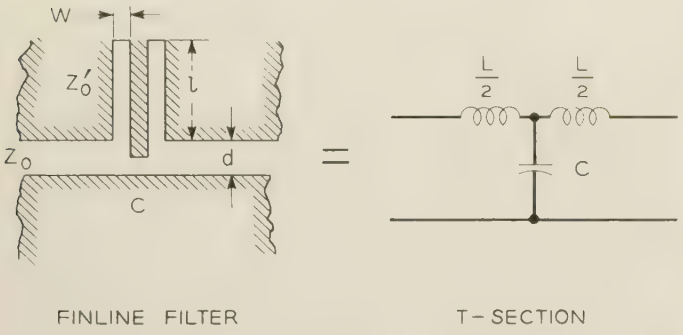

Fig. 9—The equivalence between a finline circuit and a low-pass T section.

Evidently, with a series inductor and a shunt capacitor, one may design a low-pass, T-section filter having a specified iterative impedance Z_0, a cut-off frequency f_c, and a frequency of infinite attenuation f_∞ corresponding to the frequency at which the series slots become antiresonant.

The standard low-pass T-section design equations are

$$f_c = 1/\pi(LC)^{1/2} \tag{3}$$

and

$$Z_0 = (L/C)^{1/2}[1 - (f/f_c)^2]^{1/2}. \tag{4}$$

In the usual filter, L and C are both constants. In the present case, however, C is a constant, but L varies with frequency according to the relation

$$L = (Z_0'/\pi f) \tan \beta l \tag{5}$$

where $\beta = 2\pi f/c$ and Z_0' is the characteristic impedance of the stub lines. Since L is a function of f, the value for f_c in (3) also varies with f. This means that, at any particular frequency below the true cut-off frequency, f_c in (3) gives the apparent cut-off frequency for the particular value of L then prevailing. The true cut-off f_c' is the particular value of f_c defining the point where Z_0 passes from a real to an imaginary value.

The variation of L with f leads to a similar difficulty in (4) in that Z_0 approaches zero as the frequency decreases. This can be evaded, however, in the microwave case since the frequencies of interest will not approach zero but will have a lower bound defined by the low-frequency cutoff of the finline waveguide itself. The problem may be resolved quite easily by defining the lowest operating frequency of interest f_1 and designing the filter so that it will exhibit the correct value of Z_0 at that frequency.

If f_c' is substituted for f in (3) and (5), one may combine these equations and solve for C. Likewise, if f_1 is substituted for f in (4) and (5), one may obtain a second expression for C. If the equations for C are then equated one obtains

$$Z_0'^2 = f_1 Z_0^2/[f_c' \tan \beta_c' l - f_1 \tan \beta_1 l] \tan \beta_1 l \tag{6}$$

where $\beta_c' = 2\pi f_c'/c$ and $\beta_1 = 2\pi f_1/c$.

It will be apparent that, having specified values for f_1, Z_0, f_c', and f_∞, one may immediately obtain $l = c/4f_\infty$, and then Z_0' the characteristic impedance of the stub line, from (6). The shunt capacitance C is given by

$$C = 1/\pi f_c' Z_0' \tan \beta_c' l. \tag{7}$$

Finally, it is necessary to determine the slot widths d and w to produce the required line impedances Z_0 and Z_0', respectively, and to compute the spacing between the stubs and the fin spacing in this region to establish the value of C.

S. P. Morgan[2] has dervied formulas for the characteristic impedance of a finline contained in a circular waveguide of a given radius. Numerical values have been obtained for the case of a circular guide of one inch radius with 1/16 inch thick fins separated by a gap spacing equal to d. For this particular fin thickness and for gaps ranging in value from 0.005 inch to 0.032 inch the characteristic impedance has been found to be given approximately by the formula,

$$Z_0 = 8d^{2/3} \qquad (d \text{ in mils}). \tag{8}$$

For finlines operating at frequencies far above cut-off, it is assumed that the characteristic impedance depends primarily upon the fin thickness and the gap spacing, and that it is relatively independent of the size or shape of the outer waveguide envelope. If this is true, one may use the above formula for calculating the required slot widths d and w in a finline filter irrespective of the form of the outer shell.

In order to test the general aspects of the theory, an experiment a filter has been designed and constructed. The specified parameters were $Z_0 = 45.5$ ohms, $f_1 = 3.0$ kmc, $f_c' = 8.5$ kmc, and $f_\infty = 11.05$ kmc. The computed quantities were $Z_0' = 25.4$ ohms, $C = 5.5 \times 10^{-13}$ farads, $d = 0.0135$ inch, $W = 0.0056$ inch, and $l = 0.268$ inch. The spacing between the stubs and the fin spacing in this

[2] Unpublished work.

region, required to establish C, were computed using the parallel plate expression for capacitance and making due allowance for fringing. These dimensions are shown in Fig. 11.

The variation of iterative impedance with frequency for this filter design has been computed and is shown in the curve of Fig. 10. It will be noted that the impedance is quite constant from 3 to 7 kmc. The impedance of a simple T-section filter, whose inductance L is constant with frequency, drops off much more rapidly with frequency than the curve given in the figure. The latter has more of the shape characteristic of the m-derived sections of filter theory.

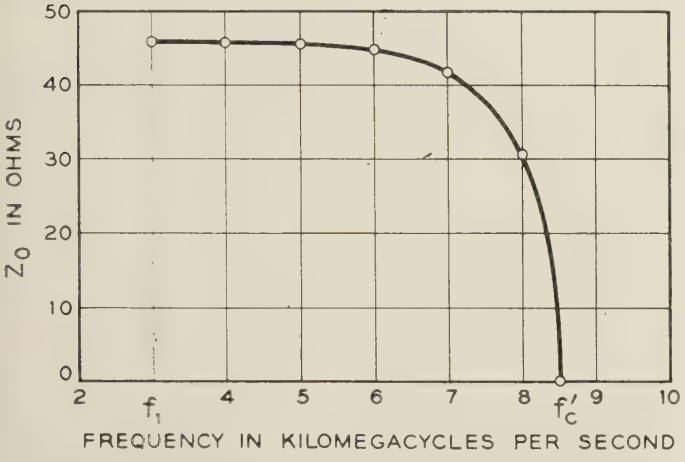

Fig. 10—Variation of the theoretical iterative impedance of a finline filter with frequency.

An experimental filter was built in conformity with the above design. Details of the filter are shown in Fig. 11. The fins were mounted in a section of 1 inch×2 inches rectangular waveguide. The ends of the fins, although not shown in the figure, were tapered in order to provide an impedance match to the waveguide.

The measured loss as a function of the frequency is shown in the lower part of the figure. The dotted portions of the curve represent frequencies which were not within the range of the measuring equipment used. Evidently the lumped-circuit design theory is capable of giving reasonably good results.

The results of these experiments show that it is possible to use finline techniques in building microwave filters. It is thought that a more detailed study of

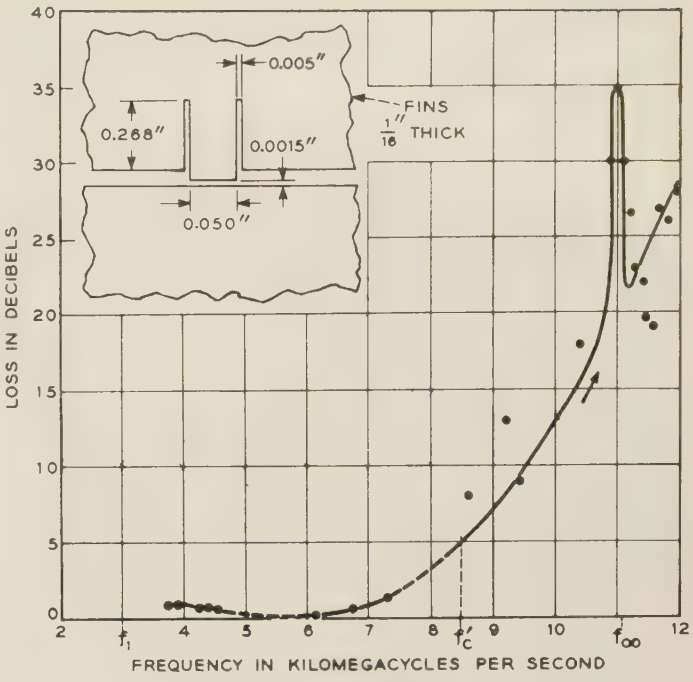

Fig. 11—Experimental transmission characteristics of a finline filter.

these techniques will lead to refinements resulting in filters having lower losses and probably sharper cutoffs than those measured with the exploratory model described here. Higher discriminations can probably be obtained by using several T sections in tandem.

The principles outlined here may possibly be applied to other wide-band microwave circuits such as equalizers, impedance transforming networks, etc.

Conclusion

Apparently finline techniques offer the means of designing certain microwave circuit components which will operate over much wider frequency bands than heretofore possible with standard components. It is thought likely that refinements and extensions of this work will lead to improved performance and unfold new applications of finline techniques.

Acknowledgment

The author wishes to express his appreciation to C. F. Chapman for his enthusiastic assistance in the experimental portions of this work.

Recent Advances in Waveguide Hybrid Junctions*

PATRICIA A. LOTH†

Summary—**Design techniques for waveguide hybrid tee junctions, resulting in convenient structures and simple internal matching elements for increased bandwidth and power-handling capacity are described, and experimental data are given.**

THE EVER-INCREASING variety of circuit applications of the waveguide hybrid junction has been the incentive for many advances in its design. Those which will be described are designs for a 12 per cent frequency band, featuring simple impedance-matching elements, high power-handling capability, or particularly convenient structures for connection to adjacent circuit elements.

To review briefly, a hybrid junction is basically a 4-port network, as shown in Fig. 1, so constructed that

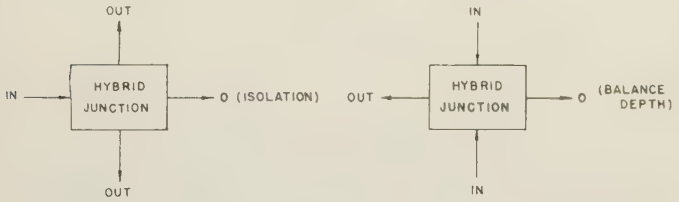

Fig. 1—Hybrid junction circuits.

power incident at one port divides equally into two of the other ports, and does not pass directly to the fourth, or conjugate, port. The inverse relationship of two equal inputs producing full output from one port and zero from another also will be obtained, and is in fact a special case of the property that two coherent inputs produce their vector sum and difference at the other two ports. One other property of a hybrid junction is of interest: it is the only branching junction capable of appearing matched looking into any port when the other ports are terminated in their characteristic impedances. Typical waveguide forms of hybrid junctions shown in Fig. 2 are the *E-H* tee, (also called "magic" tee), the hybrid ring ("rat-race") and the 3 db directional-coupler ("short-slot") hybrid.

Early applications of hybrid junctions in waveguide circuits were in balanced mixers, where two independent input signals are each divided equally between the two crystals; in impedance bridges, where two reflections are compared by observing their difference, and in power dividers, where equal power division is secured regardless of the load impedances. Later, hybrids found application in tuners, phase adjusters, balanced duplexers, and discriminator circuits. The most recent applications include the new type of "monopulse" radar described by Mr. Page of the Naval Research Laboratory at the 1955 IRE Convention, which uses the sum and difference signals from a hybrid for simultaneous determination of target range and angle; and the ferrite "circulator," a new nonreciprocal circuit element.

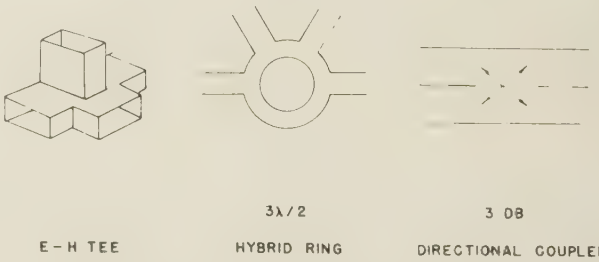

Fig. 2—Forms of waveguide hybrid junctions.

The wartime developments in hybrid junction design concerned principally tee and ring-type junctions. Many structures and matching elements for these junctions are described in detail in the M.I.T. Radiation Laboratory Series, principally volumes 8, 11, and 14, and in a comprehensive article by Tyrell.[1] Since then, Mr. Budenbom of the Bell Laboratories has presented extensive treatments of the hybrid ring junction. Mr. Riblet of the Microwave Development Laboratories has developed the directional-coupler type of hybrid to a high degree. His "short-slot" hybrids have excellent impedance match, good power capacity, and may be obtained quite inexpensively in many compact forms with various adapters. Mr. Sensiper and others at Sperry have achieved and patented a design for a hybrid tee junction with low reflection over the full 40 per cent waveguide bandwidth. This design, consisting of a wedge and pin within the junction and a small inductive iris in the *E* arm, has been adapted (with tapers where necessary) to all standard waveguide sizes, and is being defined by the Signal Corps as a military standard component.

Some of the most important needs in present applications of the waveguide hybrid junction are for easily specifiable internal dimensions, high power-handling

* Manuscript received by the PGMTT, July 16, 1956. Presented before the National Symposium on Microwave Techniques, Philadelphia, Pa., February 2, 1956.

† Wheeler Labs., Inc., Great Neck, N. Y.

[1] W. A. Tyrrell, "Hybrid circuits for microwaves," PROC. IRE, vol. 35, pp. 1294–1306; November, 1947.

capacity, convenient configurations for direct connection to adjacent circuit elements, and high isolation in both pairs of arms over a wide (12 per cent) frequency band. All of these needs have been met in varying degrees in the hybrids which will be described, which were developed by the Wheeler Laboratories for the Bell Telephone Laboratories. These are all centralized junctions, having two perpendicular, cross-polarized arms located in the plane of symmetry of the junction. An advantage of this type of structure is the inherent isolation of the perpendicular arms at all frequencies. If these two arms are also impedance-matched, the design of the junction is completed, for, by reciprocity, the collinear arms acquire the same properties of isolation and match.

For the conventional *E-H* tee structure, a new wide-band matching element has been found for the *E* arm; this is a large cone located in the junction space, replacing the narrow-band inductive iris used in early tee designs. The cone, shown in Fig. 3, acts as a power-divider

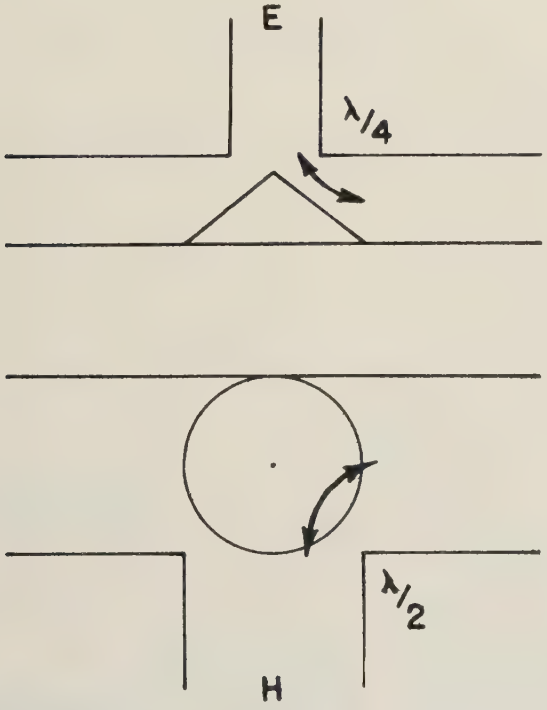

Fig. 3—Cone for matching *E* arm of hybrid tee.

in the *E* arm, a cutoff-corner 90° *E*-plane bend, and a quarter-wavelength transformer from half to full height waveguide. Its location along the plane of symmetry of the junction is less critical than the volume of material introduced into the junction. In cross section, the cone may be seen to resemble the wedge of Sensiper's wide-band design. The aspect presented to the *H* arm, however, differs somewhat from the wedge. The cone becomes a section of reduced impedance line which is a half wavelength long, and is therefore not seen from the *H* arm. With the *E* arm matched by the cone, a suitable element affecting only the *H* arm is the "post" of the early designs. Its height and distance from the back wall of the junction are adjusted for match. Since the cone location is not critical axially, it is made concentric with the pin in order to obtain a simple form for the insert. With the addition of a thin resonant window to double-tune the *E* arm, the structure and performance shown in Figs. 4 and 5 is achieved. Over the 12 per cent

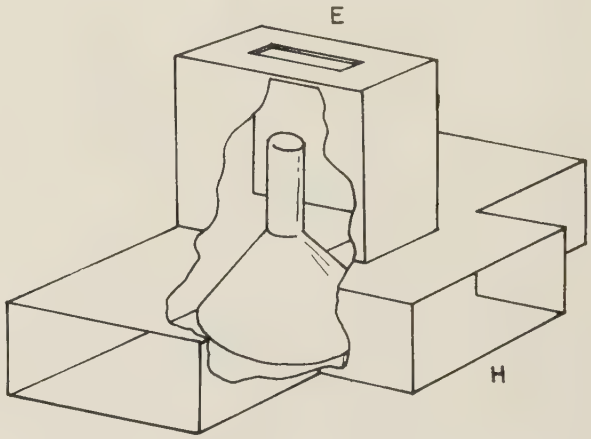

Fig. 4—Waveguide hybrid tee (WL model 201).

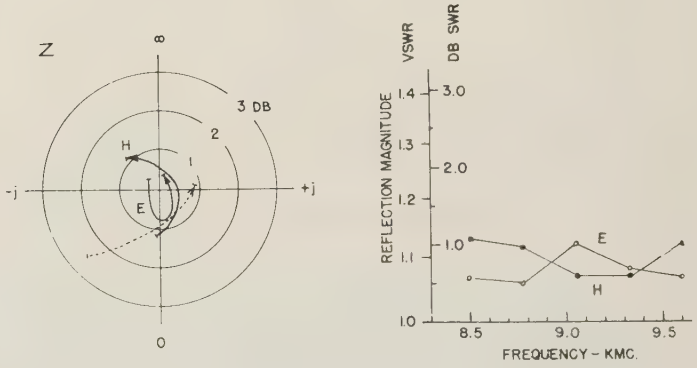

Fig. 5—Reflection of model 201 hybrid tee.

X band, reflection is within 1.2 db swr (1.15 vswr) in both the *E* and *H* arms. A consequence of this match is isolation of over 35 db between collinear side arms. The *E-H* arm isolation is, of course, limited only by constructional symmetry of the junction; values of over 50 db over the band have been obtained in our models.

When the pin is modified into the form of a rounded fin and the resonant window is widened as shown in

Fig. 6, a high-power design is obtained, with performance equivalent to that previously described. Over the 12 per cent X band, the E arm of this junction has been found to carry pulse power of up to 1 mw without breakdown. (See Fig. 7.)

Another configuration of particular convenience is the H plane fork shown in Fig. 10. The perpendicular pair of ports are easily accessible; the other pair, which are adjacent in the H plane, provide a compact connection

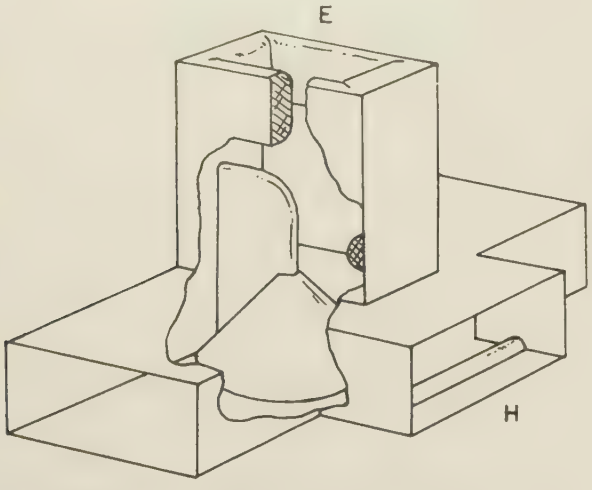

Fig. 6—High-power waveguide hybrid tee (WL model 120).

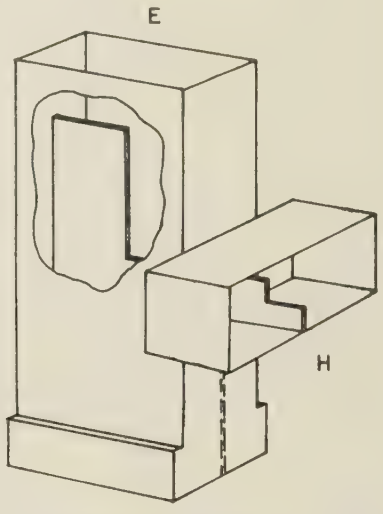

Fig. 8—E-plane forked hybrid (WL model 294).

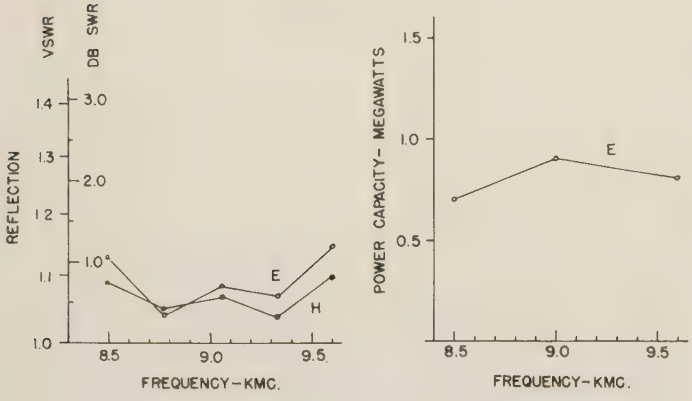

Fig. 7—Reflection and power capacity of model 120 hybrid tee.

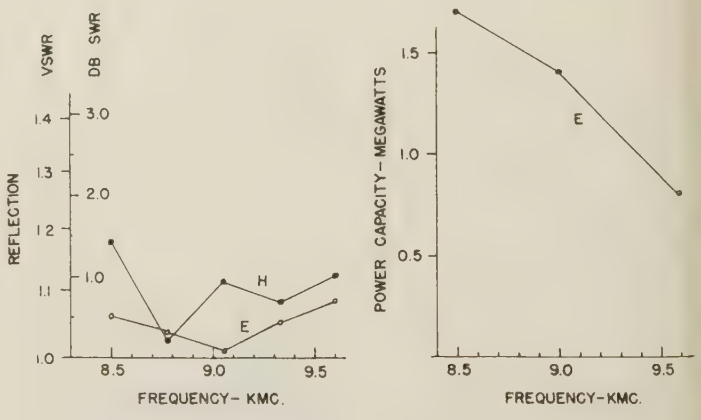

Fig. 9—Reflection and power capacity of model 294 forked hybrid.

Even higher power capacity has been attained with another structure, the E-plane forked hybrid.[2] In this junction, shown in Fig. 8, the "side" arms become parallel and are brought out in a direction opposite to the E arm. The E arm here feeds a guide having a thin partition in an equipotential plane; there is very little reduction of power by such a structure. Power tests of the E-plane fork over the 12 per cent X band indicate a pulse-power capacity of up to 1.6 mw in the E arm. The reflection of this junction, when combined with suitable adapters to bring all ports to normal waveguide size, is within 1.0 db swr (1.12 vswr), as shown in Fig. 9.

[2] W. K. Kahn, "E-plane forked hybrid-T junction," IRE Trans., vol. MTT-3, pp. 52–58; December, 1955.

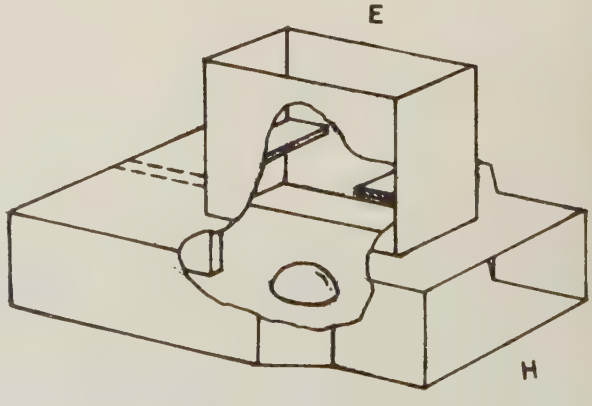

Fig. 10—H-plane forked hybrid (WL model 202).

to parallel antenna feeds, balanced mixers, or circulator elements. A similar structure has been developed by the Hughes Aircraft Co., and is presently being manufactured by Airtron. In the design shown here, the matching elements, which consist of a small round bump in the junction and an inductive iris in the E arm, achieve match within 0.8 db swr (1.10 vswr) in the E arm, and within 1.6 db swr (1.20 vswr) in the H arm, over the 12 per cent X band (see Fig. 11).

All the designs described have been carried to completion in one particular waveguide size (RG-51/U); the principles, however, are adaptable to any other size desired. By choosing a type of junction with inherent isolation in one pair of arms, it is necessary only to match that pair while maintaining symmetry in order to complete the junction design. The basic matching element for the E arm is a space-filling insert which acts as a power-divider; for the H arm, a resonant stub which couples the H arm to the side arms. Further matching may be achieved by introducing reactive irises or resonant windows in the E and H arms. Any symmetrical position of the side arms can be incorporated into a matched design; the extreme positions are represented in the designs described.

These design principles have resulted in waveguide hybrid junctions with simple matching elements, having good impedance match, isolation in both pairs of arms, and high power-handling capability.

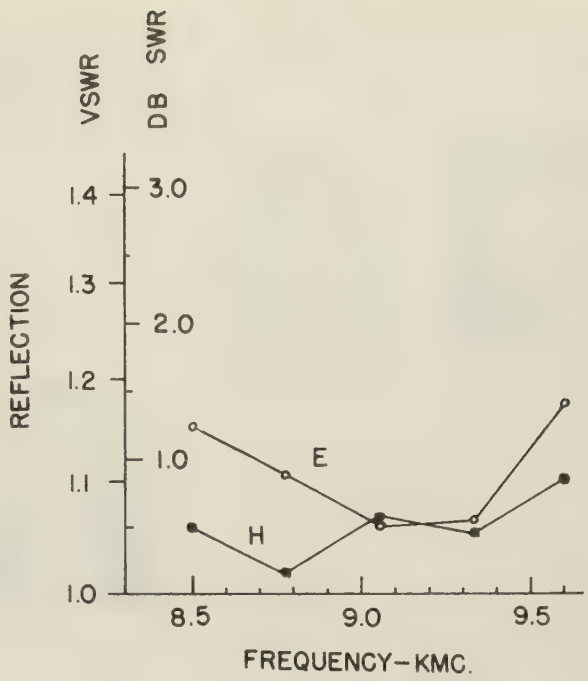

Fig. 11—Reflection of model 202 forked hybrid.

This work has been conducted under the direction of H. A. Wheeler and has been sponsored by the Bell Telephone Laboratories in connection with an Armed Services contract.

Contributors

P. J. Allen

Philip J. Allen was born in Whitinsville, Mass., on December 30, 1919. Following two years of subprofessional employment with the General Radio Company, Cambridge, Mass. Mr. Allen entered Pennsylvania State University, and in 1944 received the B.S. degree in physics.

That same year, he joined the Tracking Branch, Radar Division at the Naval Research Laboratory, Washington, D. C., where he has been engaged in developing special microwave components and antenna feeds, and in the development of automatic tracking radar systems. Since 1951, he has been serving as head of the New Techniques Section of this same branch, engaged in investigating new ideas for the improvement of tracking radar systems.

Mr. Allen is a member of RESA.

❖

Helmut M. Altschuler (S'47–A'49–M '54–SM'55) was born in Germany, in 1922. He received the B.E.E. degree in 1947 and the M.E.E. degree in 1949 from the Polytechnic Institute of Brooklyn, New York, where he is continuing his graduate studies at the present time.

In 1947–48 Mr. Altschuler held a Research Fellowship at the Microwave Research Institute of the Polytechnic Institute of Brooklyn, and since then has been employed there, presently in the capacity of research associate.

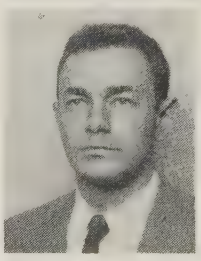

H. M. Altschuler

His work has been concerned chiefly with the development of impedance meters, microwave measurement techniques, and equivalent network representations.

Mr. Altschuler is a member of Sigma Xi and Eta Kappa Nu.

Tore N. Anderson (S'49–A'49–SM'55) was born on May 1, 1920, in Sweden. In 1943 he completed the electrical engineering program at Oregon State College, and in 1948 received the B.S.E.E. degre from Cooper Union.

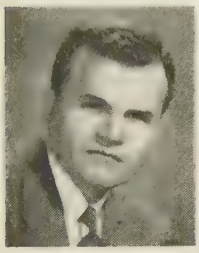

T. N. Anderson

During the war, Mr. Anderson served with the Engineering Research and Development Agency as project officer on underwater mine detectors and as chief of the Laboratory and Test Section, engaged in the design and development of mine detectors. After the war he was engineer-in-charge of radio frequency measurements at Electrical Testing Laboratories in New York.

He has been associated with Airtron, Inc. since 1948, working on the development of transmission line components and on the development of rigid and flexible waveguide components. In 1951, he was appointed Chief Engineer, and in 1953, was elected to the Board of Directors and appointed Vice-President. He is now Director of Engineering and in charge of the Research and Development Division.

He is a member of AIEE and Tau Beta Pi.

❖

Franklin S. Coale (A'53) received the B.S. degree in engineering physics from Lehigh University in 1952, subsequently taking post graduate work in applied mathematics at N.Y.U. In 1953 he joined Sperry Gyroscope Co. as an associate engineer in microwave components and antennas engineering. In 1955, he joined Stanford Research Institute in the Microwave Group of the Antenna Systems Laboratory. He is engaged in research and development on filters, multiplexers, ferrite devices, and antennas.

F. S. Coale

He is a member of the American Physical Society and the Research Society of America.

❖

Albert D. Frost (S'45–A'52) was born in Boston, Mass., in 1922. He received the B.S. degree from Tufts College in 1945, the A.M. degree in applied science from Harvard in 1947, and the Sc.D. degree in physics from M.I.T. in 1952. Since 1947, he has been a faculty member of the Department of Physics and a research associate in the Research Laboratory of Physical Electronics at Tufts University. Presently, Dr. Frost is assistant professor of physics.

A. D. Frost

He is a member of Phi Beta Kappa, Sigma Xi, Sigma Pi Sigma, the Acoustical Society of America, and the American Association of Physics Teachers.

❖

Georg Goubau (A'49) was born in Munich, Germany, on November 29, 1906. He received the M.S. and Ph.D. degrees in physics from the Munich Technical University. From 1931 to 1939 he was employed in research and teaching in the physics department of the same university, under Professor Zenneck. During this time, he established and was in charge of the first German ionospheric research station. In 1939, Dr. Goubau was appointed professor and director of the department of applied physics of the Friedrich-Schiller University in Jena, Germany.

G. Goubau

Since 1947, he has been a member of the research staff of the Signal Corps Engineering Laboratories in Fort Monmouth, N. J. His chief research activities have been principally concerned with wave propagation and microwave circuits.

❖

John W. E. Griemsmann (A'45) was born May 31, 1916, in Brooklyn, N. Y. He received the B.E.E. degree in 1936 and the M.E.E. degree in 1938 from the Polytechnic Institute of Brooklyn, and remained there as a research fellow until September, 1939.

J.W.E. Griemsmann

From 1939 to 1942 he was associated with the Westinghouse Research Laboratories as a research engineer in the Insulation Department. During this time he studied at the University of Pittsburgh toward the Ph.D. degree in physics.

In 1942 he returned to the Polytechnic Institute of Brooklyn as a research associate working on radar components and microwave measuring instruments under O.S.R.D. He received the D.E.E. degree from the Polytechnic Institute of Brooklyn in 1946. Since that time, Dr. Griemsmann has been associated with the Microwave Research Institute, becoming associate director in 1952, and research professor at P.I.B. in 1953.

Since 1945 he has also been active in standardization work on microwave transmission lines and components, as a participant in the Army-Navy RF Cable Coordinating Committee, a member of the R.D.B. Sub-Panel on Transmission Lines and Components, and a member of RETMA active in the Special Quality Components group. He was joint chief delegate for the United States to Subcommittee 12-5 of the International Electrotechnical Commission at the 1954 meeting in Philadelphia and the 1955 meeting in London.

Dr. Griemsmann is a member of Eta Kappa Nu, Sigma Xi, the American Association for the Advancement of Science, and the AIEE Insulation Conference (NRC).

❖

Walter K. Kahn (S'50–A'51–M'56) was born on March 24, 1929, in Mannheim, Germany, and came to the United States in 1938. He completed his undergraduate studies at the Cooper Union School of Engineering, receiving the Bachelor's degree in electrical engineering in 1951.

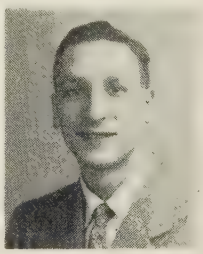

W. K. Kahn

Upon graduation, Mr. Kahn was employed at the Wheeler Laboratories, New York where he was engaged in microwave radar system development. Concurrently he engaged in graduate study at the Polytechnic Institute of Brooklyn, receiving the Master's degree in electrical engineering in 1954.

At that time he joined the staff of the Microwave Research Institute of the Polytechnic Institute of Brooklyn, where he is presently studying general diffraction theory and propagation in multimode waveguides.

Mr. Kahn is an associate of Sigma Xi.

❖

George Kasai (S'49–A'49) was born April 28, 1927, in San Francisco, Calif. He received the B.S. degree in electrical engineering from the University of California in Berkeley in 1949. From 1949 until 1952, he was engaged as Electronic Engineering Assistant at the Evans Signal Laboratory of the Signal Corps Electronic Laboratory in Belmar, N.J. In 1952 he was granted a Junior Research Fellowship at the Polytechnic Institute of Brooklyn where he participated in a research program at the Microwave Research Institute. He received the M.E.E. degree in 1954. Mr. Kasai is presently employed at the North American Aviation Corporation in Downey, Calif.

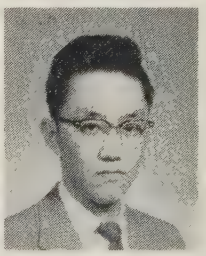

G. S. Kasai

Mr. Kasai is a member of Sigma Xi, Eta Kappa Nu, and Tau Beta Pi.

Patrick J. Kelly (S'54–M'56) was born in Minneapolis, Minn., on June 13, 1930. He attended the University of Minnesota, Macalester College and the U. S. Naval Academy where he received the B.S. degree in 1953. After one and one-half years in the Navy he came to the Moore School of Electrical Engineering, University of Pennsylvania to study for advanced degrees. Mr. Kelly is currently on the staff of the Moore School where he is a Research Engineer.

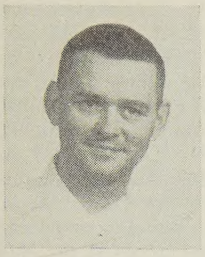

P. J. KELLY

❖

Ralph W. Klopfenstein (S'44–A'46–M'50–SM'54) was born on June 3, 1923, in Aberdeen, S. D. He received the B.S. in E.E. degree from the University of Washington in 1944 and the M.S. and Ph.D. degrees in applied mathematics from Iowa State College in 1951 and 1954.

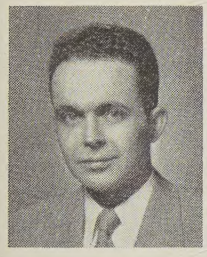

R.W. KLOPFENSTEIN

From 1945 to 1946, he was a radio materiel officer in the U. S. Naval Reserve. He became an instructor in the mathematics department of South Dakota School of Mines and Technology in 1946. In 1948, he joined RCA Victor in Camden, N. J., where he worked on the advanced development of television and fm transmitting antennas and filters. After three years as an instructor in mathematics at Iowa State, from 1950 to 1953, he returned to RCA Laboratories Division in Princeton, N. J., where he is now a member of the research staff.

Dr. Klopfenstein is a member of Sigma Xi, Phi Kappa Phi, the Mathematical Association of America, and the Society for Industrial and Applied Mathematics.

❖

Pietro P. Lombardini (A'53) was born in Bologna, Italy. He received the degree of Doctor of nautical science in 1937 in Naples, Italy and the degree of Doctor in physics in 1950 in Pisa, Italy. From 1938 to 1941 he served in various capacities in the Italian Navy. From 1941 to 1943 he was engaged in radar research for the Italian Navy. From 1945 to 1946 he was with the National Research Council in Rome, Italy. From 1946 to 1952 he was engaged in microwave research and radar design at the Center for Microwave Physics, National Research Council, Florence, Italy. In the summer and fall of 1950 he held a UNESCO Fellowship for work with the National Research Council of Canada in Ottawa. Since 1952 he has been engaged in microwave research at the Moore School of Electrical Engineering, University of Pennsylvania, Philadelphia, where he is an Assistant Professor. He is the author of several technical papers. He is a member of Sigma Xi.

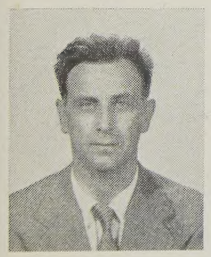

P. P. LOMBARDINI

❖

Patricia A. Loth (A'48–SM'55) was born in New York, N. Y. in 1921. She graduated from St. Joseph's College for Women in Brooklyn, N.Y., in 1942 with the B.A. degree in mathematics, and is presently doing graduate study in the physics department of the Polytechnic Institute of Brooklyn. She was employed until 1943 as an assistant engineer in the Physical and Electrical Standardization Laboratory of the Western Electric Company in Kearny, N.J. From 1943 to 1947, she was a member of the Test Laboratory at Hazeltine Electronics Corp., in Little Neck, N.Y., eventually being in charge of the group. In 1947, she joined the engineering staff of the Wheeler Laboratories in Great Neck, N.Y. and is presently a project supervisor specializing in microwave design.

P. A. LOTH

She is an associate member of Sigma Xi.

❖

Charles R. McGeoch, Jr. was born in Pelham, Mass., on October 23, 1928. He received the B.S. degree in mathematics from the University of Massachusetts in 1952 and the M.S. degree in physics from Tufts University in 1956.

C. R. MCGEOCH, JR.

Formerly associated with the department of physics at Tufts, Mr. McGeoch is presently employed at Bomac Laboratories, located in Beverly, Mass., where he holds the position of development engineer working on microwave electron tubes.

Mr. McGeoch is a member of Sigma Pi Sigma and Sigma Xi.

❖

Charles R. Mingins (A'36–SM'46) was born in Lawrence, Mass., in 1899. He received the A.B. degree from Wesleyan University in 1925. During 1928–1929 he was Heckscher research assistant in wave propagation at Cornell University. He remained at Cornell as an instructor in physics, and was in charge of the electric wave laboratory from 1930 to 1935 He received the Ph.D. degree in 1935. For two years thereafter, Dr. Mingins was acting instructor in physics at State College in Albany, N. Y. He is presently at Tufts College as professor of physics and director of the Research Laboratory of Physical Electronics.

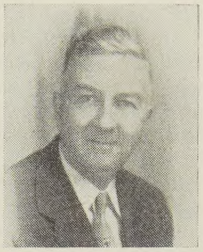

C. R. MINGINS

He is a member of Sigma Xi, Phi Beta Kappa, and the American Physical Society.

❖

Edward A. Ohm (S'51–A'54) was born on July 4, 1926 in Milwaukee, Wis. He received the degrees of B.S., M.S. and Ph.D. in Electrical Engineering from the University of Wisconsin in 1950, 1951, and 1953, respectively. Since 1953 he has been a member of the technical staff of the Bell Telephone Laboratories in the Radio Research Department at Holmdel, N. J. Dr. Ohm is presently working on extremely broad-band microwave filter and channel branching problems, including many with ferrite devices.

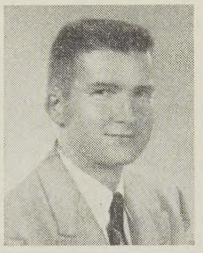

E. A. OHM

He is a member of Tau Beta Pi and of Sigma Xi.

❖

John Reed (A'48–SM'53) was born in Cambridge, Mass., on March 9, 1922. He received the B.S. degree in applied physics from M.I.T. in 1943, and for two years thereafter was on the staff of the M.I.T. Radiation Laboratory in the Radio Frequency Components Group. After graduate study at Cornell University he joined the Submarine Signal Company in 1947 and then transferred to the Raytheon Manufacturing Company in 1948, where he is currently employed as consultant on microwave problems.

J. REED

❖

Sloan D. Robertson (S'37–A'40–SM'45) received the B.E.E. degree from the University of Dayton in 1936 and the M.S. and

Ph.D. degrees in communication engineering from Ohio State University in 1938 and 1941. In 1940 he taught electrical engineering at the University of Dayton.

S. D. ROBERTSON

From 1940 to 1956 Dr. Robertson was with Bell Telephone Laboratories, Holmdel, N.J., where he was engaged in research on microwave radar, microwave circuits, millimeter-wave amplifiers, and finline circuits. He is now Engineering Section Head with Goodyear Aircraft Corp., Litchfield Park, Arizona.

Dr. Robertson is a registered Professional Engineer in New Jersey and is a member of Tau Beta Pi, Eta Kappa Nu, and Sigma Xi.

❖

Richard F. Schwartz (S'43–A'45–M'53–SM'55) was born in Albany, N. Y. on May 31, 1922. He attended Rensselaer Polytechnic Institute where he received the B.E.E. degree in 1943, and the M.E.E. degree in 1948. He served with the U. S. Army Signal Corps from 1944 to 1946. From 1946 to 1948 he was an instructor in electrical engineering at Rensselaer Polytechnic Institute. From 1948 to 1951 he was with the Radio Corporation of America in Camden, N. J. where he did advanced development work on transmitting systems. Since 1951 he has been engaged in teaching and research at the Moore School of Electrical Engineering, University of Pennsylvania, where he holds the title of Associate in electrical engineering. He holds two patents and is the author of several technical articles. He is a member of AIEE, Sigma Xi, Eta Kappa Nu, the American Association for the Advancement of Science, and the American Society for Engineering Education.

R. F. SCHWARTZ

❖

Jorgen P. Vinding (A'54) was born in Copenhagen, Denmark, on January 9, 1925. He received the M.S. degree in electrical engineering from the Technical University of Denmark in January, 1950. After a few months in commercial engineering he joined Storno, a division of the Great Northern Telegraph Company in Copenhagen, where he designed vhf transmitters and receivers for mobile communication. After a year of study at Brooklyn Polytechnic Institute under the Rotary Foundation program during 1951–1952, he rejoined Storno to plan a microwave relay system for tv and telephone and to design the microwave parts of this system.

J. P. VINDING

Since 1954, Mr. Vinding has worked for Cascade Research Corporation, Los Gatos, Calif., where he has designed microwave load isolators and other ferrite components and is now directing the development of a series of special microwave test instruments.

He is a member of the Institution of Danish Engineers and of the American Society of Danish Engineers.

Max T. Weiss (S'43–A'45) received the B.S. degree in electrical engineering from the College of the City of New York in 1943, and the M.S. in E.E. and Ph.D. in physics from M.I.T. in 1947 and 1951, respectively. He worked for the Radio Corporation of America in Camden, N. J., from 1943 to 1944 and then served in the U. S. Navy, working on underwater mines at the Naval Ordnance Laboratory. From 1946 to 1950 he was connected with the Research Laboratory of Electronics at M.I.T. He joined Bell Telephone Laboratories in 1950 and for one year was concerned with dielectric waveguide transmission. Since then he has chiefly done research in microwave properties and applications of ferrites.

M. T. WEISS

He is a member of the American Physical Society, Sigma Xi, and Eta Kappa Nu.

❖

Gershon J. Wheeler (SM'54) was on the the staff of Radiation Laboratory, M.I.T., from 1942 to 1945. From 1945 to 1949 he was an engineer at Naval Research Laboratory Field Station in Boston, and from 1949 to 1950, was a project engineer at Andrew Alford Company. Since 1950 he has been at Raytheon Manufacturing Company where he is currently a consultant on special microwave problems.

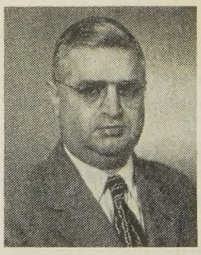

G. J. WHEELER

INSTITUTIONAL LISTINGS (Continued)

MICROWAVE DEVELOPMENT LABS., INC., 92 Broad St., Babson Park, Mass.
Design, Development & Production of Waveguide Components & Complete RF Assemblies

NATIONAL INSTRUMENT CO., INC., 23 E. 26 St., New York, N. Y.
Wide-Band Microwave Equipment, Simulated Flight Instruments, Lobe Switches, Custom Built Precision Apparatus

RAYTHEON MANUFACTURING CO., 148 California St., Newton, Mass.
Microwave Communications Systems, Radar, Missiles, Cooking Equipment, Tubes & Components

WEINSCHEL ENGINEERING CO. INC., Kensington, Md.
Attenuation Standards, Coaxial Attenuators and Insertion Loss Test Sets

WHEELER LABORATORIES, INC., 122 Cutter Mill Road, Great Neck, N. Y.
Consulting Services, Research & Development, Microwave Antennas & Waveguide Components

The charge for an Institutional Listing is $50.00 per issue or $140.00 for four consecutive issues. Applications for Institutional Listings and checks (made out to the Institute of Radio Engineers) should be sent to Mr. L. G. Cumming, Technical Secretary, Institute of Radio Engineers, 1 East 79th Street, New York 21, N. Y.

INSTITUTIONAL LISTINGS

The IRE Professional Group on Microwave Theory and Techniques is grateful for the assistance given by the firms listed below, and invites application for Institutional Listing from other firms interested in the Microwave field.

AIRCRAFT RADIO CORPORATION, Boonton, N. J.
Airborne Electronic Equipment, Associated Test Equipment

CASCADE RESEARCH CORPORATION, 53 Victory Lane, Los Gatos, Calif.
Res., Dev., & Prod. Microwave Ferrite Devices, Backward Wave Oscillators & Microwave Test Equip.

COLLINS RADIO CO., Cedar Rapids, Iowa
Complete Industrial Microwave, Communication, Navigation and Flight Control Systems

ESPEY MFG. CO., INC., Congress and Ballston St., Saratoga Springs, N. Y.
Mfgrs. of X-Band and S-Band Wavemeters, Attenuators, Thermistor Mounts and Signal Generators

HUGHES AIRCRAFT COMPANY, Culver City, California
Radar Systems, Guided Missiles, Antennas, Radomes, Tubes, Solid State Physics, Computers

MARYLAND ELECTRONIC MANUFACTURING CORPORATION, College Park, Md.
Development and Production of Microwave Antennas and Waveguide Components

MEASUREMENTS CORPORATION, Box 180, Boonton, N. J.
Specialists in the Design and Development of Electronic Test Instruments

(Please see inside cover for additional names.)